



**HAL**  
open science

# New insights on Intraflagellar Transport and flagellum length control in *Trypanosoma brucei*

Eloïse Bertiaux

► **To cite this version:**

Eloïse Bertiaux. New insights on Intraflagellar Transport and flagellum length control in *Trypanosoma brucei*. Cellular Biology. Sorbonne Université, 2018. English. NNT : 2018SORUS113 . tel-02341168

**HAL Id: tel-02341168**

**<https://theses.hal.science/tel-02341168>**

Submitted on 31 Oct 2019

**HAL** is a multi-disciplinary open access archive for the deposit and dissemination of scientific research documents, whether they are published or not. The documents may come from teaching and research institutions in France or abroad, or from public or private research centers.

L'archive ouverte pluridisciplinaire **HAL**, est destinée au dépôt et à la diffusion de documents scientifiques de niveau recherche, publiés ou non, émanant des établissements d'enseignement et de recherche français ou étrangers, des laboratoires publics ou privés.

Thèse de doctorat

De l'Université Pierre et Marie Curie

Ecole doctorale Complexité du Vivant

Présentée par

M<sup>lle</sup> Eloïse Bertiaux

Pour obtenir le grade de  
Docteur de l'Université Pierre et Marie Curie

**New insights on Intraflagellar  
Transport and flagellum length control  
in *Trypanosoma brucei*.**

Soutenue le 20 septembre 2018

Devant le jury composé de :

Sylvie SCHNEIDER-MAUNOURY, Présidente du jury  
Juliette AZIMZADEH, Rapporteuse  
André SCHNEIDER, Rapporteur  
Sue VAUGHAN, Examinatrice  
Manuel THERY, Examineur  
Philippe BASTIN, Directeur de thèse  
Brice ROTUREAU, Co-Directeur de thèse

Thèse de doctorat

De l'Université Pierre et Marie Curie

Ecole doctorale Complexité du Vivant

Présentée par

M<sup>lle</sup> Eloïse Bertiaux

Pour obtenir le grade de  
Docteur de l'Université Pierre et Marie Curie

**New insights on Intraflagellar  
Transport and flagellum length control  
in *Trypanosoma brucei*.**

Soutenue le 20 septembre 2018

Devant le jury composé de :

Sylvie SCHNEIDER-MAUNOURY, Présidente du jury  
Juliette AZIMZADEH, Rapporteuse  
André SCHNEIDER, Rapporteur  
Sue VAUGHAN, Examinatrice  
Manuel THERY, Examineur  
Philippe BASTIN, Directeur de thèse  
Brice ROTUREAU, Co-Directeur de thèse



# Acknowledgments

First of all, I would like to thank the members from my thesis defence committee, Juliette Azimzadeh and André Schneider, for accepting to become my thesis referees. Also, I am grateful to my thesis examiners, Sue Vaughan and Manuel Thery. Finally, I would like to thank Sylvie Schneider-Maunoury, for accepting to chair my thesis committee.

Je tiens à remercier mes directeurs de thèse Philippe Bastin et Brice Rotureau, de m'avoir acceptée dans l'Unité de Biologie Cellulaire des Trypanosomes au départ pour mon stage de Master 2. Merci ensuite de m'avoir soutenue pour obtenir ma bourse de thèse. A tous les deux, merci pour votre enthousiasme pour la science. Merci de m'avoir toujours poussée et soutenue tout au long de ces 4 années. Merci également pour votre aide et vos corrections lors de la rédaction de ce manuscrit. Merci Philippe pour ta gentillesse et ta bonne humeur et tes encouragements. Merci Brice pour ta gentillesse également et tes conseils quand j'en ai eu besoin.

Je remercie tous les membres de l'Unité de Biologie Cellulaire des Trypanosomes. Je ne vais pas être très originale mais de façon générale merci pour votre soutien, votre aide et votre bonne humeur qui rendent le quotidien dans le laboratoire très agréable.

Merci Adeline ma binôme de choc sur cette fin de thèse. On se souviendra de nos nombreux essais sur le FIB-SEM et nos heures à dessiner des flagelles et des IFT.

Merci Aline, pour les nombreuses heures dissection et pour toujours avoir eu une oreille attentive quand j'ai eu des coups de mou.

Merci Anne, pour sa gentillesse, son aide et son soutien. Merci également pour nos échanges littéraires.

Merci Christelle ma binôme de congrès. Merci pour ton soutien et nos discussions tout au long de ces quatre années.

Merci Elise, la petite dernière du labo. Toujours de bonne humeur et avec le sourire. J'espère que tu trouveras quelque chose qui te plaira à Bordeaux.

Thanks Estefania for your support and at the start to have dedicated some time to speak with me in spite of my poor english.



Thanks Jamin for sharing the office with me and supporting my music.

Thanks Moara, for your cheerfulness and your support.

Thanks Sebastian, for your help and your advices for the discussion and my post-doctoral fellowship application.

Merci Serge, pour nos discussions scientifiques, mais pas que, d'avoir partagé l'enseignement des TPs avec moi et pour ton coup de main sur la discussion.

Merci Sylvain, pour ton aide précieuse sur cette fin de thèse dans les analyses de FIB-SEM et ta bonne humeur.

Merci Thierry d'avoir été une oreille attentive surtout à la fin et pour ton aide. Merci de m'avoir formée au MEB et à la préparation des figures.

Je remercie Linda pour sa gentillesse et pour m'avoir permis de faire une partie de mon monitorat dans son unité d'enseignement.

Je tiens à remercier également toute l'équipe de Lucy Glover, qui partage les lab-meetings avec nous et leurs conseils.

Merci à l'Unité de Biologie des Interactions Hôte-parasite et en particulier Christine, Patty et Aurélie pour nos discussions aux détours des couloirs.

Un grand merci à mes amis de licence et M2 : Marie, Charlotte M, Charlotte G, Nicolas et Veronica. Merci pour nos conversations, d'avoir partager les mêmes doutes et parler de nos expériences respectives.

Merci Benoît, mon chéri qui a été d'un soutien hors pair depuis le départ. Tu as toujours cru en moi (souvent même plus que moi même) et tu as toujours eu les mots pour me remotiver. Merci tout simplement d'être là à mes côtés et surtout lors de ces dernières semaines qui ont été par moment très compliquées.

Merci à toute ma famille et en particulier à mes parents. Merci de m'avoir donnée le goût du travail et de m'avoir offert la possibilité de continuer des études qui me plaisaient et d'être tout simplement de supers parents. Merci à Manon ma petite sœur chérie, Aurélien mon petit frère chéri et Florian, mon beauf préféré pour votre soutien. Merci à tous d'être au quotidien à mes côtés.



# Abbreviations

AAT	Animal African Trypanosomiasis
ADP	Adenosine DiPhosphate
ADPKD	Autosomal Dominant Polycystic Kidney Disease
AE	Attached Epimastigote
AK3	Arginine kinase 3
AMP	Adenosine MonoPhosphate
APOL1	Apolipoprotein L1
ARPKD	Autosomal Recessive Polycystic Kidney Disease
ATP	Adenosine TriPhosphate
BARP	Bloodstream Alanine Rich Protein
BBS	Bardet-Biedl Syndrome
BSF	Bloodstream form
CALK	Aurora like protein kinase
CATT	Card Agglutination Test for Trypanosomiasis
CC2D	Coiled-Coil and C2-domain
CDK	Cyclin dependent kinase
CEP164	Centrosomal protein 164
CEP290	Centrosomal protein 290
CEP83	Centrosomal protein 83
CH	Calponin-Homology
CHE-3	Chemosensory protein 3
CLEM	Correlative light and Electron Microscopy
DAPI	4',6-diamidino-2-phenylindole
DE	Dividing Epimastigote
DHC	Dynein Heavy chain
DIC	Differential Interference Contrast
DNA	Deoxyribo-Nucleic Acid
DNA	Deoxyribonucleic Acid
DNAI1	Dynein Axonemal Intermediate chain 1
DRC	Dynein Regulatory Complex
Epi	Epimastigote



FAP133	Flagellar Associated protein 133
FAZ	Flagellum Attachment Zone
FC	Flagellar Connector
FIB-SEM	Focuss Ion Beam and Scanning Electron Microscopy
FLA1	Flagellum Attachment glycoprotein 1
FLA10	Flagellar kinesin-like protein 10
FLA11	Flagellar kinesin-like protein 11
FLA1BP	FLA1-binding protein
FLAM3	Flagellar Member 3
FLAM8	Flagellar Member 8
FP	Flagellar Pocket
FPC	Flagellar Pore Complex
FRAP	Fluorescence Recovery After Photobleaching
GFP	Green Fluorescent Protein
gHAT	gambiense Human African Trypanosomiasis
GPI	Glycosyl-Phosphatidylinositol
HAT	Human African Trypanosomiasis
Hh	Hedgehog
HRP	Haptoglobin related protein
IDA	Inner Dynein Arm
IFT	IntraFlagellar Transport
Ig	Immunoglobulin
KAP	Kinesin Associated Protein
KIF17	Kinase-like protein 17
KIF9B	Kinesin 9 family
LE	Long Epimastigote
MAP	Microtubule Associated protein
MKS	Meckel-Gruber Syndrome
MS	Mesocyclic
MT	Metacyclic
NECT	Nifurtimox/Eflornithine Combination Therapy
NF	New Flagellum
NPC	Nuclear Pore Complex
ODA	Outer Dynein Arm



ODF2	Outer Dense Fibre 2
OF	Old Flagellum
OSM-3	Osmotic avoidance abnormal protein 3
OSM-9	Osmotic avoidance abnormal protein 9
PC1	Polycystin-1
PC2	Polycystin-2
PCD	Primary Ciliary Dyskinesia
PCF	Procyclic form
PCM	Peri-Centriolar Material
PCR	Polymerase Chain Reaction
PCR	Polymerase Chain Reaction
PFR	ParaFlagellar Rod
PFR1	ParaFlagellar Rod protein 1
PFR2	ParaFlagellar Rod protein 2
PKD	Polycystic Kidney Disease
RABL5	RAS in the brain-like 5
RNA	Ribonucleic Acid
RNAi	RiboNucleic Acid Interference
RP2	Retinal Pigmentosa 2
RSP	Radial Spoke Proteins
ScIt1	Sodium Channel and Clathrin Linker 1
SE	Short Epimastigote
SEM	Scanning Electron Microscopy
Shh	Sonic hedgehog
SIT	Sterile Insect Technique
SL	Slender form
Smo	Smoothened
SRA	Serum Resistance Associated protein
ST	Stumpy form
TAC	Tripartite Attachment Complex
TBBC	Trypanosome Basal Body Component
TEM	Transmission Electron Microscopy
TF	Transition Fiber
TIRF	Total Internal Fluorescence
TLF1	TrypanoLytic Factor 1



TLF2	TrypanoLytic Factor 2
TPR	Tetratricopeptid repeat
TRPV	Transient Receptor potential vanilloid
Trypo	Trypomastigote
TZ	Transition Zone
VSG	Variant Surface Glycoprotein
WHO	World Health Organization



<b>INTRODUCTION</b>	<b>1</b>
<b>I. CILIA AND FLAGELLA</b>	<b>5</b>
1) HISTORY	5
2) THE STRUCTURE OF CILIA AND FLAGELLA	6
a) Basal bodies and centrioles	7
b) The transition zone	8
c) The axoneme	9
d) The membrane of cilia and flagella	10
e) Extra-axonemal structures	11
3) DIFFERENT TYPES OF CILIA AND FLAGELLA	12
1) The motile "9+2" cilia and flagella	12
2) The immotile "9+0" cilia and flagella	13
3) Other types of cilia and flagella	14
4) CILIOPATHIES	15
a) Primary ciliary dyskinesia	15
b) Polycystic kidney disease	16
c) Retinal degeneration	17
5) MODEL ORGANISMS TO STUDY CILIA AND FLAGELLA	18
a) The green alga <i>Chlamydomonas reinhardtii</i>	19
b) The nematode <i>Caenorhabditis elegans</i>	20
c) The mouse	20
<b>II. TRYPANOSOMA BRUCEI</b>	<b>23</b>
1) <i>TRYPANOSOMA BRUCEI</i> AS A PARASITE	23
a) African trypanosomiasis: history and epidemiology	23
b) African trypanosomiasis: actors of the infection	25
i. The trypanosomes	25
ii. The tsetse	26
iii. Mammalian host and reservoir	27
c) Parasite cycle	28
i. Mammalian stages	28
ii. Tsetse fly stages	29
d) Human infection and symptoms	30
e) Diagnosis and treatment	31
2) THE FLAGELLUM OF <i>TRYPANOSOMA BRUCEI</i>	33

a)	Conserved and unique features in the architecture of the trypanosome flagellum	33
I.	Flagellar pocket	34
II.	Basal body and transition zone	34
III.	Axoneme	35
IV.	ParaFlagellar Rod (PFR)	36
V.	Flagellar attachment zone (FAZ)	37
VI.	Flagella connector (FC)	38
b)	Duplication of the flagellum during the cell cycle	39
c)	Roles of the trypanosome flagellum	40
I.	Motility	40
II.	Immune evasion	41
III.	Salivary gland adhesion	42
IV.	Cell morphology	42
V.	Sensory functions	43
<b>III.</b>	<b>FLAGELLUM BIOGENESIS</b>	<b>44</b>
1)	HISTORY	44
2)	INTRAFLLAGELLAR TRANSPORT (IFT)	46
a)	The IFT trains	46
b)	IFT-B complex	48
I.	The IFT-B core (IFT-B1)	48
II.	The Peripheral IFT-B complex	50
c)	The IFT-A complex	51
d)	The IFT associated motors	51
e)	IFT regulation	53
I.	Initiation of flagellum assembly	53
II.	IFT Regulation at the base of the flagellum	54
III.	Entry into the flagellar compartment and anterograde transport	55
IV.	Cargo protein transport	56
V.	Transition at the flagellum tip	57
VI.	Retrograde transport	59
<b>IV.</b>	<b>MODELS FOR FLAGELLUM LENGTH CONTROL</b>	<b>60</b>
I.	Balance point model	60
II.	The limited precursor availability	61
III.	The flagellum length sensor theory	62

<b>QUESTIONS</b>	<b>65</b>
<b>I. WHERE DO IFT TRAINS TRAVEL ON THE TRYPANOSOME AXONEME?</b>	<b>67</b>
<b>II. HOW IS THE FLAGELLUM LENGTH CONTROLLED IN <i>T. BRUCEI</i>?</b>	<b>69</b>
<b>RESULTS</b>	<b>71</b>
<b>I. BIDIRECTIONAL INTRAFLAGELLAR TRANSPORT IS RESTRICTED TO ONLY TWO MICROTUBULE DOUBLETS IN THE TRYPANOSOME FLAGELLUM.</b>	<b>73</b>
1) SUMMARY	73
<b>II. FLAGELLUM LENGTH CONTROL IN TRYPANOSOMES.</b>	<b>131</b>
1) SUMMARY	131
<b>III. PRODUCTION OF FLAGELLA WITH DIFFERENT LENGTH DURING THE TRYPANOSOME PARASITE CYCLE.</b>	<b>210</b>
1) INTRODUCTION	210
2) MATERIALS AND METHODS	211
Tsetse fly maintenance, infection and dissection	212
Immunofluorescence	212
Live imaging of parasites isolated from tsetse fly	213
Inhibition of cell division	214
3) RESULTS	215
The IFT concentration remains constant in the flagellum during the entire parasite cycle	215
IFT trafficking remains constant during all the parasite cycle	215
IFT protein repartition is different in short epimastigote flagella	217
Modulation of FLAM8 concentration is not responsible for flagellum length control in short epimastigote.	218
Cell division timing contributes to the control of flagellum length.	219
<b>DISCUSSION</b>	<b>222</b>
<b>I. IFT ON SPECIFIC DOUBLETS</b>	<b>224</b>
1) WHY DO IFT TRAINS TRAVEL ONLY ON SPECIFIC DOUBLETS?	224
2) WHY DOES IFT ONLY USE 2 OF THE 9 MICROTUBULE DOUBLETS?	227
3) HOW DOES IFT ONLY TAKE PLACE ON SPECIFIC MICROTUBULE DOUBLETS?	230
4) WHY ARE ONLY DOUBLETS 4 AND 7 BE MODIFIED?	235
5) HOW ANTEROGRADE AND RETROGRADE TRAINS AVOID COLLISIONS?	236
<b>II. FLAGELLUM LENGTH CONTROL</b>	<b>238</b>
1) WHAT COULD REGULATE FLAGELLUM GROWTH?	238

2) WHAT COULD BE THE MECHANISM(S) RESPONSIBLE FOR FLAGELLUM LOCKING?	239
3) COULD THE "GROW AND LOCK" MODEL APPLY TO OTHER STAGES OF THE <i>T. BRUCEI</i> PARASITE CYCLE?	242
4) COULD OTHER MODELS EXPLAIN FLAGELLUM LENGTH CONTROL?	244
5) DISCOVERY OF A NEW STAGE DURING THE PARASITE CYCLE.	245
6) FLAGELLUM LENGTH CONTROL DURING EPI-TRYPO DIVISION.	246
<b>III. CONCLUSION AND PERSPECTIVES.</b>	<b>247</b>

**REFERENCES** **249**

---

1) TEXT REFERENCES	251
2) FIGURE REFERENCES	284



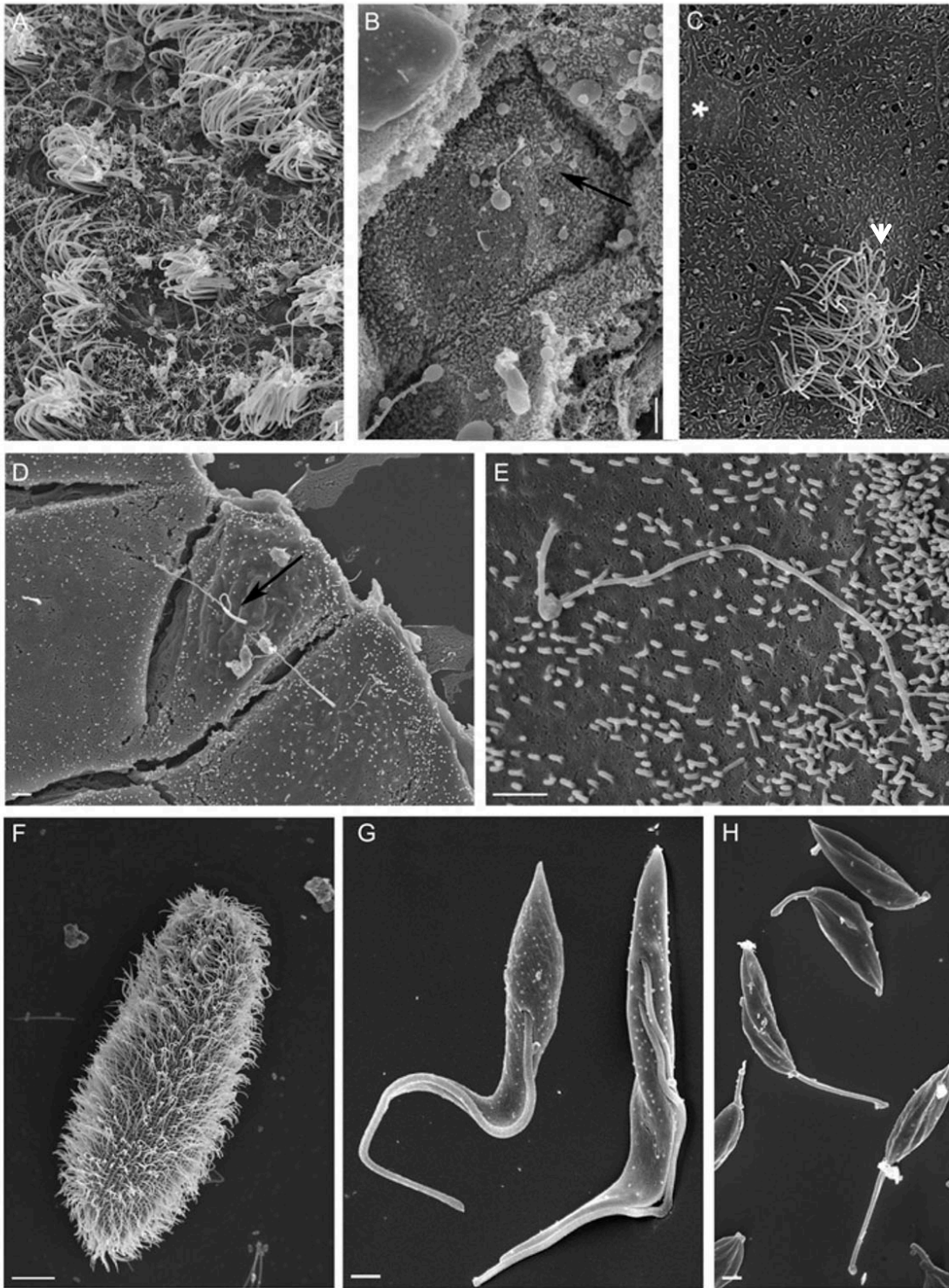
# Introduction



## **Introduction**

Cilia and flagella are organelles present in most eukaryotic cells. They share a canonical cylindrical structure composed of 9 microtubule doublets called the axoneme that is conserved during evolution. Despite some variations in composition and length between different types of cilia, the length for a given cell type is tightly controlled. Any defect in this length can lead to serious cellular dysfunctions, including in humans where it is associated to genetic diseases called ciliopathies. Two major questions result directly from these observations: (1) how are these organelles assembled? (2) Which are the mechanisms implicated in the control of their length?

Ribosomes are absent from the ciliary compartment meaning that all the constituents necessary for construction are synthesized in the cytoplasm. Axonemal component incorporation takes place at the distal end of the organelle (Rosenbaum and Child 1967). It is proposed that they are transported to the assembly site by Intraflagellar Transport (IFT), a bidirectional movement of protein complexes driven by molecular motors along the axoneme. IFT proteins are associated in trains or particles visible by electron microscopy as electron dense material found between the ciliary membrane and the axoneme microtubules. It is possible to visualize IFT in live cell by tagging one of its constituents with a fluorescent protein. IFT defects are responsible for defaults in flagellum construction or / and in the control of flagellum length. During my thesis, I have studied the IFT machinery and the mechanisms implicated in flagellum length control by using the parasite *Trypanosoma brucei* as a model. First, using a combination of high-resolution electron microscopy and light microscopy we have investigated how and where IFT trains move within the flagellum of *T. brucei*. Second, we have proposed a new model named “grow and lock” to explain how flagellum length could be controlled. We have evaluated the impacts of both the flagellum growth rate and the timing of the locking event in the control of the flagellum length. We have investigated the relevance of other potential models for length regulation in *T. brucei* and none of them can explain the results. Finally we have started to investigate how flagellum length could be regulated during the parasite cycle, where trypanosomes construct flagella of very different lengths. This could be controlled by the “grow and lock” model or by other models such as the existence of a length sensor for example. Mechanisms implicated in length regulation

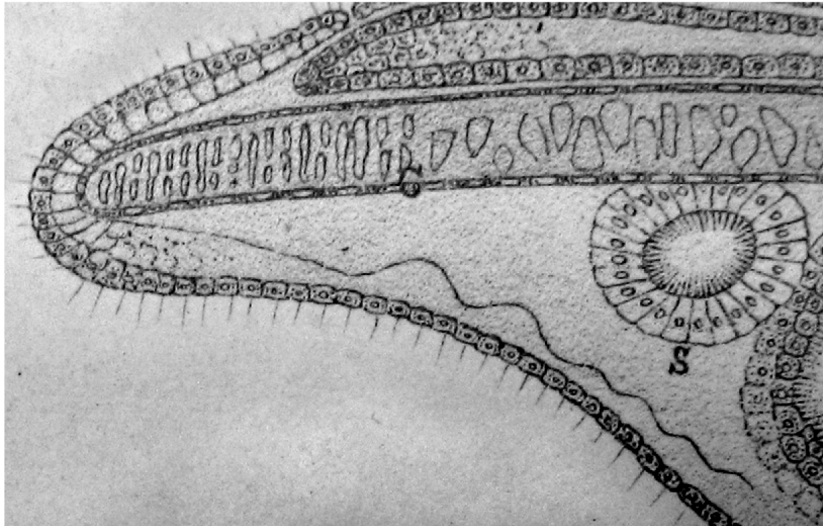
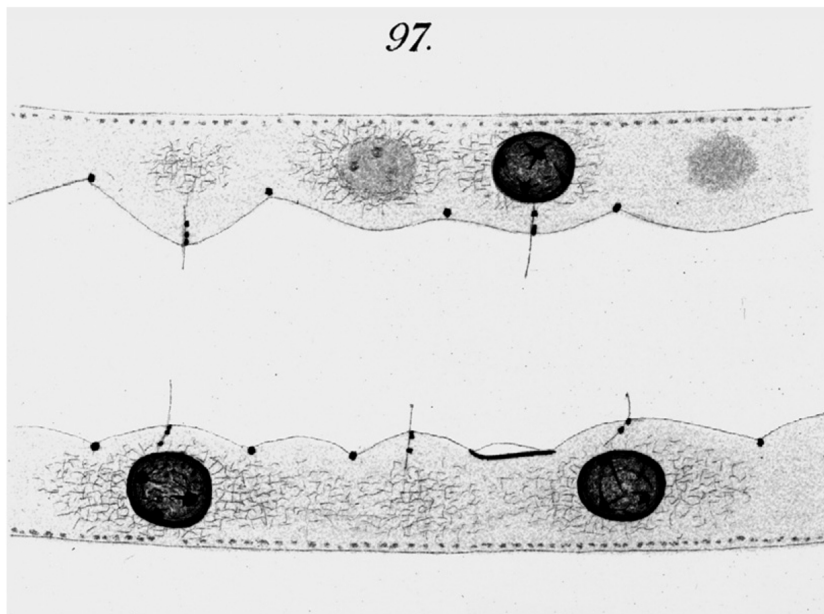


**Figure 1: Diversity of cilia and flagella.**

Images acquired by scanning electron microscopy showing different ciliated type of **(A)** mouse ependymal cilia covering the epithelium of the brain ventricles. **(B)** Cilia present on collecting tubule from mouse kidneys observed after cryo-fracture. **(C)** Mucociliary epithelium in *Xenopus* with one multi-ciliated cell (arrowhead) and one sensory cell (asterisk). **(D)** Cultured inner medullary collecting duct cells (IMCCD) and **(E)** Madin-Darby canine kidney cells (MDCK). **(F)** The ciliate *Paramecium tetraurelia* **(G)** *Trypanosoma brucei*, procyclic stage found in the midgut of the tsetse fly **(H)** and *Leishmania donovani*, promastigote stage. Scale bars: 1 $\mu$ m except for *Paramecium*, 10 $\mu$ m. Figure courtesy of (Vincensini, Blisnick et al. 2011)

## ***Introduction***

could be specific for each stage of the parasite cycle. This could be also the case in multicellular organisms where specific mechanisms could be activated to produce different types of cilia depending on the cell type.

**A****B**

**Figure 2: First observations of cilia and flagella.**

(A) Illustration made by Kowalevsky in 1867 showing a portion of a 30-hours old *Amphioxus* embryo. The epithelium is made of a simple layer of cuboidal cells, that each possesses a single flagellum. (Bloodgood 2009) (B) Drawing of rabbit kidney tubule epithelia with central primary cilia made by Zimmerman in 1898. Dark dots at the cell surface represent cell junctions. (Zimmermann 1898)

# I. Cilia and flagella

---

Eukaryotic cells are highly structured and separated from their environment by a plasma membrane. The cytoplasm contains specialized organelles such as the nucleus surrounded by a double nuclear envelope, enclosing the genetic material organised in chromosomes. Each compartment or organelle is associated to particular biological processes like polymer degradation associated to lysosomes. Most cells from unicellular or multicellular eukaryotic organisms exhibit at their surface a complex organelle called cilium or flagellum (interchangeable terms). They share a common structure and are highly conserved throughout evolution. Nevertheless, each type of cilium presents variation in number, length, positioning and roles from one organism to the other, but also between different cell types in the same organism (Figure 1).

## 1) History

Cilia are the oldest known cellular organelles, first described in 1675 by Anthony van Leeuwenhoek, using homemade light microscopes to observe ciliary beating in protozoa. In 1786, Otto Muller proposed the term *cilium* to define this organelle and Dujardin introduced the term *flagellum* much later in 1841 (Muller 1786, Dujardin 1841). At that time, the use of two different terms was codified; the term “*flagellum*” was used for cells having one or few numbers of organelles and the term “*cilium*” at the opposite, was used when a cell exhibited many similar organelles. From the cilium discovery until the 19<sup>th</sup> century, the study of cilia was only focused on their motility that was a defining feature to identify them. During the second half the 19<sup>th</sup> century, Langerhans described a new class of non-motile cilia (Langerhans 1876). This type of cilia was first observed on a wide variety of epithelia in *Amphioxus* (Figure 2A). In mammalian cells, they were observed for the first time at the surface of rabbit and human epithelia by Zimmermann 22 years later (Figure 2B)

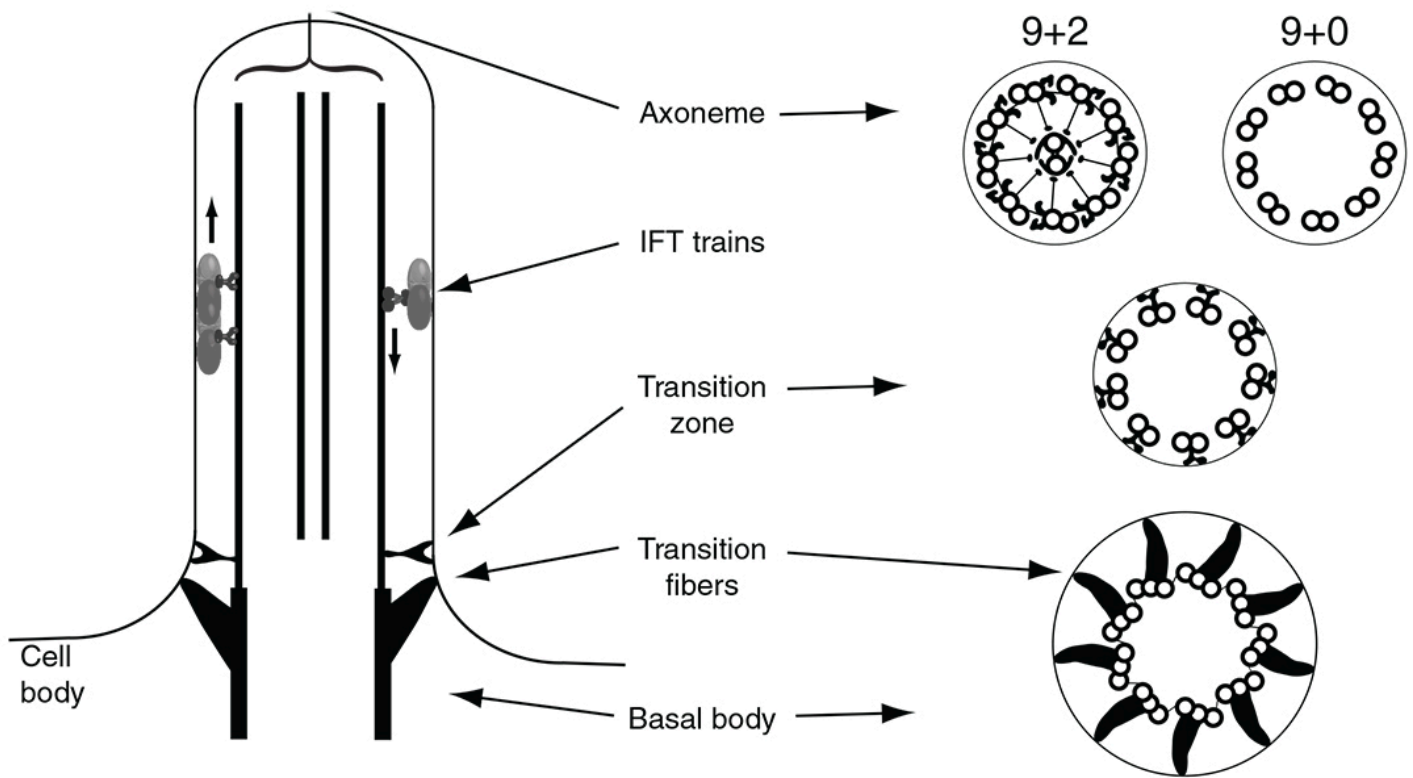


**Figure 3: Schema of the ciliary / flagellar structure.**

On the left is a longitudinal representation of the organelle. On the right are cross sections at different levels of the cilium / flagellum including the basal body, the transition zone and the axoneme. The two common configurations called “9+2” and “9+0” are represented. IFT: Intraflagellar transport (Brown and Witman 2014).

(Zimmermann 1898). He proposed the name of “central flagellum” and correctly predicted its sensory role. During the 20<sup>th</sup> century, Joseph hypothesized that cells with a “central flagellum” could represent a transition between non-ciliated cells and multi-ciliated cells (Joseph 1903). In 1968, the term “primary cilia” was proposed to refer to “the rudimentary or abortive cilia” which “ have only a transitory existence” (Sorokin 1968). More recently, this hypothesis was confirmed in mouse, where ependymal cells emerge with a primary cilium and become multi-ciliated cells during embryogenesis (Banizs, Pike et al. 2005). Once called the “forgotten organelles”, cilia are today a central interest for research due to their importance in many sensory and developmental processes. Moreover, disorders in cilia assembly and / or functions can cause a wide array of pathologies called ciliopathies. Understanding the exact aetiology of these diseases is now a major interest for a growing scientific community.

## **2) The structure of cilia and flagella**

Most cilia and flagella share a common architecture conserved throughout evolution. It contains three different structural regions from the base to the tip of the organelle: the basal body, the transition zone and the axoneme (Figure 3). Cilia and flagella can be separated in two major categories: motile and non-motile. Both show the basic axonemal structure composed of nine microtubule doublets. In motile cilia the axoneme is organized following a “9+2” conformation: nine microtubule doublets associated to dynein arms (essential for ciliary beating) surround a central pair of single microtubules (Figure 3). On the contrary, non-motile cilia possess a “9+0” structure where the central pair and the dynein arms are absent (Figure 3). The cilium possesses a specific membrane surrounding the axoneme and, in some specific cases, extra-axonemal structures.

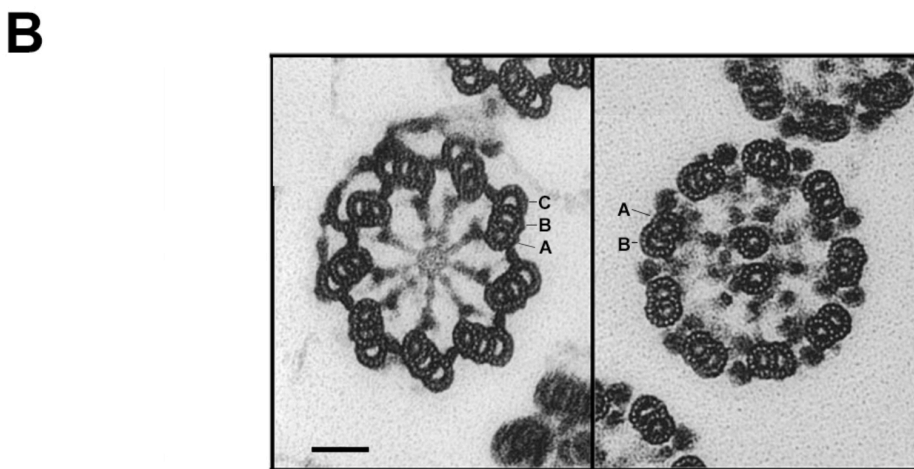
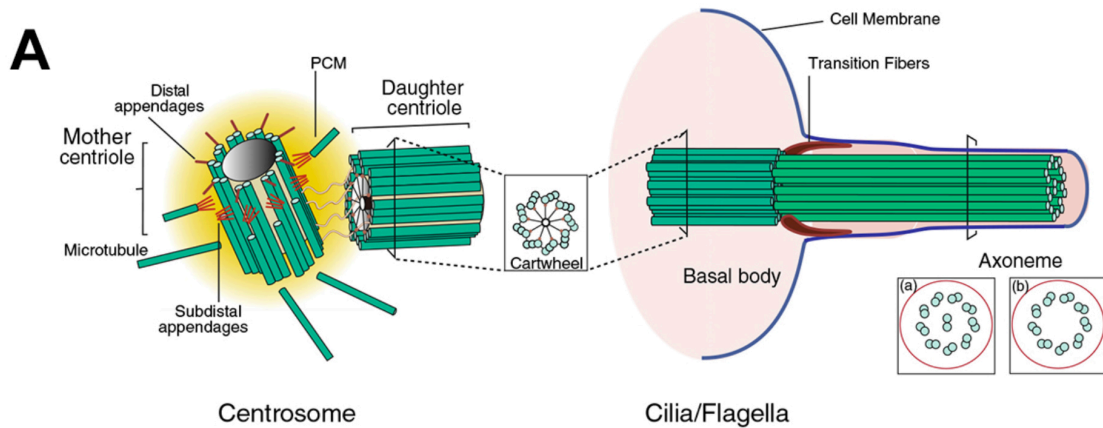


**Figure 4: Centrosomes and basal body structure.**

**(A)** A centriole is the main structural constituent of centrosomes or basal bodies when it is anchored at the membrane. The canonical centriole has nine microtubule triplets. Each centrosome is composed of a mother and a daughter centriole presenting an orthogonal configuration and surrounded by the pericentriolar material (PCM). The basal body anchors the cilium to the cellular membrane. (a) and (b) boxes showing respectively the structure of “9+2” and “9+0” axoneme (Bettencourt-Dias 2013). **(B)** Electron microscopy images of a cross section through the basal body and the axoneme of *Chlamydomonas*. The name of each microtubule of a triplet basal body and of a doublet axoneme is indicated in these images. Scale bar: 0.95  $\mu\text{m}$ . (Linck and Stephens 2007)

### a) Basal bodies and centrioles

Basal bodies and centrioles are large, evolutionary conserved organelles; that display nine triplets of microtubules organised in a 9-fold symmetry determined by the cartwheel (Figure 4A). This scaffold appears at the initial step of centriole assembly and is composed of a core from which irradiate 9 spokes. Each triplet is composed of a complete A tubule made of 13 protofilaments, fused with the incomplete B tubule (11 protofilaments), the latter being associated with the incomplete C tubule also built with 11 protofilaments (Figure 4B, left panel). Some exceptions have been described such as in *Drosophila melanogaster* embryos where basal bodies present 9 doublets instead of triplets (Callaini, Whitfield et al. 1997). The A and B tubules of the basal body extend into the axonemal part whereas the C tubule stops before the transition zone (Figure 4B, right panel). The distal end of the basal body is anchored to the cell membrane thanks to transition fibers. The transition fibers contribute to the separation of the flagellar compartment from the rest of the cell, as electron microscopy pictures from various cell types show that the inter-fibre spaces are too small to allow vesicle trafficking (Reiter, Blacque et al. 2012, Garcia-Gonzalo and Reiter 2017). The flagellum base forms a flagellar pore complex (FPC) thought to be related to the nuclear pore complex (NPC) enabling a selective entry inside the flagellar compartment (Rosenbaum and Witman 2002, Dishinger, Kee et al. 2010, Kee, Dishinger et al. 2012).

The centrosome is composed of usually two perpendicular centrioles surrounded by a peri-centriolar material (PCM) made of proteins essential for microtubule nucleation and anchoring such as  $\gamma$ -tubulin or pericentrin. The mature, appendage-bearing centrosome is called the mother centriole and the immature; often shorter is named the daughter centriole (Figure 4A) (Chretien, Buendia et al. 1997). The centrosome is the microtubule-organizing center in most animal cells where it is essential for mitosis. In its absence, chromosomes alone fail to organize a bipolar spindle and kinetochore microtubules (Sluder and Rieder 1985). The basal body has the ability to nucleate the polymerisation of the axoneme into cilia and flagella (Figure 4A). Basal bodies and centrioles are related functionally, as illustrated by one centriole of the

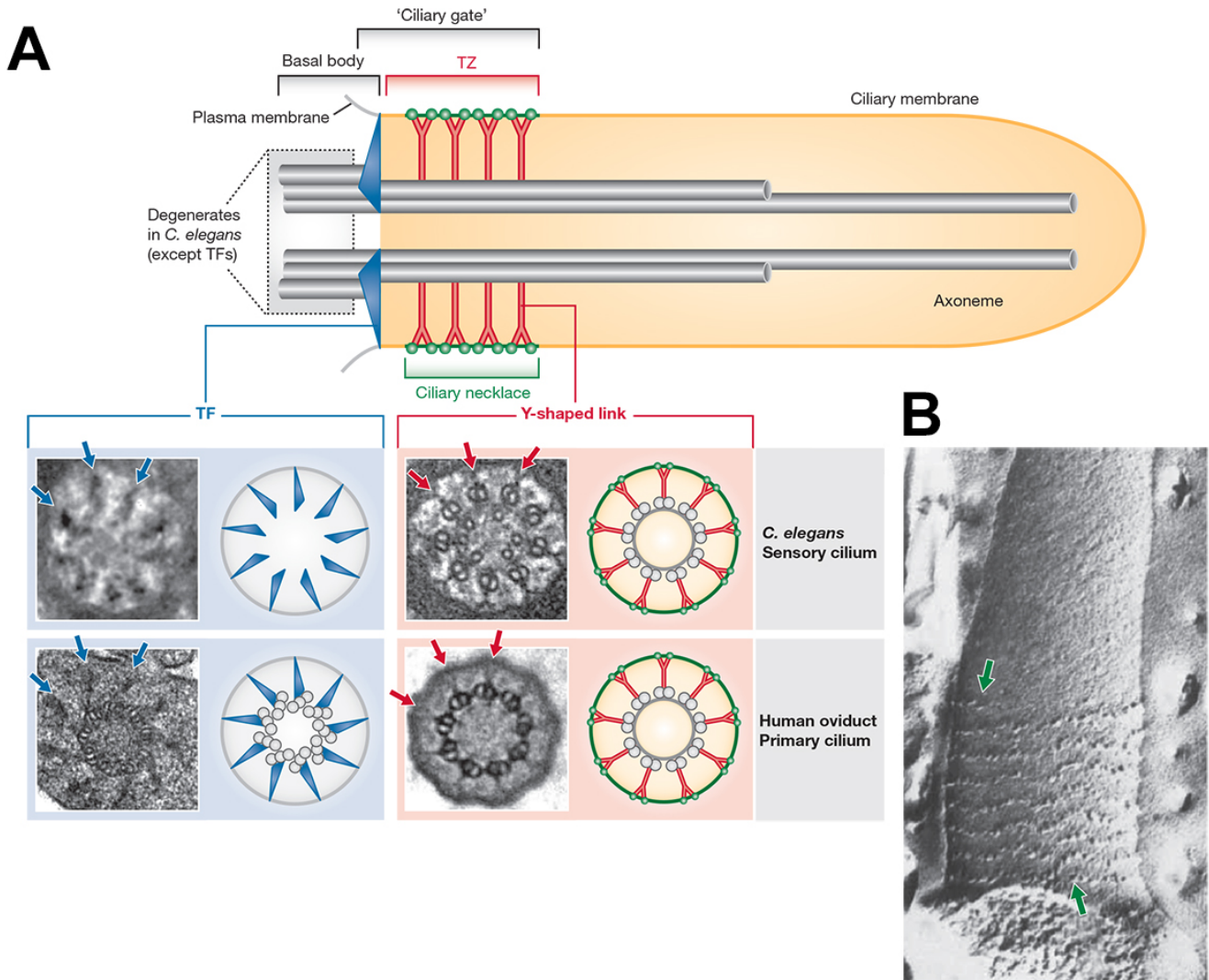


**Figure 5: The transition zone.**

**(A)** Schematic representation of the transition zone (TZ). The transition zone is defined by the transition fibers (TF) that link the basal body to the membrane, the Y-links and the ciliary neck. Cross-sections of the transition fibers (blue arrows) and Y-links (red arrows) from *C. elegans* sensory cilium and human oviduct primary cilium. **(B)** Ciliary neck from a hamster respiratory cilium visualized by freeze fracture scanning electron microscopy indicated by the green arrows (Reiter, Blacque et al. 2012).

centrosome becoming basal body during ciliogenesis in animal cells. This is also found in other organisms such as *Chlamydomonas*. Once the flagella are removed, basal bodies are transformed into centrioles, migrate at the nucleus periphery and drive mitosis by nucleating the spindle (Cavalier-Smith 1974). By contrast, most protists like *Paramecium* maintain their cilia with the basal bodies anchored to the membrane during all the cell cycle. In this context, the basal body is not used as a centriole but is only dedicated to axoneme assembly.

### **b) The transition zone**

The transition zone ensures the separation between the cytoplasm and the ciliary compartment. At the base of the transition zone, electron-dense appendages called transition fibres connect the basal body to the membrane (Figure 5A) (Garcia-Gonzalo and Reiter 2017). The nine transition fibres emerge from the distal portion of the basal body and end as electron-dense buttons on the ciliary membrane (Ringo 1967). At an early stage of ciliogenesis, the transition zone is formed and anchors the basal body to the plasma membrane. Cross-sections of the transition zone show a 60nm space between each transition fibre, and it has been proposed that this space could act as a gateway for the cilium (Nachury, Seeley et al. 2010). Transition fibres are composed of at least of five proteins, including CEP83 (CEntrosomal Protein 83) and Sclt1 (Sodium channel and clathrin linker 1) that are both important for the correct localization of the other transition fibre proteins (Tanos, Yang et al. 2013) but their exact spatial distribution remains to be determined. The proteins ODF2 (Outer dense fibre 2) and CEP164 (CEntrosomal Protein 164) are also localized in the transition fibres. These two proteins are required for the proper anchoring of the basal body to the cell membrane in mice and human, hence for ciliogenesis (Ishikawa, Kubo et al. 2005, Graser, Stierhof et al. 2007). Depending of the ciliary type, the transition zone measures 0.1µm to 1µm from the basal body to the basal plate, the structure allowing the nucleation of the central pair microtubules in motile cilia ("9+2"). In each of the nine triplets, only two microtubules (A and B) further elongate to form the transition zone that is therefore composed of nine doublets of

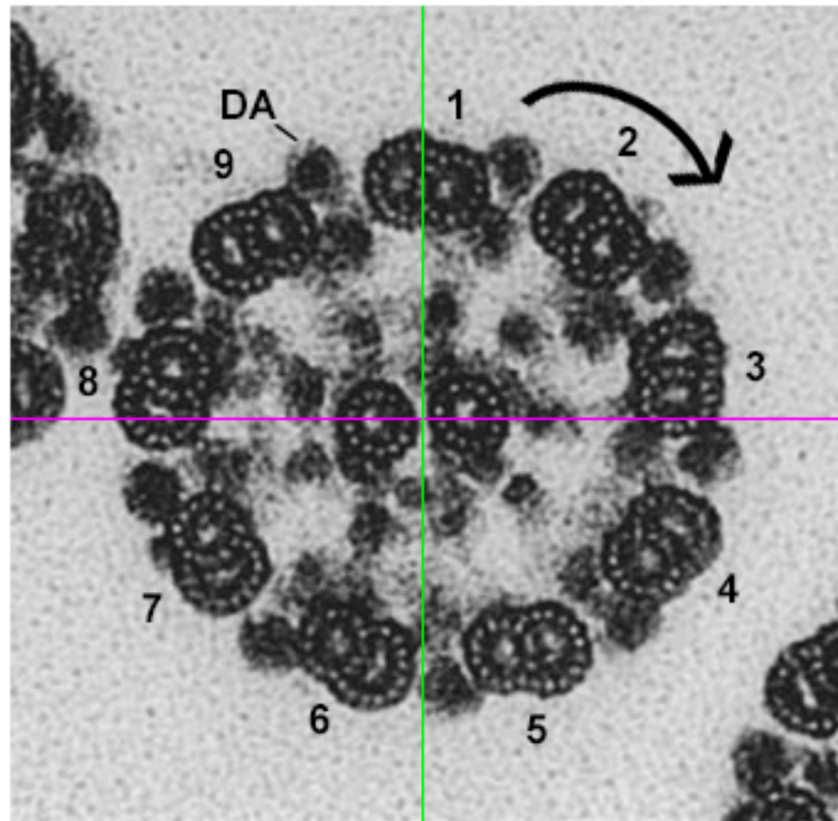


**Figure 6: Determination of doublet orientation.**

The pink line crosses the central pair and the green line is drawn perpendicularly the first one and crossing between microtubules of the central pair. The only doublet crossed by this line (green), defined as doublet 1. In this electron microscopy section, dynein arms are in clockwise orientation, so doublet 2 is at the right of the doublet 1. DA: Dynein arms. Electron microscopy images of a cross section through the axoneme of *Chlamydomonas*. Adapted to (Linck and Stephens 2007).

microtubules. The interface between each tubule doublet is connected to the ciliary membrane by unique structures called Y-links (Figure 5A) (Gilula 1972). Freeze fracture revealed that the ciliary membrane of the transition zone is decorated with intra-membrane particles forming the ciliary necklace (Figure 5B) (Gilula 1972). CEP290 is the only protein known to localize in the Y-links of *Chlamydomonas*, but this protein is also predicted to be associated to the cylinder microtubule shaft of the transition zone in mammals and in *C. elegans* revealing the occurrence of species-specific adaptations (Craigie, Tsao et al. 2010, Yang, Su et al. 2015). Of note, other proteins such as the Nephrocystin NPHP1 or some trans-membrane proteins such as MKS-2 (Meckel-Gruber syndrome) present a periodic pattern similar to that of the ciliary necklace or the Y-links (Lambacher, Bruel et al. 2016).

### c) The axoneme

In continuity with the transition zone, the axoneme constitutes the main core of cilia and flagella. Its ultrastructure has been well described by classical electron microscopy studies as well as cryo-tomography (Fawcett 1975, Nicastro, McIntosh et al. 2005). The axoneme is made of nine parallel microtubule doublets, which are composed of  $\alpha$ - $\beta$  tubulin heterodimers as in cytoskeletal microtubules. The doublets are disposed at regular intervals and their (+) end is located at the tip of the flagellum. Each doublet consists of one A-tubule, made with 13 protofilaments fused with one incomplete B-tubule composed of 11 protofilaments (Figure 4B). The orientation of the axoneme has been established by using the central pair and the dynein arms as referential cues. First, a line is drawn crossing through the central pair (Figure 6). A second line is drawn perpendicularly to the first one and crossing in between the two microtubules of the central pair. Only one doublet can be crossed by it and it is defined as doublet 1. Second the visualization of dynein arms allows determining the flagellum orientation: if the dynein arms are in clockwise orientation, the doublet 2 will be on the right side of the doublet 1. By knowing the relative position of the basal body and the flagellum tip, flagellum orientation can be determined. Indeed from the base to the tip, the dynein arms are always in clockwise

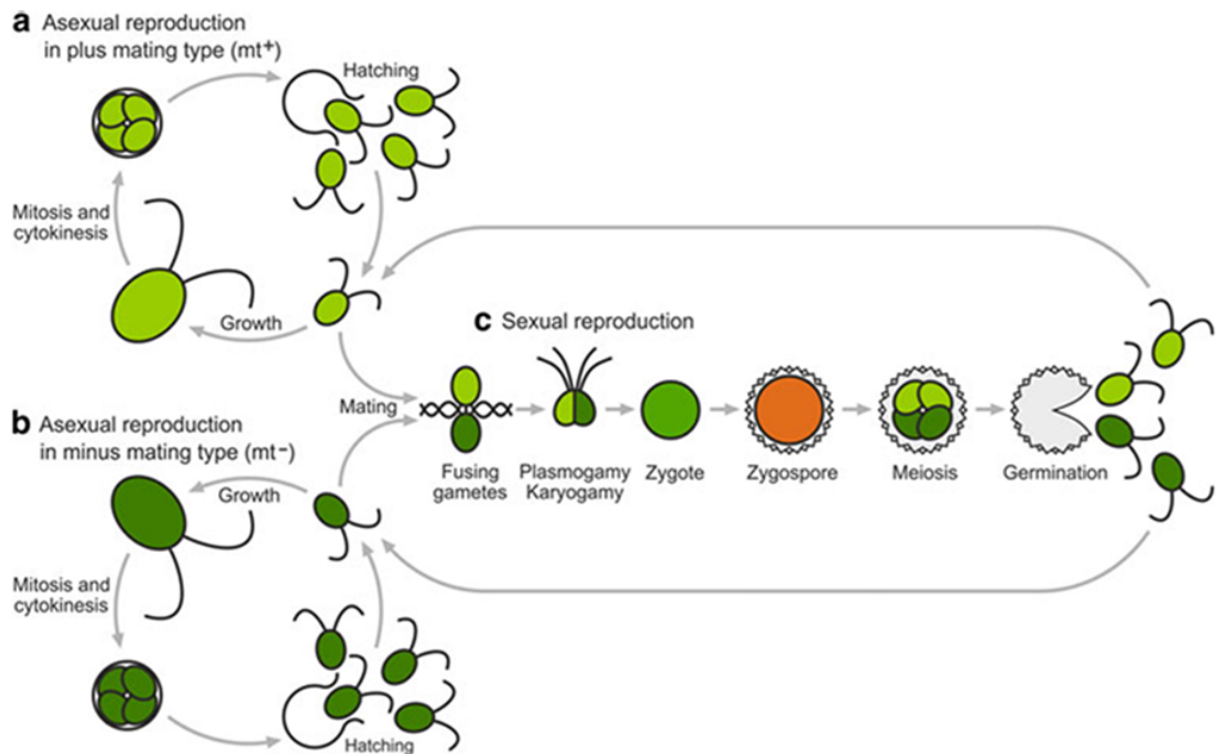


**Figure 7: Asexual and sexual reproduction in *Chlamydomonas*: importance of the flagellar membrane.**

Schematic representation of the *Chlamydomonas* reproductive cycles. When gametes of opposite mating types ( $mt^+$  (a) and  $mt^-$  (b)) are mixed for sexual reproduction (c), flagellar adhesion is characterized by membrane-membrane contacts and is followed by gamete activation. Membrane-membrane is possible thanks to a set of agglutinins that are trans-membrane flagellar proteins (Hallmann 2011).

orientation. This aspect will be essential to orientate flagella in 3D electron microscopy.

### d) The membrane of cilia and flagella

The axoneme is wrapped by the ciliary membrane that is an extension of the plasma membrane with a unique set of proteins and lipids. It can be enriched in trans-membrane receptors involved in transduction of various extra-cellular signals.

In *T. brucei*, a recent study based on mass spectrometry analysis of purified flagella showed an enrichment of raft-forming phospholipids in the flagellum membrane as compared to whole cell (Serricchio, Schmid et al. 2015). These candidate lipid rafts could have a major role in protein localization and trafficking (Tyler, Fridberg et al. 2009), and might be essential for several signalling cascades. Indeed, a recent lipid raft proteomic analysis revealed an enrichment in calpains that are proteins proposed to detect external  $Ca^{2+}$  concentration and could be associated to signalling functions (Sharma, Olson et al. 2017). Cilia can also be involved in adhesion function and the membrane is a key player in this phenomenon. For example, during the sexual cycle of *Chlamydomonas*, gametes of opposite mating types ( $mt^+$  and  $mt^-$ ) get in contact via their flagella that adhere thanks to trans-membrane agglutinins. This interaction activates a signalling pathways required for gamete fusion (Figure 7) (Goodenough 1989, Pan 2002).

One major question concerns the transport of membrane proteins from the cell body to the ciliary compartment. A study in rat trachea showed that the ciliary necklace region is depleted of filipin-sterol complexes (Montesano 1979). It has been demonstrated that filipin binds specifically to cholesterol in cell membrane meaning that the ciliary necklace contains little or no cholesterol (de Kruijff and Demel 1974). Cholesterol contributes to the fluidity of the cell membranes and its absence in the ciliary necklace is thought to act as a diffusion barrier and as it can restrict the exit of ciliary membrane components and prevent mixing between two compartments (Montesano 1979, Rohatgi and Snell 2010). One model proposes that proteins targeted to the ciliary membrane are transported on vesicles from the Golgi to the

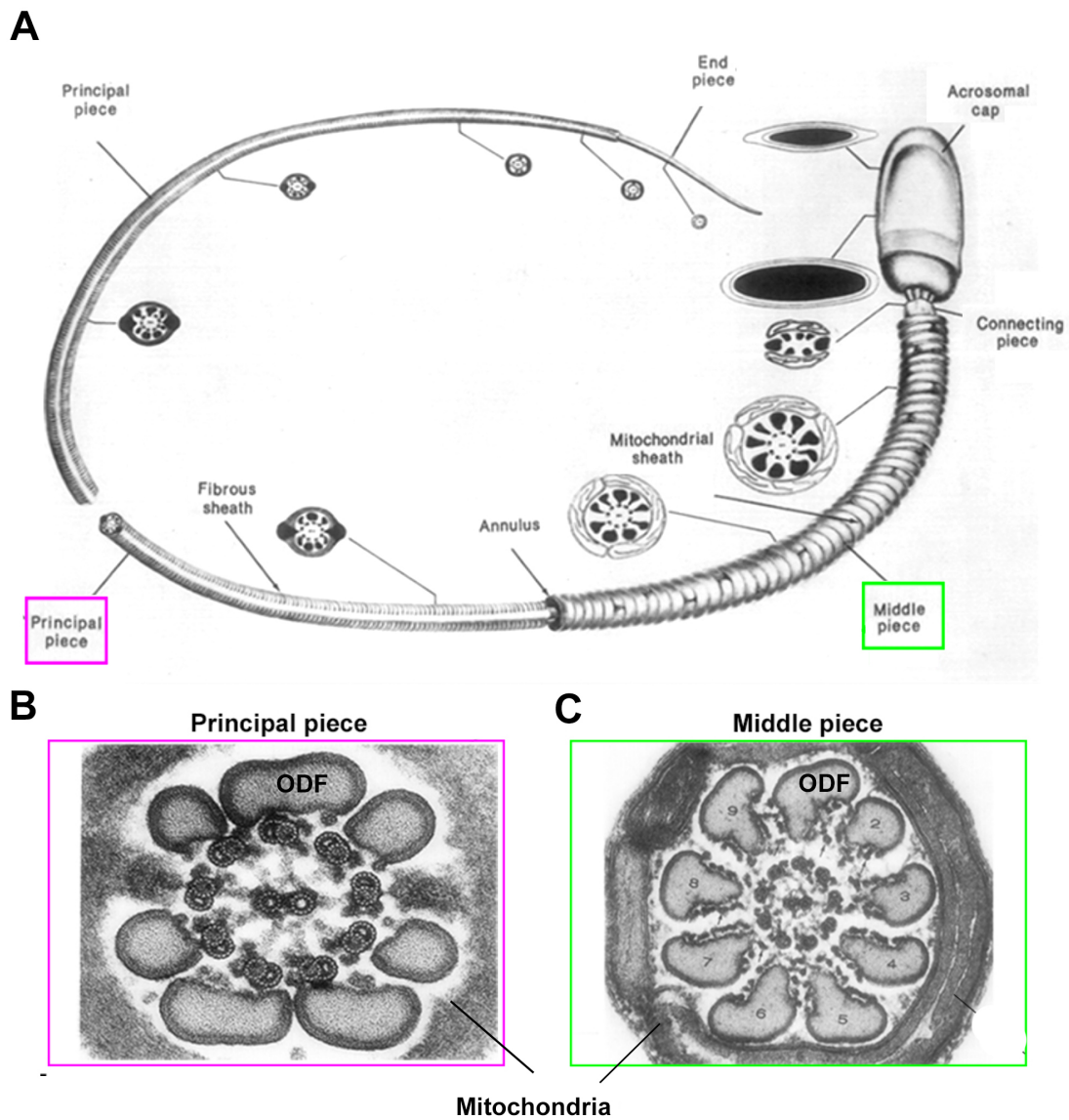


**Figure 8: Extra-axonemal structures in spermatozoa.**

**(A)** Carbon of the mammalian spermatozoa. In the middle piece, each doublet is attached to a row of dense fibers and mitochondria, visible on the right cross section of a guinea pig sperm cell **(B)**. In the principal piece, a fibrous sheath surrounds the axoneme, visualized in the left cross section **(C)**. ODF: Outer dense fibers (Fawcett 1975).

base of the cilium as shown for opsin in photoreceptors (David Papermasrer 1985). Proteins need to enter through the transition zone gateway and then can be transported or either diffuse in the ciliary compartment. Another model proposes that the proteins from the plasma membrane can move laterally and enter in the cilium compartment. This phenomenon has been shown for the agglutinins that access the ciliary membrane from the plasma membrane during *Chlamydomonas* adhesion (Hunnicuttt 1990). In mammalian cells, an elegant microscopy-based pulse-chase approach revealed the lateral transport of the Hedgehog (Hh) pathway protein Smoothened (Smo) from the plasma membrane to the ciliary membrane (Milenkovic, Scott et al. 2009).

### e) Extra-axonemal structures

In some specific cell types, such as spermatozoa or protists, supplementary structures are associated with the axoneme. For example, the axoneme of the human spermatozoa is divided in three main regions: the middle, principal and end pieces (Figure 8A Top panel) (Fawcett 1975). In the middle piece, an outer dense fibre is linked to each outer microtubule doublet of the axoneme. Moreover, a large number of mitochondria and the outer dense fibre surrounding the axoneme provide the ATP necessary for flagellum beating (Figure 8C). The axoneme of the principal piece of the sperm tail is surrounded by a fibrous sheath (Figure 8B). The later could be involved in enzyme regulation and notably glycolytic enzymes that are probably essential for producing energy for sperm swimming (Miki, Qu et al. 2004). Extra-axonemal structures are also found in many protists. *Giardia intestinalis*, a parasite pathogen of mammals, possesses four pairs of flagella termed anterior, posterior lateral, ventral and caudal flagella, each with specific localization, structure and functions (Figure 9A). The proximal part of each axoneme is localized in the cytoplasm and not surrounded by any membrane but it is associated with extra-axonemal structures (Figure 9B) (Friend 1966, Elmendorf, Dawson et al. 2003). These extra-axonemal structures confer a unique structural identity to each flagellar pair. For example, two distinguish structures are associated with the anterior flagella

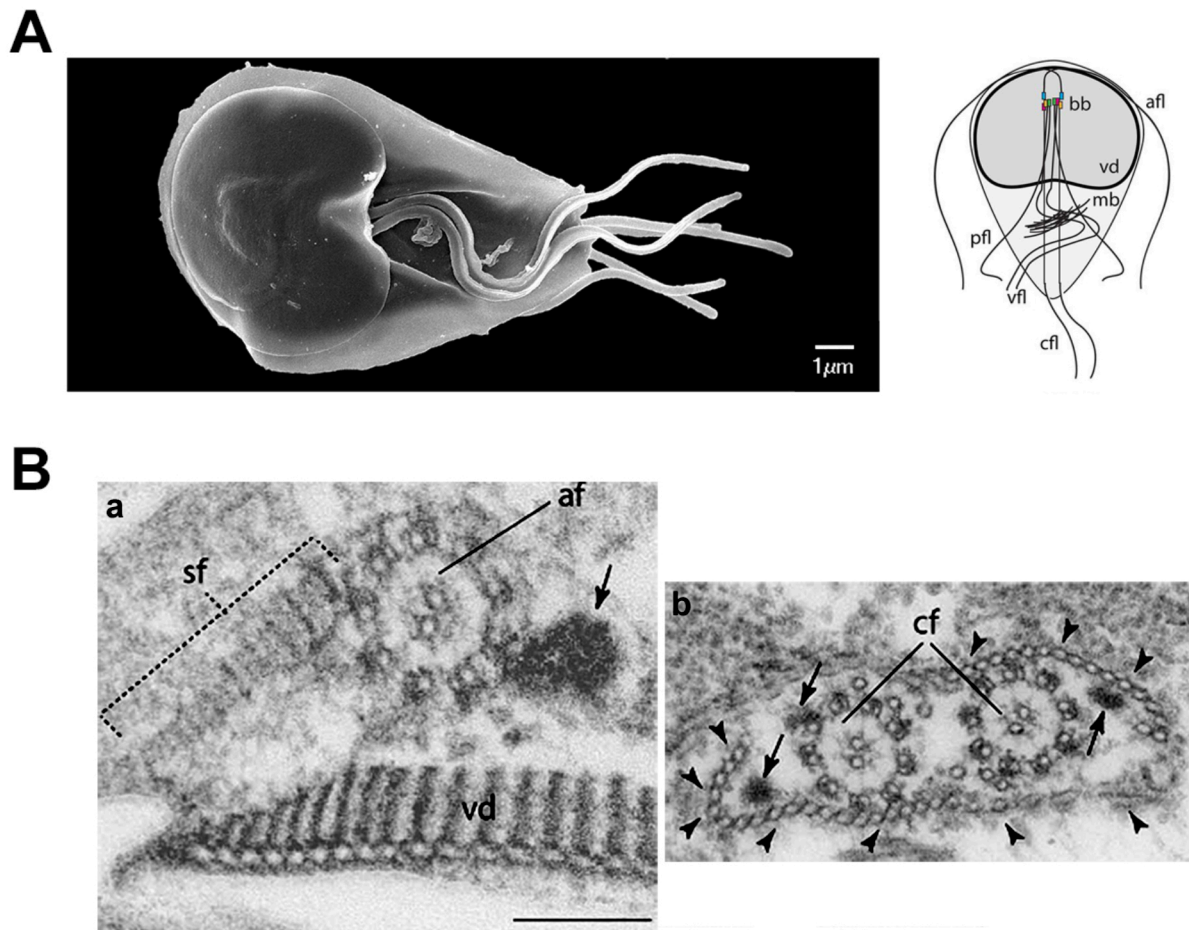


**Figure 9: Extra-axonemal structures in *Giardia intestinalis*.**

**(A)** Scanning electron micrograph of *Giardia intestinalis* parasite (T.Blisnick) and a schematic representation of *Giardia lamblia*. bb: basal body, afl: anterior flagella, cfl: caudal flagella, pfl: posterior-lateral flagella, vfl: ventral flagella, vd: ventral disc and mb: median body (McInally and Dawson 2016). **(B)** Transmission electron microscopy (TEM) image of the anterior flagella (af) of *Giardia intestinalis* with the classical “9+2” organization, with some striated fibers (sf) and dense rod pointed by the arrow (Left image) (vd: ventral disk). On the right transversal section, the additional array of microtubules (arrowheads) surrounding the caudal flagella (cf) of *Giardia intestinalis* is visible, as well as some dense rods (arrows) (b). Scale bar: 0.2 μm. (Elmendorf, Dawson et al. 2003).

(Friend 1966). The first structure corresponds to the “dense rods”, located just below the axoneme and the second one is a system of striated filaments found in the upper portion of the flagellum (Figure 9Ba). It was proposed that these filaments help the motility and behaviour of the anterior flagella (Maia-Brigagao, Gadelha et al. 2013). On caudal flagella, there is the “caudal complex” or “funis” that surround and extend the axoneme (Figure 9Bb) (Filice 1952, Benchimol, Piva et al. 2004). Based on several ultra-structural studies, it was shown that the “funis” is composed of microtubule sheets that fan out laterally at the emergence of the caudal axonemes. The “funis” has no known function, yet has been suggested to have a structural role in maintaining the *Giardia* cell shape (Benchimol, Piva et al. 2004).

### 3) Different types of cilia and flagella

#### 1) The motile “9+2” cilia and flagella

The typical motile “9+2” cilia are characterised by the presence of inner dynein arms (IDAs) and outer dynein arms (ODAs) that are attached at a precise positions of the A-tubule of the axoneme. Axonemal dyneins are multi-subunit complexes, composed of a variable number of dynein light, intermediate and heavy chains (Figure 10) (DiBella, Sakato et al. 2004). In ODA and IDA complexes, the dynein heavy chain possesses ATPase and molecular-motor activities that are necessary to generate ciliary beating. Using ATP as an energy source, the dynein arms present on the A-tubule of any doublet create a force against the B-tubule of the adjacent doublet, inducing the sliding of the adjacent microtubule doublets (Porter and Sale 2000, Satir and Christensen 2007). Because the nexin / DRC complex links connect microtubule doublets to each other and the microtubule are attached at the basal body, the inter-doublet sliding results into flagellar bending.

The “9+2” cilium possesses a central pair of microtubules. The later emerges from the basal plate (a region lying above the transition zone) and extends to the distal tip of the cilium. The central pair is formed by two singlet microtubules called C1 and C2,

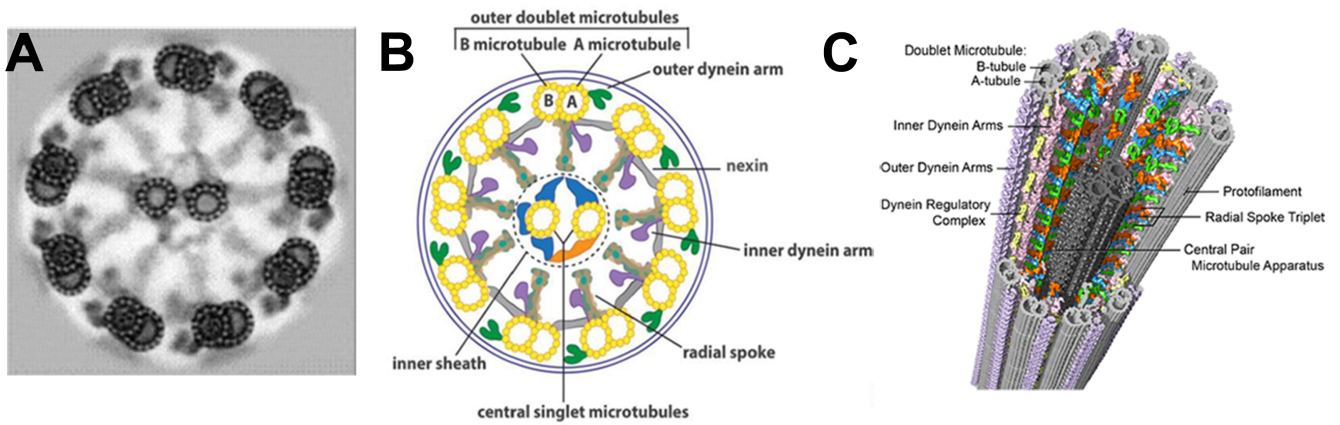


**Figure 10: The axoneme.**

(A) Computer averaging of TEM micrographs of cross-sectioned axonemes from human sperm showing the classic “9+2” axoneme structure. Only the axoneme portion is shown (Afzelius 2004). (B) Corresponding cross-section schematic illustration of the classic “9+2” axoneme, with the nine peripheral doublet microtubules surrounding the central pair (Bustamante-Marin and Ostrowski 2017). (C) A three-dimensional representation of a “9+2” axoneme (from sea urchin sperm flagellum) obtained after cryo-electron tomography analysis. Adapted from (Linck, Chemes et al. 2016).

that are structurally and biochemically distinct (Porter and Sale 2000). They are connected to each other by a protein bridge and surrounded by a unique set of accessory proteins that facilitate the contact with radial spokes (Figure 10B and C). The later are T-shape structure composed of (1) an elongated stem that is attached to the A-tubules of peripheral doublets and (2) a head that could contact the central pair and its associated projections (Warner and Satir 1974, Goodenough and Heuser 1985). The radial spokes are made of at least 23 distinct proteins, termed radial spoke proteins (RSP) that are conserved throughout evolution in organisms with motile cilia (Yang, Diener et al. 2006).

Motile flagella can be found at the surface of multiple protists where they are responsible for cell motility. In mammals this is the case of spermatozoa that use their flagellum to propel themselves through the female reproductive tract. “9+2” motile cilia line the surface of the respiratory epithelium and brain ventricles, where they produce and maintain the movement of the surrounding fluids. The fallopian tube epithelium is made with two major cell types: the secretory and ciliated cells. After ovulation, the ciliary beating is essential for the ovum transport from the ovary to the uterus.

## **2) The immotile “9+0” cilia and flagella**

Immotile “9+0” cilia are defined by the absence of a central pair of microtubules, of radial spokes and both types of dynein arms (ODAs and IDAs). The “9+0” cilia are found at the surface of most mammalian cells and are also called primary cilia. Primary cilia are involved in sensory functions such as the detection of flow sensing at the surface of the epithelial cells of kidney tubules (Praetorius and Spring 2003). One of the best-known “9+0” cilium is found in photoreceptors in the retina where they contribute to light detection (Figure 13B). The rod and cone photoreceptors are found on the outermost layer of the retina; they have both the same basic structure. Photoreceptors can be divided in four main regions from the visual field in the eye to the brain tissues: the axon termination that releases neurotransmitters, the cell body that contains the nucleus and the cell organelles, the inner segment full of

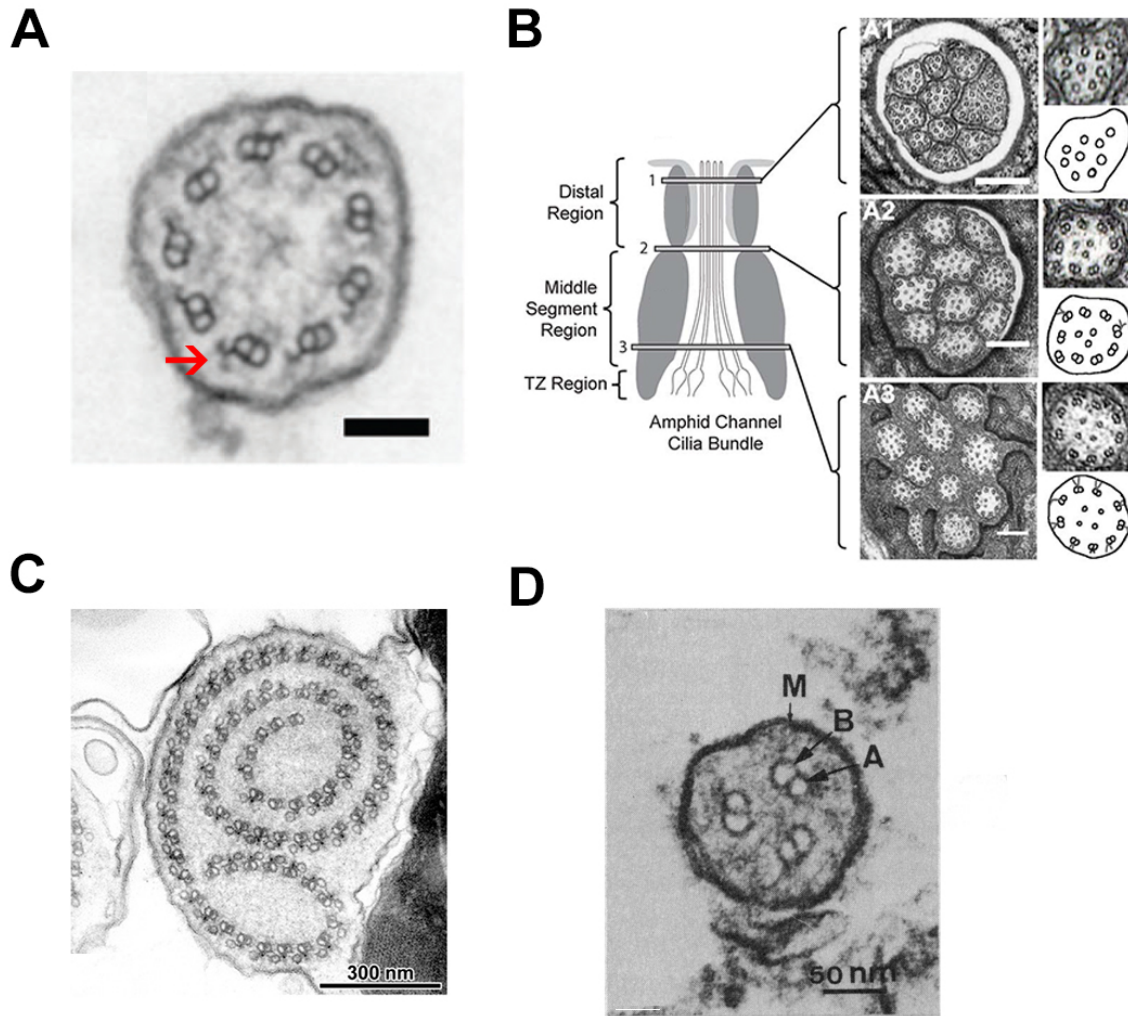


### Figure 11: Other types of axonemes.

(A) Typical nodal cilium of mice in the “9+0” conformation bearing dynein arms (red arrow). Scale bar: 50 nm (Odate, Takeda et al. 2016). (B) *C. elegans* cilia ultrastructure. Cross sections of the different regions of the amphid channel containing sensory cilia showing the different architecture. (A1) Distal microtubule singlets are devoid of B-tubule. Microtubule doublets containing B-tubule are present in (A2) and (A3), and additional singlet microtubules are present in the lumen of these two later regions. TZ: transition zone Scale bar: 250nm (Warburton-Pitt, Silva et al. 2014). (C) Cross-section of *Sciara coprophila* sperm cell axoneme consisting of microtubule doublets and accessory microtubules disposed in a spiral arrangement (Dallai, Lupetti et al. 2006). (D) Cross section of the flagellum of the male gamete of *Diplauxis hattii* presenting a “3+0” organisation. A: A-tubule B: B-tubule M: Membrane (Prensier, Vivier et al. 1980).

mitochondria and the outer segment. A connecting cilium is present between the inner segment and the outer segment. The latter contains stacks of membrane with membrane-associated molecules (opsin and rhodopsin) capable of transducing information coded by light energy into a specific neuronal electro-chemical activity that can be processed by neurons (Calvert, Strissel et al. 2006).

### 3) Other types of cilia and flagella

Some noticeable exceptions to the general patterns of motile or immotile cilia detailed in the previous sections have been described in various organisms. For instance, “9+0” cilia of embryonic node cells possess outer-dynein arms and are capable to generate a rotational movement to produce the leftward fluid flow necessary to initiate left-right asymmetry (Nonaka, Tanaka et al. 1998) (Figure 11A). At the periphery of the node, some classical non-motile “9+0” cilia can detect this flow and activate a  $\text{Ca}^{2+}$  dependent pathway. This pathway is only activated in the cells situated on the left side of the embryo and is essential to determine the left-right axis (Nonaka, Tanaka et al. 1998, McGrath, Somlo et al. 2003).

The nervous system of the nematode *C. elegans* is made of 302 neurons among which 60 possess cilia at the ends of their dendrites. All these sensory cilia are immotile with an axoneme separated in three distinct regions: a transition zone, a middle segment and a distal segment. The middle segment is made of nine microtubule doublets that surround a few central singlets and the distal segment is only made of microtubule singlets (Figure 11B).

The flagella of some insect spermatozoa do not possess a central pair and can present a “12+0” or a “14+0” architecture and in general they are immotile (Baccetti 1986). Even more spectacular is the axoneme of the sperm flagellum of the fly *Sciara coprophilia* made of 70 microtubule doublets each being associated to a peripheral singlet tubule (Figure 11C) (Phillips 1966). Smaller microtubule combinations are encountered in the male gametes of the gregarines *Lecudina tuzetae* and *Diplauxis hattii* that possess axonemes with respectively “6+0” and “3+0” architecture (Figure 11D) (Schrevel and Besse 1975, Prensier, Vivier et al. 1980).

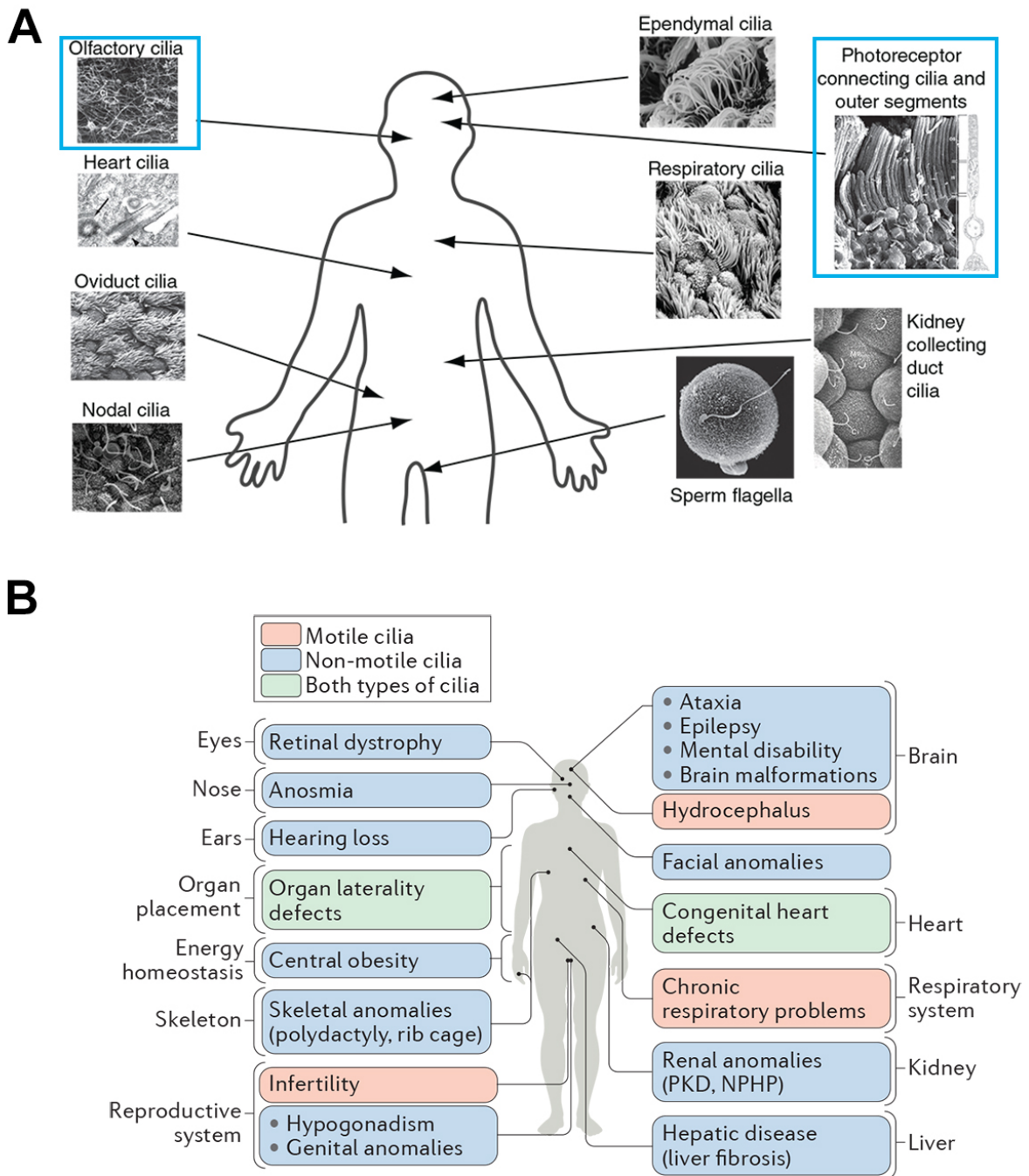


**Figure 12: Cilia and ciliopathies.**

**(A)** Schematic representation of the localization of some cilia dedicated to sensing (framed in blue) and motile cilia in the human body observed by SEM (Brown and Witman 2014). **(B)** Cartoon showing the different organs or tissues that are affected in diverse ciliopathies, and the main disease phenotypes for each organ. Ciliopathies that are caused by defects in motile cilia are highlighted in orange, those that result from defects in non-motile cilia in blue and those associated with defects in both types of cilia in green. NPHP, nephronophthisis; PKD, polycystic kidney disease. (Reiter and Leroux 2017)

## **4) Ciliopathies**

Ciliopathies are a group of genetic diseases caused by defects in ciliary assembly and / or functions that affect 1 in 400 births (Reiter and Leroux 2017). In humans, a large diversity of cells possesses one or more cilia. Motile cilia are found at the surface of several epithelia such as in the respiratory tract, where they sweep mucus (Figure 12A). The beating of sperm flagella is essential for the male gamete to migrate in the female sexual tract and fertilize the ovum. Immotile cilia are generally associated to sensory functions such as those found in the odorant receptors in the dendritic knob of the olfactory neurons (Figure 12A). In case of a defect associated to ciliogenesis, many organs can be affected resulting in several disorders induced by a single underlying cause (Cf next session). Dysfunctions in motile cilia induce primary ciliary dyskinesia, while defects in sensory cilia are responsible for a diversity of diseases such as polycystic kidney, retinal degeneration, Bardet-Biel or Alstrom syndromes (Figure 12B) (Reiter and Leroux 2017). Here, I will briefly describe three examples of ciliopathies.

### **a) Primary ciliary dyskinesia**

The first ciliopathy that have been identified is “immotile cilia symptom” or primary ciliary dyskinesia (PCD) that is caused by genetic abnormalities impacting motile cilia (Afzelius 1976). This is an autosomal recessive disorder with genetically heterogeneous manifestations. PCD roughly affects 1 in every 20-60 000 individuals in the United States, although this may be an underestimate in general population because diagnosis relies on a difficult combination of cilia structure analysis by electron microscopy and genetic analysis (Zariwala, Knowles et al. 2007). So far, mutations in more than > 30 genes have been associated with this disease (Reiter and Leroux 2017). Most of them encode for proteins directly involved in cilia motility such as components of the outer dynein arms, the radial spokes and the nexin links (Figure 13A) (Chilvers 2003). Patients with PCD frequently present chronic bronchitis



due to a dysfunction of their cilia involved in mucus clearance. Male patients are usually infertile because of reduced motility of their sperm flagellum. Moreover in female patients defects in the beating of cilia in the epithelium of the Fallopian tubes can also induce infertility due to problems in ovum migration from the ovary to the uterus. In addition, half of the patients present a *situs inversus*, a spectacular phenotype in which the position of the heart and other internal organs are reversed during embryonic development. This symptom is due to impaired motility of nodal cilia that initiate left-right asymmetry in early embryo (See previous section). More rarely, patients with PCD present *hydrocephalus* symptoms (an abnormal intracranial accumulation of cerebrospinal fluid) that could be caused by the defective motility of the ependymal “9+2” cilia (Lee 2013). Although it is a rare human symptom, *hydrocephalus* is a common manifestation of the disease in mice, suggesting that distinct genetic mechanisms underlie the differences in the development and physiology of human and mouse brains (Lee 2013).

### **b) Polycystic kidney disease**

Polycystic kidney disease (PKD) is the most common disease caused by sensory cilia dysfunctions (frequency 1: 1 000) and more generally one of the most life threatening inherited diseases, affecting 12.5 million people worldwide (Brown and Witman 2014). Two different types of PKD have been identified: autosomal dominant PKD (ADPKD) that mostly affects adults and the autosomal recessive PKD (ARPKD) occurring in neonates and children. Both types of PKD are characterized by an excessive proliferation of the kidney epithelial cells, ultimately leading to a massive organ enlargement and a loss of function. The first connection between PKD and cilia came from studying cilia in *C. elegans* where two homologues of human polycystin-1 (PC1) and polycystin-2 (PC2) (mutated in most cases of ADPKD) were detected in sensory cilia involved in mating behaviour (Barr and Sternberg 1999). PC1 and PC2 are two trans-membrane proteins that can interact to form a complex. The PC1/PC2 complex may function as a receptor-ion channel with PC1 transducing environmental

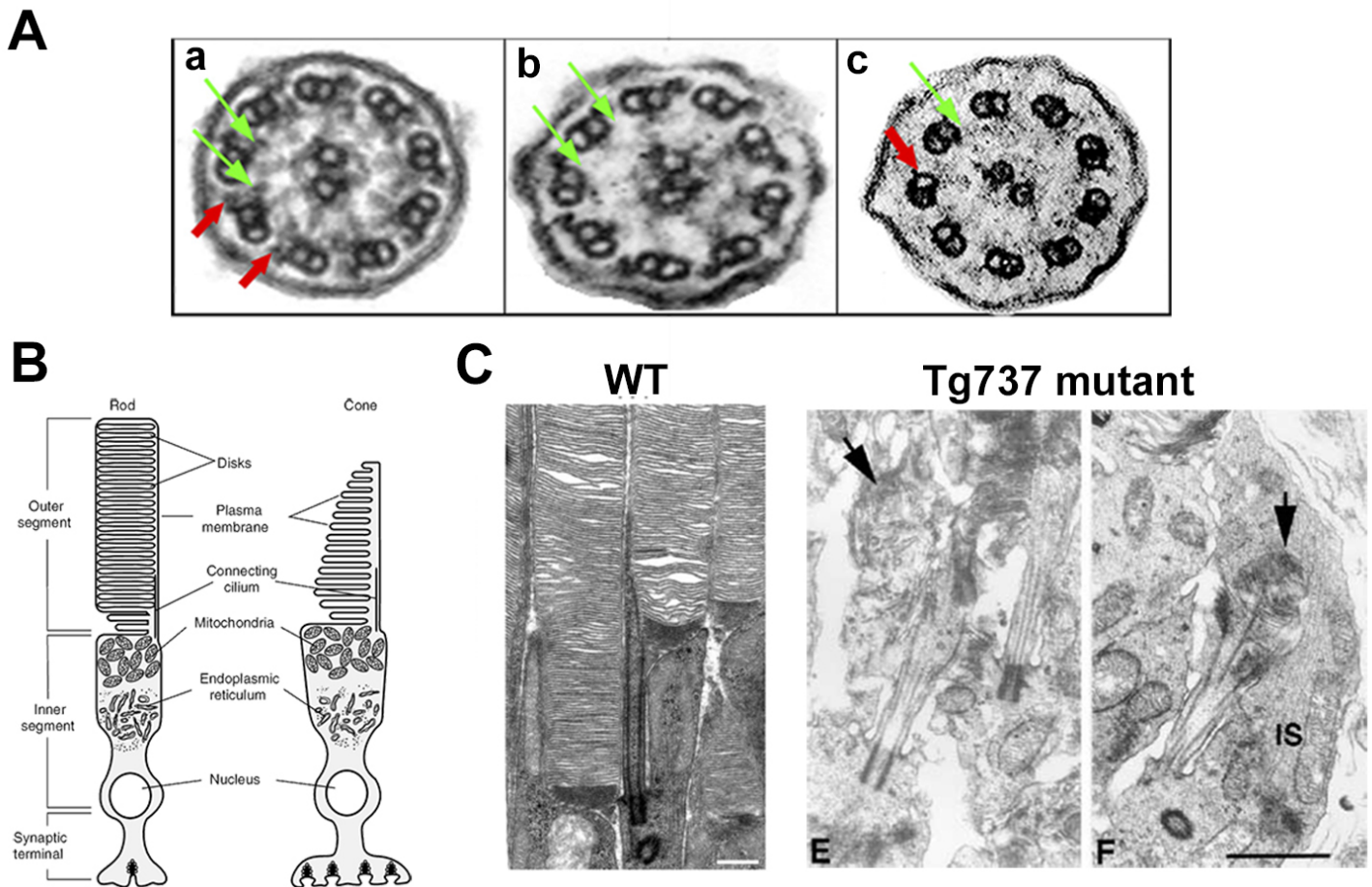


### Figure 13: Phenotypes of ciliopathies

**(A)** Electron microscopy images from a healthy human subject (a) and patients with PCD (b and c). (a) Red arrows point ODAs and green arrows IDAs. (b) Patient with *CCDC40* mutations. Abnormal IDAs defects are indicated with green arrows. (c) Abnormal ODAs and IDAs defects are pointed with red and green arrows respectively. Adapted from (Knowles, Daniels et al. 2013). **(B)** Schematic diagram of vertebrate rod and cone photoreceptors. The outer and inner-segments are connected by the connecting cilium (Cote 2006). **(C)** Typical outer segments of rod cells in wild type animal (mice). Scale bar: 500nm **(E and F)** Typical examples of aberrant outer segments in Tg737 mutant mice. (Salinas, Pearing et al. 2017) **(E)** The arrow indicates disrupted discs. **(F)** Outer segment extending into the inner segment. IS: Inner segment Scale bar: 1 $\mu$ m. (Pazour, Baker et al. 2002)

signals to PC2 that in turn mediates a  $\text{Ca}^{2+}$  influx (Chapman and Schrier 1991, Lakkis and Zhou 2003).

The analyses of kidney cells in the mouse model for ARPKD (Tg737<sup>orpk</sup>) revealed the crucial role of cilia in PKD (Pazour, Dickert et al. 2000). The gene mutated in this mouse lineage is the homologue of *IFT88* that is essential for ciliogenesis. Scanning electron microscopy of kidney in the ARPKD murine model revealed that their primary cilia were shorter and it was proposed that the cystic kidney might be a consequence of ciliary defect (Pazour, Dickert et al. 2000). Shortly after, Pazour and colleagues revealed that polycystin-2 was specifically localized in the primary cilium at the surface of mouse and human kidney cells (Pazour, San Agustin et al. 2002). In that case, primary cilia function as a sensory antenna to detect and transduce signals from the environment to the cell body. Mutations in PC1 or PC2 genes can result in defective ciliary signalling that block the pathway implicated in proper kidney development and function. This highlights an important role of cilia in kidney functions, as further supported by the common presence of kidney defects in multiple ciliopathies.

### c) Retinal degeneration

Blindness is associated to photoreceptor cell degeneration *Retinitis pigmentosa* and is one of the most common symptoms observed in ciliopathies. The rod and cone photoreceptors are composed of an inner segment and an outer segment that can be considered as a modified cilium (Figure 13B). The connecting cilium separates these two segments, and can be seen as an elongated transition zone. Defects in proteins of the connecting cilium such as CEP290 (protein important in early and late steps of ciliogenesis) cause Leber's congenital amaurosis, a disease characterized by an early form of retinal degeneration (den Hollander, Koenekoop et al. 2006). Many of the proteins necessary for constructing the outer segment are likely to be dependent on the IFT machinery to pass through the connecting cilium (Crouse, Lopes et al. 2014). Accordingly, several mutations in the IFT machinery can cause abnormal



outer segment development resulting in photoreceptor death (Figure 13C) (Marszalek, Liu et al. 2000, Pazour, Baker et al. 2002).

There are many more ciliopathies associated with a large panel of symptoms / phenotypes such as defects in left-right asymmetry establishment, polydactyly, cystic kidneys, liver, and pancreatic diseases, behavioural and cognitive defects and obesity (Figure 12B). The difficulty of prenatal diagnosis is due to the absence of diagnostic criteria that appear later on during childhood. Moreover the phenotypic overlap between the different syndromes and their clinical and genetic heterogeneity does not facilitate the diagnosis. Therefore, basic research is essential to understand what could be the impact of mutations in gene implicated in ciliogenesis and to evaluate if the impact will be the same in all the different types of cilia present in the human body. Moreover, the knowledge of ciliary protein localisation and their timing of expression could facilitate the comprehension of symptoms associated to ciliopathies.

## **5) Model organisms to study cilia and flagella**

Ciliopathies are characterized by a large diversity of sometimes overlapping symptoms. Mutation in the same gene can result in different clinical manifestations whereas mutations in different genes can cause the same phenotype. This complexity is explained by the diversity in cilium structure, composition and function. Studies of gene function can be performed *in vitro* in human cultured cells or tissues, but multi-ciliated cells are terminally differentiated and difficult to manipulate. The primary cilium can be assembled but mostly when the cells exit from the cell cycle necessitating to incubate cells in starvation conditions. Physiological relevance is therefore questionable. The use of model organisms is essential to try to understand the complex ciliary biology and mechanisms involved in ciliopathies (Vincensini, Blisnick et al. 2011). Fortunately cilia and flagella exhibit a high level of structural and molecular conservation throughout evolution, allowing the use of simpler model organisms to reveal complex phenomena. Pioneering studies carried out in



*Tetrahymena* and *Chlamydomonas* permitted respectively the discovery of the first axonemal microtubule motor, the dynein motor and the IFT (Gibbons and Rowe 1965, Kozminski, Johnson et al. 1993). Moreover, multicellular organisms such as mouse, *C. elegans* or zebrafish and protists such as *Tetrahymena* or *T. brucei* each bring specific advantages to the study of cilium biology.

### a) The green alga *Chlamydomonas reinhardtii*

The green alga *Chlamydomonas* possesses two flagella in the “9+2” conformation that emerge from the apical end of the cell. They are important for motility, light detection and gamete adhesion. Flagella are not essential for the cell cycle and are disassembled at mitosis, allowing the transformation of basal bodies in centrioles that migrate at the nuclear pole to nucleate the mitotic spindle. Several biological and technical advantages make *Chlamydomonas* one of the most efficient models to understand mechanisms implicated in ciliogenesis. *Chlamydomonas* may be grown synchronously and large amounts of flagella can be purified for biochemical or proteomic analyses. Since flagella are not essential, forward genetics is possible allowing the generation and characterization of many mutant strains defective in flagellum formation or functions. After deflagellation, *Chlamydomonas* is able to synchronously regrow new flagella allowing the study of mechanisms implicated in flagellum elongation. IFT was first observed in *Chlamydomonas* using differential interference contrast (DIC) microscopy (Kozminski, Johnson et al. 1993). Numerous genes involved in flagellum motility (Dynein arms) and construction have been discovered in *Chlamydomonas* (Kozminski, Beech et al. 1995, Piperno and Mead 1997, Cole, Diener et al. 1998, Porter, Bower et al. 1999). As the specific genes and proteins involved in IFT were identified, it became possible to control flagellum assembly by interfering with IFT. This has led to a better understanding of cilia and flagella formation and functions and comprehension of their importance in Human.



### **b) The nematode *Caenorhabditis elegans***

*C. elegans* is a transparent nematode of about 1mm in length that lives in soil. It does not possess motile cilia and the only ciliated cell types are the sensory neurons. A hermaphrodite adult has 60 neurons with cilia at their ends, that present a wide diversity of structure including membranous elaborations of different shapes (Perkins, Hedgecock et al. 1986). Ciliated neurons are essential to detect external stimuli (e.g. surrounding salt concentration) but are not essential for the worm to survive. A large collection of mutants has been generated based on their non-lethal failure to respond to external stimuli and have been separated in two categories: chemosensory or osmosensory mutants. Some of them were mutated in *IFT* genes, resulting in several defects in ciliogenesis (Tabish, Siddiqui et al. 1995, Collet, Spike et al. 1998). In addition to the generation of functional mutants, gene tagging with a GFP reporting construct is possible, allowing the first *in vivo* visualization of GFP::IFT fusion protein (Orozco, Wedaman et al. 1999). Studies in *C. elegans* have brought key discoveries on the IFT machinery (Prevo, Scholey et al. 2017) but also on the regulation of ciliary gene expression by transcription factors. Many genes involved in ciliogenesis are under the control of the same RFX-like transcription factor that recognizes a specific sequence present upstream of the start codon (Swoboda, Adler et al. 2000). RFX-like factors have been shown to be important in other organisms such as *Drosophila* to regulate genes implicated in ciliogenesis (Laurencon, Dubruille et al. 2007). Studies in *C. elegans* have brought important insight into the ciliogenesis machinery, the mechanisms of ciliary gene expression and permitted to establish a list of known and candidate ciliary proteins.

### **c) The mouse**

The mouse is the most common model to study human diseases in basic and preclinical research. It offers the advantage to be evolutionarily closer to humans than unicellular model organisms and reasonably easy to breed. The use of hypomorph mutants or conventional mutants using the Cre-lox system allowed for

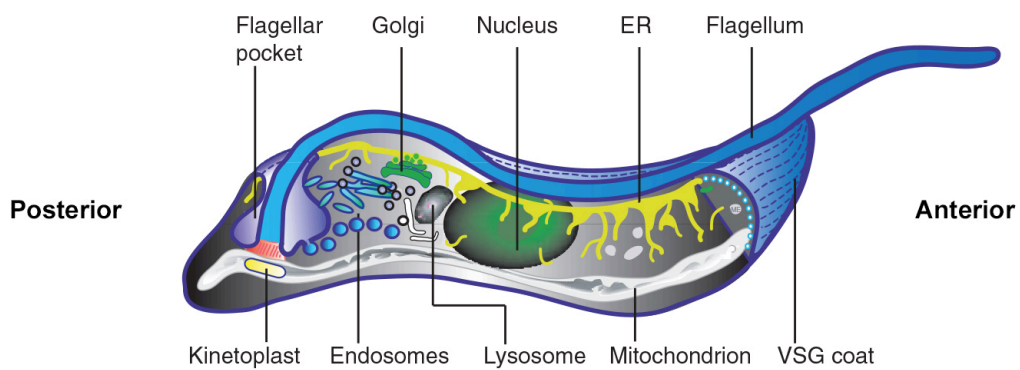


**Figure 14: Trypomastigote morphotype of *Trypanosoma brucei*.**

Schematic representation of the trypanosome cell in trypomastigote morphotype. This model shows the localization of the major organelles and the anterior and posterior poles of the cell. (Overath and Engstler 2004)

## **Introduction**

detailed analysis of genes involved in human ciliogenesis. The first series of IFT mutants revealed that the primary cilium is essential for mouse embryo survival and brought understanding of the ciliary role in mammalian development. Moreover, mouse mutants provided important highlights in Shh (Sonic hedgehog) signalling pathway and its role in ciliogenesis (Huangfu, Liu et al. 2003). Indeed key actors of Shh pathway are enriched in vertebrate cilia and their disruption mimics many ciliopathy symptoms such as polydactily or craniofacial abnormalities (Mullor, Sanchez et al. 2002, Brancati, Iannicelli et al. 2009). Specifically, the main advantage for using mouse models is to assess the impacts of gene mutations on different ciliary types present on several tissues and to compare these defects with human symptoms. However, it is more time-consuming compared in other organisms such as zebrafish.

In the lab, we have selected the protist *Trypanosoma brucei* as model. This organism is well known for being the causative agent of sleeping sickness. *T. brucei* is a typical unicellular eukaryote with an elongated and highly polarized cell body shape that measures from 3 to 45  $\mu\text{m}$  depending on the parasite cycle stage (Rotureau, Subota et al. 2011). The cell polarity is defined by the microtubules of the cytoskeleton, with the (+) end of the microtubules at the posterior part of the cell and the (-) end at the anterior part (Figure 14) (Robinson 1995). The trypanosome flagellum emerges from the flagellar pocket near the posterior end of the cell and is attached along the cell body with the exception of its distal tip (Figure 14). Trypanosomes possess several biological and technological advantages to study ciliogenesis. First, the *T. brucei* genome has been fully sequenced and annotated. The absence of introns facilitates gene identification and cloning (Berriman, Ghedin et al. 2005). Thanks to intense research efforts over the last decade, a powerful and diversified genetic toolbox is currently available for functional studies including constitutive or conditional gene knockout, overexpression, inducible or constitutive expression of fluorescently tagged proteins, inducible or constitutive RNAi silencing (Clayton 1999, Julkowska and Bastin 2009) and recently CRISPR-cas9 gene editing (Rico, Jeacock et al. 2018). Many of the human genes currently known to be involved in ciliogenesis are



## **Introduction**

conserved in trypanosomes. Indeed comparison of *T. brucei* and *H. sapiens* showed that all IFT proteins are conserved and share 30-45% identity despite the large evolutionary distance (van Dam, Townsend et al. 2013). Trypanosomes maintain the existing flagellum while constructing the new one during the cell cycle, providing the opportunity to study flagellum construction and maintenance in the same cell (Sherwin and Gull 1989). Two trypanosome stages can be easily cultivated in liquid medium where they can reach high cell densities with a doubling time of less than 12 hours. During my thesis I studied the control of flagellum length in *T. brucei*. At the procyclic stage, cells proliferate but always produce a flagellum with a final length of 20  $\mu\text{m}$ . In this context, we can study how one cell is able to control the construction of a flagellum always presenting the same fixed length. During the complex life cycle, other stages are characterized by large morphological modifications including different stage-specific flagellum lengths (Rotureau, Subota et al. 2011). By studying parasites isolated from tsetse fly, we can evaluate parameters implicated in the production of the different flagella that could possibly be distinct for each parasite stage. Indeed, using the same genome, a given parasite stage can produce a flagellum with a very different length, and distinct functions as compared to those of the previous or next stages and that could be regulated by stage-dependant pathways. It is also the case in multicellular organisms such as in Human where cell types possessing cilia with different functions, structures and compositions originate from the same genome.



## II. *Trypanosoma brucei*

---

### 1) *Trypanosoma brucei* as a parasite

#### a) African trypanosomiasis: history and epidemiology

Human African Trypanosomiasis (HAT), also known as sleeping sickness is a vector-borne parasitic disease. An equivalent disease exists in animals and is called Animal African trypanosomiasis (AAT) or nagana. Although it has probably been existing since prehistoric times, the Arab historian Ibn Khaldun was the first to describe sleeping sickness in writings from the 14<sup>th</sup> century, when reporting the death of King Diata II, sultan of Mali. *"His end was to be overtaken by the sleeping sickness which is a disease that frequently befalls the inhabitants of these countries especially their chieftains. Sleep overtakes one of them in such a manner that it is hardly possible to awake him."* In the 19<sup>th</sup> century, it was the explorer David Livingstone who first suggested a link between the bite of tsetse flies and nagana (Livingstone 1857). In 1895, David Bruce demonstrated that cattle were sick due to the presence of parasitic agents in their blood and cerebrospinal fluid. Robert Forde made the first observation of the causative agent in the human blood few years later. David Bruce established the conclusive evidence that it is the bite of the tsetse flies that transmits the causative agent of sleeping sickness (Bruce 1895). Ten years later, Friedrich Kleine started to describe the overall cyclical transmission of African trypanosomes between mammals and tsetse flies (Kleine 1909). Three major human outbreaks have occurred over the last century. The first one occurred between 1896 and 1906 mostly in Uganda and the Congo Basin. The second one occurred in 1920 in several African countries and was controlled thanks to massive screening and treatment of populations at risk. In the 1960s, the disease seemed under control with less than 5 000 reported cases per year and the surveillance was relaxed. The disease reappeared and reached epidemic level from 1970 to the late 1990s. Today, the

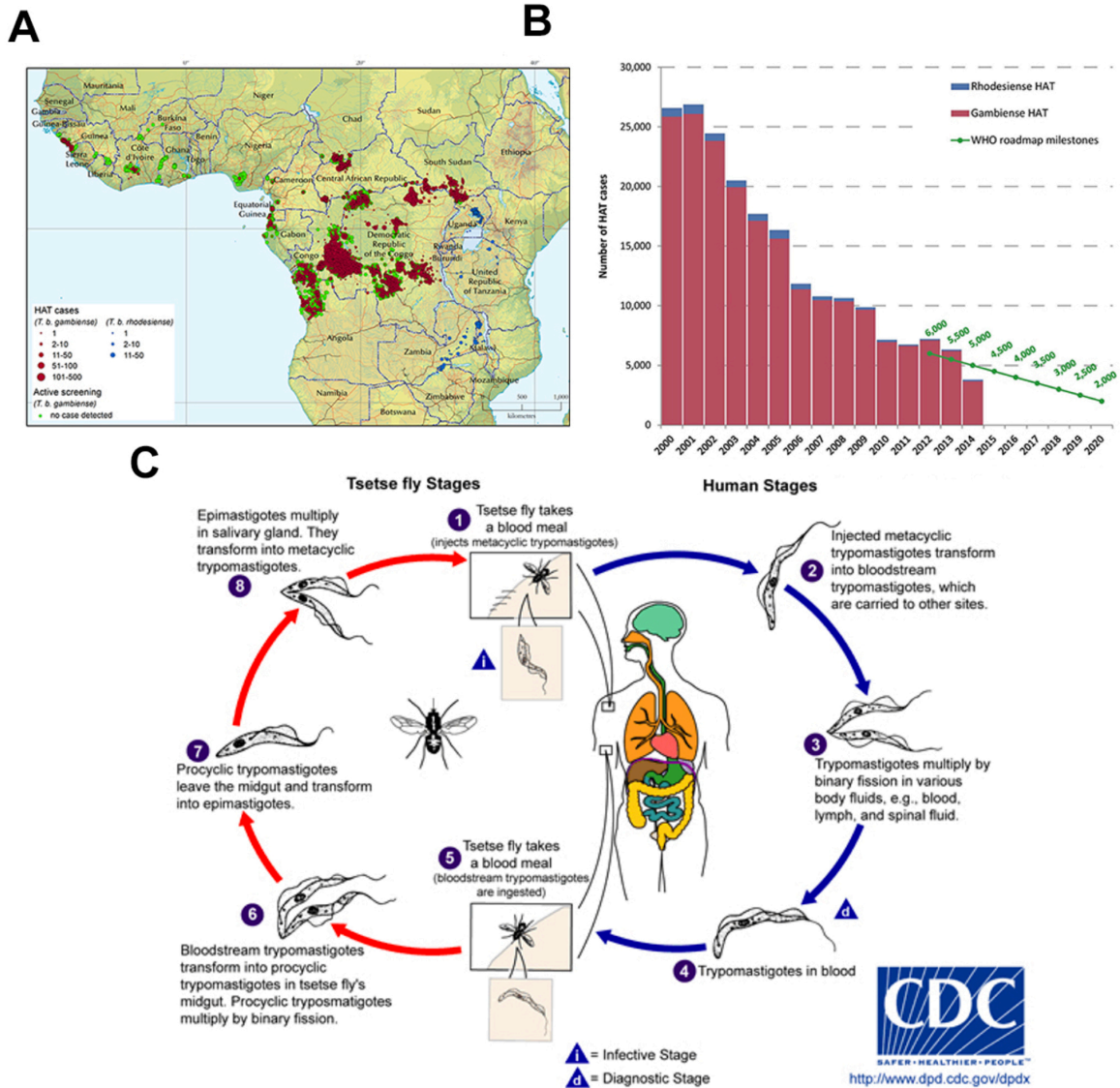


**Figure 15: Human African Trypanosomiasis.**

(A) Maps representing the foci distribution of the HAT cases reported to WHO from 2010 to 2014 (Franco, Cecchi et al. 2017). (B) Numbers of new HAT cases caused by *T. brucei gambiense* and *T. brucei rhodesiense* annually reported to WHO since 2000 and epidemiological projections until 2020 (Franco, Cecchi et al. 2017). (C) Simplified life cycle of *T. brucei*. During a blood meal, a tsetse fly ingests stumpy forms that are pre-adapted to life in the midgut. After a complex journey from the posterior midgut to the salivary glands, infective metacyclic forms are produced in the saliva for being injected in a new mammalian host. Cycle from the American Center of Diseases Control and Prevention web site.

burden of sleeping sickness has been reduced thanks to continuous international control efforts. The number of new HAT cases reported between 2000 and 2012 dropped by 73% (WHO 2018) (Figure 15B). Today, the World Health Organization (WHO) considers HAT as a neglected tropical disease. It threatens 36 countries in Sub-Saharan Africa, with around 65 million people living at risk (WHO 2018) (Figure 15A). In addition, nagana threatens 50 million heads of cattle and still represents the most economically important livestock disease in Africa, with annual losses estimated between US\$ 1-1.2 billion per year (Kennedy 2008). However, despite these numerous campaigns of mass screening and treatment, some transmission foci have been persisting and the disease is not yet eliminated. The goal of the WHO is elimination of HAT as a public health problem for 2020, and the transmission interruption in humans for 2030 (Figure 15B) (Informal Expert Group on Gambiense, Buscher et al. 2018).

During the last Ebola outbreak in Guinea, HAT active screening and surveillance was interrupted over two years (2014-2016). This arrest of screening activities led to a dramatic resurgence of HAT (Kagabadouno 2018). Recently, experiment in mouse models suggested that the skin could act as a reservoir for parasites transmission. After the bite of a tsetse fly, extravascular trypanosomes remain abundantly present in the skin (Capewell, Cren-Travaille et al. 2016). Using intra-vital imaging it was shown that these extravascular trypanosomes are highly motile, consistent with viability. Moreover, they are able to infect tsetse flies even in absence of blood parasitemia demonstrating that parasites in the skin could contribute to transmission. Skin biopsies collected from humans as part of a National onchocerciasis screening programme showed the presence of parasites in the extravascular tissue meaning that the situation is also encountered in the field (Capewell, Cren-Travaille et al. 2016). Importantly, these people did not report for sleeping sickness, suggesting the existence of asymptomatic patients. Presence of asymptomatic subjects could explain why HAT has not yet been eliminated and the rapid resurgence of HAT in Guinea (Informal Expert Group on Gambiense, Buscher et al. 2018).



## **b) African trypanosomiasis: actors of the infection**

### **i. The trypanosomes**

Trypanosomes are eukaryotic organisms belonging to the Kinetoplastidae family that is characterized by the presence of large amount of concatenated DNA in a single and large mitochondrion, forming a structure called the kinetoplast. Besides their unique mitochondrion, trypanosomes possess several typical organelles such as the nucleus, the endoplasmic reticulum, a Golgi apparatus and a single flagellum (Figure 14 and 16A) (Lacomble, Vaughan et al. 2009). Kinetoplastids include a number of human parasites such as *Trypanosoma brucei*, the parasite causing sleeping sickness, *Trypanosoma cruzi*, the agent of Chagas disease, also called American Trypanosomiasis and several *Leishmania* species that are responsible for visceral and cutaneous leishmaniases. The genus *Trypanosoma* is subdivided in two groups depending on their behaviour in the insect vector. The first group is composed of stercorian trypanosomes that are transmitted to the next recipient host in the feces of the insect vector. This is the case of *T. cruzi* that is transmitted by the feces of reduviid bugs (subfamily *Triatomine*). The members of the second group are called salivarian trypanosomes because their infective forms are present in the salivary glands of the insect vector and penetrate in their vertebrate host during a blood meal. *T. brucei* is a member of this group and is transmitted to the mammalian host by the bite of tsetse flies (Figure 15C and 16B). Two sub-species are able to infect humans and cause different forms of HAT in Africa. *T. brucei gambiense* accounts for 97% of the reported cases and is found in West and Central Africa where it causes the chronic form of the disease. The infection may remain latent for months or even years before the emergence of the first symptoms (Brun, Blum et al. 2010). The remaining cases are caused by *T. brucei rhodesiense* that is found in Southern and Eastern Africa, where it causes a faster and more severe disease often resulting in death within a few weeks after the first symptoms in absence of treatment (Simarro, Jannin et al. 2008).



Natural human immunity to *T. brucei brucei*, *T. vivax* and *T. congolense*, causative agents of AAT is due to two trypanolytic factors (TLF1 and -2), found in the serum. These complexes contain haptoglobin-related protein (HPR) and apolipoprotein L1 (APOL1) (Pays, Vanhollebeke et al. 2006). APOL1 kills trypanosomes by lysis after insertion into endosomal and lysosomal membranes. The two subspecies that cause HAT can resist APOL1. *T. brucei gambiense* resists TLFs via a hydrophobic  $\beta$ -sheet of the *T. brucei gambiense* specific glycoprotein (TgsGP) that prevents APOL1 toxicity by inducing a stiffening of the membrane (Uzureau, Uzureau et al. 2013).

*T. brucei rhodesiense* resistance is conferred by a truncated form of the variant surface glycoprotein (VSG) (See section below) termed serum resistance associated protein (SRA). SRAs interact strongly with APOL1 preventing its association with trypanosome membranes (Vanhamme, Paturiaux-Hanocq et al. 2003).

### ii. The tsetse

Tsetse flies can be considered as obligatory host for trypanosomes due their critical role to complete life cycle and as vector because they transmit trypanosomes to mammalian hosts. Tsetse flies are biting flies that are found exclusively in Africa (Figure 16B). Tsetse flies include all the species in the genus *Glossina* and are found in three main ecosystems: savannah, forest and riverbanks. Males and females are exclusive blood-feeders. Tsetse fly saliva is injected in the dermis during the blood meal to avoid blood coagulation and to induce vasodilatation. If the saliva contains infective trypanosomes, they are transferred during the blood meal and can develop an infection in mammal. During the bite of an infected tsetse fly, up to hundreds of trypanosomes can be injected in the inoculation site (Otieno and Darji 1979). Presently, 31 species of *Glossina* have been identified among which 12 are recognized as efficient trypanosome vectors and 6 are directly incriminated in the transmission of the two human-infective trypanosomes sub-species (WHO 1998, Franco, Simarro et al. 2014). During the different outbreaks, vector control strategies were used to disrupt the transmission cycle. Odor baited traps and screen impregnated with insecticide have been used to suppress tsetse population by 99%



in Uganda and The Republic of Congo (WHO 2018). Despite the simplicity of these traps, they require a lot of maintenance. Sometimes they are applied on too small scale to prevent tsetse reinvasion. The sterile insect technique (SIT) is another approach to reduce tsetse populations. This is based on the fact that females mate only once in their life. Mating a female with a sterile male will prevent new births. *Glossina* was eradicated in less than 4 years in the island of Unguja (Zanzibar) by using this approach (Vreysen, Saleh et al. 2000). SIT was efficient in this island because it is a closed ecosystem. However in African countries, effective suppression using other methods is prerequisite. Indeed, the cost of SIT is very high and large of numbers of sterile male flies would be needed to be released to out-compete the wild population to prevent future reinvasion.

### iii. Mammalian host and reservoir

The role of animal reservoirs and humans is different in the two forms of HAT. In HAT associated to *T. brucei gambiense*, the role of animal reservoirs is thought to be minor in most transmission foci, while HAT associated to *T. brucei rhodesiense* is a zoonotic disease mostly affecting mainly animals and where humans are only accidental hosts (Franco, Simarro et al. 2014). In *gambiense* HAT, asymptomatic patients infected with trypanosomes could be a source of infection for vectors that would sustain the transmission (Checchi, Filipe et al. 2008, Capewell, Cren-Travaille et al. 2016, Informal Expert Group on Gambiense, Buscher et al. 2018). The role of animal reservoirs in maintaining *T. brucei gambiense* is currently not clear. In some West African foci, data suggest that *T. brucei gambiense* was also found in domestic pigs but in others foci the parasites were exclusively present in humans (Njiokou, Nimpaye et al. 2010, Balyeidhusa, Kironde et al. 2012). In *rhodesiense* HAT, the population of trypanosomes is maintained in wild and domestic animal reservoirs (Franco, Simarro et al. 2014, Berthier, Breniere et al. 2016). In some cases, the trypanotolerant animal just carries the parasite and survives for many years, but in other cases, the disease affects the animal. In this context, the incidental contact between humans and animals (mainly cattle) can explain small and limited outbreaks



of the disease in humans. Non-endemic cases of rhodesiense HAT encountered over the past 20 years have been imported largely due to tourists traveling to endemic areas, primarily for safari, but also soldiers training in endemic areas (Migchelsen, Buscher et al. 2011).

### c) Parasite cycle

The parasite cycle of *T. brucei* alternates between mammalian hosts, such as humans, wild or domestic animals and the tsetse flies (Figure 15C). After the passage from the reservoir host to the vector host, parasites multiply, differentiate and migrate in the different organs of the tsetse, leading to the production of the only infective stage that can be transmitted to a new mammalian host during a blood meal (Figure 16D). During their parasite cycle, trypanosomes adapt their metabolism in order to optimize the benefits from the nutrients available in their micro-environments, especially glucose in the mammalian host and mostly proline in the tsetse fly (Smith, Bringaud et al. 2017).

#### i. Mammalian stages

*T. brucei* is exclusively extracellular and colonizes both the blood and interstitial tissues including the skin and the brain at the final stage of the disease (See next section) (Caljon, Van Reet et al. 2016, Capewell, Cren-Travaille et al. 2016). Parasites are permanently exposed to the immune system. Bloodstream trypanosomes possess a dense surface coat made of 10 million copies of the same type of variant surface glycoproteins (VSG) linked to the cell membrane by a unique GPI-anchor (glycosyl-phosphatidylinositol) (Cross 1975, Ferguson, Homans et al. 1988). VSGs allow trypanosomes to evade the immune system by an intensive antigenic variation. A given VSG is recognized by the immune system and cleared by an antibody response specifically directed against them. However, a small proportion of the population is able to modify its VSG coat by expressing a different VSG gene and escape the antibody response. These parasites proliferate until a new antibody

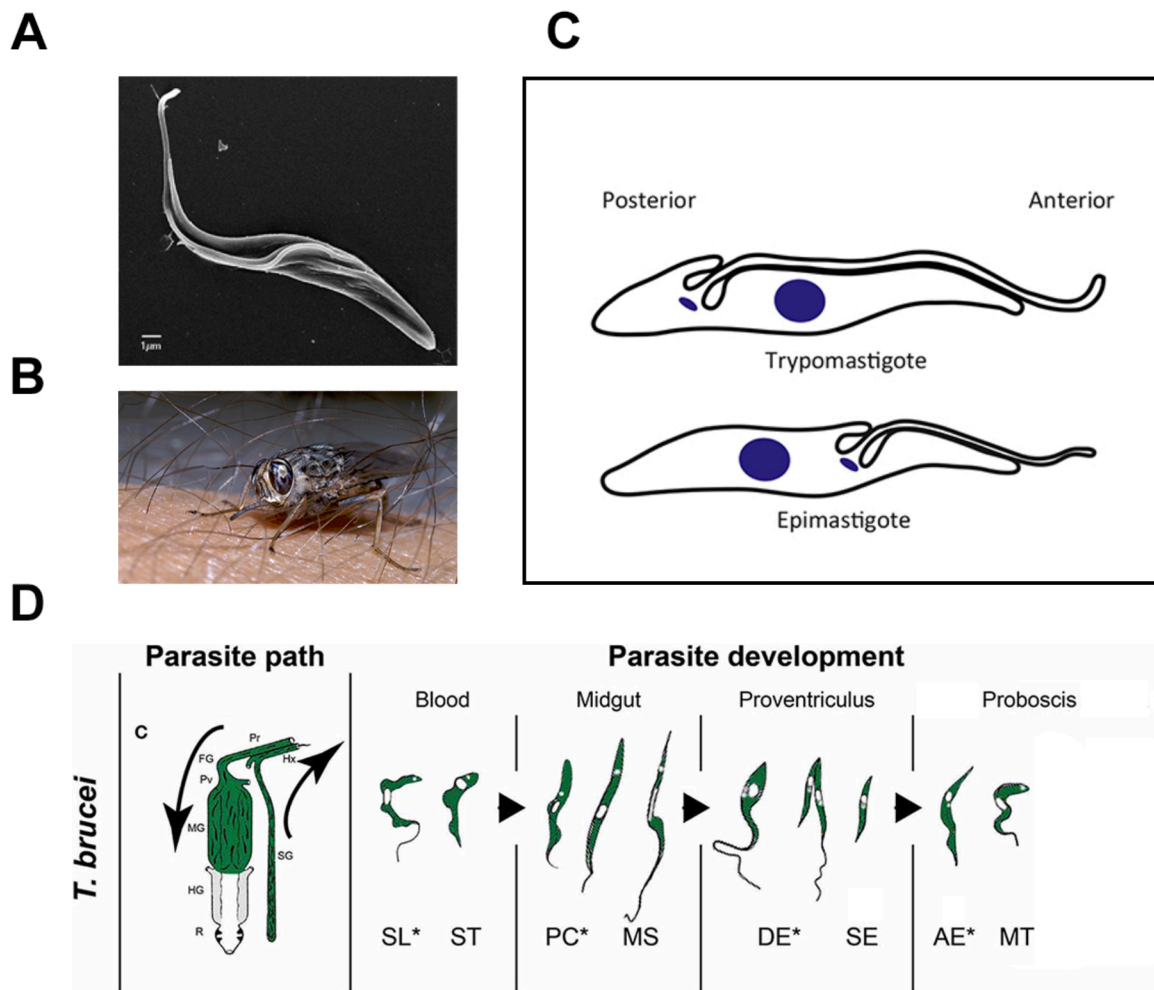


**Figure 16: Life cycle of *Trypanosoma brucei*.**

**(A)** Scanning electron micrograph of a *T. brucei* procyclic found in the tsetse posterior midgut **(B)**. Tsetse fly *Glossina morsitans morsitans*, the main vector of *T. brucei brucei* (B. Rotureau). **(C)** Cartoons showing the two common morphologies of *T. brucei*. The nucleus is the large circle and the kinetoplast is the small blue oval linked to the base of the flagellum. The trypomastigote possesses the kinetoplast posterior to the nucleus. In epimastigote conformation, the kinetoplast is anterior to the nucleus (Sunter and Gull 2016). **(D)** Schema of *T. brucei* development in the tsetse fly. The parasitic path is represented in the left part of the drawing and the successive forms found in different organs and tissues are represented in chronological order on the right part. \* indicate proliferative stages. Pr: proboscis, FG: foregut, Pv: proventriculus, MG: midgut, HG: hindgut, R: rectum, Hx: hypopharynx, SG: salivary glands, SL: slender trypomastigote, ST: stumpy trypomastigote, PC: procyclic trypomastigote, MS: mesocyclic trypomastigote, DE: long dividing epimastigote, SE: short epimastigote, AE: attached epimastigote, MT: metacyclic trypomastigote (Rotureau and Van Den Abbeele 2013).

response is mounted against the new VSG coat. The infection can persist for a long time because the trypanosome genome contains about 1000-2000 VSG and VSG-related genes, constituting a diversified repertoire of antigenic forms of VSGs (Horn 2014). Moreover, segmental gene conversion has been observed in *T. brucei* infections in mouse, generating mosaic VSGs not previously encoded in the genome and offering an even greater potential for diversification (Mugnier, Cross et al. 2015). In mammals, trypanosomes exist in two different forms: the slender form (SL) that can multiply every 7 hours by binary fission and the stumpy form (ST), which is pre-adapted to survive in the tsetse midgut and does not proliferate. As parasite number increases, an irreversible differentiation from slender to stumpy form occurs (Reuner, Vassella et al. 1997, Tyler, Matthews et al. 1997).

### ii. Tsetse fly stages

After the tsetse fly has taken a blood meal on an infected mammal, parasites start a long developmental programme of up to three weeks that will lead to the production of the metacyclic stage, the only stage able to infect mammals. In tsetse fly, *T. brucei* parasites successively travel through the midgut and the proventriculus and finally reach the salivary glands (Vickerman 1985). During their journey, they switch between two morphotypes defined by the relative position of the kinetoplast to the nucleus and the posterior end (Figure 16C) (Frolov 1994). In the trypomastigote morphotype, the kinetoplast is found between the nucleus and the posterior end of the cell, while it is located between the nucleus and the anterior end of the cell in epimastigotes (Figure 16C). Upon ingestion by the tsetse fly, 99% of parasites are eliminated, but some cells at the stumpy stage are pre-adapted to survive in the gut and can transform into procyclic forms (PCF) that colonize the midgut (Figure 16A). The development of PCF is marked by the replacement of the VSG coat by a new surface coat composed of two distinct classes of procyclin: EP and GPEET (Roditi and Clayton 1999). There are seven procyclin genes (EP) that encode unusual proteins with extensive tandem repeat units of glutamic acid (E) and proline (P) and two genes that encode proteins with internal pentapeptide GPEET repeat (Butikofer,



Ruepp et al. 1997). During this colonization, a parasite population called mesocyclic (MS) differentiates and migrates toward to the proventriculus (Figure 16D) (Vickerman 1985). Cytoskeleton elongation at the posterior end and an increase in cell length characterize this differentiation from PCF to MS (Rotureau, Subota et al. 2011). In the proventriculus, they differentiate into long dividing epimastigotes (DE). This differentiation is characterized by nucleus migration toward the posterior end beyond the kinetoplast position. This cell asymmetrically divides to give birth to two distinct cells: the short epimastigote (SE) and the long epimastigote (LE) (Figure 16D). The exact role of the LE is currently being debated but the community has proposed a transfer role to bring the SE to the salivary glands. Indeed, the SE is not able to swim alone to get to the salivary glands due to the short length of its flagellum (3  $\mu\text{m}$ ). Once in the salivary glands, the SE can differentiate in attached epimastigote (AE), covered by a coat composed of BARP proteins (Urwyler, Studer et al. 2007). BARPs (Bloodstream alanine rich protein) are a glycosylphosphatidyl inositol anchored proteins that form a stage-specific coat for epimastigote forms (Urwyler, Studer et al. 2007). The transition from SE to AE is also accompanied by a significant increase in cell volume and an important elongation of the posterior end (Rotureau, Subota et al. 2011). At the early stage of salivary glands infection, the AE proliferate (Epi-Epi) and colonize the epithelium by creating extensive membrane outgrowths and desmosome-like connections inducing physical contact with microvilli of epithelial cells (Vickerman 1985). AEs can enter in asymmetric division (Epi-Trypo) to produce the infective metacyclic stage (MT) in the saliva, ready to be injected in a new mammalian host (Figure 16D) (Rotureau, Subota et al. 2012). The proportion of Epi-Epi divisions decrease in favour of Epi-trypo divisions during the course of infection (Rotureau, Subota et al. 2012). MT trypomastigotes are non-proliferative cells that have re-acquired a VSG coat in preparation for being injected into mammalian hosts.

### **d) Human infection and symptoms**

During the first stage of the disease known as the hemo-lymphatic phase, trypanosomes multiply in the blood, the lymph and probably in the dermis. Fever



spikes, weakness, headaches, cutaneous itching, joint pains and swollen cervical lymph nodes are characteristic symptoms associated with this phase. Fever is intermittent with weeks or months between episodes and parasite burdens in fluids are accompanied by a swelling of the lymph nodes. As the symptoms are fairly generic and other infectious diseases such as malaria are present in the same areas, the diagnosis is difficult to establish solely from clinical observations. Occasionally, trypanosomes proliferate at the inoculation site, which leads to an inflammatory nodule, called chancre. The first phase of the disease may last for years in the case of infection with *T. brucei gambiense*, whereas in the case of *T. brucei rhodesiense*, the infection is more virulent and neurological symptoms progress over a matter of weeks. The second phase of the disease known as the meningo-encephalitic phase, begins when parasites cross the blood-brain barrier and invade the central nervous system. Neurological symptoms include sensory disturbances, confusion, tremor and altered behaviour. At this stage, parasites impair the circadian rhythm of their host with an alteration of sleep/wake cycles, hence the name “sleeping sickness”. The neurological damages caused by the parasites are irreversible. Without treatment, the natural evolution of the disease is invariably lethal, with a progressive mental deterioration, a systemic organ failure, cachexia, coma and finally death.

### **e) Diagnosis and treatment**

The diagnosis of a potential infection starts by an evaluation of the clinical signs and especially the palpation of swollen cervical lymph nodes. However, due to the non-specificity of the symptoms, the diagnosis need to be first completed by serological tests. A field-adapted test called Card Agglutination Test for Trypanosomiasis (CATT) is available for Gambian HAT to identify anti-trypanosome antibodies present in the patient’s whole blood or plasma (Magnus, Vervoort et al. 1978). If there is suspicion of infection, a second and compulsory step is the visualization of parasites in a blood sample or in a lymph node aspirate by microscopy. If negative, it is possible to examine the cerebrospinal fluid obtained by lumbar puncture and to determine whether parasites are present. This will also confirm the disease stage. The



presence of parasite DNA can be detected by polymerase chain reaction (PCR) permitting the identification of the subgenus *Trypanozoon* (Mitashi, Hasker et al. 2012). In addition, the existence of skin-dwelling parasites may now require the development of new non-invasive detection techniques (Capewell, Cren-Travaille et al. 2016). These new diagnostic tools could permit to screen large population, detect and treat asymptomatic patients in order to prevent future trypanosome transmission. The type of treatment depends on the trypanosome species and on the stage of the disease. In the early stage of *T. brucei gambiense* sleeping sickness, patients are treated with pentamidine that is generally well tolerated. For patients infected with *T. brucei rhodesiense*, suramin is recommended, but this can lead to adverse effects like allergic reactions and nephrotoxicity. Due to a low cerebral fluid entry-rate, pentamidine and suramin cannot be used to treat the second phase of the disease. In that case, melarsoprol is still used against *T. brucei rhodesiense* infections. This old arsenical derivative can cross the blood-brain barrier and is highly trypanocidal. However, it has many side effects: the most dramatic one being a possible fatal encephalopathy observed in 5-10% of the cases. Moreover, drug resistance is observed in several foci in Central Africa (Baker, de Koning et al. 2013). Eflornithine is a molecule less toxic than melarsoprol that is used in combination with Nifurtimox. This combination reduces and simplifies the use of Eflornithine alone. Indeed Eflornithine alone should be administered intravenously every six hours during 14 days while the combination of the two molecules reduces the duration of treatment to one week (Priotto, Kasparian et al. 2009). The Nifurtimox/Eflornithine combination is only efficient against *T. brucei gambiense*. Therefore, WHO recommends using it in first line treatment for this form rather than melarsoprol in stage two gHAT patients. A new oral medicine called Fexinidazole is about to obtain a market authorization to treat the late-stage of African *T. brucei gambiense* trypanosomiasis. This drug is a little less efficient than the Nifurtimox/Eflornithine combination therapy (NECT) but the advantages of an oral treatment compensate this loss due the absence of complication related to intravenous catheter and offer the possibility to receive home-based treatment, which is important when all patients live in rural areas without hospitals nearby (Mesu, Kalonji et al. 2018). Anti-trypanosomiasis vaccination could be the best option to eliminate the disease but antigenic variation has been a major



obstacle to vaccine development. Non-variable intra-cellular vaccine targets have been tested such as microtubule-associated proteins (MAPp15). The same level of protection against *T. brucei* was observed in the mice vaccinated with MAPp15 antigen and in the mice injected with PIPES as negative control (Rasooly and Balaban 2004). In view of the available treatments and the absence of a vaccine, patient care in the early stages of the disease is therefore essential.

## **2) The flagellum of *Trypanosoma brucei***

In addition to being a parasite, *T. brucei* is also a robust model to study a variety of biological processes such as GPI anchors, mono-allelic expression or RNA editing to cite only few. In my thesis I have used *T. brucei* to investigate flagellum assembly. The flagellum is particularly interesting because it is essential for parasite development and has conserved and specific structural components. The conserved features of the trypanosome flagellum provide a model to study flagellum assembly, maintenance and functions including in the context of ciliopathies. The flagellum is present throughout the cell and parasite cycles and its assembly is carried out while the old one is maintained. These particular characteristics enable the comparison of flagellum assembly and maintenance within the same cell (Bastin, MacRae et al. 1999, Fort, Bonnefoy et al. 2016).

### **a) Conserved and unique features in the architecture of the trypanosome flagellum**

The flagellum emerges from a specific membrane invagination called the flagellar pocket and contains two main structures: a classical “9+2” axoneme and an extra-axonemal structure called paraflagellar rod (PFR). The flagellum is attached along the cell body by the flagellar attachment zone (FAZ) except at its distal tip that remains free (Figure 14 and 16A). When the procyclic cell possesses two flagella, a specific structure called the flagella connector is present, connecting the tip of the



new flagellum to the side of the old one (Moreira-Leite, Sherwin et al. 2001, Briggs, McKean et al. 2004). Proteomic analysis revealed the complexity of the trypanosome flagellum that is composed of at least 600 proteins (Broadhead, Dawe et al. 2006, Oberholzer, Langousis et al. 2011, Subota, Julkowska et al. 2014).

### **I. Flagellar pocket**

The typical trypanosome cell shape is due to the presence of a subpellicular array of microtubules orientated with the (+) end at the posterior part of the cell (Robinson 1995). The flagellum exits through a gap between this microtubule skeleton where a membrane invagination called the flagellar pocket is present (Figure 14 and 17a). The flagellar pocket is the unique site of endocytosis and exocytosis of the cell and plays an essential role in immune evasion (see next section) (Engstler, Pfohl et al. 2007, Lacomble, Vaughan et al. 2009). The flagellar pocket is closed by the flagellar collar that appears as an electron-dense ring. BILBO1 was the first protein identified in this structure. It is a trypanosome specific cytoskeletal protein with two EF-hand domains and a large C-terminal coiled-coiled domain. This protein is essential for flagellar pocket formation. In its absence the flagellar pocket is not formed and vesicular trafficking is stopped (Bonhivers, Nowacki et al. 2008). Moreover the new flagellum is made too short and is not correctly positioned for cytokinesis that fails (Absalon, Blisnick et al. 2008, Bonhivers, Nowacki et al. 2008). In a recent study, a yeast two-hybrid screen identified several BILBO1 protein partners, including FPC4; a multi partner protein that can also bind microtubules and that is involved in flagellar pocket collar segregation (Albisetti, Florimond et al. 2017).

### **II. Basal body and transition zone**

The basal body is the microtubule-organizing center of the flagellum. In trypomastigote stages, the basal body is located at the posterior part of the cell but it can be found in an anterior position relative to the nucleus during the parasite cycle when trypanosomes adopt the epimastigote conformation. The basal body is

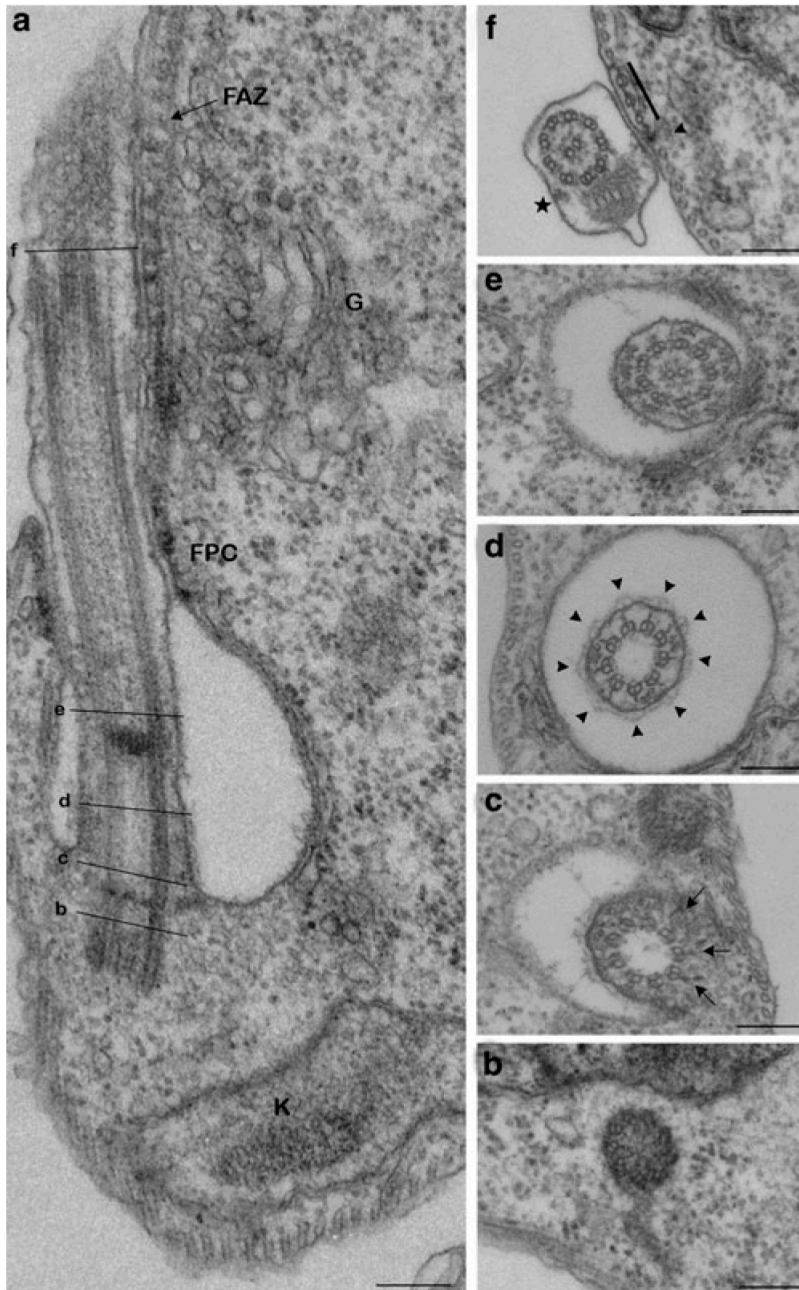


**Figure 17: Ultra-structure of the flagellum in the *T. brucei* procyclic cell.**

(a) TEM pictures of a longitudinal section through the flagellar pocket and the base of the flagellum. (b-f) TEM cross-sections through the flagellum at different regions indicated by the lines on picture (a) (b) Basal body. (c) Base of the transition zone (arrows indicate transition fibers). (d) Transition zone (arrowheads indicate the collarette). (e) Axoneme within the flagellar pocket. (f) Axoneme and the PFR after the flagellum exits from the flagellar pocket. The bar indicates the position of the FAZ-associated microtubule quartet and the arrowhead points the FAZ filament. The star indicates an IFT particle. FPC: Flagellar pocket collar, FPL: Flagellar pocket lumen, G: Golgi, K: Kinetoplast. Scale bars: 100nm (Buisson and Bastin 2010).

composed of nine triplet of microtubules (A, B and C) and is linked to the kinetoplast by a filament network called the Tripartite attachment complex (TAC) (Robinson and Gull 1991, Ogbadoyi, Robinson et al. 2003). At the distal portion of the basal body, C-tubules stop whereas A and B-tubules continue to form the transition zone and the axoneme (Figure 17 b-d).

The transition zone is localized in the flagellar pocket and it is comprised between the distal end of the basal body and the basal plate where the central pair nucleation is initiated. The proximal region of the transition zone has an invariant length of 150 nm and is characterized by the collarette surrounding the membrane (Vaughan and Gull 2015, Trepout, Tassin et al. 2018). The collarette is likely equivalent of the ciliary necklace and is composed of fibers connected to the microtubules of the transition zone (Figure 17d). The distal part of the transition zone presents more length variations (from 55 nm to 235 nm) and contains the typical Y-links following a more complex organisation than observed in previous studies (Trepout, Tassin et al. 2018). At the base of the transition zone, electron-dense projections appear to connect each outer microtubule doublets to the flagellar membrane. The tubulin-folding co-factor C or RP2 (Retinal Pigmentosa 2) is the only protein that has been clearly localized at the transition fibres in *T.brucei*, where it could play a role of quality control gateway for tubulin (Stephan, Vaughan et al. 2007).

### III. Axoneme

Microtubule doublets of the axoneme are the continuity of those of the transition zone. The axoneme compartment starts when the flagellum is still in the flagellar pocket (Figure 17e). The “9+2” axoneme presents a typical structure with nine doublet microtubules surrounding a central pair of singlet microtubules (Figure 17f). Peripheral A-tubules are decorated with ODA and IDA that are responsible for flagellum beating (Figure 18). The outer microtubule doublets are linked to one another with a nexin link and radial spokes project from the A microtubules toward the central pair (Figure 18) (Hughes, Ralston et al. 2012). The microtubules are composed of  $\alpha$  and  $\beta$  tubulin subunits that are modified by classical post-translational



modifications such as glutamylation or acetylation (Sherwin 1987, Schneider, Plessmann et al. 1997). Genes encoding less abundant tubulin types such as  $\gamma$ - $\delta$ - $\epsilon$ -tubulin and the trypanosomatid-specific  $\xi$ -tubulin are present in the genome, but their localisation remains to be clarified (Vaughan, Attwood et al. 2000). Proteomic and genomic analyses showed that the vast majority of axonemal proteins are conserved in *T. brucei* (Ralston, Kabututu et al. 2009). The dynein regulatory complex (DRC) that is essential to transmit mechanochemical signals from the central pair to the axonemal dynein.

#### IV. ParaFlagellar Rod (PFR)

When the flagellum emerges from the flagellar pocket, an additional structure called the PFR follows the axoneme until its distal tip (Figure 17f). This structure is described as a complex lattice-like structure (Vickerman 1962). Cross-sections of the PFR reveal 3 different domains defined by their relative position to the axoneme (Figure 18) (M. Farina 1986). The proximal region is connected to the axoneme with fibers attached to doublets 4 to 7 and organised in stacks of plates. The intermediate domain is constituted of filaments perpendicular to the plates whereas the distal one has a very similar pattern to the proximal region (M. Farina 1986, Koyfman, Schmid et al. 2011, Hughes, Ralston et al. 2012).

Proteomic analyses revealed that the PFR of *T. brucei* is made of at least 20 proteins (Portman, Lacomble et al. 2009). The major components are two coiled-coil proteins called PFR1 and PFR2. Homologues of these two proteins have been found in other kinetoplastids such as *Leishmania mexicana* and in *Euglena* (Moore, Santrich et al. 1996, Ngo and Bouck 1998). In trypanosomes, the absence of PFR2 leads to disruption of the distal and intermediate domains of the PFR and to the accumulation of the PFR1 protein at the distal tip of the flagellum (Bastin, MacRae et al. 1999). The absence of PFR in *T. brucei* or *Leishmania* is characterized by a pronounced motility defect demonstrating the importance of the PFR in flagellum beating (Santrich, Moore et al. 1997, Bastin, Sherwin et al. 1998, Maga, Sherwin et al. 1999). Based on



cryo-electron microscopy, it was suggested that PFR could act as a biomechanical spring to successively absorb and transmit the energy produced by axoneme beating (Koyfman, Schmid et al. 2011). The PFR is also proposed to be a storage place for ATP that is essential for dynein arms to generate flagellum movement. Moreover, two adenylate kinase proteins has been identified and localized in the PFR (Pullen, Ginger et al. 2004). These proteins could convert two ADP molecules in one ATP and 1 AMP.

### **V. Flagellar attachment zone (FAZ)**

The flagellum emerges from the flagellar pocket and is attached to the cell body along most of its length with the exception of the distal tip. The site of attachment defines a specialised region of the cell body that has been called the flagellum attachment zone (FAZ) (Figure 18) (Kohl and Gull 1998). The FAZ contains two distinct structures: the microtubule quartet, a unique set of four microtubules and the FAZ filament. The microtubule quartet is integrated into a gap within the sub-pellicular microtubule corset. This set of four microtubules is distinct from the other sub-pellicular microtubules. The polarity of the quartet is the same as for the axonemal microtubules with the (+) end at the anterior of the cell. This is in anti-parallel orientation compared to all the other sub-pellicular microtubules (Robinson 1995). Moreover these microtubules are distinct from the other cytoplasmic microtubules by their higher chemical stability, as they are resistant to high NaCl treatment (Sherwin and Gull 1989). They are also associated to the smooth endoplasmic reticulum (Angelopoulos 1970). The molecular composition of these four microtubules is still unclear but the quartet seems to host a specific version of  $\beta$ -tubulin recognized by the monoclonal antibody 1B41 (Gallo, Precigout et al. 1988). The quartet is also enriched in  $\gamma$ -tubulin (Scott, Sherwin et al. 1997).

The FAZ filament is linked to both the cell body and the flagellum by a network of regularly spaced connectors localized across the cell and flagellar membranes (Vickerman 1969). It appears as regular arrays of electron dense staple-like structures alternating with less contrasted portions on longitudinal flagellum sections.

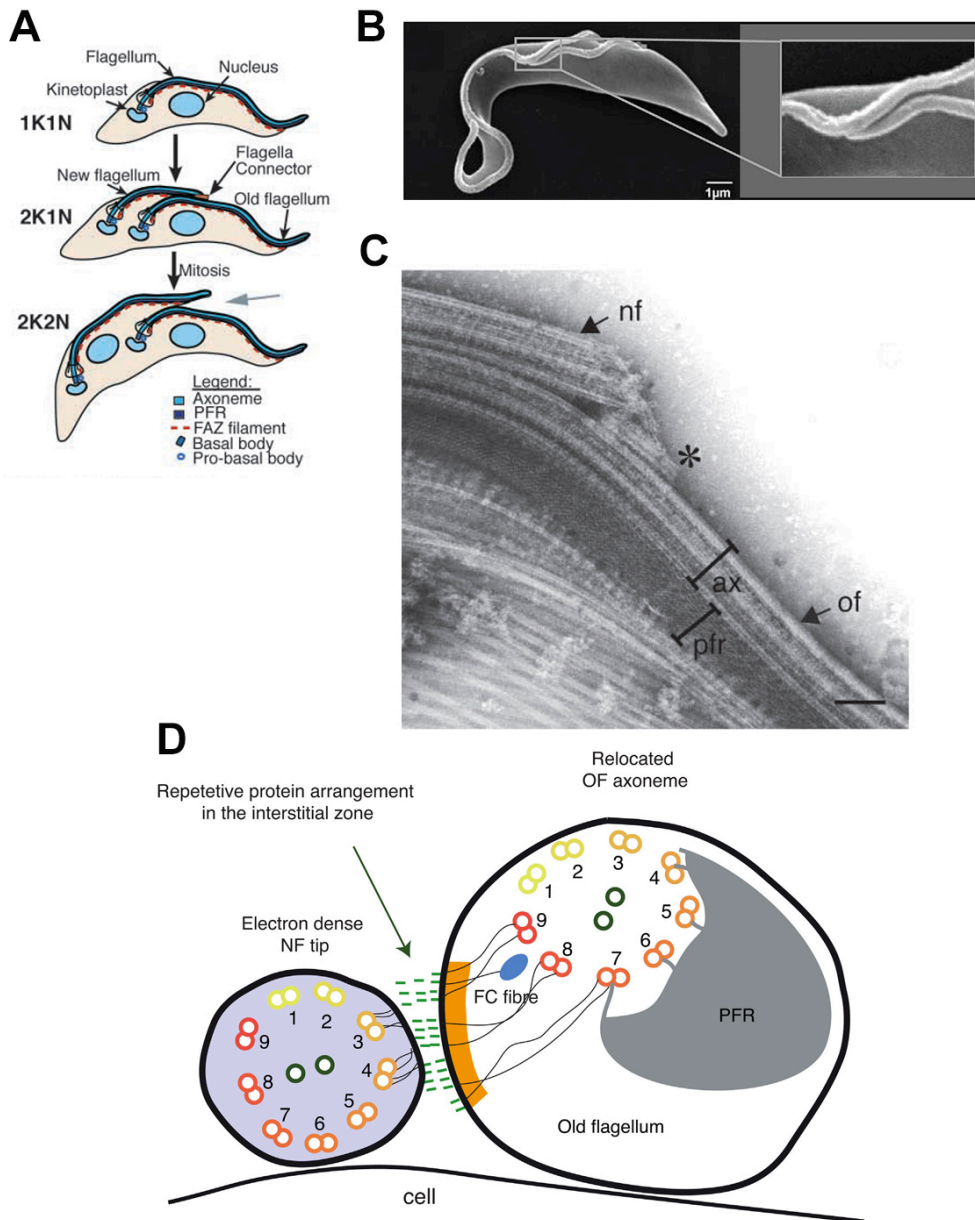


**Figure 19: The flagella connector.**

**(A)** Schematic representation of *T. brucei* procyclic cell cycle. At G1 phase the cell possesses one kinetoplast, one nucleus and one flagellum. During the cell cycle, new flagellum elongation occurs in parallel to basal body and kinetoplast segregations. The new flagellum is connected to the old flagellum via the flagella connector (FC) (Briggs, McKean et al. 2004). **(B)** Scanning micrograph of procyclic *T. brucei* where the new and old flagella are connected by the FC (zoom on this area) (Hoog, Lacomble et al. 2016) **(C)** Negative stained whole-mount cytoskeleton. The flagella connector (asterisk) is positioned at the tip of the new flagellum (nf) and along the axoneme (ax) of the old flagellum (of) (Briggs, McKean et al. 2004). **(D)** Cartoon showing the structure of the FC. Microtubule doublets of the axonemes connected to the FC are indicated. PFR: Paraflagellar rod (Hoog, Lacomble et al. 2016).

This filament is composed of multiple molecular components; some of them have been first identified using antibodies from infected patients or animals or from proteome analysis (Vaughan and Gull 2008, Sunter, Benz et al. 2015, Zhou, Hu et al. 2015). The FAZ1 protein was the first to be identified; it is a large protein (close to 200kDa) containing from 36 to 70 repetitions of a unique 14 amino-acid-sequence. This protein is not essential for FAZ filament assembly but its absence perturbs nucleus segregation and flagellum adhesion, further implicating this filament in cell morphogenesis (Vaughan and Gull 2008).

Transversal flagellar sections show the presence of filamentous structures that link the FAZ-associated membrane and the proximal domain of the PFR (Sherwin and Gull 1989). The flagellum attachment glycoprotein 1 (FLA1), a transmembrane protein with a very long extracellular domain that is highly glycosylated is also essential for flagellum attachment in *T. brucei* and *T. cruzi* (Cooper, de Jesus et al. 1993, LaCount, Barrett et al. 2002). The *T. brucei* FLA1-binding protein (FLA1BP) binds the flagellar membrane to the plasma membrane linking FAZ elongation to flagellum growth (Sun, Wang et al. 2013). On the axoneme side, a unique protein called FLAM3 was shown to be essential for flagellar connection (Rotureau, Blisnick et al. 2014, Sunter, Benz et al. 2015).

## VI. Flagella connector (FC)

During its elongation, the tip of the new flagellum of procyclic *T. brucei* is tethered to the lateral region of the old flagellum by a pyramidal structure termed the flagella connector (Moreira-Leite, Sherwin et al. 2001) (Figure 19). The flagella connector is separated in three plates with an overall width of ~90nm. The central core layer is ~18nm wide and is the thickest of the three layers. The layer closest to the old axoneme is the next thickest layer with ~16 nm and the layer closest to the tip of the new flagellum is the thinnest with ~13 nm (Briggs, McKean et al. 2004). A recent analysis described the protein composition of the flagella connector and revealed the existence of two kinesin motors. It was proposed that kinesins could contribute to the flagella connector movement along the old flagellum and render the connection

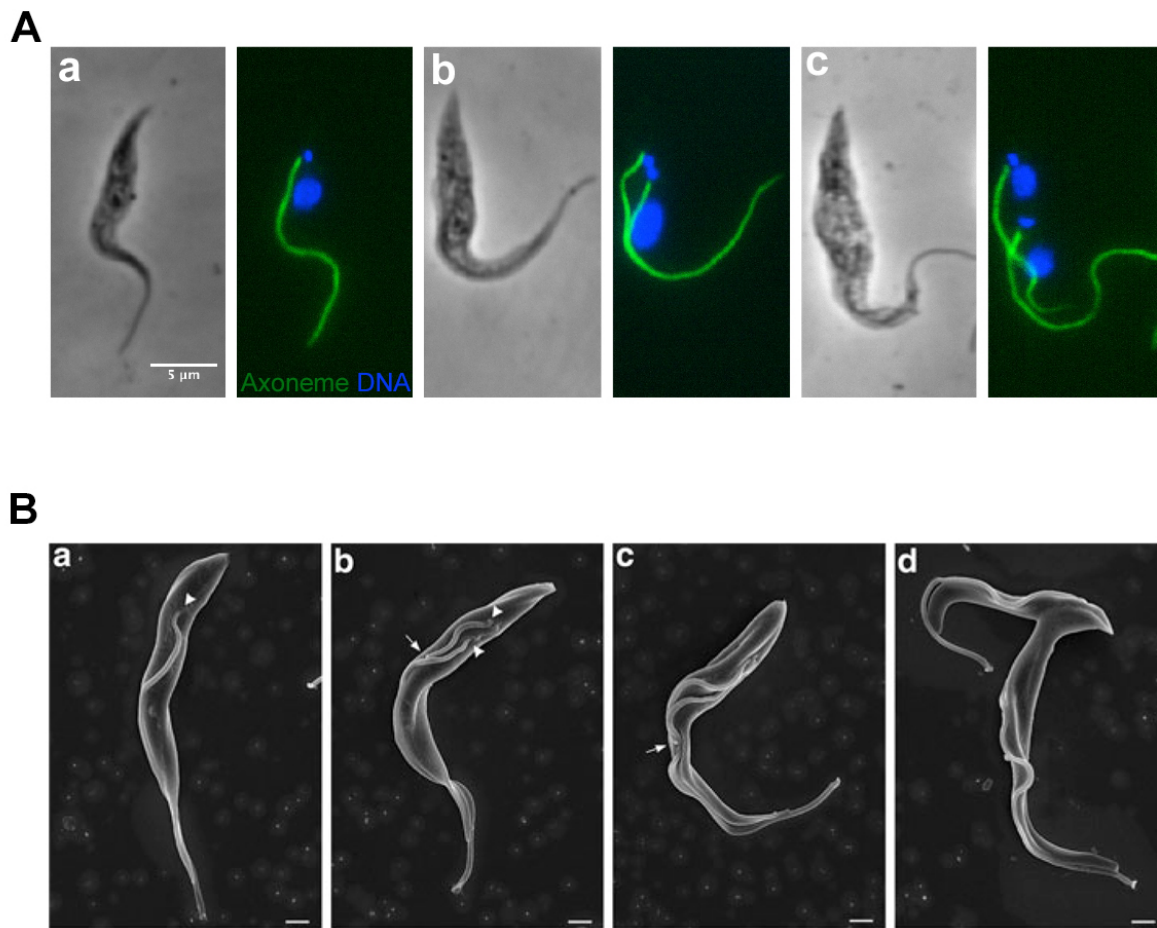


**Figure 20: The *T. brucei* procyclic cell cycle.**

**(A)** Immunofluorescence images of the different stages of the procyclic trypanosome cell cycle. **(a)** At the G1 stage, trypanosomes possess a single flagellum, one kinetoplast and one nucleus. **(b)** After basal body duplication, a new flagellum is assembled that is found in a posterior position relative to the old flagellum. **(c)** Mitosis occurs and the new flagellum further elongates. **(B)** Scanning electron microscope images of the different cell cycle steps in the procyclic cells. **(a)** A single flagellum emerges from the flagellar pocket (arrowhead) at the posterior end. **(b)** A new flagellum is assembled and emerges from its own flagellar pocket (arrowhead). Its tip elongates towards the anterior end of the cell in close proximity of the old flagellum (arrow). **(c)** The new flagellum continues to elongate with its distal tip physically connected to the old flagellum by the flagella connector (c, arrow). **(d)** Cell division takes place at the anterior end and progresses through the posterior end. At this final step, flagella are disconnected (Buisson and Bastin 2010) Scale bar: 1  $\mu\text{m}$ .

flexible robust and dynamic (Varga, Moreira-Leite et al. 2017). The flagella connector is associated to one side of the old flagellum axoneme and its tip is connected to the extremity of the elongating microtubules in the new flagellum (Figure 19 C and D). At the early steps of flagellum construction, the old and the new flagella are already connected in the same flagellar pocket by the flagella connector found in a distal position to the transition zone of the new flagellum. The flagella connector moves toward the distal end of the old flagellum in parallel to the growth of the new flagellum (Figure 19A) (Absalon, Kohl et al. 2007). During flagellum construction, the basal body of the new flagellum migrates towards the posterior end of the cell. Using (Trypanosome Basal Body Component) *TBBC<sup>RNAi</sup>* mutant where the new flagellum was disconnected from the old one, it was demonstrated that flagella connection is important for basal body migration (Absalon, Kohl et al. 2007). The flagella connector has not been found in bloodstream forms nor in *T. brucei*, in *T. cruzi* and in *Leishmania* species (Briggs, McKean et al. 2004).

### **b) Duplication of the flagellum during the cell cycle**

During its cell cycle, *T. brucei* grows a new flagellum in parallel to the maintenance of the existing one. In the G1 phase, a trypanosome cell possesses one kinetoplast (1K), one nucleus (1N) and one flagellum (1F) (Figure 20 Aa and Ba). During their cell cycle, BSF and PCF divide by binary fission without disassembling their cytoskeleton to produce two similar daughter cells after the duplication of all the organelles in a defined chronological order. First, the basal body duplicates and nucleates the formation of a new flagellum (NF) in an anterior position compared to the old flagellum (OF) (Sherwin and Gull 1989). During its elongation, the new flagellum migrates to a posterior position to emerge from a new flagellar pocket (Lacomble, Vaughan et al. 2010). Kinetoplast duplication and segregation start before mitosis, resulting in cells with two kinetoplasts, two flagella and one nucleus (2K2F1N) (Figure 20Ab and Bb). Kinetoplast segregation depends on basal body segregation (Robinson and Gull 1991). The microtubule corset elongates at the posterior end of the cell, resulting in an increase of 20% of the initial volume of the



cell (Sherwin and Gull 1989, Rotureau, Subota et al. 2011). The connection between the NF and the OF via the flagella connector during NF elongation induces the re-localisation of the new basal body-kinetoplast complex to the posterior end of the cell (Absalon, Kohl et al. 2007). NF elongation occurs in parallel to the construction of a new FAZ, allowing its attachment. Mitosis leads to cells with 2 kinetoplasts, 2 flagella and 2 nuclei (2K2F2N) (Figure 20 Ac). As in most protists, the nuclear membrane stays intact. The new flagellum keeps on elongating and cytokinesis is initiated from the anterior end of the cell. In PCF, the cell inheriting the NF is smaller than the cell retaining the pre-existing one. The ratio between the length of the NF and the OF in cells about to divide is close to 80% (Figure 20 Bd) (Robinson 1995, Subota, Julkowska et al. 2014). The NF continues growing after division until it reaches its definitive length and the cell can undergo then another duplication cycle.

### c) Roles of the trypanosome flagellum

#### I. Motility

*T. brucei* possesses a flagellum with the classical “9+2” characteristics; its motility is associated to ATP-dependent structural changes in the dynein arms connected to the A-tubule (Satir 1968). The flagellum is attached to the surface of the cell body and tracts the swimming trypanosome. Trypanosomes move due to the beating wave initiated at the tip of the flagellum and that propagates to the base. This wave is characterized by a low amplitude but a high frequency and is responsible for the forward movement (Hill 2003). The opposite wave causes the re-orientation of the cell, it starts from the base with a high amplitude and a low frequency and finishes at the distal tip. In high-viscosity medium, the proportion of trypanosomes undergoing propulsive motility increases as compared to liquid culture medium. To better understand this phenomenon, researchers monitored trypanosome motility in a homemade microfluidic environment containing silicone micropillars homogeneously distributed, yet with variable interspaces. Parasite exhibited maximal velocity when the pillar spacing was approximating that estimated for red blood cells in the

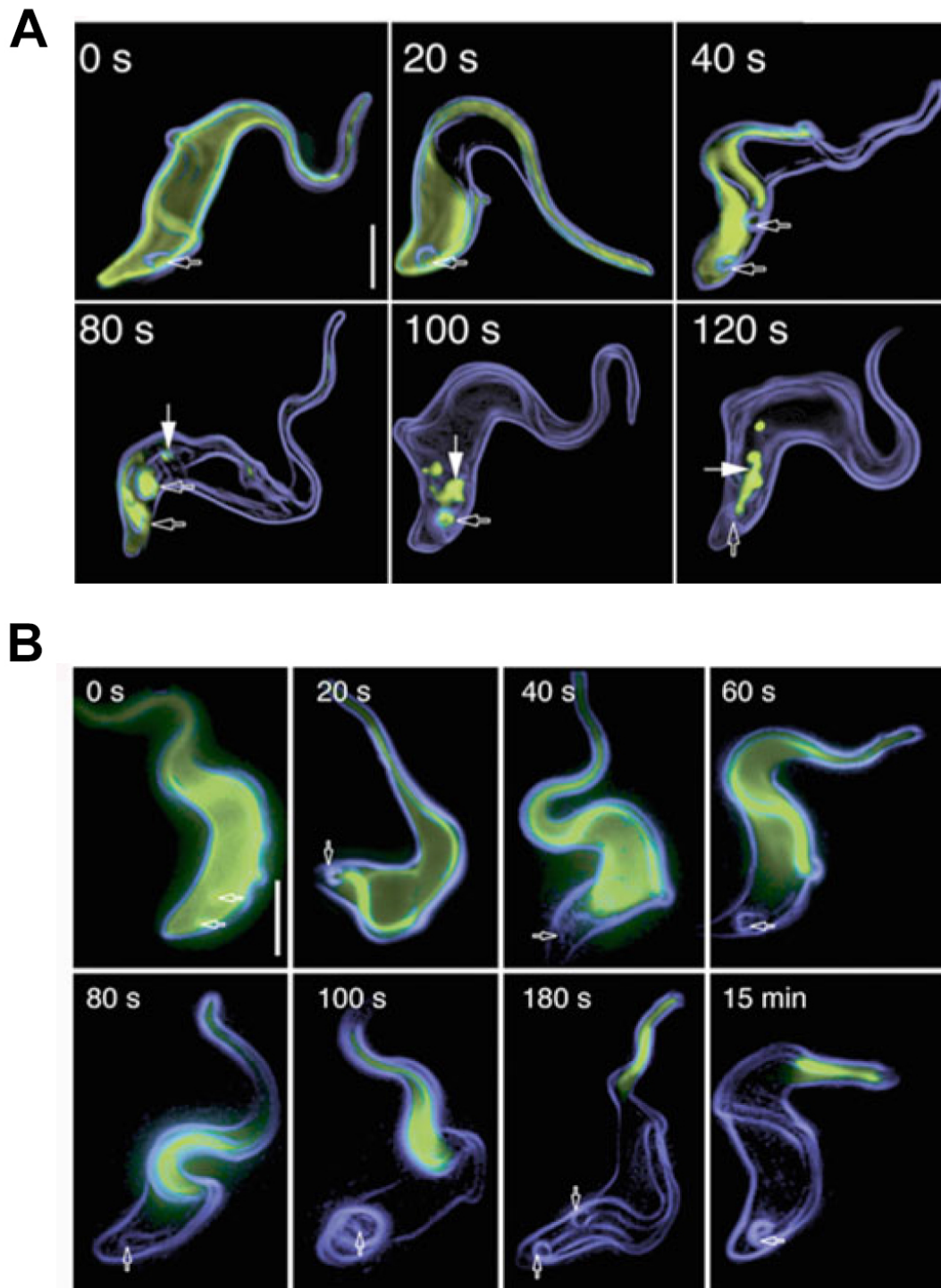


**Figure 21: The importance of the flagellum in *T. brucei* : Immune evasion.**

**(A)** Forward motility is essential in immune evasion to eliminate IgG-VSG complexes. Visualization of antibody removal. Cells were surface labelled with a blue-fluorescent dye and incubated for 10 min on ice with anti-VSG-specific IgG (green). Following 0-3 min of incubation at 37°C, cells were fixed and permeabilised. Open arrows indicate the position of the flagellar pocket, and filled arrows point to the lysosome. **(B)** The trypanosome *DNAI1<sup>RNAi</sup>* mutant shows backward motility and reversed direction of VSG-IgG movement with an accumulation at the anterior part of the cell. Scale bar: 3  $\mu$ m (Engstler, Pfohl et al. 2007).

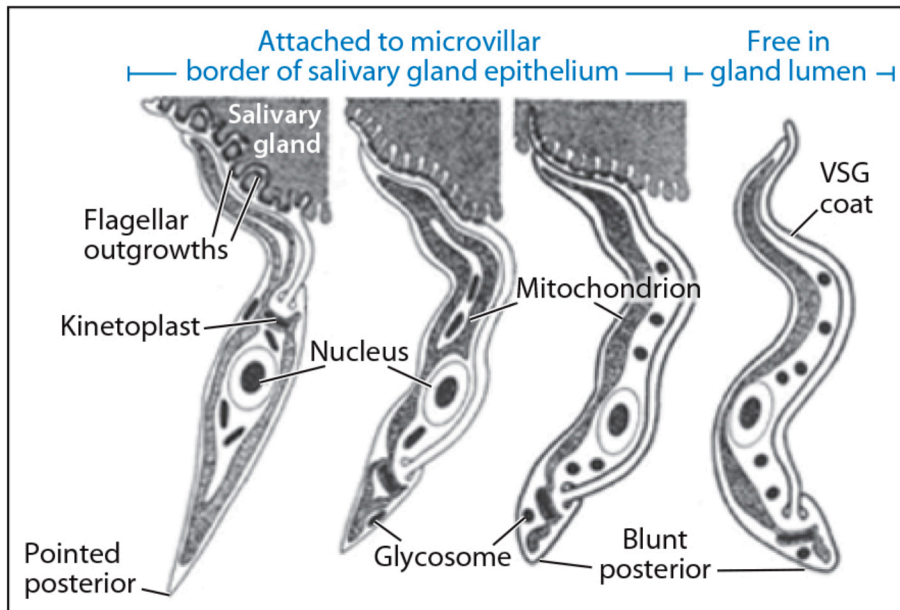
bloodstream, suggesting that trypanosomes have optimized their motility according to their environment (Heddergott, Kruger et al. 2012).

Trypanosome motility is crucial for parasite transmission and affects parasite virulence. In the mammalian host, the parasites circulate from the inoculation site to the dermis to finally penetrate the blood barrier endothelium and reach the central nervous system. Bloodstream parasites knockdown for the paraflagellar rod protein (PFR2), are rapidly cleared in mice potentially due to a reduction of their motility (Griffiths, Portman et al. 2007). In the insect vector, trypanosomes need to travel from the midgut to the salivary glands to be transmitted to the next mammalian host. Like in other eukaryotes, the dynein intermediate chain protein DNAI1 is essential for dynein arm assembly and its absence leads to forward motility defects (Branche, Kohl et al. 2006). A *DNAI1* null mutant strain is able to infect the midgut but fails to access the proventriculus and salivary glands, showing for the first time the role of motility in the insect vector (Rotureau, Ooi et al. 2014).

Flagellum motility is also crucial for the final step of the cell cycle. Once cytokinesis is almost complete when the two future daughter cells face each other, flagella point and swim in opposite directions allowing the separation of these two cells. Many paralyzed mutant fail to separate at this stage, a phenotype that can be compensated by shaking the culture flasks (Branche, Kohl et al. 2006, Broadhead, Dawe et al. 2006, Ralston, Lerner et al. 2006).

## II. Immune evasion

The flagellum of *T. brucei* is also essential for immune evasion. In mammals, bloodstream trypanosomes are exposed to the host immune system and particularly to antibodies against VSG proteins. Parasites are able to clear a part of these antibodies from their membrane by endocytosis in order to resist for longer to the immune system. Forward motility is required for this process to orientate the cells against the hydrodynamic flow that causes the “sailing” of immunoglobulins associated to VSGs at the cell surface toward the flagellar pocket, where they are captured by endocytosis (Figure 21A) (Engstler, Pfohl et al. 2007). The acidic

**A****B**

**Figure 22: The importance of the flagellum in *T. brucei*: salivary gland adhesion.**

**(A)** Diagram showing the different stages present in the tsetse salivary glands. The attached epimastigote use its flagellum to attach to the microvillar salivary gland epithelium. Metacyclics possess a VSG and are free in the saliva ready to be injected (Vickerman 1985, Ralston, Kabututu et al. 2009) **(B)** Electron microscopy section through the apical region of microvillar border of the tsetse salivary glands with attached flagella of *T. brucei*. The flagellar membrane has been highlighted in black. The membrane presents extensive outgrowth to create contact with salivary gland epithelium. Mv: Microvillosity Magnification x42 000

environment of the endosomes leads to dissociation of the antibodies from the VSG. VSG proteins are rapidly recycled and re-integrated in the parasite surface coat while the lysosome pathway eliminates the antibodies. In the *DNAI1<sup>RNAi</sup>* mutant, antibodies accumulate at the anterior end of the cell demonstrating the crucial role of forward motility in surface molecule recycling (Figure 21B) (Engstler, Pfohl et al. 2007).

### **III. Salivary gland adhesion**

In the tsetse salivary glands, the flagellum is essential for the colonization of the epithelium. The flagellum membrane of the attached epimastigote elaborates extensive outgrowths that create contacts with the epithelium microvilli of the salivary glands (Figure 22). The production of “hemidesmosome-like” junctions between the flagellar membrane and the host cell membrane creates strong physical links (Vickerman 1985). The adhesion to the epithelium prevents release of non-infective trypanosomes in the saliva during a blood meal. These close contacts may facilitate interactions with molecules present at the surface of host cells such as flagellar receptors that could initiate pathways essential for parasite adaptation at its new environment (metabolic responses, etc).

### **IV. Cell morphology**

Trypanosomes are highly polarized cells and during mitosis the respective positions of their organelles have to be maintained. As previously detailed, the emergence and the elongation of the flagellum are strictly linked to the cell cycle. Modifications of flagellum assembly by RNAi silencing targeting components of the IFT machinery (See section below) have important effects on cell morphology (Figure 23). Cells with a shorter flagellum are smaller than control cells, with an almost linear correlation between flagellum and cell length (Kohl, Robinson et al. 2003). This is accompanied by restricted elongation of the FAZ and reduced body migration. It was shown that this is not due to a defect in cell body elongation but rather to a mispositioning of the cleavage furrow suggesting that the tip of the FAZ could define the point of initiation

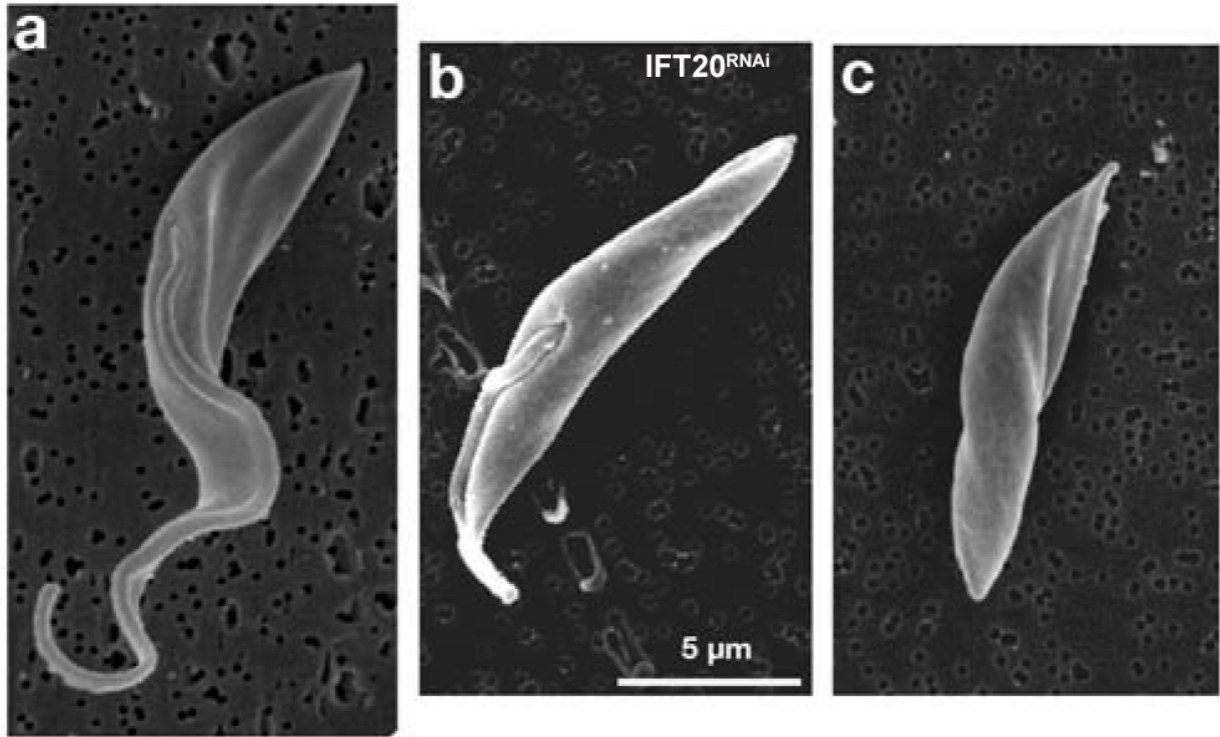


**Figure 23: The importance of the flagellum in *T. brucei*: cell morphology.**

Scanning electron micrographs of *IFT20<sup>RNAi</sup>* cells induced for 72h. (a) cells with normal flagellum (b) with short flagellum and (c) no flagellum. Disruption of the flagellum assembly machinery (IFT) by RNAi silencing targeting one of its component leads to the formation of short cells with small flagellum and smaller cell body (Absalon, Kohl et al. 2007)

of division. RNAi knockdown of CC2D, a structural protein of the FAZ, disrupted elongation of the FAZ filament and led to the formation of smaller cells confirming the importance of the FAZ in defining cell length (Zhou, Liu et al. 2011).

### **V. Sensory functions**

During their complex parasite cycle, trypanosomes need to detect signals from their surrounding microenvironment in order to activate or repress the appropriate differentiation programs as well as to evade the antimicrobial host immune responses. Recently cilia and flagella have emerged as critical sensory organs for unicellular or multicellular organisms (Singla and Reiter 2006). They can be compared to cellular antenna due to their positioning at the cell surface and to the original composition of their membrane that is enriched in lipid raft platforms known to organize trans-membrane signalling events (Tyler, Fridberg et al. 2009). Some proteins present at the surface of the flagellum in bloodstream forms have been characterized by proteomic analysis. The proteins identified take in a large range of molecular functionalities, including many candidates to signalling functions and host-parasite interactions (Oberholzer, Langousis et al. 2011). These include adenylate cyclases and calflagins that are predicted to function in host-parasite signalling. Moreover, uncharacterized flagellum surface proteins have been identified. They possess domain architectures typical of cell surface receptors with a large extracellular domain suitable for binding host ligands and an intracellular signalling module compatible with receptor functions (Oberholzer, Langousis et al. 2011).



## III. Flagellum biogenesis

---

### 1) History

Cilia and flagella are sophisticated organelles that exhibit a complex structure and molecular composition. Proteomic studies of purified *Chlamydomonas* flagella revealed that it contains more than 600 proteins (Pazour, Agrin et al. 2005). Other studies in different organisms confirmed this molecular complexity. In *T. brucei*, the cytoskeletal scaffold of the flagellum is composed of at least 330 different polypeptides (Broadhead, Dawe et al. 2006, Oberholzer, Langousis et al. 2011). However, mass spectrometry analysis performed on intact flagella of procyclic stage cells identified a total of 751 proteins and revealed the existence of 212 proteins that were not previously reported to be associated with flagella (Subota, Julkowska et al. 2014). All these proteins need to be assembled at the right place and at the right time. Since their discovery, the ultrastructure of cilia and flagella has been extensively studied by electron microscopy and understanding the mechanisms responsible for their construction and length control have attracted the interest of biologists for decades.

The first experiment describing flagellum assembly was performed 50 years ago using four different species of flagellated protozoa (*Astasia*, *Chlamydomonas*, *Euglena* and *Ochromonas*) (Rosenbaum and Child 1967). Rosenbaum and colleagues followed flagellum regeneration after amputation, focussing on the kinetic of the process. They showed that there was a lag phase during which there was no apparent growth followed by a rapid growth of the flagellum that ended in a slow elongation phase as the original length of the organelle was reached. The lag phase was highly reproducible, although its duration and the regeneration rate were specific to each species without any relations with the expected final flagellum length. The lag phase could be associated to the production of flagellar components. To test this hypothesis, cycloheximide (an inhibitor of protein synthesis) was added just after

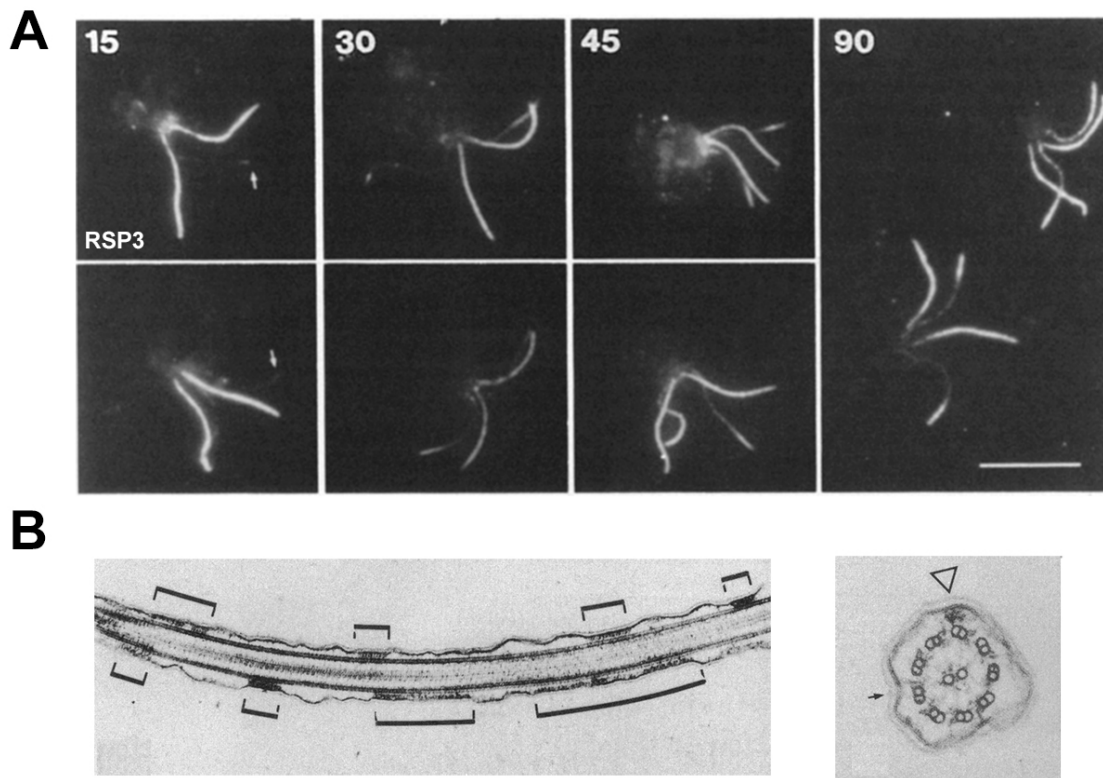


**Figure 24: Flagellum assembly: first discoveries.**

**(A)** Visualisation of the flagella assembly site in *Chlamydomonas*. Immunofluorescence images obtained after staining mating algae cells with an antibody directed against the radial spoke protein 3 (RSP3) in *Chlamydomonas*. 15 min after mating between wild-type algae and mutant cells that lacked radial spokes. RSP3 is localised along full lengths of the two wild-type axonemes, whereas no signal is detected in the two mutant axonemes indicated with arrows. An increasing signal progressively appears at the distal tips of these two mutated flagella observed for 90 minutes. Scale bar: 10  $\mu\text{m}$ . Adapted from (Johnson and Rosenbaum 1992)

**(B)** Electron micrographs of longitudinal (left) and cross (right) sections of *Chlamydomonas* flagella. In the longitudinal sections, IFT particles appear as a linear array distinct from the membrane (bold segments). In the cross section, IFT particles appear as electron-dense material between the axonemal microtubules and the membrane (big arrowhead) (Kozminski, Johnson et al. 1993)

deflagellation and this resulted in an inhibition of flagella elongation. In contrast, addition of the inhibitor after the lag phase was followed by the production of a flagellum with a length of around 10  $\mu\text{m}$  (half of their normal size) before the elongation stopped. This means that the synthesis and accumulation of flagellar proteins necessary for elongation was occurring during the lag phase (Rosenbaum and Child 1967).

The first flagellar components whose incorporation was revealed *in vivo* were tubulin and radial spoke protein 3 (RSP3). By using donor *Chlamydomonas* cells expressing tagged tubulin or RSP3 in their flagella and fusing them with wild type cells, Johnson *et al.* followed the incorporation of tagged proteins in wild type flagella. They revealed that the assembly site of the tagged protein was at the distal tip of the organelles (Figure 24A) (Johnson and Rosenbaum 1992). Although the axonemal components were incorporated at the distal tip, the delivery system was still unknown. Flagellar components were thought to be delivered actively via unknown transport mechanisms or passively, by diffusion.

Less than one year later, the system necessary to deliver building block from the base to the tip of the flagellum was discovered using differential interference contrast (DIC) microscopy to observe paralyzed flagella of *Chlamydomonas*. Kozminski *et al.* revealed the presence of two distinct sets of granule-like particles moving along the flagellum in a manner independent of flagellum beating. First, some particles moved from the base to the tip of the flagellum at a speed of  $\sim 2\mu\text{m}/\text{sec}$  and others travelled in the opposite direction at  $\sim 3.5\mu\text{m}/\text{sec}$  (Kozminski, Johnson *et al.* 1993). Second, the movement of these particles was dependent on FLA10, a subunit of the heterotrimeric kinesin II complex (Kozminski, Beech *et al.* 1995). The *Chlamydomonas* FLA10 null mutant cells have wild-type flagella at the permissive temperature ( $20^{\circ}\text{C}$ ) and resorb their flagella at the restrictive temperature ( $33^{\circ}\text{C}$ ) due to the absence of FLA10 subunit. In this mutant, the incorporation of tagged proteins at the distal tip of the flagellum was not observed any more. The process was termed IntraFlagellar Transport (IFT).

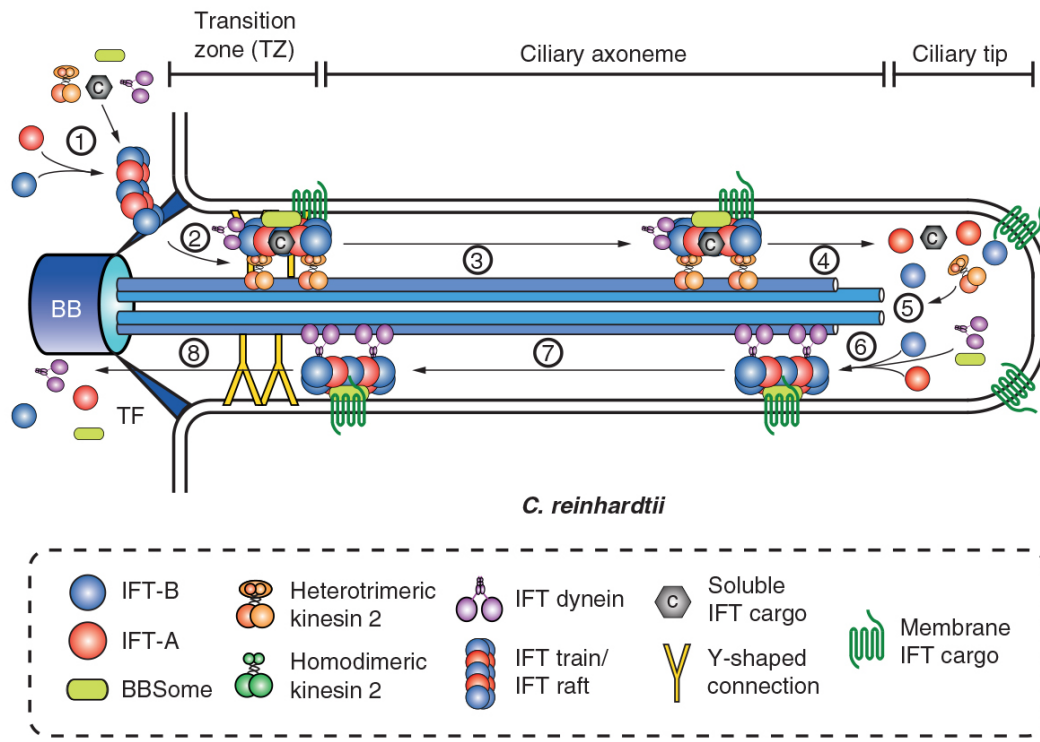


**Figure 25: Schema of IFT process in *Chlamydomonas*.**

Schematic representation of the main steps of Intraflagellar transport in *Chlamydomonas*. (1) Assembly of IFT-A and IFT-B proteins, kinesin (active) and dynein motors (as a cargo) and other cargo proteins such as the tubulin. (2) IFT trains enter into the cilium and (3) move toward the tip. (4) IFT trains are remodelled and cargo proteins are released. (5) Kinesins going back independently from the other components to the base (6) Activation of the dynein motor and formation of retrograde trains (7) Retrograde transport to return to the ciliary base (8) Exit from the ciliary compartment. BB: Basal body (Taschner and Lorentzen 2016).

## **2) Intraflagellar Transport (IFT)**

Intraflagellar transport (IFT) is the motor-dependent and bidirectional microtubule-based movement along the axoneme of multi-protein complexes called IFT particles or IFT trains (Pedersen and Rosenbaum 2008). IFT can be decomposed in several steps: (1) entry of IFT proteins into the axoneme compartment, (2) assembly of trains, (3) loading of trains with cargo proteins, (4) transport of IFT trains towards the distal tip using kinesin motors (anterograde transport), (5) reorganisation of IFT trains at the distal tip, (6) return to the ciliary base driven by dynein motors (retrograde transport) and (7) finally exit or recycling of IFT proteins (Figure 25). It was shown that IFT is involved in flagellum assembly, maintenance and signalling functions depending on the organism. Four different situations have been encountered so far regarding the contribution of IFT in flagellum construction and maintenance. First, IFT is active in both growing and mature flagella and is essential for both construction and maintenance of flagellum length, as shown in *Chlamydomonas* (Marshall and Rosenbaum 2001). Second, IFT is only active during flagellum construction and becomes absent once the organelle has reached its full length. This case has been reported in mouse spermatozoa where IFT proteins are highly abundant during flagellum elongation but are not detectable in mature spermatozoa (San Agustin, Pazour et al. 2015). Third, an intermediate situation has been described in *T. brucei* where IFT is active in both growing and mature flagella but is essential only for the construction and not for flagellum length maintenance (Fort, Bonnefoy et al. 2016). Fourth, IFT is not required for flagellum construction when the latter one takes place in the cytoplasm, as described for male gametes in *Plasmodium* and *Drosophila* (Han, Kwok et al. 2003, Briggs, McKean et al. 2004).

### **a) The IFT trains**

By using correlative light microscopy and transmission electron microscopy (TEM) in *Chlamydomonas* flagella, it was demonstrated that the IFT particles consist of linear

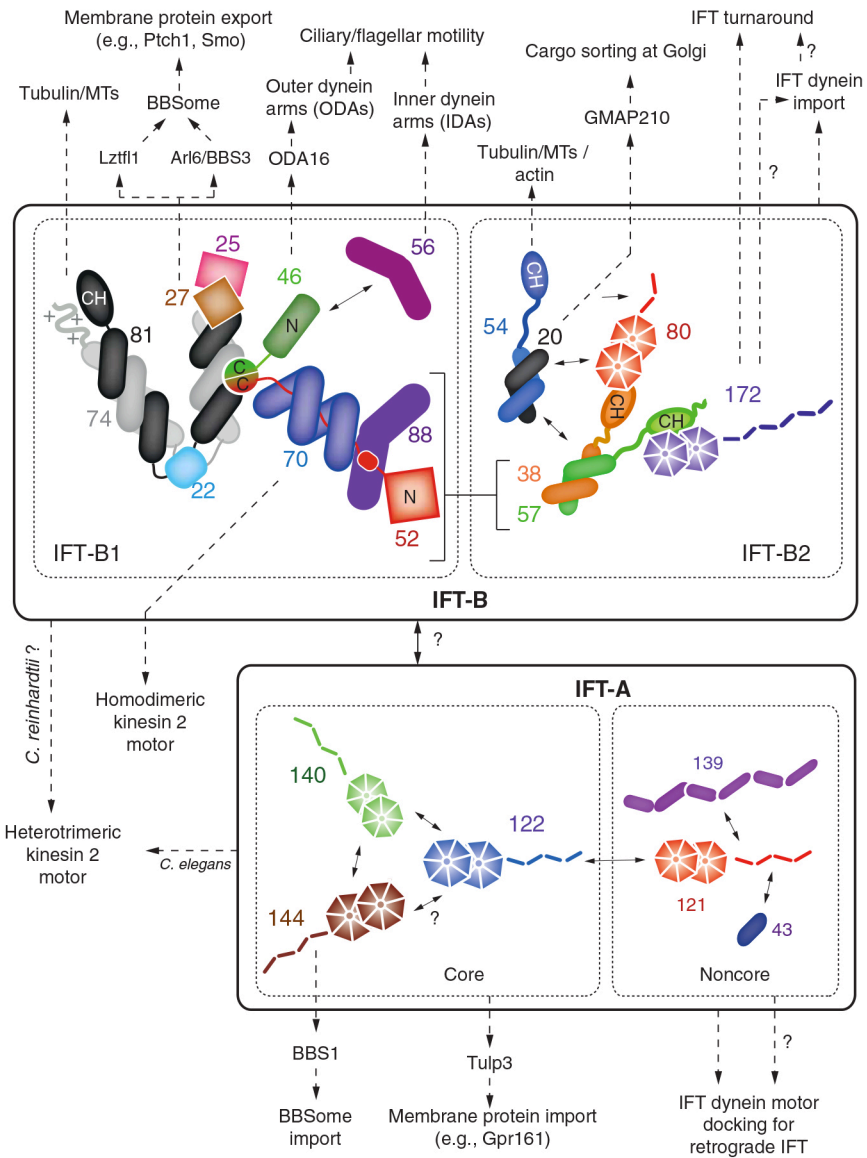


**Figure 26: Schematic representation of the IFT-A and IFT-B complexes in *Chlamydomonas*.**

Schematic map of the predicted interactions between different proteins of the IFT complexes (Taschner and Lorentzen 2016).

arrays of lollipop-shaped structures located between the outer doublet microtubules and the flagellar membrane (Figure 24B) (Kozminski, Beech et al. 1995). The identity of these electron-dense structures was confirmed by immunogold labelling with antibodies directed against kinesin motors and later on IFT proteins (Kozminski, Beech et al. 1995, Pedersen, Geimer et al. 2006). IFT trains were first isolated from the matrix of *Chlamydomonas* flagella, which allowed identifying a “17S” complex made of at least 13 different polypeptides (Piperno and Mead 1997). Following this study, the purification of IFT particles revealed the existence of 15 polypeptides forming a complex that dissociated at increasing ionic strength into two biochemically distinct sub-complexes called IFT-A and IFT-B (Cole, Diener et al. 1998). Presently, 20 IFT proteins have been identified and characterised. The IFT-B complex is composed of at least 14 subunits and the IFT-A complex consists of 6 subunits (Figure 26) (Taschner, Bhogaraju et al. 2012). The different proteins of these two IFT complexes were named according to their apparent molecular weight in *Chlamydomonas* as judged by migration in SDS-PAGE. IFT polypeptide orthologues were found in most ciliated / flagellated eukaryotes suggesting a high conservation throughout evolution (Pazour, Baker et al. 2002, Follit, Xu et al. 2009). It has been proposed that the IFT complexes originated from vesicle coat similar to coat protein complex and clathrin (Avidor-Reiss, Maer et al. 2004, Li, Gerdes et al. 2004). Recently, the origins and acquisition of the IFT system were studied by comparing the genome of 52 different ciliated and non-ciliated eukaryotes. This suggests that the BBSome (an octameric protein complex involved in trafficking cargos into the primary cilium) and IFT-A emerged from an IFT-B-like complex by intra-complex duplications (van Dam, Townsend et al. 2013). It is proposed that the cilium emerged in association with a “proto-IFT” complex itself derived from protocoatamer, followed by the acquisition of the IFT-A complex and the BBSome. This is the likely situation of the last common eukaryotic ancestor. For non-ciliated species, one could imagine a scenario with successive loss of the BBSome, the IFT-A subcomplex and ultimately the IFT-B complex. Intermediate with less elaborate cilia have been observed (van Dam, Townsend et al. 2013). In general, mutations in proteins of the IFT-B complex result in the formation of abnormally short or absent flagella suggesting a role of the IFT-B complex in anterograde transport (Figure 27) (Pazour, Dickert et al. 2000,



Absalon, Blisnick et al. 2008). By contrast, defects in IFT-A proteins lead to the apparition of short flagella full of IFT proteins, suggesting a role of the IFT-A complex in retrograde transport (Figure 28). In this case, IFT trains can enter and travel toward the tip of the flagellum by anterograde transport but cannot go back to the base. These results not only showed that IFT-A and IFT-B complexes are biochemically distinct complexes, but also indicated that they have specific and distinct roles in the IFT process.

### **b) IFT-B complex**

Bioinformatics analyses of IFT protein sequences revealed the existence of well-known protein:protein interaction domains such as tetra-tricopeptide repeats (TPRs), WD-40 repeats, and coiled coils domains, consistent with their assembly into large macromolecular complexes and with their predicted binding to ciliary cargo proteins (Taschner, Bhogaraju et al. 2012). The IFT-B complex can be separated in two sub-complexes, a salt-stable complex called IFT-B core (IFT-B1) and a peripheral complex (IFT-B2) dissociated at a NaCl concentration of 300mM (Figure 26).

#### **I. The IFT-B core (IFT-B1)**

The IFT-B core was first isolated from *Chlamydomonas* and consisted of 6 proteins (IFT88, 81, 74, 52, 46 and 27) (Lucker, Behal et al. 2005) to which four newly identified members were added later on (IFT70, 25, 22 and 56) (Lechtreck, Luro et al. 2009, Wang, Fan et al. 2009, Fan, Behal et al. 2010). Most of the IFT-B core members are essential for ciliogenesis and the absence of one of these factors leads to severe defects in cilium assembly. The most studied protein is IFT88 that is essential for flagellum formation in *Chlamydomonas*, *T. brucei*, *C. elegans* and its mutation is associated to kidney disease in mammals. Indeed, the mouse lineage with a hypomorphic mutation in the *Tg737* gene (an orthologue of IFT88) is a classic model to study polycystic kidney and presents very short cilia at the surface of kidney epithelial cells (Pazour, Dickert et al. 2000). IFT88 plays a central role in the

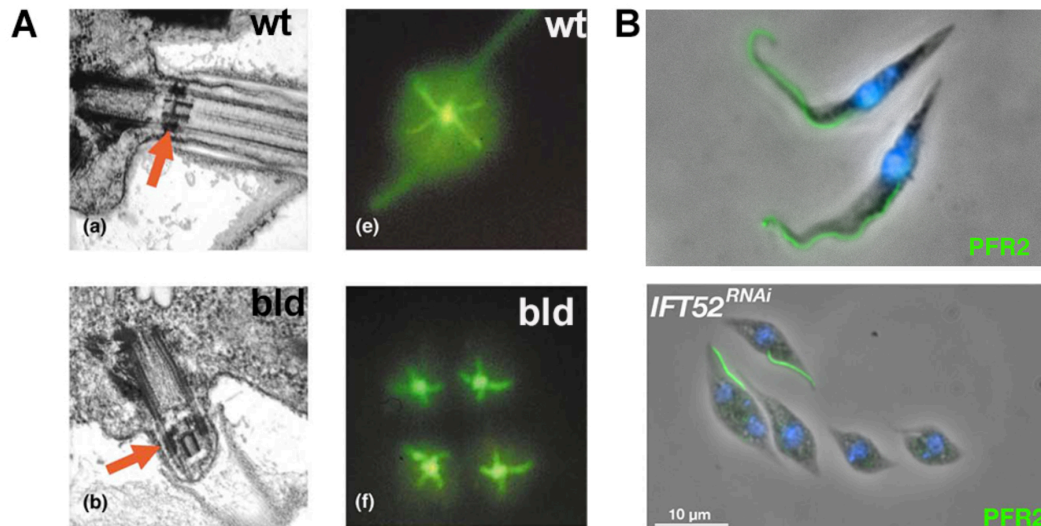


**Figure 27: Absence of on IFT-B protein results in defect in flagellum formation.**

**(A)** Electron microscopy images of wild-type (wt) (top) and IFT52 *Chlamydomonas* mutant (called *b/b*) (bottom). WT cells present normal transition zone (red arrow) and normal axoneme whereas in *b/b* mutant no cilium assembly occurs but the transition zone (red arrow) looks normal. Immunofluorescence images using an antibody against  $\alpha$ -tubulin, the cruciform array of stable microtubules found in the cells remains unaffected (Brazelton, Amundsen et al. 2001). **(B)** Immunofluorescence with antibody against PFR2 in IFT52<sup>RNAi</sup> mutants non-induced (top panel) and induced (bottom panel) of *T. brucei* after RNAi induction. When IFT52 is absent, cells possess short flagellum (two cells) or they are not able to construct flagellum (Absalon, Blisnick et al. 2008).

interaction between IFT-B1 and IFT-B2 via its TPR domains (Taschner, Weber et al. 2016).

It was shown that IFT52 occupies a central position and interacts with other IFT-B core members such as IFT46/70/88 as well as with the tetramer formed by IFT81/74/27/25 suggesting that IFT52 plays a crucial role in IFT-B assembly and stability. The *IFT52* gene is mutated in the *bld1 Chlamydomonas* strain. The mutation leads to the production of 'bald' algae that are unable to construct flagella (Brazelton, Amundsen et al. 2001) (Figure 27A). This protein travels along the axoneme of *T. brucei* and *C. elegans*, and is essential for cilium formation since its disruption triggers the apparition of cell without flagellum (Figure 27B) (Collet, Spike et al. 1998, Absalon, Blisnick et al. 2008).

*In vitro*, IFT81 and IFT74 form a stable complex with IFT27/25 (Taschner, Bhogaraju et al. 2011). IFT81/74 contain calponin-homology (CH) domains known to recognize and bind tubulins (Bhogaraju, Cajanek et al. 2013). *In vitro* it was shown that the IFT81 CH domain binds tubulin with a low affinity that was reinforced by interactions of the E-hooks with the high basic end of IFT74.

IFT22/RABL5 is a small G-protein first discovered in *C. elegans*. In the nematode, IFT22 is not essential for cilium formation (Ishikawa, Ide et al. 2014). By using *in vivo* imaging of GFP fusion proteins it was shown that IFT22 traffics within the cilium (Ishikawa, Ide et al. 2014). The *T. brucei* IFT22 also traffics in the flagellum but by contrast, its depletion induced the formation of very short flagella where IFT material accumulates (Adhiambo, Blisnick et al. 2009). Another small G protein called IFT27 was first characterized in *Chlamydomonas* and proposed to be essential for flagellum formation and cytokinesis (Qin, Wang et al. 2007). IFT27 forms a stable complex with IFT25 (Wang, Fan et al. 2009). In *T. brucei*, IFT27 is essential for retrograde transport by controlling the entry of the IFT dynein (Huet, Blisnick et al. 2014).

IFT56 and IFT70 are also part of the IFT-B core. IFT70 has first been identified in *C. elegans* (DYF-1) and is thought to link the homodimeric motor OMS-3 to the IFT-B complex (Ou, Blacque et al. 2005). A recent study in mammalian cells shows that the homodimeric kinesin motor KIF17 interacts with IFT46-IFT56 dimer and this interaction is essential for KIF17 entry in the ciliary compartment (Funabashi, Katoh et al. 2017). IFT56 plays a role in IFT-B core complex stability and its contribution to



flagellum construction is variable (Lucker, Miller et al. 2010, Taschner, Bhogaraju et al. 2011). Knockdown of IFT56 in zebrafish embryos or mutation in *Chlamydomonas* leading to the production of a truncated IFT56 proteins did not interfere with train speed or frequency, but resulted in the formation of shorter flagella (Inglis, Blacque et al. 2009, Ishikawa, Ide et al. 2014). In *T. brucei* IFT56 is essential for ciliogenesis exactly like other IFT-B proteins (Absalon, Blisnick et al. 2008).

## II. The Peripheral IFT-B complex

The peripheral IFT-B complex is composed by IFT172, IFT80, IFT57, IFT54 and IFT20. These proteins can be dissociated from the IFT-B core complex with high NaCl concentration, suggesting a potential peripheral localisation (Lucker, Behal et al. 2005, Taschner, Bhogaraju et al. 2011, Taschner, Weber et al. 2016). The first four proteins seem to have an important role in IFT regulation. For example, IFT172 plays a role in the transition between anterograde and retrograde transport. In *Chlamydomonas*, IFT172 is encoded by *FLA11*. When *fla11* is point mutated in *Chlamydomonas*, there is an accumulation of IFT material at the distal tip of the flagellum (Pedersen, Miller et al. 2005). However, this was not observed in *T. brucei* *IFT172* knockdown mutant (Absalon, Blisnick et al. 2008). These differences could be due to the different approaches used to generate the *IFT172* mutants. Indeed RNAi is characterized by a strong reduction in protein abundance; while the point mutation leads to the production of malfunctioning protein.

In mammals, IFT20 does not only localize to the cilium but also to the Golgi complex and it was proposed that IFT20 could be involved in membrane protein sorting before entering the cilium (Follit, Tuft et al. 2006). In *T. brucei* and *Chlamydomonas*, IFT20 is essential for flagellum assembly but it is not found in the Golgi apparatus (Absalon, Blisnick et al. 2008). IFT54 possesses a CH-domain tubulin binding that could contribute to the transport of two tubulin subunits per IFT-B complex (with the domain present on IFT81/74) compatible with the kinetics of ciliogenesis in *Chlamydomonas* (Taschner, Weber et al. 2016).

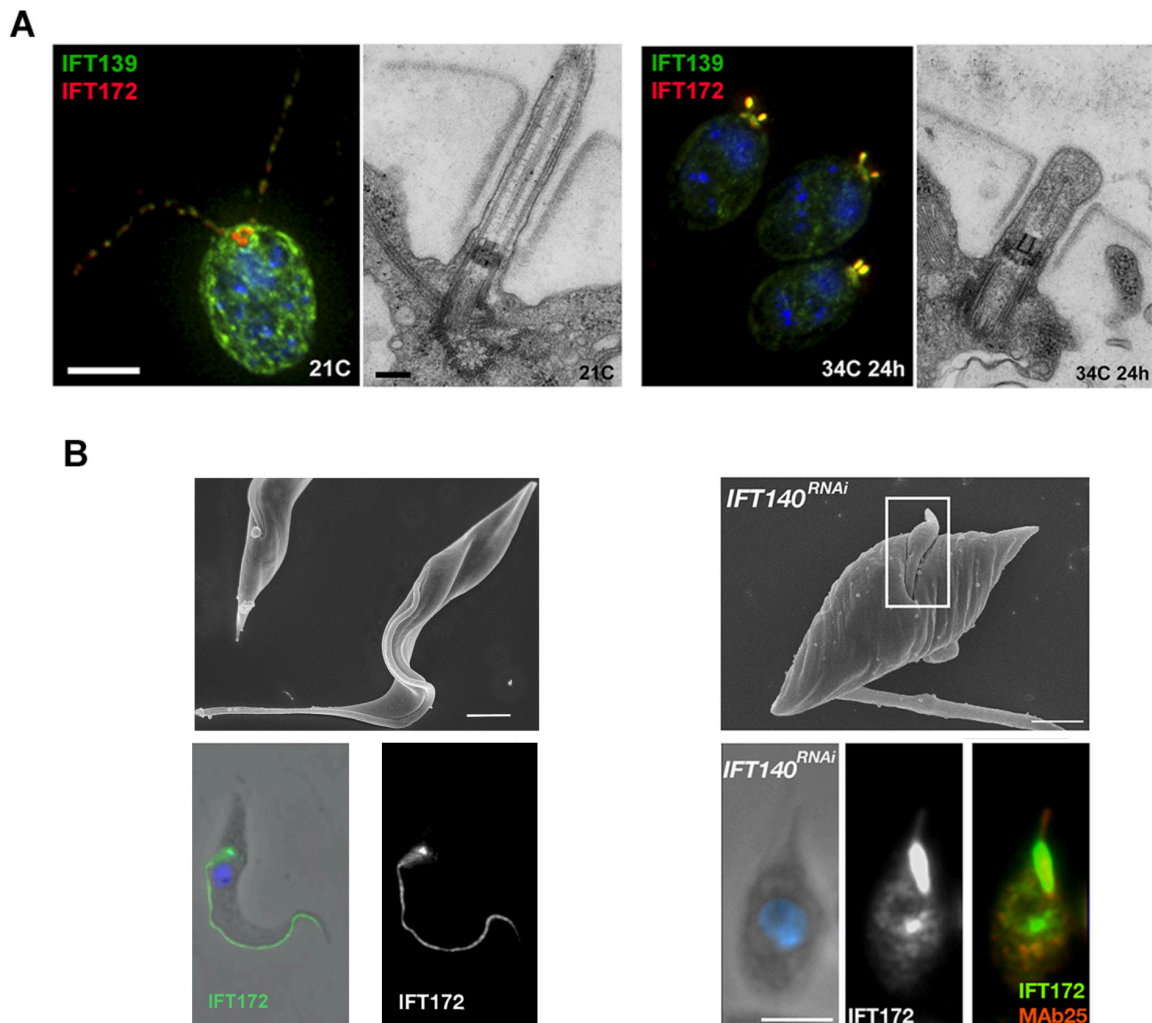


### Figure 28: Phenotypes caused by defects in retrograde IFT.

Disruption of the IFT-A components leads to the formation of short flagella full of IFT material (**A**) *Chlamydomonas* temperature-sensitive *dhc1b-1* mutant. At 21°C the mutant appeared to have a regular distribution of IFT proteins along the flagella. At 34°C flagella appear smaller and a strong accumulation of IFT proteins in these flagella is visible. This accumulation is also visible on TEM images, where dense material is visible in the flagellum. Scale bare 5μm (IFA) and 200nm (TEM) (Engel, Ishikawa et al. 2012). (**B**) Localization and distribution of IFT172 protein in wild-type procyclic and *IFT140<sup>RNAi</sup>* trypanosome mutants. In wild-type flagellum, IFT172 is present all along the flagellum and at its base. In *IFT140<sup>RNAi</sup>* trypanosome mutants' a strong accumulation of IFT protein is visible in the small flagellum. Scanning electron image showing wild type cell with a long flagellum attach to the cell body and *IFT140<sup>RNAi</sup>* mutant that exhibit short and dilated flagellum. Scale bar: 1μm (Absalon, Blisnick et al. 2008).

### **c) The IFT-A complex**

The IFT-A complex is made of 6 proteins, and with the exception of IFT43, they have a molecular weight superior to 120kDa and a similar domain organization. Most of their protein sequences exhibit some similarity with the presence of WD-40 repeats at the N-terminal region and TPRs at the C terminal part. Co-immunoprecipitation experiments suggested the existence of a core sub-complex made of IFT144, IFT140 and IFT122 (Mukhopadhyay, Wen et al. 2010).

IFT140 is the most studied IFT-A protein. In *T. brucei*, RNAi knockdown of *IFT140* expression induced the formation of short flagella full of IFT172 proteins, indicating a default in retrograde transport (Figure 28B) (Absalon, Blisnick et al. 2008). In *Drosophila*, a similar phenotype was observed as well as defaults in mechanosensory functions (Lee, Sivan-Loukianova et al. 2008).

By contrast, IFT122 seems to play different roles depending on the organism. In *Tetrahymena thermophila*, the protein is not required for cilia assembly but for efficient return of IFT proteins from the ciliary tip to the cell body (Tsao and Gorovsky 2008). The trypanosome orthologue of IFT122 is required for retrograde IFT whereas the *IFT122* mutant mice display an anterograde phenotype with defective Sonic hedgehog signalling (Absalon, Blisnick et al. 2008, Cortellino, Wang et al. 2009).

### **d) The IFT associated motors**

According to DIC microscopy and GFP-tagged fusion proteins in *Chlamydomonas*, IFT trains travel at an average speed of ~ 2µm/sec in anterograde direction and ~ 4µm/sec in retrograde direction. Other live-cell studies confirmed the existence of two different speeds associated to each transport in *T.brucei*, *C. elegans* and primary cilia (Hsiao, Tuz et al. 2012, Buisson, Chenouard et al. 2013). Two microtubule-based motors drive IFT: kinesin-2 and cytoplasmic dynein 1b, which are respectively associated to the anterograde and retrograde movements of IFT particles along the axoneme.



## Introduction

The first motor family to be identified was kinesin-2 after purification from sea urchin eggs. This is a trimeric complex displaying a movement towards the (+) ends of microtubules (Cole, Chinn et al. 1993). Further studies revealed that this complex was made of KIF3A and KIF3B, two kinesin-related motors and a kinesin-associated protein (KAP). In *Chlamydomonas*, kinesin localization between microtubules and the ciliary membrane was demonstrated by immunogold using an antibody against the protein FLA10, a subunit of the trimeric kinesin complex (Kozminski, Beech et al. 1995). The inactivation of *FLA10* induces a dramatic reduction of IFT frequency and a default in ciliogenesis. Likewise, the disruption of the kinesin-2 protein in mice embryos led to the absence of nodal cilia that are essential to establish the left-right asymmetry during embryogenesis (Nonaka, Tanaka et al. 1998).

In *C. elegans*, two types of kinesin complexes participate to anterograde transport. In this organism, sensory cilia are made of two different parts called the middle and distal segments. The middle segment is made of nine doublet microtubules whereas the distal segment consists of nine singlet microtubules extending from the middle segment toward the distal tip. In these particular cilia, heterotrimeric kinesin-2 cooperates with a second motor called OSM-3 that is made of two identical subunits but that does not contain a KAP. These two motors travel together along the middle segment. When arriving at the end of the middle segment, the kinesin-2 motors undergo turnaround and liberate OSM-3. The OSM-3 motor continues moving to reach the distal end of the axoneme and construct the distal segment. The *osm-3* mutants are still able to build the middle segment of the axoneme, suggesting that kinesin-2 and OSM-3 can travel independently (Snow, Ou et al. 2004). Conversely, the absence of kinesin-2 leads to the formation of apparently normal cilia constructed by OSM-3 alone (Pan, Ou et al. 2006). The genome of *T. brucei* encodes two kinesin II proteins potentially forming a homodimer but no kinesin-associated protein (KAP) (Julkowska and Bastin 2009).

The second molecular motor implicated in IFT is cytoplasmic dynein 1b. The dynein heavy chain (*DHC2*) was first identified in sea urchin embryos where it was up-regulated prior ciliogenesis (Gibbons, Asai et al. 1994). This motor is composed of copies of the two heavy chains (*DHC2*) and at least three intermediate or light



chains. Each of these components is required for proper IFT. A direct role for this dynein in driving retrograde IFT is supported by work done in *Chlamydomonas* and *C. elegans* cilia. Mutation in genes coding for heavy (DHC-1b or CHE-3), light intermediate (D1bLIC/XBX1/FAP133) or light (LC8) chains cause the formation of very short cilia containing large amounts of accumulated IFT material, suggesting a role in retrograde transport (Figure 28A) (Pazour, Dickert et al. 1999, Porter, Bower et al. 1999, Signor, Wedaman et al. 1999, Perrone, Tritschler et al. 2003, Schafer, Haycraft et al. 2003). In kinetoplastids, two genes encode for IFT dyneins heavy chain (DHC2.1 and DHC2.2) and both have been shown to be essential for flagellum assembly (Kohl, Robinson et al. 2003, Adhiambo, Forney et al. 2005). By contrast, gene encoding the intermediate chain proteins (FAP133/DICS/WDR24) and DL11 (D1bLIC/XBX1) are present as single copy. Inducible RNAi-mediated knockdown of any IFT *dynein* gene resulted in the production of small-inflated flagella full of IFT material. Dynein motors are probably assembled in the cytoplasm and associated to the IFT-A complex at the base of the flagellum (Blisnick, Buisson et al. 2014).

### e) IFT regulation

IFT is a complex multi-step process, and most of its components have now been identified and characterized. However, several key steps remain unclear such as the entry of IFT material in the flagellar compartment or the assembly of the IFT trains *per se*. In this section, we summarize the different steps and mechanisms of flagellum assembly.

#### I. Initiation of flagellum assembly

The migration of the basal body to the cellular membrane precedes the initiation of axoneme elongation. In *Chlamydomonas* and mammals, the mother centriole needs to be liberated from its centrosomal role in mitosis before it could migrate to the membrane. In some mammalian cells, ciliogenesis is initiated by the addition of Golgi-derived vesicles to the distal end of the mother centriole (Sorokin 1962)



(Sorokin 1968). Basal body migration seems to be dependent on the actin cytoskeleton and other membrane-associated components of the transition zone (Dawe, Farr et al. 2007). Once the basal body docks to the plasma membrane, the axoneme elongates and one face of the Golgi-derived vesicle becomes the ciliary membrane, forming a membrane sheath around the emerging axoneme. The initiation of axoneme formation and the role of IFT in this process remain unclear. How is IFT initiated in the absence of axoneme? The initiation of microtubule polymerisation could be independent of IFT and the presence of short microtubules would permit to create railway of IFT trains and launch further axoneme elongation. However the absence of a short axoneme in IFT-B<sup>RNAi</sup> mutants does not support in the sense of this first hypothesis. IFT motors at the base could be essential for the entry of tubulin in the ciliary compartment and then for the early elongation of microtubules, subsequently followed by initiation of transport. It is also proposed that the high concentration of IFT proteins and cilium constituents at the base of the cilium could initiate microtubule formation and initiate axoneme elongation. Once the basal body docks into the plasma membrane, axonemal elongation occurs thanks to the IFT machinery and the cilium becomes isolated from the rest of the cell as the different elements of the transition zone are added to the structure.

## II. IFT Regulation at the base of the flagellum

IFT particles, motors are highly concentrated at the base of the flagellum as demonstrated by immuno-localisation or GFP::IFT fusion proteins in several organisms (Cole, Diener et al. 1998, Orozco, Wedaman et al. 1999, Pazour, Dickert et al. 1999, Buisson, Chenouard et al. 2013, Blisnick, Buisson et al. 2014). In *Chlamydomonas*, immuno-electron microscopy revealed that a pool of IFT52 is localized near the site where the transition fibres contact the flagellar membrane, suggesting that IFT is initiated by the gathering of IFT components cargo proteins at this level (Deane, Cole et al. 2001). This was confirmed in *C. elegans* and photoreceptor; hence transition fibres are proposed to be the site of docking and



assembly for the intraflagellar machinery (Deane 2001, Sedmak and Wolfrum 2010, Williams, Li et al. 2011).

Recently, a study showed that IFT particles are injected by pulses in avalanche-like releases of accumulated material at the base of flagella. This supports that IFT entry regulation could be controlled by a self-organizing physical mechanism (Ludington, Wemmer et al. 2013). Double staining of *Chlamydomonas* IFT-A and IFT-B complexes revealed that the proteins are found in distinct regions within the basal body area, IFT-A proteins are located more apically whereas IFT-B proteins are more basal, with a partial staining overlap at the apical end of the peri-basal body region (Hou, Qin et al. 2007). However, these studies were performed with conventional light microscopy and will need confirmation with more resolutive approaches. These observations suggest that IFT proteins would be segregated into separate compartments and then subsequently assembled before their injection in the flagellum. The overlapping region could correspond to transition fibers (Reiter, Blacque et al. 2012).

In *T. brucei*, photobleaching experiments demonstrated that when IFT proteins are coming back from retrograde trains to the base of the flagellum, they appear to follow each other. Then, they are mixed with the existing pool at the base of the flagellum to be used to build new anterograde trains (Buisson, Chenouard et al. 2013). In *Chlamydomonas*, IFT-A and dynein motor proteins were shown to be recruited from the cell body to the basal body pool, to be assembled into trains, to move through the cilium, and disperse back into the cell body after retrograde transport. This means that IFT-A and motors proteins evolve in an “open-system”. In contrast, IFT-B proteins from retrograde trains re-enter the pool present at the base where a portion is reused directly in anterograde trains indicating a ‘semi-open’ system, closer to what has been observed in trypanosomes (Wingfield, Mengoni et al. 2017).

### III. Entry into the flagellar compartment and anterograde transport

After their assembly, IFT particles adopt a linear shape and travel toward the flagellar tip as part of the anterograde transport system. The speed of IFT trains depends on



the type of molecular motors involved as well as on the organism. In *Chlamydomonas*, kinesin-2 transports IFT trains and the inactive dynein motors towards the tip at the mean speed of 1.9  $\mu\text{m}/\text{sec}$  (Dentler 2005). In *T. brucei*, the quantification by kymograph analysis of GFP::IFT52 speeds revealed different anterograde velocities. About 67% of these trains travel at a speed of 2.5  $\mu\text{m}/\text{sec}$  and the second population travels at a slower speed of 1.53  $\mu\text{m}/\text{sec}$  (Buisson, Chenouard et al. 2013). In this experiment the tagged version of IFT52 was overexpressed. By contrast, only one population of anterograde trains was detected (speed 1.75  $\mu\text{m}/\text{sec}$ ) when IFT81 was endogenously tagged (Bhogaraju, Cajanek et al. 2013). Expression of GFP fused IFT27 using the PFR regulatory sequences led to an intermediate expression level and here also only one population was detected travelling at a speed of 2.5  $\mu\text{m}/\text{sec}$  (Huet, Blisnick et al. 2014). The situation is more complex in *C. elegans* where two different motors are involved in anterograde transport. Along the middle segment microtubule doublets, kinesin-2 and OSM-3 travel together at a 0.7  $\mu\text{m}/\text{sec}$  rate, whereas OSM-3 continues alone along the distal segment to reach the tip of the cilium at a 1.3  $\mu\text{m}/\text{sec}$  speed (Snow, Ou et al. 2004).

#### IV. Cargo protein transport

For cilia and flagella construction, IFT trains need to transport axonemal precursors from the base to the assembly site at the distal tip. The most abundant cargo is obviously tubulin. In *Chlamydomonas*, IFT protein inside flagella can be imaged by total internal reflection fluorescence microscopy (TIRF) (Wren, Craft et al. 2013). TIRF microscopy permits to restrict the excitation and detection of fluorophores to a thin region. This technique permitted an improvement of the signal to-noise-ratio and the spatial resolution. Using double channel fluorescent live imaging, it was shown that GFP-tagged  $\alpha$ -tubulin molecules enter in flagellum as IFT cargoes or by simple diffusion (Craft, Harris et al. 2015). Simultaneous monitoring of mNeonGreen- $\alpha$ -tubulin and IFT20-mCherry movements further showed that  $\alpha$ -tubulin is an IFT cargo protein. More recently, the same team attenuated the tubulin IFT-based transport by altering the tubulin binding sites in IFT81 and IFT74. They showed that despite a



strong reduction in transported tubulin rates, the length of the axoneme was only moderately reduced. They proposed that ~80% of axonemal tubulin could enter in the flagellar compartment or access to the assembly site by simple diffusion and that IFT trains would rather be important to concentrate the tubulin in the flagellar compartment as well as to favour its polymerization {Harris, <https://doi.org/10.1101/268573>}. In *Chlamydomonas*, IFT transports other axonemal components to the distal end of the cilium such as DRC2 and DRC4 proteins and the central pair protein PF16 (Wren, Craft et al. 2013). In *C. elegans*, OSM-9 and OCR-2 two transient receptor potential vanilloid (TRPV) move in ciliary membrane at rates similar to IFT trains. Moreover, in IFT mutant their motility is disrupted confirming the role of the IFT machinery to transport these cargo proteins (Qin, Burnette et al. 2005).

### V. Transition at the flagellum tip

The flagellum tip is the site where axonemal growth occurs. When IFT trains arrive at the tip of the flagellum, they release their cargoes. The anterograde trains are at least probably disassembled and retrograde trains are formed in association with dynein motors in order to return back to the flagellum base.

On transmission electron microscopy images of several *Chlamydomonas* mutants, analysis with non-growing flagella showed that anterograde trains appeared twice large as retrograde one (Dentler 2005). Tomography of *Chlamydomonas* flagella showed the existence of two populations of IFT trains. The first one was made of electron-dense material, measured 250nm in length and exhibited a ~16 nm periodicity. The second population showed a less electron-dense material with a length of 700nm and a ~ 40 nm periodicity (Pigino, Geimer et al. 2009). A recent CLEM analysis of *Chlamydomonas* flagellum revealed that anterograde (~ 233nm) and retrograde (~ 209 nm) trains are similar in length (Stepanek and Pigino 2016). Stepanek *et al* developed a novel method that allows millisecond resolution in TIRF compatible with IFT trafficking analysis and 3D electron microscopy. A *Chlamydomonas* cell in gliding position was fixed with glutaraldehyde during TIRF



acquisition of GFP::IFT trains. In these conditions it was not possible to identify the nature of each train before checking their structure in electron microscopy. The anterograde trains appear like compact electron-dense structures as previously described. The retrograde trains appear less condensed and less regular suggesting that in previous studies they could have been missed or not considered as IFT particles. Another class of IFT trains was identified that were not motile with a length of ~ 650nm (Stepanek and Pigino 2016). Their structure and size was similar to the long trains described previously (Pigino, Geimer et al. 2009).

The analysis of IFT train frequency in live *T. brucei* cells expressing GFP::IFT52 showed a 1:3 ratio of anterograde versus retrograde train (Buisson, Chenouard et al. 2013). This suggests that one anterograde train is remodelled to produce three retrograde trains at the distal tip within 3-4s. In *Chlamydomonas*, a recent analysis using photo-gate experiments allowing to track individual trains, showed that this remodelling occurs within 1.3s. Then 1.7s average waiting time is necessary between the departure of successive retrograde trains (Chien, Shih et al. 2017).

Since the flagellum tip is the site where the axoneme elongates, cargo proteins transported by IFT trains need to be unloaded in this region. In *Chlamydomonas*, it was shown that GFP-tubulin was predominantly released from anterograde IFT trains near the flagellar tip accompanied by a deceleration of the trains (Craft, Harris et al. 2015). In addition, the anterograde motors have to be inactivated; the IFT complexes (A and B) must be associated to the IFT dynein. This one has to be activated to drive retrograde transport. Due to the presence of many IFT trains, very little is known about the regulatory mechanisms promoting IFT remodelling. IFT trains could be totally disassembled and all IFT proteins would mix together before forming new retrograde trains. By contrast, anterograde trains could be split to produce retrograde trains without disassembly.

At the tip of the *Chlamydomonas* flagellum, the (+) end microtubule-binding protein (EB1) is able to associate with IFT172 only when IFT-A and IFT-B complexes are separated (Pedersen, Geimer et al. 2006). EB1 could therefore play a role in the remodelling of IFT complexes at the flagellar tip.



## **VI. Retrograde transport**

Studies in several organisms have shown that retrograde transport is faster than anterograde transport. During retrograde IFT, the inactivated kinesin could be transported back to the base of the flagellum by IFT dynein or going back by simple diffusion. Immunofluorescence experiments of *Chlamydomonas D1bLIC* (Dynein light intermediate chain) mutant demonstrated that the two-kinesin subunits do not accumulate in the dilated flagellum (Hou, Pazour et al. 2004). The same result was obtained in *T. brucei* IFT dynein RNAi mutants (Blisnick, Buisson et al. 2014). In *Chlamydomonas* expressing KAP-GFP proteins, recent live imaging studies demonstrated that kinesin is coming back to the base by diffusion (Engel, Ludington et al. 2009, Chien, Shih et al. 2017). In contrast to *Chlamydomonas*, both heterotrimeric (OSM-3) and homodimeric kinesin-II motors of *C. elegans* are recycled by retrograde IFT (Prevo, Mangeol et al. 2015).

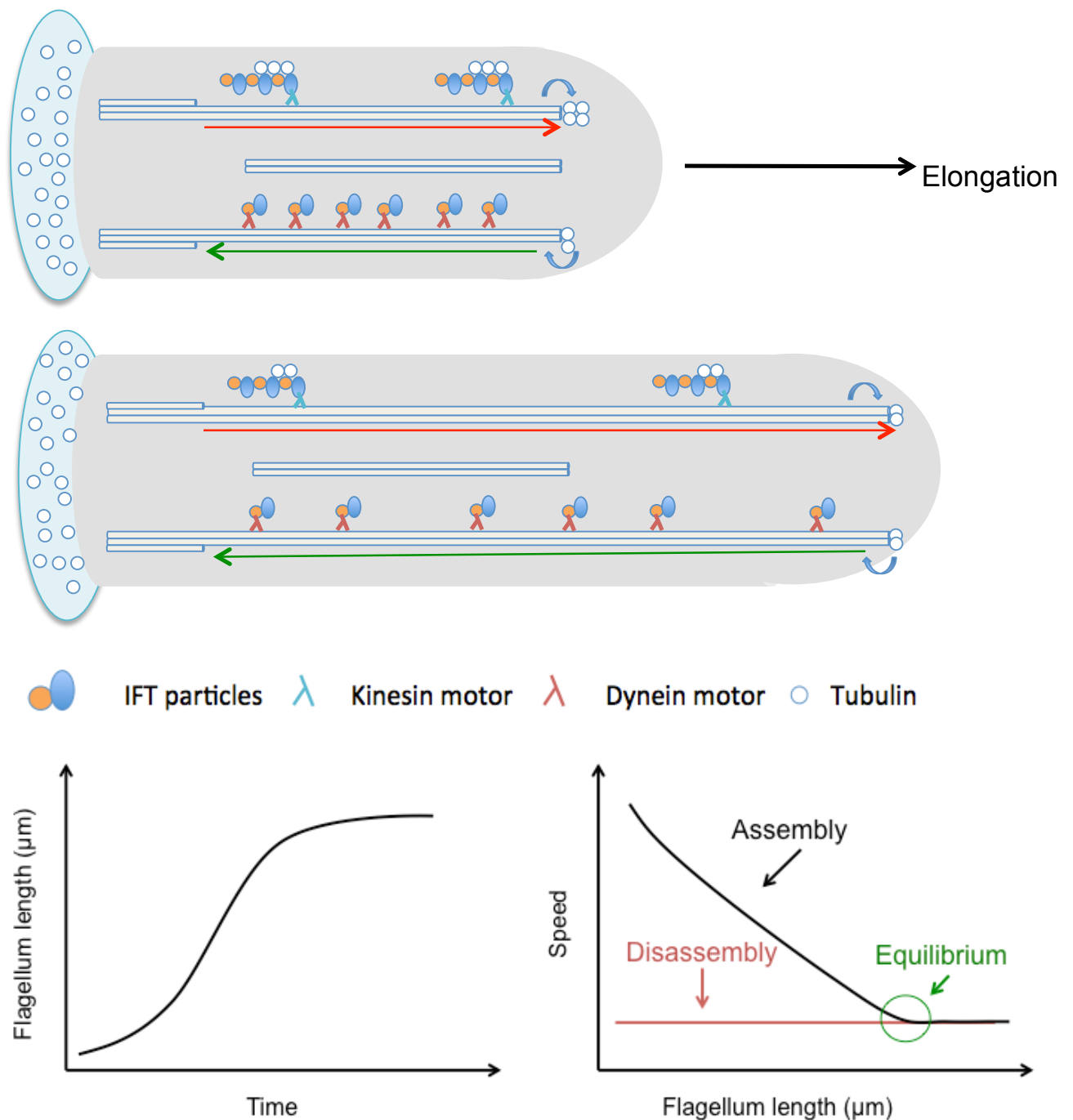


**Figure 29: The balance point model.**

Schematic representation of the “balance point” model (Marshall and Rosenbaum 2001). During flagellum elongation, tubulin assembly is faster at the distal tip than disassembly. In parallel to flagellum elongation, the rate of delivery is going down. In full-length flagellum, a dynamic equilibrium between assembly and disassembly occurs to maintain the flagellum at its final length. The concentration of IFT proteins decreases in parallel to flagellum elongation, hence the initial number of IFT proteins recruited into flagellum determines its final length.

## IV. Models for flagellum length control

---

The way by which cells control the size of their organelles is a major question for cell biologists. Eukaryotic cilia and flagella are excellent models to answer this question because they are present in many tissues and in many organisms and because their length is easily measurable in one-dimension. The ciliary length is tightly regulated in a cell-type specific manner. Mutations inducing the production of shorter or longer flagella can modify the swimming speed in protists and result in several diseases in humans (Barsel, Wexler et al. 1988). Some patients with nephronophthisis possess shorter or longer cilia in kidney cells that could be responsible for disorders in the associated mechanosensory signalling pathways. Three main models are currently proposed to explain the various mechanisms of flagellum length control.

### I. Balance point model

The balance point model is based on the principle that flagellum length is the result of an equilibrium between assembly and disassembly of tubulin at the distal end (Figure 29). To explain growth, it was proposed that tubulin disassembly is totally independent of flagellum length while the rate of tubulin assembly is initially faster than disassembly but decreases in parallel to flagellum elongation (Figure 29). A constant disassembly was observed in the absence of IFT in the *fla10* conditional kinesin-2 *Chlamydomonas* mutant, regardless of flagellar length (Kozminski, Beech et al. 1995, Marshall and Rosenbaum 2001). Furthermore, flagella also naturally shorten in a length-independent manner during mitosis (Marshall, Qin et al. 2005). Therefore the balance-point model proposes that the flagellar assembly rate decreases as the organelle elongates until the assembly and disassembly rates are equivalent (Marshall and Rosenbaum 2001). Marshall *et al.* observed that elongating and mature flagella contain the same quantity of IFT proteins (Marshall, Qin et al. 2005). They proposed that the quantity of IFT determines flagellar length. At the initial step of ciliogenesis, a fixed quantity of IFT proteins is injected in the flagellum.

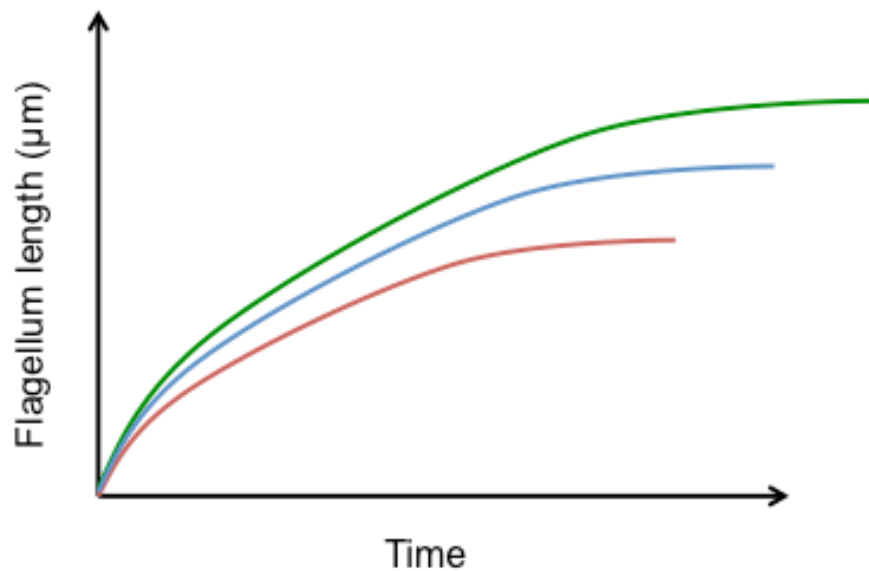
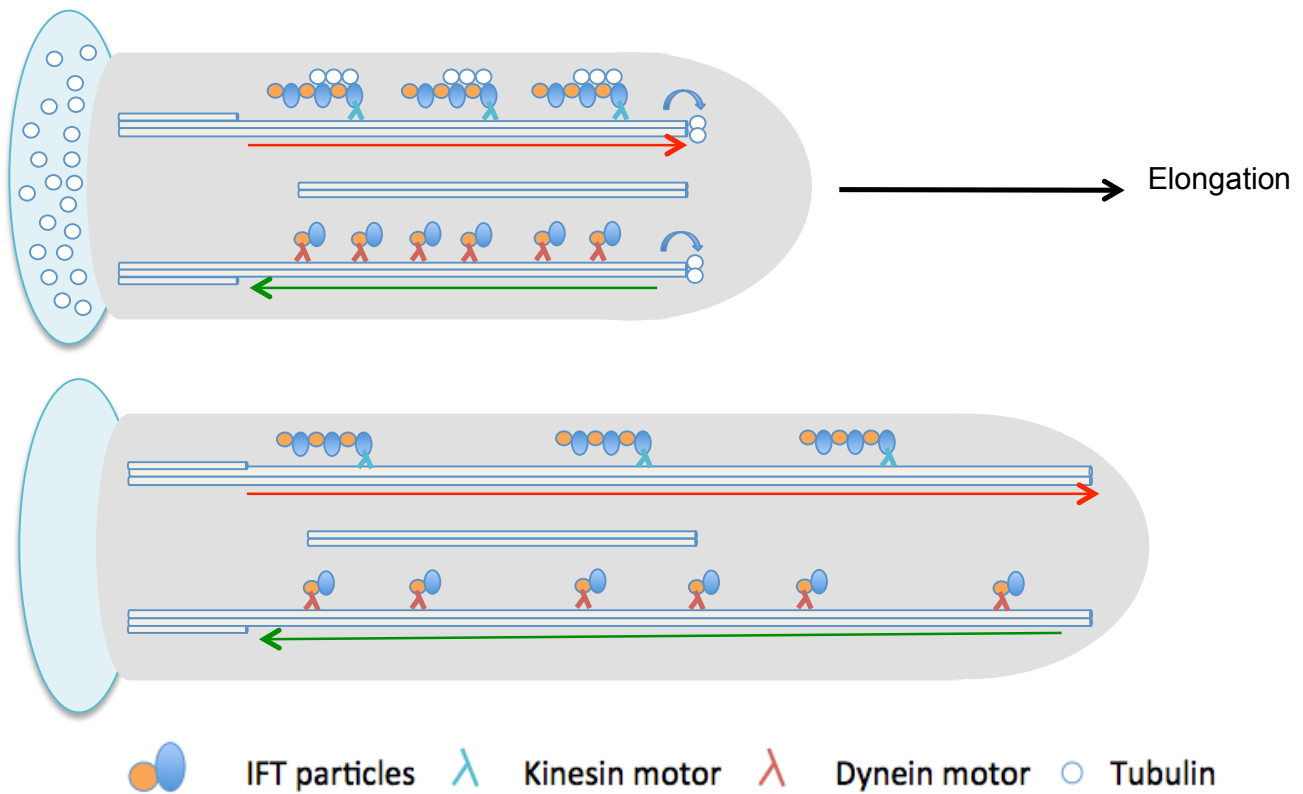


**Figure 30: Precursor availability model.**

A limiting pool of precursor component such as tubulin is produced at the initial step of the ciliogenesis. Flagellum elongates until the entire protein pool is exhausted. The initial quantity of flagellar precursors therefore determines the final length of the flagellum. Production of less precursors results in a shorter flagellum (red curve) whereas larger amounts will lead to the production of a longer flagellum (green curve).

As flagella elongate, IFT speed does not change and IFT particles will spend more and more time in transit. Surprisingly, the frequency at which IFT trains reach the flagellar tip and release their cargoes is constant during flagellum elongation (Dentler 2005). This is due to a decrease of IFT train size in parallel to flagellum elongation, allowing the production of more trains but of shorter size using the same amount of proteins in the flagellum (Vannuccini, Paccagnini et al. 2016). Indeed, it was demonstrated that anterograde IFT trains in short flagella are composed of more kinesin-associated protein and IFT27 proteins than trains in long flagella (Engel, Ludington et al. 2009).

Accordingly to this model, cells can regulate their flagellum length by modifying the number of IFT trains during assembly without controlling the production of axonemal precursors or sensing the ciliary length. This model is only valid assuming that the cargo loading on IFT trains is constant during all the steps of ciliogenesis. However, direct imaging analysis revealed that IFT trains are loaded with tubulin and other axonemal proteins whereas mature flagella are largely devoid of these cargo proteins once they reach their expected length (Wren, Craft et al. 2013, Craft, Harris et al. 2015). Including these observations, the “balance point” model remains valid but the mechanisms would rely more on tubulin transport rather than IFT amounts.

## **II. The limited precursor availability**

An elegant model proposes that if the cytoplasmic pool of flagellar components were simply maintained at high levels such that precursor concentrations were not limiting, the longer flagellum did not need to depolymerize to facilitate the growing of the severed flagellum (Goehring and Hyman 2012). The simplest hypothesis for the modification of the control of flagellum length is the presence of a limiting pool of flagellar precursors (Figure 30). At the initial step of ciliogenesis, a fixed number of precursors is produced. Available precursors enter the flagellum during the growing phase and flagellum elongation would stop once the entire precursor pool has been exhausted. In mammalian cells, the modification of free tubulin availability by pharmaceutical agents impacts on the length of the primary cilium (Sharma, Kosan et

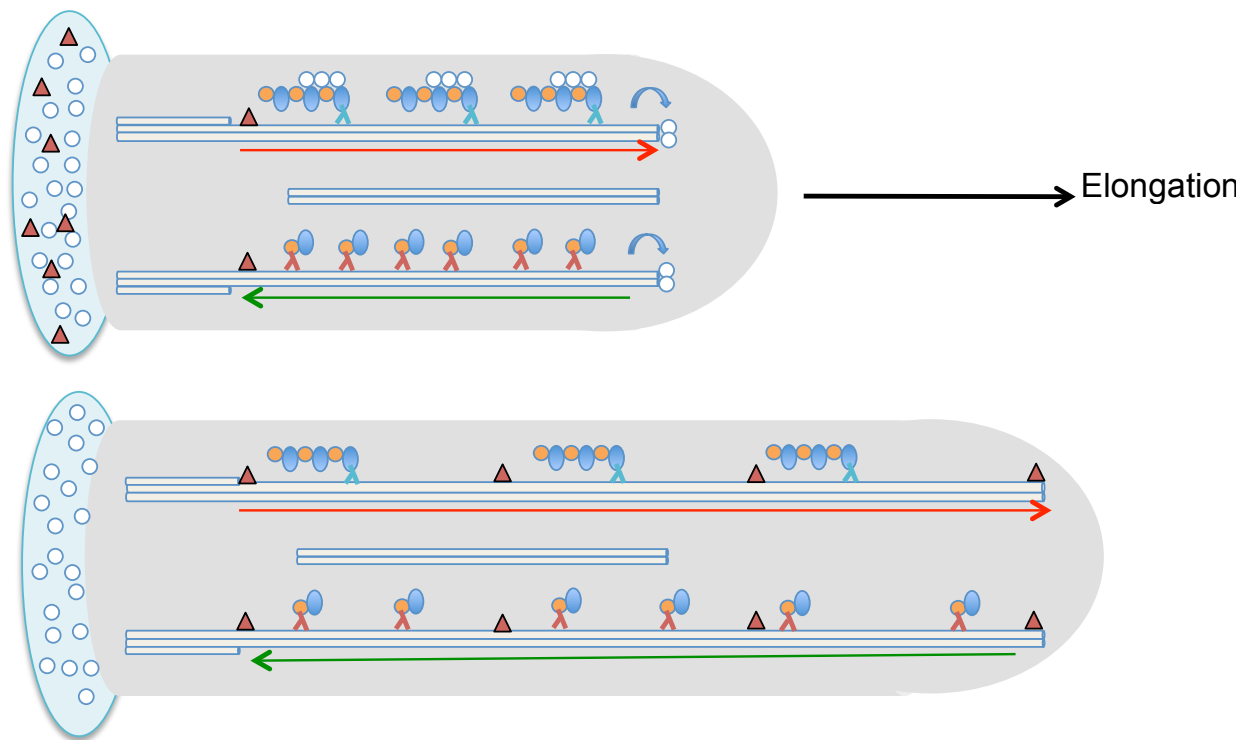


**Figure 31: Regulation of the flagellum length by sensor molecule.**

Schematic representation of a model based on the central regulatory role of a sensor molecule in the control flagellum length. At the initial step of ciliogenesis a fixed quantity of sensor molecules is produced. This sensor molecule is injected into flagellum at fixed and regular intervals. When all the sensor molecules are used the flagellum stops to grow. The sensor molecule can act as stabilizer of the axoneme to prevent depolymerisation.

al. 2011). These drugs act on the microtubule network and can increase (nocodazole) or decrease (taxol) the soluble pool of tubulin. This revealed an increase of the soluble tubulin pool results in an increase of ciliary length while the depletion of this pool using taxol induced ciliary shortening. In addition, nocodazole treatment induced ciliogenesis under conditions in which cilia are not normally present and increased cilia length on cells that have already established cilia.

In *Chlamydomonas*, it is possible to sever one of the flagella independently of the other one. As the severed flagellum begins to regrow, the longer flagellum reduces in length until the two flagella are equal in length after which both grow out in parallel (Marshall and Rosenbaum 2001). The severing of a flagellum results in an important decrease of the total pool of flagellar components available in the cell. Before the synthesis of new flagellar components, the availability of flagellar components is limiting and the disassembly of the longer flagellum ensures that there is enough material to elongate the short flagellum. This experiment demonstrates also that in *Chlamydomonas*, flagella can communicate and share a common pool of material.

### III. The flagellum length sensor theory

A third model proposed that cells possess dedicated reporter molecules to detect and measure ciliary length in real time in order to adapt their responses and finely tune the organelle size by elongating, reducing or maintaining its length. There are several possibilities by which a sensor molecule could provide the cell some readout of its organelle length. First, this could be a variant of the limiting pool model but associated to sensor molecules. The sensor molecule could be inserted into the cilium at regular intervals and stabilise the axoneme. Higher the number of sensor molecules, the longer the flagellum will be (Figure 31). Second, if ruler molecules were delivered to a certain region of the flagellum at some rate, then transport or diffusion of this molecule would create a concentration gradient whose properties will be directly linked to the flagellum length. Third the ruler proteins might change and / or induce a change in the structure of flagellar elements such as the axoneme depending on organelle length. Fourth, in the 'time-of-flight' model, the activity of a



length-regulating sensor could change as it moves along the cilium for example under the action of IFT. Assuming that IFT trains move at constant velocity, the time necessary for a sensor to cycle through a cilium would be proportional to ciliary length. The increase in travel time would be a way to measure flagellum length. This model has only been tested in *Chlamydomonas* using a temperature sensitive dynein mutant. When transferred at restricted temperature, retrograde transport speed is slow thereby IFT trains take more time to back to the ciliary base. Because of the reduced frequency of retrograde trains, less IFT material is available at the basal pool to produce new anterograde trains. Surprisingly using the KAP (Kinesin associated protein) tagged with GFP, it was shown that IFT injection increases. This observation does not support the “time-of-flight” model to explain the control of flagellum length in *Chlamydomonas* (Ishikawa and Marshall 2017).

The exact molecular mechanisms by which cells are able to sense the length of their cilia remain unknown but some kinases have been proposed to be involved in this process. In *Chlamydomonas*, mutation in several CDK-related proteins and MAP-kinases result in the production of abnormally long cilia (Tam, Wilson et al. 2007, Wilson, Iyer et al. 2008). These kinases could phosphorylate kinesin 2 subunits and prevent its fixation to IFT-B proteins, thereby regulating the entry of IFT trains in the ciliary compartment (Liang, Pang et al. 2014). Using two *Chlamydomonas* mutants that produce long (20  $\mu\text{m}$ ) and short flagella (6-8  $\mu\text{m}$ ), it was shown that CALK (aurora-like protein kinase) was dephosphorylated when flagella reached the length of 6  $\mu\text{m}$  (Luo, Cao et al. 2011). They observed changes in the CALK phosphorylation pattern in response to ciliary length variations provide strong evidence that cells could sense the status of their cilia. However, the phosphorylation site on the kinesin-2 subunit is not universally conserved.





# Questions



# I. Where do IFT trains travel on the trypanosome axoneme?

---

Several studies have shown that Intraflagellar transport (IFT) is essential for cilium / flagellum formation in most eukaryotic organisms. The first *in vivo* observations of IFT particles using DIC microscopy, that was rapidly followed by many further studies revealed the existence of two types of transport moving along the flagellum: the anterograde transport from the base to the tip and the faster retrograde transport in the opposite direction. Classical light microscopy allows monitoring of IFT trains in real time by using one of their constituents tagged with a fluorescent protein (Buisson, Chenouard et al. 2013, Huet, Blisnick et al. 2014, Craft, Harris et al. 2015). In the trypanosome flagellum, anterograde trains move at different speeds and regularly fuse meaning that at least part of the IFT anterograde trains travel on same set of microtubule doublet(s). However, no similar interactions are observed between retrograde trains and trains that moving in opposite directions do not apparently collide (Buisson, Chenouard et al. 2013). How do trains traveling in opposite directions avoid each other? Are there multiple IFT railways along the axoneme?

The axoneme is made of 9 doublets of microtubules and all are in theory available to be used for IFT. One could consider that IFT trains select randomly any of the 18 possible tracks, meaning that the risk of collision is relatively low. Alternatively, trains could select specific tracks for anterograde IFT and distinct tracks for retrograde IFT, hence avoiding collision. This is challenging to visualise because the diameter of the axoneme is 180 nm in *T. brucei*, which is below the resolution of classic light microscopy (250nm). In these conditions, it is not possible to distinguish microtubules doublets in live cells.

By contrast, this is quite straightforward to do using electron microscopy. IFT trains appear as electron dense particles sandwiched between the axonemal microtubules and the flagellar membrane. In *T. brucei* procyclic forms, IFT particles are mostly found on doublets 3-4 and 7-8, that are on each the side of the PFR (Absalon,

Blisnick et al. 2008). These 4 doublets might be different and can somehow facilitate IFT. This restricted localisation also raises different hypotheses. First, anterograde trains and retrograde trains could each travel preferentially on specific doublets of the axoneme in order to prevent collision. Second, both train types could travel on the two sides of the axoneme but using preferentially the A-tubule for one direction and the B-tubule for the other one.

In cross sections of the flagellum, the localization of IFT trains around the axoneme can be evaluated but not their length and although we can evaluate the position of one particle, it is not possible to determine whether this positioning on a given doublet is the same along the entire length of the train.

Therefore, we have investigated IFT train distribution along the trypanosome flagellum using Focused Ion Beam Scanning Electron Microscopy (FIB-SEM) to obtain a 3D-view of these structures with a high z-resolution (10nm) and on which the length of each IFT train could be accurately measured. However, IFT is a dynamic process and FIB-SEM analysis does not inform on the train directions (anterograde and retrograde). To challenge these two hypotheses, we have also used high-resolution light microscopy in order to determine where IFT trains traffic along the axoneme in live *T. brucei* cells.

## II. How is the flagellum length controlled in *T. brucei*?

---

*T. brucei* has a complex life cycle alternating between the tsetse vector and a mammalian host, involving many successive stages with significant different cellular morphologies and spectacular variations of flagellum length (Rotureau, Subota et al. 2011). Trypanosomes assemble flagella of precise length depending of the stage of the parasite cycle. Currently, three main models presented in the introduction have been proposed to explain the control of flagellum length. Do any of these models fit the strict flagellum length control observed during the *T. brucei* parasite cycle?

First the “balance point” model is based on a dynamic equilibrium between assembly and disassembly rates using the IFT machinery to deliver tubulin (Marshall and Rosenbaum 2001). This model is relevant for cilia that display a microtubule turnover such as *C. elegans* or *Chlamydomonas* (Engel, Ludington et al. 2009, Hao, Thein et al. 2011). Although IFT is essential for *T. brucei* flagellum construction, it has recently been demonstrated that it is not required to maintain its length (Fort, Bonnefoy et al. 2016). It means that a balance point model could only work if other motors were insuring the tubulin transport. Unfortunately, tubulin turnover at the distal tip cannot be investigated directly because tagged-tubulin is not incorporated in the trypanosome flagellum (Bastin, Bagherzadeh et al. 1996, Sheriff, Lim et al. 2014). Thus, we decided to scrutinize the turnover of structural proteins associated to tubulin, such as the outer dynein arm heavy chain B (ODAB) at the distal tip of the old flagellum by using fluorescence recovery after photobleaching (FRAP) experiments. Since the dynein arms are firmly anchored to the microtubules, we reasoned that the ODAB turnover would reflect the tubulin turnover. In cultured procyclic form, we have not observed any turnover of ODAB at the distal end of the mature flagellum, demonstrating little or no turnover of the axoneme microtubules. This demonstrates that the “balance point” model is not compatible with situation observed in *T. brucei* procyclic forms.

We next challenged the model of the limiting pool of cytoplasmic components (Goehring and Hyman 2012). The production of flagella of different lengths could be controlled by modifying the abundance of axonemal components. Using the mutant targeting *T. brucei* IFT kinesins (*KIN2A2B<sup>RNAi</sup>*) and that produces shorter flagella (12  $\mu\text{m}$ ), we have determined the amount of soluble tubulin by cell fractionation. In these cells with short flagella, we found out that a significant pool of soluble tubulin was still available, which could not explain the production of shorter flagella in *KIN2A2B<sup>RNAi</sup>* cells. This result demonstrates that the “limiting pool” model is not compatible with the situation observed in *T. brucei* procyclic forms.

Third we have developed and evaluated a new model called the “grow and lock” model. We propose that the flagellum can elongate at a constant growth rate until a signal blocks further any elongation or shortening and locks the flagellum in a mature conformation. To validate this hypothesis, we have manipulated the two control parameters: the axoneme growth rate and the timing of the locking event. This was investigated in cultured procyclic form parasites that all produce mature flagella of a fixed length of 20 $\mu\text{m}$ . This new model is compatible with the existence of a length sensor. Indeed, the length sensor could initiate the locking event when the flagellum has reached its expected length.

Trypanosomes precisely set the length of their flagella during their parasite cycle. In bloodstream forms and attached epimastigotes, the new flagellum has always the same length than the old one like in procyclics. However the short epimastigote and metacyclic stages are produced following an asymmetric division. For the first case, the new flagellum is made shorter than the old one while the new flagellum of the metacyclic is longer than the old one.

How is it possible that the same parasite cell can produce flagella with different fixed lengths at different times of its development? Is it the same strategy to control flagellum length to being used for asymmetric divisions? To answer these questions, we started to evaluate the pertinence of different models in the other stages of *T. brucei* parasite cycle. We focused our preliminary studies on the astonishing asymmetric division resulting in the production of the short epimastigotes in the tsetse proventriculus and tried to evaluate how a cell can produce a flagellum ten times shorter than the old one.



# Results



## I. Bidirectional Intraflagellar

Transport is restricted to only two microtubule doublets in the trypanosome flagellum.

---

### 1) Summary

On transversal sections of flagella observed by transmission electron microscopy, IFT trains are easily detectable as electron dense particles sandwiched between the microtubule doublets and the flagellar membrane. In *T. brucei*, these particles are exclusively found on doublets 3-4 and 7-8 but are absent in several IFT mutants confirming their identity. Using Focussed Ion Beam Scanning Electron Microscopy (FIB-SEM) in collaboration with Adeline Mallet (Engineer at the UTechs UBI, Institut Pasteur), we have studied the distribution of IFT trains along the trypanosome flagellum. We have confirmed that IFT trains are restricted to doublets 3-4 and 7-8 all along the length of the axoneme and demonstrated the existence of two distinct populations of trains defined by their length and present on both sets of doublets. The average particle length in the two populations is statistically different, possibly representing the larger anterograde trains and smaller retrograde trains although alternative explanations are possible. However since FIB-SEM analysis does not allow discriminating anterograde, retrograde and arrested trains, two hypotheses are possible. First, one of these two doublets could be dedicated to anterograde trafficking and the other one for retrograde trafficking, hence allowing independent control of each mode of transport and theoretically preventing any collision. Second,

each doublet could serve for the two types of transport, with the same principle at the level of A and B microtubules.

To discriminate these two hypothesis, Jean-Yves Tinevez (Engineer at the Image analyse hub, Institut Pasteur) and Cécile Fort (Previous PhD student in the lab) went to Janelia Campus (USA) to use recently developed high-resolution microscopy system to monitor the trafficking of GFP::IFT52 containing particles and confirmed the existence of two tracks for IFT in live cells. At the Institut Pasteur, we have reproduced similar observation conditions using a confocal spinning disk with a high numerical aperture objective (NA= 1.57). We were able to visualize IFT trafficking on two distinct tracks in live cells expressing mNg::IFT81 upon endogenous tagging, revealing that anterograde and retrograde transport take place on each of these two tracks. Once IFT anterograde particles reach the distal tip, they are converted in smaller retrograde trains in 3-4 sec (Buisson, Chenouard et al. 2013). Due to an improved imaging resolution, we have further demonstrated that anterograde trains were converted into retrograde trains on the same track and no exchange of fluorescent proteins was observed between the two tracks.

**Bidirectional Intraflagellar transport is restricted to only two microtubule doublets in trypanosome flagellum.**

Article submitted to Journal of Cell Biology.

Eloïse Bertiaux, Adeline Mallet, Cécile Fort, Thierry Blisnick, Serge Bonnefoy, Jamin Jung, Moara Lemos, Sergio Marco, Sue Vaughan, Sylvain Trépout, Jean-Yves Tinevez and Philippe Bastin.



# **Bidirectional intraflagellar transport is restricted to only two microtubule doublets in the trypanosome flagellum**

Eloïse Bertiaux<sup>1,2\*</sup>, Adeline Mallet<sup>1,2,3\*</sup>, Cécile Fort<sup>1,2</sup>, Thierry Blisnick<sup>1</sup>, Serge Bonnefoy<sup>1</sup>, Jamin Jung<sup>1</sup>, Moara Lemos<sup>1</sup>, Sergio Marco<sup>4,5</sup>, Sue Vaughan<sup>6</sup>, Sylvain Trépout<sup>4,5</sup>, Jean-Yves Tinevez<sup>7,8</sup> and Philippe Bastin<sup>1, +</sup>

## **Affiliations:**

<sup>1</sup>Trypanosome Cell Biology Unit, INSERM U1201, Institut Pasteur, 25 Rue du Docteur Roux, 75015 Paris, France

<sup>2</sup>Université Pierre et Marie Curie Paris 6, Cellule Pasteur-UPMC, 25 rue du Docteur Roux, 75015 Paris, France

<sup>3</sup>UtechS Ultrastructural Bioimaging (Ultrapole), Institut Pasteur, 28 Rue du Docteur Roux, 75015 Paris, France

<sup>4</sup>Université Paris Sud, Université Paris-Saclay, CNRS UMR9187, F-91405 Orsay, France

<sup>5</sup>Institut Curie, PSL Research University, INSERM U1196, F-91405 Orsay, France

<sup>6</sup>Department of Biological and Medical Sciences, Faculty of Health and Life Science, Oxford Brookes University

<sup>7</sup>UtechS Photonic Bioimaging (Imagopole), Institut Pasteur, 28 Rue du Docteur Roux, 75015 Paris, France

<sup>8</sup>Image Analysis Hub, Institut Pasteur, 28 Rue du Docteur Roux, 75015 Paris, France

\*These authors contributed equally

+ Correspondence to Philippe Bastin: [pbastin@pasteur.fr](mailto:pbastin@pasteur.fr)

## Summary

Intraflagellar transport (IFT) is the rapid bidirectional movement of large protein complexes driven by kinesin and dynein motors along microtubule doublets of cilia and flagella. Here we used a combination of high-resolution electron and light microscopy to investigate how and where these IFT trains move within the flagellum of the protist *Trypanosoma brucei*. Focused Ion Beam Scanning Electron Microscopy (FIB-SEM) analysis of trypanosomes showed that trains are found almost exclusively along doublets 4 and 7 and that trains distribute in two categories according to their length. High-resolution live imaging of cells expressing mNeonGreen::IFT81 or GFP::IFT52 revealed for the first time IFT trafficking on two distinct tracks within the flagellum and that anterograde and retrograde IFT takes place on each of these tracks. At the distal end, a large individual anterograde IFT train is converted in several smaller retrograde trains in the space of 3-4 seconds while remaining on the same track.

## Introduction

Intraflagellar transport (IFT) is the movement of molecular motors and multi-protein complexes that carry tubulin and other flagellar components to the tip of cilia and flagella for assembly (Craft et al., 2015; Kozminski et al., 1993). One or more kinesin motors are responsible for anterograde transport whereas a dynein motor returns the trains to the base during retrograde transport (Prevo et al., 2017). These moving protein complexes have been termed IFT trains (Pigino et al., 2009). Absence of IFT prevents construction of most cilia and flagella whereas perturbation of IFT components can impact on the structure and function of the organelle, as observed in multiple human genetic diseases (Beales et al., 2007; Dagonneau et al., 2009; Halbritter et al., 2013; Perrault et al., 2012).

Quantification of IFT in animal cells, green algae, trypanosomes or ciliates revealed remarkably high speed (0.5-5  $\mu\text{m}$  per second) and frequency ( $\sim$ 1-3 trains per s) of IFT trains in both directions (Besschetnova et al., 2010; Brooks and Wallingford, 2012; Buisson et al., 2013; Iomini et al., 2001; Prevo et al., 2015; Snow et al., 2004; Wheeler et al., 2015; Williams et al., 2014; Wingfield et al., 2017). Trains are fairly large complexes of  $>20$  proteins (Taschner and Lorentzen, 2016) associated to molecular motors whose size is above 1 megadalton (Rompolas et al., 2007), raising the question of their organisation within the flagellum during anterograde and retrograde trafficking.

In transmission electron microscopy (TEM), trains appear as electron dense particles sandwiched between microtubule doublets and the flagellum membrane. This was visualised in only two species so far: the green algae *Chlamydomonas reinhardtii* (Pigino et al., 2009; Ringo, 1967; Vannuccini et al., 2016) and the protist *Trypanosoma brucei* (Absalon et al., 2008). Recently, an elegant study using correlative light electron microscopy in *Chlamydomonas* cells expressing a fluorescent IFT protein showed that anterograde trains are

positioned on the B-tubule of each microtubule doublet whereas retrograde trains are found on the A-tubule (Stepanek and Pigino, 2016). In this organism, IFT trains appeared on all 9 microtubule doublets (Stepanek and Pigino, 2016). By contrast, transmission electron microscopy (TEM) suggested that electron dense particles looking like IFT trains are restricted to microtubule doublets 3-4 and 7-8 of the axoneme in *Trypanosoma brucei* (Fig. 1A)(Absalon et al., 2008; Hoog et al., 2016). The restricted presence of IFT trains on two doublets raises two hypotheses. First, a tantalising explanation would be that one of these two doublets serves as track for anterograde transport and the other one for retrograde trafficking, hence allowing independent control of each mode of transport (Fig. 1B, Model 1). Second, each doublet could serve as a double track for IFT (Fig. 1B, Model 2), as shown in *Chlamydomonas*. In that situation, train frequency and speed could be similar or different between the two doublets. In both models, anterograde trains need to be converted to retrograde trains. Does it happen on the same doublet or is from a common pool of material shared at the distal end? Here, we investigated IFT train distribution along the length of the trypanosome flagellum using Focused Ion Beam Scanning Electron Microscopy (FIB-SEM) to get a three dimensional view and to measure the length of each IFT train using a 10nm Z-axis increment. We formally demonstrate that trains are indeed mostly found on doublets 4 and 7 and that they fall in two categories defined by their length. Using high-resolution live cell imaging, we reveal which hypothesis is correct for the distribution of anterograde and retrograde trafficking and we apply kymograph analysis to examine the conversion of anterograde to retrograde trains.

## RESULTS

### *FIB-SEM analysis revealed the length and 3-D distribution of IFT trains*

To obtain a global view of the 3-D distribution of IFT trains by electron microscopy, different approaches are available. Since the twisted shape of the trypanosome flagellum (Sherwin and Gull, 1989) restricts the use of conventional transmission electron tomography to short portions of the axoneme, we turned to FIB-SEM that allows trimming a fixed sample over several  $\mu\text{m}$  (Kizilyaprak et al., 2014). Wild-type trypanosomes were chemically fixed, dehydrated and embedded in resin in conditions similar to classic transmission electron microscopy. The block was milled with 10 nm increments using the ion beam, hence providing a better resolution than serial sectioning. Four samples were reconstructed, each containing several trypanosomes. Navigating through the volume of each sample revealed the typical trypanosome architecture with the cell body containing the subpellicular microtubules, the nucleus, the large mitochondrion and its kinetoplast (mitochondrial DNA), the endoplasmic reticulum, the Golgi apparatus or the glycosomes (Video S1)(Fig. 2A). The shape, size and distribution of these organelles were in agreement with published data based on electron tomography (Lacomble et al., 2009) or serial block face sectioning (Hughes et al., 2017). Flagella were clearly recognised in both cross and longitudinal sections, including multiple cases where the proximal portion was seen to emerge from the flagellar pocket (Video S1). The base of the flagellum displayed the typical organisation with the basal body, the transition zone, the axoneme, and finally the axoneme and the paraflagellar rod (PFR), a lattice-like structure (Hughes et al., 2012) essential for motility (Bastin et al., 1998). Flagella were correctly attached to the cell body with the exception of the distal end that is always free as expected (Sherwin and Gull, 1989).

Importantly, IFT trains can be seen without ambiguity as electron dense particles found between the flagellar membrane and microtubule doublets (Video S1 and Fig. 2A, arrows on bottom panels). To determine doublet number, the fixed orientation of the axoneme relative to the PFR (Branche et al., 2006; Gadelha et al., 2006; Ralston et al., 2006) was exploited (Fig. 1A). Indeed, the presence of a thick projection that connects the B tubule of doublet 7 to the PFR makes doublet numbering straightforward (Fig. 1A). In case this projection was not visible, the proximal to distal orientation of the axoneme was determined by travelling through the volume knowing that dynein arms are orientated clockwise when starting from the base of the flagellum (Sherwin and Gull, 1989). Because several portions of flagella were encountered in a single volume, each axoneme was individually marked with a different colour and IFT trains were indicated in red (Fig. 2B,C)(Video S2). Most trains were found along doublets 4 and 7 and exhibited various lengths (Fig. 2B,C). We detected 52 trains on doublet 4 and 56 trains on doublet 7 in 27 distinct flagella (total cumulated axoneme length 166  $\mu\text{m}$ , the average length of visible axoneme was  $6.25 \pm 4.21 \mu\text{m}$ ). Only 2 trains were not found on these doublets (both were present on doublet 1). The calculated average number of trains reported to the theoretical full-length flagellum of 20  $\mu\text{m}$  was 6.15 on doublet 4 and 6.6 on doublet 7. This is below the expected numbers of 8.6 anterograde trains and 8.9 retrograde trains per flagellum deduced from their speed and frequency in live cells (Buisson et al., 2013), suggesting that some trains might be missed in the FIB-SEM analysis. Statistical analysis using R software indicated the presence of two distinct populations on each doublet, with 61% of short trains ( $202 \pm 94 \text{ nm}$ ) and 39% of longer trains of ( $822 \pm 515 \text{ nm}$ ) on doublet 4 (n=52) and 68% of short trains ( $207 \pm 99 \text{ nm}$ ) and 32% of longer trains of ( $968 \pm 239 \text{ nm}$ ) on doublet 7 (n=56) (Fig. 2D).

These results demonstrate that IFT trains are restricted to doublets 4 and 7 along the length of the flagellum in trypanosomes. The average train number and train length is

undistinguishable between the two doublets, hence suggesting that similar trains travel on each doublet, supporting the second hypothesis of anterograde and retrograde IFT trafficking taking place on each doublet. However, FIB-SEM does not give information on train direction and the possible presence of arrested trains (Stepanek and Pigino, 2016) cannot be ruled out and could interfere with the interpretation. Now that the spatial distribution of IFT trains has been established, we turned to live cell imaging in order to investigate their dynamics.

### ***Immunofluorescence analysis indicates the existence of separate tracks for IFT***

Measurements of flagellar sections by transmission electron microscopy showed that the outer face of doublets 4 and 7 are separated by  $190 \pm 11$  nm (n=20), which is below the resolution of conventional light microscopy. To evaluate the feasibility of detecting IFT on these two separate tracks, we tried different fixation protocols and examined the distribution of IFT proteins by immunofluorescence assay with antibodies against the IFT172 protein (Absalon et al., 2008) and the axonemal protein TbSAXO1 (Dacheux et al., 2012). Fixation of trypanosomes in paraformaldehyde followed by a post-fixation in methanol led to the detection of TbSAXO1 as a single thick line (second column, Fig. 3) as expected from immunogold analysis that showed that this protein was present throughout the axoneme (Dacheux et al., 2012). By contrast, IFT172 staining appeared as two parallel lines decorating both sides of the TbSAXO1 staining (third column, Fig. 3). This was observed in the single flagellum of G1 cells (Fig. 3A) and in both mature and growing flagella of duplicating cells (Fig. 3B). Methanol fixation results in dehydration and flattens the sample on the slide, possibly leading to a better separation of IFT trains allowing their detection as two separate lines by conventional light microscopy. This is promising because this suggests that IFT positioning on distinct doublets could be discriminated by light microscopy.

The next step was the investigation of IFT in live cells, which requires the expression of a fluorescent reporter in trypanosomes (Adhiambo et al., 2009; Bhogaraju et al., 2013; Buisson et al., 2013; Huet et al., 2014). Cell lines expressing GFP::IFT52 have been used reproducibly to detect IFT (Absalon et al., 2008; Buisson et al., 2013) but in this set-up, GFP::IFT52 was expressed from the ribosomal DNA locus with a strong promoter (Wirtz and Clayton, 1995). This led to bright flagellar signal but also to significant cytoplasmic signal (Buisson et al., 2013). To avoid any risk of potential artefacts due to over-expression, an *in situ* tagging approach (Dean et al., 2017; Kelly et al., 2007) was selected to generate a cell line expressing IFT81 fused to mNeonGreen (mNG)(Shaner et al., 2013) from its endogenous locus. IFT81 is a well-known member of the IFT-B complex involved in tubulin binding and transport (Bhogaraju et al., 2013; Kubo et al., 2016) and was shown previously to traffic within the trypanosome flagellum (Bhogaraju et al., 2013). Western blotting with an anti-mNG antibody demonstrated that the fusion protein displayed the expected mobility on SDS-PAGE (Fig. S1A). Live analysis showed the classic distribution with a strong signal at the base of the flagellum and train trafficking in both anterograde and retrograde direction within the flagellum that was detected by kymograph analysis (Video S3 & Fig. S1B-C). Kymograph analysis revealed that the frequency and speed of anterograde trains (Fig. S1D-E) was similar to what was reported previously for other IFT-B proteins (Bhogaraju et al., 2013; Buisson et al., 2013; Huet et al., 2014). Finally, applying the paraformaldehyde/methanol fixation protocol followed by direct observation of the mNG::IFT81 fluorescent signal led to the detection of two parallel lines within flagella (Fig. S1F). The behaviour of mNG::IFT81 is therefore comparable to that of GFP::IFT52 and both cell lines were used for imaging IFT in trypanosomes.

### ***High-resolution live cell imaging reveals bidirectional IFT on two tracks***

These results are encouraging because they suggest that live imaging by light microscopy could permit the visualisation of IFT on two distinct tracks. We turned to super-resolution based on structured illumination microscopy (SIM)(Gustafsson, 2000; Gustafsson et al., 2008) to visualise IFT trafficking. SIM imaging provided the spatial resolution and demonstrated the existence of two parallel lines within the flagellum for fluorescent mNG::IFT81 in live cells (Fig. S2A and Video S4). Next, we tried to record IFT trafficking over time using the GFP::IFT52 cell line (Fig. S2B and Video S5). This demonstrated that IFT trains move on two distinct tracks in trypanosomes, in agreement with the electron microscopy data. However, the acquisition time (800 milliseconds) was not compatible with the rapid speed of IFT in trypanosomes ( $\sim 2 \mu\text{m/s}$  for anterograde and  $\sim 5 \mu\text{m/s}$  for retrograde transport) and images of multiple trains overlapped, precluding analysis (Video S5).

To find an appropriate compromise between sufficient resolution and fast acquisition, “high-resolution” imaging was performed using objectives with superior numerical aperture (1.49 NA for GFP::IFT52, imaging performed at the Janelia Farm Research Campus, 1.57 NA for mNG::IFT81, imaging performed at the Institut Pasteur)(Li et al., 2015). In these conditions, the theoretical resolution for a green fluorescent molecule should be  $\sim 160 \text{ nm}$ , a value compatible with the discrimination of IFT trafficking on doublets separated by  $190 \text{ nm}$ . Remarkably, examination of cells expressing mNG::IFT81 (Video S6) or GFP::IFT52 (Video S7) with the high numerical aperture objectives revealed the presence of trains on two separate tracks within the flagellum. This was clearly confirmed with time projections (Fig. 4A and Fig. S3A). Closer examination of IFT trafficking demonstrated that anterograde and retrograde IFT trafficking was taking place on each of these tracks (Fig. 4B, Fig. S3B, Video S6 and Video S7). This was further supported by kymograph analysis that showed the presence of distinct anterograde and retrograde trains on each track (Fig. 4C & Fig. S3C).

These results demonstrate that IFT takes place on two separate tracks in the trypanosome flagellum presumably corresponding to doublets 4 and 7, and that anterograde and retrograde trafficking occurs on each of them. This supports the hypothesis of bidirectional IFT on both doublets and invalidates the model with one track for each direction.

To be able to quantify and compare IFT train trafficking on each track, it was necessary to find a way to identify them. To do that, the cellular asymmetry of trypanosomes was exploited. Cells were orientated with the posterior end towards the top of the image and with the flagellum lying on the left-hand side, hence defining a left and a right track (Fig. 4A and Fig. S3A). Quantification of anterograde IFT train trafficking showed a similar frequency close to 0.5 anterograde train per second on the left and on the right track for both fluorescent proteins (Fig. 4D, Fig. S3D and Table 1). There was no statistically significant difference between these two parameters in cells expressing mNG::IFT81 (one-way ANOVA test,  $p=0.29$ ) or GFP::IFT52 ( $p=0.14$ ). The anterograde speed was  $\sim 2.5$   $\mu\text{m}$  per second on each track in both cell lines (Fig. 3E, Fig. S3E and Table 1) although we noted a trend towards slower IFT speed by 10-15% on the right track ( $p=0.20$  for mNG::IFT81 and  $p=0.067$  for GFP::IFT52). Trains trafficking simultaneously on each track might not be discriminated with conventional light microscopy. Hence, the anterograde IFT train frequency was compared using videos of mNG::IFT81 cells acquired in the same experiment but where two tracks could not be discriminated (Fig. 4E, “unresolved”). The frequency calculated from the total of left and right kymographs in cells where the two tracks could be detected was consistently higher (0.98 anterograde trains per second) compared to cells where only one track was visible (0.76 anterograde trains per second)(Table 1) with statistical confidence ( $p=0.02$ ). This result suggests that up to 15% of trains could be missed when IFT was imaged at low resolution. By contrast, their average train speed was indistinguishable (Table 1,  $p=0.21$ ), suggesting that the “missed” trains are not a specific population at least in terms of speed.

Although retrograde transport was detected in almost all videos (Video S5 and Video S6), the lower intensity of these trains made their quantification quite challenging, especially for the frequency. Nevertheless, it was possible to estimate the speed of the brightest retrograde trains, which was between 4 and 5  $\mu\text{m}$  per second, in agreement with data obtained using conventional imaging (Buisson et al., 2013).

To visualise the conversion of anterograde to retrograde transport, we looked at the distal end of the flagellum of cells expressing mNG::IFT81 (Fig. 5A & Video S8). On both left and right tracks, the arrival of large anterograde trains at the distal end of the flagellum was clearly visible. This was followed by a lag phase (seen as vertical lines on the kymograph) where the fluorescent material remained at the distal end but its intensity progressively went down while multiple retrograde trains were released during a ~3-4 second period (Fig. 5B). It should be noted that the anterograde trains do not all stop exactly at the same place (merged panel, Fig. 5B). Data also showed that anterograde trains convert to retrograde trains on the same track and that no exchange of IFT-B material could be detected between left and right tracks. To confirm these results, the signal for GFP::IFT52 was bleached only at the distal end of the flagellum and IFT was recorded in this portion (Fig. 5C & Video S9). This led to a significant improvement of the signal-to-noise ratio and facilitated visualisation of retrograde trains on videos and on kymographs. Analysis of such kymographs confirmed the findings above (Fig. 5D, see magnified area).

Overall, these results obtained with two different cell lines (expression of mNG::IFT81 and GFP::IFT52) at two different imaging centres (Janelia Farm, USA and Institut Pasteur, France) using different techniques demonstrate that IFT takes place on two distinct tracks and that anterograde and retrograde trafficking occur on each of these tracks. To our knowledge, this is the first time that bidirectional IFT trafficking at the level of individual doublets has been formally demonstrated.

## DISCUSSION

*T. brucei* is only the second organism where IFT trains have been visualised in both light and electron microscopy. Here we reveal train distribution on doublets 4 and 7 using FIB-SEM and demonstrate bidirectional trafficking on two separate tracks by high-resolution live cell imaging. These tracks presumably correspond to doublets 4 and 7 but definitive confirmation will require the identification of specific markers of each of these doublets at the axoneme level.

FIB-SEM detected two distinct populations of trains on each doublet. The first possibility is that long trains correspond to anterograde ones and short trains to retrograde ones, as expected from the distinctive size on videos and kymographs (Buisson et al., 2013). The higher frequency of short trains (2.3 to 1.5-fold) is consistent with the higher abundance of retrograde trains detected during live imaging (Buisson et al., 2013). However, the total number of IFT trains seen in FIB-SEM (12.5 per flagellum) is lower compared to what was detected by live imaging (17.5). Moreover, the average length of long trains is close to 1  $\mu\text{m}$  and this was extremely rare on kymographs. Intriguingly, two populations of IFT trains were also found using electron tomography analysis of *Chlamydomonas* flagella, with average lengths fairly close to what is reported here for trypanosomes (Pigino et al., 2009). Long trains were initially thought to correspond to anterograde trains because they accumulate in the *fla14* retrograde transport mutant whereas small trains disappear. However, correlative light and electron microscopy revealed that long trains correspond to standing material and that short particles correspond to anterograde trains (Stepanek and Pigino, 2016). Based on this, we propose that short and long trains observed by FIB-SEM in *T. brucei* flagella correspond to anterograde trains and to standing material, respectively. A total of 7.2 short trains is found per flagellum, which is close to the predicted number of 8.6 (Buisson et al.,

2013). Observation of kymographs indicated the presence of standing trains that look larger than moving trains (Fig. 5B, stars). It should be noted that this material does not remain stuck forever as it appears to be picked up by other anterograde trains after a few seconds (stars on Fig. 5B and Fig. S1E). In this scenario, retrograde trains would be missed either because they are too short or because their morphology is different and difficult to identify by FIB-SEM. In *Chlamydomonas*, retrograde trains appear less condensed and less regular compared to anterograde trains, and had been missed in conventional transmission electron microscopy until their identification by correlative techniques (Stepanek and Pigino, 2016).

The use of superior numerical aperture objectives appears to be an optimal compromise between speed of acquisition and spatial resolution. It revealed the existence of bidirectional IFT on two tracks but it also showed that the frequency of IFT measured with conventional microscopy might be underestimated. Moreover, it revealed the transition of anterograde trains to retrograde trains with IFT-B proteins spending up to 3-4 seconds at the distal end while being progressively associated to the emergence of several retrograde trains. This value is in agreement with previous low-resolution analysis based on photobleaching experiments (Buisson et al., 2013). In *Chlamydomonas* (Chien et al., 2017) and in *C. elegans* (Mijalkovic et al., 2017)(Mijalkovic et al, in revision), IFT-B proteins also spend a few seconds at the distal end of microtubules before returning towards the base as components of several retrograde trains.

The restriction of IFT to only two doublets is different from the situation encountered in *Chlamydomonas* where trains appear to be present on the majority of the doublets (Stepanek and Pigino, 2016). So far, IFT trains have only been visualised by electron microscopy in these two organisms. To understand the significance of IFT presence on all or only some doublets, it will be essential to determine which doublets are being used in different types of cilia in various organisms. This raises the question of why restricting IFT to

some doublets. We propose a scenario where the restriction of IFT to some doublets would represent an evolutionary advantage by liberating the other doublets from constraints imposed by IFT train presence, thereby offering the opportunity for acquiring new structures or functions. In trypanosomes and related protists, the PFR is tightly associated to the axoneme (Hughes et al., 2012; Koyfman et al., 2011) and brings an essential contribution to flagellum motility (Bastin et al., 1998; Santrich et al., 1997). Restricting IFT to some doublets could allow the passage of other molecular motors on the remaining doublets. These could transport different cargoes, hence increasing the range of functions performed by cilia and flagella. In trypanosomes, an unusually large number of genes encoding for kinesins has been identified (more than 40, (Berriman et al., 2005)) and several of the protein products have been localised to the flagellum (Chan and Ersfeld, 2010; Demonchy et al., 2009) or found in proteomic analyses of purified flagella (Broadhead et al., 2006; Oberholzer et al., 2011; Subota et al., 2014).

The trypanosome flagellum is attached to the cell body for most of its length towards the PFR side. Doublets 1-2-3-8-9 are towards the surface of the flagellum and the absence of IFT could favour interactions with host tissues. For example, parasites interact with the epithelium of the salivary glands of the tsetse fly via their flagellum and the development of electron-dense material resembling hemi-desmosomes (Tetley and Vickerman, 1985). In other organisms, the cilia of sensory neurons of *C. elegans* spring to mind. They are composed of a middle segment made of 9 doublet microtubules and of a distal segment with only singlet microtubules. Bidirectional IFT was reported on both segments without collisions (Snow et al., 2004). If some microtubules were used only for anterograde IFT and others only for retrograde IFT, it would provide a way to avoid collisions (Kuhns and Blacque, 2016).

Here, we show a striking functional difference between doublets 4 & 7 and the others that cannot sustain IFT. Although microtubule doublets look similar, discrete molecular and

structural differences have been noted between them in several organisms (Heuser et al., 2012; Lin et al., 2012). This is also the case in trypanosomes where doublets 4, 5, 6 and 7 are physically linked to the PFR by different structures (Hughes et al., 2012; Sherwin and Gull, 1989) that could contain unique proteins (Imboden et al., 1995). Other molecular differences between doublets start to be unveiled with the recent example of CFAP43 and CFAP44, two proteins required for motility that have been located to doublets 5 and 6 using super-resolution microscopy (Coutton et al., 2018).

What could make doublets 4 and 7 different from the others and why would they be used for IFT? One possibility is that they contain biochemical information that is preferentially recognised by the IFT molecular motors. Promising candidates are post-translational modifications of tubulin such as (poly)glycylation or (poly)glutamylolation. These are found at the surface of the tubulin dimer where one would expect interactions with molecular motors (Konno et al., 2012; Sirajuddin et al., 2014). Insights into a potential molecular mechanism are provided by *in vitro* experiments using engineered tubulin with various post-translational modifications. This revealed that recruitment and processivity of the IFT kinesin motor KIF17 was stimulated by polyglutamylolation (Sirajuddin et al., 2014). Polyglutamylolation and polyglycylation are overwhelmingly represented in cilia and flagella and their alteration affect these organelles (Bosch Grau et al., 2013; Lee et al., 2012; Pathak et al., 2011; Rogowski et al., 2009; Wloga et al., 2009). Mass spectrometry showed that trypanosome tubulin is extensively polyglutamylolated, with variable numbers of glutamate residues added to both cytoplasmic and flagellar microtubules (Schneider et al., 1997). Investigating the role of tubulin glutamylolation in the definition of microtubule heterogeneity will be an exciting but challenging future axis for research given the large number of enzymes involved in this process (Janke et al., 2005; van Dijk et al., 2007) including in *T. brucei* (Casanova et al., 2014).

## Methods

### Trypanosome cell lines and cultures

Cell lines used for this work were derivatives of *T. brucei* strain 427 cultured at 27°C in SDM79 medium supplemented with hemin and 10% foetal calf serum (Brun and Schonenberger, 1979). IFT imaging in live cells was carried out with a cell line expressing GFP::IFT52 from the pHD430 vector (Absalon et al., 2008) under the control of the tet-repressor (produced by plasmid pHD360 (Wirtz and Clayton, 1995)) and a Tandem Tomato::IFT81 fusion produced from its endogenous locus (Bhogaraju et al., 2013). For the generation of the mNeonGreen::IFT81 expressing cell line, the first 500 nucleotides of *IFT81* (Gene DB number Tb927.10.2640) were chemically synthesised (GeneCust, Luxembourg) and cloned in frame with the *mNeonGreen* gene (Shaner et al., 2013) within the HindIII and ApaI sites of p2675 vector (Kelly et al., 2007) The construct was linearised within the *IFT81* sequence with the enzyme XcmI and nucleofected (Burkard et al., 2007) in the wild-type 427 cell line, leading to an integration by homologous recombination in the endogenous locus and to expression of the full-length coding sequence of IFT81 fused to mNeonGreen.

Transfectants were grown in media with the appropriate antibiotic concentration and clonal populations were obtained by limited dilution.

### Focused Ion Beam-Scanning Electron Microscopy (FIB-SEM)

Trypanosomes were fixed directly in medium with 2.5% glutaraldehyde (Sigma), cells were spun down, the supernatant was discarded and the pellet was incubated for 15 minutes in fixation buffer made of 2.5% glutaraldehyde and 4% paraformaldehyde in cacodylate 0.1M buffer (pH 7.4). Samples were washed 3 times with 0.1M cacodylate buffer (5 minutes each) and post fixed with 1% osmium (EMS) and 1.5% potassium ferrocyanide (Sigma) in 0.1M cacodylate buffer for 1h. Samples were treated for 30 minutes with 1% tannic acid (Sigma)

and 1h with 1% osmium tetroxide (EMS), rinsed in water and dehydrated in ethanol (Sigma) series of 25%, 50%, 75%, 90% and 100% (15 minutes each). Cells were embedded in epoxy resin (EMS) after 48h at 60°C of polymerization. Embedded samples were mounted on aluminium stubs. Blocks were trimmed with glass knives in such a way that exposure of vertical faces allowed lateral milling by Focused Ion Beam FIB. Tomographic datasets were obtained using a FESEM Zeiss Auriga microscope equipped by a CrossBeam workstation (Carl Zeiss) and acquired using ATLAS 3D software (Carl Zeiss). For milling with the focused Ga-ion beam, the conditions were as follows: 0.5–1nA milling current of the Ga-emitter, leading to the removal of 10 nm at a time from the epoxy resin. SEM images were recorded with an aperture of 60  $\mu\text{m}$  in the high-current mode at 1.5 or 2 kV of the in-lens EsB detector with the EsB grid set to  $-1000$  V. Depending on the respective magnification, voxel size was in a range between 10 and 20 nm in  $x/y$  and 10 nm in  $z$ . Contrast of the images was inverted to conventional bright field. Two different persons performed the manual annotation of IFT trains. These were defined as electron dense structures sandwiched between the axoneme and the flagellum membrane and present on a minimum of 3 consecutive slices (30 nm). Densities associated to membrane distortions were excluded. Trains were defined as different when separated by a minimum of 3 slices (30 nm).

### **Data processing and 3-D-reconstruction**

Alignment of image stacks was done with the open source software ImageJ for data alignment (Schneider et al., 2012) and Amira Software for visualization (FEI Thermofisher, v6.0.1). Segmentation and 3-D reconstructions were performed semi-automatically using Amira software and were corrected manually.

### **Length measurement of IFT trains**

Segmentations of flagella and IFT trains were first split according to their segmented colours then skeletonized in ImageJ (Schneider et al., 2012) using the Skeletonize 3D plugin (Arganda-Carreras et al., 2010). The number of voxels composing the generated skeletons was computed in ImageJ using the Object Counter 3D plugin (Bolte and Cordelieres, 2006). The length of analysed biological structures (flagella and IFT trains) was calculated as the number of voxels constituting the skeletonized structure multiplied by the size of the voxel.

### **Statistical analyses**

In absence of other indications, all errors correspond to the standard deviation of the population. Anova tests were performed using the appropriate tool in Kaleidagraph v4.5.2. Populations of IFT trains on doublets 4 and 7 were analysed separately with the statistical analysis software R (Team, 2014) using the normalMixEM algorithm of the Mixtools package (version 1.1.0)(Benaglia et al., 2009) to check whether they were composed of sub-populations or not. This algorithm based on expectation maximisation estimates the mean and standard deviation values of Gaussian sub-populations and eventually converges to a solution if such sub-populations exist. Convergence was reached in 27 and 13 iterations for IFT trains on doublet 4 and 7 respectively.

### **Structured illumination microscopy (SIM)**

Trypanosomes expressing the mNG::IFT81 fusion protein were spread on glass coverslips in medium and SIM was performed on a Zeiss LSM780 Elyra PS1 microscope (Carl Zeiss, Germany) using 100×/1.46 oil Plan Apo objective and an EMCCD Andor Ixon 887 1 K camera for the detection at the Institut Pasteur. Fifteen images per plane per channel (five phases, three angles) were acquired to perform the SIM image. SIM image was processed

with ZEN software. The SIMcheck plugin (Ball et al., 2015) in ImageJ (Schneider et al., 2012) was used to evaluate the acquisition and the processing parameters.

### **High-resolution imaging of IFT trafficking**

The cell line expressing GFP::IFT52 and Tandem Tomato::IFT81 was grown in standard conditions and samples were mounted between glass and coverslip for observation on a custom built microscope (Gustafsson, 2000; Gustafsson et al., 2008) based on a Zeiss AxioObserver D1 stand equipped with an UAPON100XOTIRF 1.49 NA objective (Olympus) and an Orca Flash 4.0 sCMOS camera (Hamamatsu). GFP fluorophores were excited with a 488 nm laser (500 mW, SAPPHIRE 488-500, Coherent) and detected through an adequate emission filter (BP 500-550 nm). The sequence contains a series of 300 images exposed for 20 milliseconds each, for a total duration of 17.7 s. Kymographs of individual paths of IFT were extracted using Fiji (Schindelin et al., 2012). The two IFT tracks were manually annotated as segmented lines on the temporal maximal intensity projection of the sequence. These two lines were then used to re-slice the sequence data, generating the kymographs that were analysed using Icy (de Chaumont et al., 2012). The cell line expressing mNG::IFT81 was grown in standard conditions and samples were mounted between glass and quartz coverslip (Cover glasses HI, Carl Zeiss, 1787-996). For movie acquisition, a spinning disk confocal microscope (UltraVIEW VOX, Perkin-Elmer) equipped with an oil immersion objective Plan-Apochromat 100x/1.57 Oil-HI DIC (Carl Zeiss) was used. Movies were acquired using Volocity software with an EMCCD camera (C-9100, Hamamatsu) operating in streaming mode. The samples were kept at 27°C using a temperature controlled chamber. Sequences of 30 seconds were acquired with an exposure time of 100 milliseconds per frame. Kymographs were extracted and analysed with Icy software (de Chaumont et al., 2012) using the plug-in Kymograph Tracker 2 (Chenouard et al., 2010). The cells were positioned in the same

orientation with the posterior end on top and the flagellum on the left-hand side to define the left and right tracks. The two IFT tracks were manually defined as Region of Interest using the temporal projection.

### **Immunofluorescence imaging**

For paraformaldehyde-methanol fixation, cultured parasites were washed twice in SDM79 medium without serum and spread directly onto poly-L-lysine coated slides (Fisher Scientific J2800AMMZ). Cells were left for 10 minutes to settle prior to treatment with 1 volume 4% PFA solution in PBS at pH 7. After 5 minutes, slides were washed briefly in PBS before being fixed in pure methanol at a temperature of -20°C for 5 minutes followed by a rehydration step in PBS for 15 minutes. For immunodetection, slides were incubated for 1 h at 37°C with the appropriate dilution of the first antibody in 0.1% BSA in PBS; mAb25 recognises the axonemal protein TbSAXO1 (Dacheux et al., 2012; Pradel et al., 2006) and a monoclonal antibody against the IFT-B protein IFT172 (Absalon et al., 2008). After 3 consecutive 5-minute washes in PBS, species and subclass-specific secondary antibodies coupled to the appropriate fluorochrome (Alexa 488, Cy3, Jackson ImmunoResearch) were diluted 1/400 in PBS containing 0.1% BSA and were applied for 1 h at 37°C. After washing in PBS as indicated above, cells were stained with a 1 µg/ml solution of the DNA-dye DAPI (Roche) and mounted with the Slowfade antifade reagent (Invitrogen). Slides were immediately observed with a DMI4000 microscope (Leica) with a 100X objective (NA 1.4) using a Hamamatsu ORCA-03G camera with an EL6000 (Leica) as light excitation source. Image acquisition was performed using Micro-manager software and images were analysed using ImageJ (National Institutes of Health, Bethesda, MD).

### **Western blot**

Cells were washed once in Phosphate Buffer Saline (PBS). Laemmli loading buffer was added to the cells and samples were boiled for 5 minutes. 20µg of protein were loaded into each lane of a Criterion™ XT Bis-Tris Precast Gel 4-12% (Bio-Rad, UK) for SDS-Page separation. XT-Mops (1X) diluted in deionised water was used as a running buffer. Proteins were transferred onto nitrocellulose membranes using the BioRad® Trans-Blot Turbo™ blotting system (25V over 7 minutes). The membrane was blocked with 5% skimmed milk for one hour and then incubated with the monoclonal anti-mNeonGreen (32F6) primary antibody (ChromoTek, Germany) diluted 1/1000 in 0.05% PBS-Tween (PBST). As a loading control the anti-PFR L13D6 monoclonal antibody (Kohl et al., 1999) diluted 1/25 was used. After primary antibody incubation, three washes of 5 minutes each were performed in 0.05% PBST followed by secondary antibody incubation. Anti-mouse secondary antibody coupled to horseradish peroxidase, diluted to 1/20,000 in 0.05% PBST containing 0.1% milk, and the membrane was incubated with this for 1 hour. The Amersham ECL Western Blotting Detection Reagent Kit (GE Healthcare Life Sciences, UK) was used for final detection of proteins on the membrane.

## **Acknowledgements**

We thank Sylvie Perrot (Institut Pasteur Paris) for the preparation of samples for FIB-SEM, Audrey Salles (Institut Pasteur Paris) for the SIM acquisition performed on the Zeiss Elyra SP1 system, Derrick Robinson (Bordeaux University, France) for providing the Mab25 antibody and Linda Kohl (Museum of Natural History, Paris) for critical reading of the manuscript. We are grateful to the Photonic Bioimaging and Ultrastructural Bioimaging facilities for access to their equipment. Some SIM and high-resolution microscopy work was performed at the Advanced Imaging Centre, Janelia Research Campus, jointly sponsored by the Howard Hughes Medical Institute and the Gordon & Betty Moore Foundation. We are grateful to Lin Shao for training and advice. The generosity and the reactivity of Jim Morris (Clemson University, USA) are warmly acknowledged for having made this project feasible. E.B. is supported by fellowships from French National Ministry for Research and Technology (doctoral school CDV515) and from La Fondation pour la Recherche Médicale (FDT20170436836). C. F. was supported by fellowships from French National Ministry for Research and Technology (doctoral school CDV515) and from La Fondation pour la Recherche Médicale (FDT20150532023). This work is funded by ANR grants (11-BSV8-016 and 14-CE35-0009-01), by La Fondation pour la Recherche Médicale (Equipe FRM DEQ20150734356) and by a French Government Investissement d'Avenir programme, Laboratoire d'Excellence "Integrative Biology of Emerging Infectious Diseases" (ANR-10-LABX-62-IBEID). We are also grateful for support for FESEM Zeiss Auriga and Elyra PS1 equipment from the French Government Programme Investissements d'Avenir France BioImaging (FBI, N° ANR-10-INSB-04-01) and from a DIM-Malinf grant from the Région Ile-de-France. Live imaging at the AIC, Janelia Farm Research Campus was supported by the Citech (Centre d'Innovation et Recherche Technologique) of the Institut Pasteur.

## **Author contributions**

E. Bertiaux segmented FIB-SEM data, conducted all live cell acquisition with the mNG::IFT81 cell line, extracted and analysed the kymographs and performed the statistical analyses on IFT trafficking and contributed to figure preparation. A. Mallet acquired the FIB-SEM data, segmented them and produced the corresponding videos as well as the analysis of kymographs. C. Fort prepared samples for FIB-SEM and carried out some segmentation, conducted all the GFP::IFT52 acquisition and performed kymograph analyses. T. Blisnick produced the cell line expressing GFP::IFT52, acquired the still images of mNG::IFT81 cell line and assembled the figures. S. Bonnefoy developed the PFA/methanol fixation protocol and performed immunofluorescence data and acquisition. J. Jung characterised the mNG::IFT81 expressing cell line and performed some kymograph analyses. M. Lemos acquired transmission electron microscopy images and was responsible for measurement of the diameter of the axoneme. S. Marco contributed to statistical analysis. S. Vaughan participated to the coordination of the 3-D electron microscopy project. S. Trépot developed the script to perform the measurements of IFT trains from FIB-SEM data and performed the corresponding statistical analysis to identify train sub-populations. J.Y. Tinevez designed the live imaging project performed at the Janelia Farm Research Campus and participated to the high-resolution video acquisition and quantification. P. Bastin conceived and coordinated the project and wrote the paper with contributions from all authors.

The authors declare no competing financial interests.

## References

- Absalon, S., T. Blisnick, L. Kohl, G. Toutirais, G. Dore, D. Julkowska, A. Tavenet, and P. Bastin. 2008. Intraflagellar Transport and Functional Analysis of Genes Required for Flagellum Formation in Trypanosomes. *Mol Biol Cell*. 19:929-944.
- Adhiambo, C., T. Blisnick, G. Toutirais, E. Delannoy, and P. Bastin. 2009. A novel function for the atypical small G protein Rab-like 5 in the assembly of the trypanosome flagellum. *J Cell Sci*. 122:834-841.
- Arganda-Carreras, I., R. Fernandez-Gonzalez, A. Munoz-Barrutia, and C. Ortiz-De-Solorzano. 2010. 3D reconstruction of histological sections: Application to mammary gland tissue. *Microsc Res Tech*. 73:1019-1029.
- Ball, G., J. Demmerle, R. Kaufmann, I. Davis, I.M. Dobbie, and L. Schermelleh. 2015. SIMcheck: a Toolbox for Successful Super-resolution Structured Illumination Microscopy. *Sci Rep*. 5:15915.
- Bastin, P., T. Sherwin, and K. Gull. 1998. Paraflagellar rod is vital for trypanosome motility. *Nature*. 391:548.
- Beales, P.L., E. Bland, J.L. Tobin, C. Bacchelli, B. Tuysuz, J. Hill, S. Rix, C.G. Pearson, M. Kai, J. Hartley, C. Johnson, M. Irving, N. Elcioglu, M. Winey, M. Tada, and P.J. Scambler. 2007. IFT80, which encodes a conserved intraflagellar transport protein, is mutated in Jeune asphyxiating thoracic dystrophy. *Nat Genet*. 39:727-729.
- Benaglia, T., D. Chauveau, D. Hunter, and D. Young. 2009. mixtools: An R Package for Analyzing Finite Mixture Models. *Journal of Statistical Software*. 32:1-29.
- Berriman, M., E. Ghedin, C. Hertz-Fowler, G. Blandin, H. Renault, D.C. Bartholomeu, N.J. Lennard, E. Caler, N.E. Hamlin, B. Haas, U. Bohme, L. Hannick, M.A. Aslett, J. Shallom, L. Marcello, L. Hou, B. Wickstead, U.C. Alsmark, C. Arrowsmith, R.J. Atkin, A.J. Barron, F. Bringaud, K. Brooks, M. Carrington, I. Cherevach, T.J. Chillingworth, C. Churcher, L.N. Clark, C.H. Corton, A. Cronin, R.M. Davies, J. Doggett, A. Djikeng, T. Feldblyum, M.C. Field, A. Fraser, I. Goodhead, Z. Hance, D. Harper, B.R. Harris, H. Hauser, J. Hostetler, A. Ivens, K. Jagels, D. Johnson, J. Johnson, K. Jones, A.X. Kerhornou, H. Koo, N. Larke, S. Landfear, C. Larkin, V. Leech, A. Line, A. Lord, A. Macleod, P.J. Mooney, S. Moule, D.M. Martin, G.W. Morgan, K. Mungall, H. Norbertczak, D. Ormond, G. Pai, C.S. Peacock, J. Peterson, M.A. Quail, E. Rabinowitsch, M.A. Rajandream, C. Reitter, S.L. Salzberg, M. Sanders, S. Schobel, S. Sharp, M. Simmonds, A.J. Simpson, L. Tallon, C.M. Turner,

- A. Tait, A.R. Tivey, S. Van Aken, D. Walker, D. Wanless, S. Wang, B. White, O. White, S. Whitehead, J. Woodward, J. Wortman, M.D. Adams, T.M. Embley, K. Gull, E. Ullu, J.D. Barry, A.H. Fairlamb, F. Opperdoes, B.G. Barrell, J.E. Donelson, N. Hall, C.M. Fraser, et al. 2005. The genome of the African trypanosome *Trypanosoma brucei*. *Science*. 309:416-422.
- Besschetnova, T.Y., E. Kolpakova-Hart, Y. Guan, J. Zhou, B.R. Olsen, and J.V. Shah. 2010. Identification of signaling pathways regulating primary cilium length and flow-mediated adaptation. *Curr Biol*. 20:182-187.
- Bhogaraju, S., L. Cajanek, C. Fort, T. Blisnick, K. Weber, M. Taschner, N. Mizuno, S. Lamla, P. Bastin, E.A. Nigg, and E. Lorentzen. 2013. Molecular basis of tubulin transport within the cilium by IFT74 and IFT81. *Science*. 341:1009-1012.
- Bolte, S., and F.P. Cordelieres. 2006. A guided tour into subcellular colocalization analysis in light microscopy. *J Microsc*. 224:213-232.
- Bonnefoy, S., C.M. Watson, K.D. Kernohan, M. Lemos, S. Hutchinson, J.A. Poulter, L.A. Crinnion, C. O'Callaghan, R.A. Hirst, A. Rutman, L. Huang, T. Hartley, D. Grynspan, E. Moya, C. Li, I.M. Carr, D.T. Bonthron, M. Leroux, Care4Rare Canada Consortium, K.M. Boycott, P. Bastin, and E.G. Sheridan. 2018. Biallelic Mutations in LRRC56 encoding a protein associated with intraflagellar transport, cause mucociliary clearance and laterality defects. *BioRxiv*.
- Bosch Grau, M., G. Gonzalez Curto, C. Rocha, M.M. Magiera, P. Marques Sousa, T. Giordano, N. Spassky, and C. Janke. 2013. Tubulin glycyloses and glutamylases have distinct functions in stabilization and motility of ependymal cilia. *J Cell Biol*. 202:441-451.
- Branche, C., L. Kohl, G. Toutirais, J. Buisson, J. Cosson, and P. Bastin. 2006. Conserved and specific functions of axoneme components in trypanosome motility. *J Cell Sci*. 119:3443-3455.
- Broadhead, R., H.R. Dawe, H. Farr, S. Griffiths, S.R. Hart, N. Portman, M.K. Shaw, M.L. Ginger, S.J. Gaskell, P.G. McKean, and K. Gull. 2006. Flagellar motility is required for the viability of the bloodstream trypanosome. *Nature*. 440:224-227.
- Brooks, E.R., and J.B. Wallingford. 2012. Control of vertebrate intraflagellar transport by the planar cell polarity effector Fuz. *J Cell Biol*. 198:37-45.
- Brun, R., and Schonenberger. 1979. Cultivation and in vitro cloning or procyclic culture forms of *Trypanosoma brucei* in a semi-defined medium. Short communication. *Acta tropica*. 36:289-292.

- Buisson, J., N. Chenouard, T. Lagache, T. Blisnick, J.C. Olivo-Marin, and P. Bastin. 2013. Intraflagellar transport proteins cycle between the flagellum and its base. *J Cell Sci.* 126:327-338.
- Burkard, G., C.M. Fragoso, and I. Roditi. 2007. Highly efficient stable transformation of bloodstream forms of *Trypanosoma brucei*. *Mol Biochem Parasitol.* 153:220-223.
- Casanova, M., F. de Monbrison, J. van Dijk, C. Janke, M. Pages, and P. Bastien. 2014. Characterisation of polyglutamylases in trypanosomatids. *International journal for parasitology.*
- Chan, K.Y., and K. Ersfeld. 2010. The role of the Kinesin-13 family protein TbKif13-2 in flagellar length control of *Trypanosoma brucei*. *Mol Biochem Parasitol.* 174:137-140.
- Chenouard, N., J. Buisson, I. Bloch, P. Bastin, and J.C. Olivo-Marin. 2010. Curvelet analysis of kymograph for tracking bi-directional particles in fluorescence microscopy images. *International Conference on Image Processing*:in press.
- Chien, A., S.M. Shih, R. Bower, D. Tritschler, M.E. Porter, and A. Yildiz. 2017. Dynamics of the IFT machinery at the ciliary tip. *eLife.* 6.
- Coutton, C., A.S. Vargas, A. Amiri-Yekta, Z.E. Kherraf, S.F. Ben Mustapha, P. Le Tanno, C. Wambergue-Legrand, T. Karaouzene, G. Martinez, S. Crouzy, A. Daneshpour, S.H. Hosseini, V. Mitchell, L. Halouani, O. Marrakchi, M. Makni, H. Latrous, M. Kharouf, J.F. Deleuze, A. Boland, S. Hennebicq, V. Satre, P.S. Jouk, N. Thierry-Mieg, B. Conne, D. Dacheux, N. Landrein, A. Schmitt, L. Stouvenel, P. Loes, E. El Khouri, S.P. Bottari, J. Faure, J.P. Wolf, K. Pernet-Gallay, J. Escoffier, H. Gourabi, D.R. Robinson, S. Nef, E. Dulioust, R. Zouari, M. Bonhivers, A. Toure, C. Arnoult, and P.F. Ray. 2018. Mutations in CFAP43 and CFAP44 cause male infertility and flagellum defects in *Trypanosoma* and human. *Nature communications.* 9:686.
- Craft, J.M., J.A. Harris, S. Hyman, P. Kner, and K.F. Lechtreck. 2015. Tubulin transport by IFT is upregulated during ciliary growth by a cilium-autonomous mechanism. *J Cell Biol.* 208:223-237.
- Dacheux, D., N. Landrein, M. Thonnus, G. Gilbert, A. Sahin, H. Wodrich, D.R. Robinson, and M. Bonhivers. 2012. A MAP6-related protein is present in protozoa and is involved in flagellum motility. *PLoS ONE.* 7:e31344.
- Dagoneau, N., M. Goulet, D. Genevieve, Y. Sznajder, J. Martinovic, S. Smithson, C. Huber, G. Baujat, E. Flori, L. Tecco, D. Cavalcanti, A.L. Delezoide, V. Serre, M. Le Merrer, A. Munnich, and V. Cormier-Daire. 2009. DYNC2H1 mutations cause asphyxiating

- thoracic dystrophy and short rib-polydactyly syndrome, type III. *Am J Hum Genet.* 84:706-711.
- de Chaumont, F., S. Dallongeville, N. Chenouard, N. Herve, S. Pop, T. Provoost, V. Meas-Yedid, P. Pankajakshan, T. Lecomte, Y. Le Montagner, T. Lagache, A. Dufour, and J.C. Olivo-Marin. 2012. Icy: an open bioimage informatics platform for extended reproducible research. *Nat Methods.* 9:690-696.
- Dean, S., J.D. Sunter, and R.J. Wheeler. 2017. TrypTag.org: A Trypanosome Genome-wide Protein Localisation Resource. *Trends in parasitology.* 33:80-82.
- Demonchy, R., T. Blisnick, C. Deprez, G. Toutirais, C. Loussert, W. Marande, P. Grellier, P. Bastin, and L. Kohl. 2009. Kinesin 9 family members perform separate functions in the trypanosome flagellum. *J Cell Biol.* 187:615-622.
- Gadelha, C., B. Wickstead, P.G. McKean, and K. Gull. 2006. Basal body and flagellum mutants reveal a rotational constraint of the central pair microtubules in the axonemes of trypanosomes. *J Cell Sci.* 119:2405-2413.
- Gustafsson, M.G. 2000. Surpassing the lateral resolution limit by a factor of two using structured illumination microscopy. *J Microsc.* 198:82-87.
- Gustafsson, M.G., L. Shao, P.M. Carlton, C.J. Wang, I.N. Golubovskaya, W.Z. Cande, D.A. Agard, and J.W. Sedat. 2008. Three-dimensional resolution doubling in wide-field fluorescence microscopy by structured illumination. *Biophys J.* 94:4957-4970.
- Halbritter, J., A.A. Bizet, M. Schmidts, J.D. Porath, D.A. Braun, H.Y. Gee, A.M. McInerney-Leo, P. Krug, E. Filhol, E.E. Davis, R. Airik, P.G. Czarnecki, A.M. Lehman, P. Trnka, P. Nitschke, C. Bole-Feysot, M. Schueler, B. Knebelmann, S. Burtey, A.J. Szabo, K. Tory, P.J. Leo, B. Gardiner, F.A. McKenzie, A. Zankl, M.A. Brown, J.L. Hartley, E.R. Maher, C. Li, M.R. Leroux, P.J. Scambler, S.H. Zhan, S.J. Jones, H. Kayserili, B. Tuysuz, K.N. Moorani, A. Constantinescu, I.D. Krantz, B.S. Kaplan, J.V. Shah, T.W. Hurd, D. Doherty, N. Katsanis, E.L. Duncan, E.A. Otto, P.L. Beales, H.M. Mitchison, S. Saunier, and F. Hildebrandt. 2013. Defects in the IFT-B Component IFT172 Cause Jeune and Mainzer-Saldino Syndromes in Humans. *Am J Hum Genet.* 93:915-925.
- Heuser, T., C.F. Barber, J. Lin, J. Krell, M. Rebesco, M.E. Porter, and D. Nicastro. 2012. Cryoelectron tomography reveals doublet-specific structures and unique interactions in the I1 dynein. *Proc Natl Acad Sci U S A.* 109:E2067-2076.
- Hoog, J.L., S. Lacomble, C. Bouchet-Marquis, L. Briggs, K. Park, A. Hoenger, and K. Gull. 2016. 3D Architecture of the Trypanosoma brucei Flagella Connector, a Mobile Transmembrane Junction. *PLoS Negl Trop Dis.* 10:e0004312.

- Huet, D., T. Blisnick, S. Perrot, and P. Bastin. 2014. The GTPase IFT27 is involved in both anterograde and retrograde intraflagellar transport. *eLife* 2014;10.7554/eLife.02419.
- Hughes, L., S. Borrett, K. Towers, T. Starborg, and S. Vaughan. 2017. Patterns of organelle ontogeny through a cell cycle revealed by whole-cell reconstructions using 3D electron microscopy. *J Cell Sci.* 130:637-647.
- Hughes, L.C., K.S. Ralston, K.L. Hill, and Z.H. Zhou. 2012. Three-dimensional structure of the Trypanosome flagellum suggests that the paraflagellar rod functions as a biomechanical spring. *PLoS One.* 7:e25700.
- Imboden, M., N. Muller, A. Hemphill, R. Mattioli, and T. Seebeck. 1995. Repetitive proteins from the flagellar cytoskeleton of African trypanosomes are diagnostically useful antigens. *Parasitology.* 110 ( Pt 3):249-258.
- Iomini, C., V. Babaev-Khaimov, M. Sassaroli, and G. Piperno. 2001. Protein particles in Chlamydomonas flagella undergo a transport cycle consisting of four phases. *J Cell Biol.* 153:13-24.
- Janke, C., K. Rogowski, D. Wloga, C. Regnard, A.V. Kajava, J.M. Strub, N. Temurak, J. van Dijk, D. Boucher, A. van Dorsselaer, S. Suryavanshi, J. Gaertig, and B. Edde. 2005. Tubulin polyglutamylase enzymes are members of the TTL domain protein family. *Science.* 308:1758-1762.
- Kelly, S., J. Reed, S. Kramer, L. Ellis, H. Webb, J. Sunter, J. Salje, N. Marinsek, K. Gull, B. Wickstead, and M. Carrington. 2007. Functional genomics in Trypanosoma brucei: a collection of vectors for the expression of tagged proteins from endogenous and ectopic gene loci. *Mol Biochem Parasitol.* 154:103-109.
- Kizilyaprak, C., J. Daraspe, and B.M. Humbel. 2014. Focused ion beam scanning electron microscopy in biology. *J Microsc.* 254:109-114.
- Kohl, L., T. Sherwin, and K. Gull. 1999. Assembly of the paraflagellar rod and the flagellum attachment zone complex during the Trypanosoma brucei cell cycle. *J Eukaryot Microbiol.* 46:105-109.
- Konno, A., M. Setou, and K. Ikegami. 2012. Ciliary and flagellar structure and function--their regulations by posttranslational modifications of axonemal tubulin. *Int Rev Cell Mol Biol.* 294:133-170.
- Koyfman, A.Y., M.F. Schmid, L. Gheiratmand, C.J. Fu, H.A. Khant, D. Huang, C.Y. He, and W. Chiu. 2011. Structure of Trypanosoma brucei flagellum accounts for its bihelical motion. *Proc Natl Acad Sci U S A.* 108:11105-11108.

- Kozminski, K.G., K.A. Johnson, P. Forscher, and J.L. Rosenbaum. 1993. A motility in the eukaryotic flagellum unrelated to flagellar beating. *Proc Natl Acad Sci U S A.* 90:5519-5523.
- Kubo, T., J.M. Brown, K. Bellve, B. Craige, J.M. Craft, K. Fogarty, K.F. Lechtreck, and G.B. Witman. 2016. Together, the IFT81 and IFT74 N-termini form the main module for intraflagellar transport of tubulin. *J Cell Sci.* 129:2106-2119.
- Kuhns, S., and O.E. Blacque. 2016. Cilia Train Spotting. *Dev Cell.* 37:395-396.
- Lacomble, S., S. Vaughan, C. Gadelha, M.K. Morphew, M.K. Shaw, J.R. McIntosh, and K. Gull. 2009. Three-dimensional cellular architecture of the flagellar pocket and associated cytoskeleton in trypanosomes revealed by electron microscope tomography. *J Cell Sci.* 122:1081-1090.
- Lee, J.E., J.L. Silhavy, M.S. Zaki, J. Schroth, S.L. Bielas, S.E. Marsh, J. Olvera, F. Brancati, M. Iannicelli, K. Ikegami, A.M. Schlossman, B. Merriman, T. Attie-Bitach, C.V. Logan, I.A. Glass, A. Cluckey, C.M. Louie, J.H. Lee, H.R. Raynes, I. Rapin, I.P. Castroviejo, M. Setou, C. Barbot, E. Boltshauser, S.F. Nelson, F. Hildebrandt, C.A. Johnson, D.A. Doherty, E.M. Valente, and J.G. Gleeson. 2012. CEP41 is mutated in Joubert syndrome and is required for tubulin glutamylation at the cilium. *Nat Genet.* 44:193-199.
- Li, D., L. Shao, B.C. Chen, X. Zhang, M. Zhang, B. Moses, D.E. Milkie, J.R. Beach, J.A. Hammer, 3rd, M. Pasham, T. Kirchhausen, M.A. Baird, M.W. Davidson, P. Xu, and E. Betzig. 2015. Advanced Imaging. Extended-resolution structured illumination imaging of endocytic and cytoskeletal dynamics. *Science.* 349:aab3500.
- Lin, J., T. Heuser, K. Song, X. Fu, and D. Nicastro. 2012. One of the nine doublet microtubules of eukaryotic flagella exhibits unique and partially conserved structures. *PLoS One.* 7:e46494.
- Mijalkovic, J., B. Prevo, F. Oswald, P. Mangeol, and E.J. Peterman. 2017. Ensemble and single-molecule dynamics of IFT dynein in *Caenorhabditis elegans* cilia. *Nature communications.* 8:14591.
- Oberholzer, M., G. Langousis, H.T. Nguyen, E.A. Saada, M.M. Shimogawa, Z.O. Jonsson, S.M. Nguyen, J.A. Wohlschlegel, and K.L. Hill. 2011. Independent analysis of the flagellum surface and matrix proteomes provides insight into flagellum signaling in mammalian-infectious *Trypanosoma brucei*. *Molecular & cellular proteomics : MCP.* 10:M111 010538.

- Pathak, N., C.A. Austin, and I.A. Drummond. 2011. Tubulin tyrosine ligase like genes TTLL3 and TTLL6 maintain zebrafish cilia structure and motility. *J Biol Chem.* 286:11685-11695.
- Perrault, I., S. Saunier, S. Hanein, E. Filhol, A.A. Bizet, F. Collins, M.A. Salih, S. Gerber, N. Delphin, K. Bigot, C. Orssaud, E. Silva, V. Baudouin, M.M. Oud, N. Shannon, M. Le Merrer, O. Roche, C. Pietrement, J. Goumid, C. Baumann, C. Bole-Feysot, P. Nitschke, M. Zahrate, P. Beales, H.H. Arts, A. Munnich, J. Kaplan, C. Antignac, V. Cormier-Daire, and J.M. Rozet. 2012. Mainzer-Saldino syndrome is a ciliopathy caused by IFT140 mutations. *Am J Hum Genet.* 90:864-870.
- Pigino, G., S. Geimer, S. Lanzavecchia, E. Paccagnini, F. Cantele, D.R. Diener, J.L. Rosenbaum, and P. Lupetti. 2009. Electron-tomographic analysis of intraflagellar transport particle trains in situ. *J Cell Biol.* 187:135-148.
- Pradel, L.C., M. Bonhivers, N. Landrein, and D.R. Robinson. 2006. NIMA-related kinase TbNRKC is involved in basal body separation in *Trypanosoma brucei*. *J Cell Sci.* 119:1852-1863.
- Prevo, B., P. Mangeol, F. Oswald, J.M. Scholey, and E.J. Peterman. 2015. Functional differentiation of cooperating kinesin-2 motors orchestrates cargo import and transport in *C. elegans* cilia. *Nat Cell Biol.* 17:1536-1545.
- Prevo, B., J.M. Scholey, and E.J.G. Peterman. 2017. Intraflagellar transport: mechanisms of motor action, cooperation, and cargo delivery. *FEBS J.* 284:2905-2931.
- Ralston, K.S., A.G. Lerner, D.R. Diener, and K.L. Hill. 2006. Flagellar motility contributes to cytokinesis in *Trypanosoma brucei* and is modulated by an evolutionarily conserved dynein regulatory system. *Eukaryot Cell.* 5:696-711.
- Ringo, D.L. 1967. Flagellar motion and fine structure of the flagellar apparatus in *Chlamydomonas*. *J Cell Biol.* 33:543-571.
- Rogowski, K., F. Juge, J. van Dijk, D. Wloga, J.M. Strub, N. Levilliers, D. Thomas, M.H. Bre, A. Van Dorsselaer, J. Gaertig, and C. Janke. 2009. Evolutionary divergence of enzymatic mechanisms for posttranslational polyglycylation. *Cell.* 137:1076-1087.
- Rompolas, P., L.B. Pedersen, R.S. Patel-King, and S.M. King. 2007. *Chlamydomonas* FAP133 is a dynein intermediate chain associated with the retrograde intraflagellar transport motor. *J Cell Sci.* 120:3653-3665.
- Santrich, C., L. Moore, T. Sherwin, P. Bastin, C. Brokaw, K. Gull, and J.H. LeBowitz. 1997. A motility function for the paraflagellar rod of *Leishmania* parasites revealed by PFR-2 gene knockouts. *Mol Biochem Parasitol.* 90:95-109.

- Schindelin, J., I. Arganda-Carreras, E. Frise, V. Kaynig, M. Longair, T. Pietzsch, S. Preibisch, C. Rueden, S. Saalfeld, B. Schmid, J.Y. Tinevez, D.J. White, V. Hartenstein, K. Eliceiri, P. Tomancak, and A. Cardona. 2012. Fiji: an open-source platform for biological-image analysis. *Nat Methods*. 9:676-682.
- Schneider, A., U. Plessmann, and K. Weber. 1997. Subpellicular and flagellar microtubules of *Trypanosoma brucei* are extensively glutamylated. *J Cell Sci*. 110:431-437.
- Schneider, C.A., W.S. Rasband, and K.W. Eliceiri. 2012. NIH Image to ImageJ: 25 years of image analysis. *Nat Methods*. 9:671-675.
- Shaner, N.C., G.G. Lambert, A. Chamma, Y. Ni, P.J. Cranfill, M.A. Baird, B.R. Sell, J.R. Allen, R.N. Day, M. Israelsson, M.W. Davidson, and J. Wang. 2013. A bright monomeric green fluorescent protein derived from *Branchiostoma lanceolatum*. *Nat Methods*. 10:407-409.
- Sherwin, T., and K. Gull. 1989. The cell division cycle of *Trypanosoma brucei brucei*: timing of event markers and cytoskeletal modulations. *Philos Trans R Soc Lond B Biol Sci*. 323:573-588.
- Sirajuddin, M., L.M. Rice, and R.D. Vale. 2014. Regulation of microtubule motors by tubulin isoforms and post-translational modifications. *Nat Cell Biol*. 16:335-344.
- Snow, J.J., G. Ou, A.L. Gunnarson, M.R. Walker, H.M. Zhou, I. Brust-Mascher, and J.M. Scholey. 2004. Two anterograde intraflagellar transport motors cooperate to build sensory cilia on *C. elegans* neurons. *Nat Cell Biol*. 6:1109-1113.
- Stepanek, L., and G. Pigino. 2016. Microtubule doublets are double-track railways for intraflagellar transport trains. *Science*. 352:721-724.
- Subota, I., D. Julkowska, L. Vincensini, N. Reeg, J. Buisson, T. Blisnick, D. Huet, S. Perrot, J. Santi-Rocca, M. Duchateau, V. Hourdel, J.C. Rousselle, N. Cayet, A. Namane, J. Chamot-Rooke, and P. Bastin. 2014. Proteomic analysis of intact flagella of procyclic *Trypanosoma brucei* cells identifies novel flagellar proteins with unique sub-localization and dynamics. *Molecular & cellular proteomics : MCP*. 13:1769-1786.
- Taschner, M., and E. Lorentzen. 2016. The Intraflagellar Transport Machinery. *Cold Spring Harb Perspect Biol*. 8.
- Team, R.C. 2014. R: A language and environment for statistical computing. *R Foundation for Statistical Computing, Vienna, Austria*.
- Tetley, L., and K. Vickerman. 1985. Differentiation in *Trypanosoma brucei*: host-parasite cell junctions and their persistence during acquisition of the variable antigen coat. *J Cell Sci*. 74:1-19.

- van Dijk, J., K. Rogowski, J. Miro, B. Lacroix, B. Edde, and C. Janke. 2007. A targeted multienzyme mechanism for selective microtubule polyglutamylation. *Mol Cell*. 26:437-448.
- Vannuccini, E., E. Paccagnini, F. Cantele, M. Gentile, D. Dini, F. Fino, D. Diener, C. Mencarelli, and P. Lupetti. 2016. Two classes of short intraflagellar transport train with different 3D structures are present in *Chlamydomonas* flagella. *J Cell Sci*. 129:2064-2074.
- Wheeler, R.J., E. Gluenz, and K. Gull. 2015. Basal body multipotency and axonemal remodelling are two pathways to a 9+0 flagellum. *Nature communications*. 6:8964.
- Williams, C.L., J.C. McIntyre, S.R. Norris, P.M. Jenkins, L. Zhang, Q. Pei, K. Verhey, and J.R. Martens. 2014. Direct evidence for BBSome-associated intraflagellar transport reveals distinct properties of native mammalian cilia. *Nature communications*. 5:5813.
- Wingfield, J.L., I. Mengoni, H. Bomberger, Y.Y. Jiang, J.D. Walsh, J.M. Brown, T. Picariello, D.A. Cochran, B. Zhu, J. Pan, J. Eggenschwiler, J. Gaertig, G.B. Witman, P. Kner, and K. Lechtreck. 2017. IFT trains in different stages of assembly queue at the ciliary base for consecutive release into the cilium. *eLife*. 6.
- Wirtz, E., and C. Clayton. 1995. Inducible gene expression in trypanosomes mediated by a prokaryotic repressor. *Science*. 268:1179-1183.
- Wirtz, E., S. Leal, C. Ochatt, and G.A. Cross. 1999. A tightly regulated inducible expression system for conditional gene knock-outs and dominant-negative genetics in *Trypanosoma brucei*. *Mol Biochem Parasitol*. 99:89-101.
- Wloga, D., D.M. Webster, K. Rogowski, M.H. Bre, N. Levilliers, M. Jerka-Dziadosz, C. Janke, S.T. Dougan, and J. Gaertig. 2009. TTLL3 Is a tubulin glycine ligase that regulates the assembly of cilia. *Dev Cell*. 16:867-876.

## **Abbreviations**

FIB-SEM, Focused Ion Beam Scanning Electron Microscopy

IFA, immunofluorescence assay

IFT, intraflagellar transport

PFR, paraflagellar rod

TEM, transmission electron microscopy

**Table 1. Speed and frequency of anterograde IFT trafficking**

	Speed ( $\mu\text{m/s}$ )	Frequency (trains/s)	n
<u>mNG::IFT81</u>			
Left	$2.43 \pm 0.68$	$0.52 \pm 0.22$	284
Right	$2.27 \pm 0.65$	$0.45 \pm 0.18$	245
Left + right	$2.35 \pm 0.62$	$0.98 \pm 0.33$	529
Unresolved*	$2.60 \pm 0.46$	$0.76 \pm 0.11$	389
 <u>GFP::IFT52</u>			
Left	$2.56 \pm 0.26$	$0.43 \pm 0.10$	138
Right	$2.18 \pm 0.29$	$0.34 \pm 0.17$	110
Left + right	$2.37 \pm 0.26$	$0.77 \pm 0.15$	248

\*Corresponds to videos acquired in high-resolution conditions but where only one track could be visualised, presumably due to the orientation of the flagellum during the acquisition.

Hence, two tracks could not be resolved.

## Figure legends

### **Fig. 1. Positioning of IFT trains in the trypanosome flagellum and models for IFT**

**trafficking. (A)** Cross-section of the trypanosome flagellum observed by conventional TEM. The arrowhead indicates an IFT particle positioned at the level of doublet 4. The cartoon shows the main structural components of the axoneme with the numbering of microtubule doublets (Branche et al., 2006) superposed on the original image. Doublet numbering follows the conventional rules: a line perpendicular to the middle axis of the central pair microtubules is drawn and makes contact with the A-tubule of only one doublet that is defined as number 1. The numbering follows the clockwise orientation defined by the dynein arms. Dynein arms are shown in orange, radial spoke in violet, central pair projections in yellow and the PFR in blue. **(B)** The restricted presence of IFT on doublets 4 and 7 can be explained by two models: either one track is used for anterograde and the other one supports retrograde IFT (Model 1) or bidirectional trafficking takes place on both (Model 2).

**Fig. 2: IFT trains of similar length are distributed on doublets 4 and 7. (A)** Successive images from Video S1 showing wild-type trypanosomes analysed by FIB-SEM. Each image corresponds to a Z-stack of 3 slices between positions 424 and 475. The progression is from posterior to anterior. The top panels show low magnification of the cell body where major organelles are indicated (ER, endoplasmic reticulum, F, flagellum, G, glycosomes, M, mitochondrion). Bottom: A zoom of the flagellum area is shown with the axoneme (A) and the PFR. The arrows indicate IFT particles. **(B)** Portions of flagella reconstructed after FIB-SEM. Each axoneme is shown with a different colour and IFT trains are in red (for animation, see Video S2). Doublet numbers and flagellum orientation (BB, basal body and tip) are indicated for a couple of flagella. **(C)** Other example of a flagellum from a wild-type

trypanosome coming from a different stack than the one presented in A-B with the axoneme (sky blue) and several IFT trains (red). **(D)** Length of the IFT trains on doublets 4 (green) and 7 (magenta) determined from FIB-SEM analysis. Data are coming from 27 portions of flagella representing a total axoneme length of 166  $\mu\text{m}$ . Two populations can be separated with short trains (green) and longer ones (magenta, see text for details).

**Fig. 3. IFT proteins are found on two distinct lines along the axoneme in fixed cells.**

Control trypanosomes (strain expressing YFP::ODA8 (Bonney et al., 2018)) were fixed in paraformaldehyde followed by methanol post-fixation and processed for immunofluorescence using a marker antibody for the axoneme (middle panel, magenta on the merged image) and a monoclonal antibody against IFT172 (right panel, green on the merged image). The first panel shows the phase contrast image merged with DAPI staining (cyan). **(A)** Cell with one flagellum. **(B)** Cell assembling a new flagellum. In both cases, a single continuous thick line is observed for the axoneme marker whereas discontinuous staining spreading on two close but distinct lines is visible for IFT172.

**Fig. 4. Bidirectional IFT trafficking takes place on two tracks in live trypanosomes expressing mNG::IFT81.**

**(A)** Temporal projection of a stack of images corresponding to Video S6 showing the presence of two tracks for IFT in the flagellum in addition to the pool of IFT at the base. The left (green) and right (magenta) tracks were defined after orientating the cell with the posterior end on top of the image and the flagellum on the left-hand side. **(B)** Still images from Video S6 of live trypanosomes expressing mNG::IFT81 imaged at high-resolution. Green and magenta arrowheads indicate trains on the left and right tracks with light arrowheads pointing at anterograde trains and darker arrowheads showing retrograde trains. The time point for each image is indicated. **(C)** Kymograph analysis of the same cell

showing trafficking on the left track (green), on the right track (magenta) and the merged images for the region of interest indicated in A. Scale bars are 2.5  $\mu\text{m}$  for length (horizontal bar) and 2.5 seconds for time (vertical bar). **(D)** Dot plot of the frequency of anterograde IFT trains visible on the left (green) and the right (magenta) track, the sum of both (cyan) and from videos where only one track was visible (unresolved, grey). **(E)** Same representation but for the speed of anterograde trains. Only statistically significant differences are shown.

**Fig. 5. Anterograde trains are converted to retrograde trains whilst remaining on the same track.** **(A)** Temporal projection of the flagellum in a cell expressing mNG::IFT81. The region of interest at the tip of the flagellum is indicated, with left (green) and right (magenta) tracks. **(B)** The kymographs are shown for each of them in the corresponding colour. Note the presence of an anterograde train that arrested for a few seconds before the material it contained was picked up by other anterograde trains (stars). Scale bars are 2.5  $\mu\text{m}$  for length (horizontal bar) and 5 seconds for time (vertical bar). **(C)** The distal tip of a cell expressing GFP::IFT52 was photobleached and the transition from anterograde to retrograde trains was monitored in the indicated region of interest. **(D)** Kymographs are highlighted in green and magenta as above. Scale bars are 2.5  $\mu\text{m}$  for length (horizontal bar) and 5 seconds for time (vertical bar). The enlarged portion shows the distal end of the flagellum where fluorescent proteins present in anterograde trains are seen transiting for a few seconds before leaving in association to multiple but discrete retrograde trains. No evidence for transfer between the left and right tracks could be observed.

## Legends for supplementary figures

**Fig. S1. Endogenous tagging of IFT81 with mNG provides a clean marker for monitoring IFT.** (A) Western blotting with an anti-mNG antibody reveals the expected mobility on SDS-PAGE. No signal is detected with the 29-13 (Wirtz et al., 1999) control cell line. The L13D6 monoclonal antibody recognising the PFR proteins was used as loading control. (B) Still images of Video S3 showing anterograde (green arrowheads) and retrograde (dark green arrowheads) IFT trafficking in a uniflagellated cell using conventional light microscopy. Focusing was made on the flagellum and the base of the flagellum is not in the same plane. The star shows an arrested IFT train. (C) Temporal projection shows only one track in these imaging conditions. (D-E) A region of interest was drawn on the indicated position of the image (D) and the kymograph was extracted showing typical robust anterograde and more discrete retrograde trains (E). The position of the arrested train marked in B is highlighted with stars. Scale bars are 2.5  $\mu\text{m}$  for length (horizontal bar) and 2.5 seconds for time (vertical bar). (F) Cells expressing mNG::IFT81 were fixed using the paraformaldehyde-methanol protocol and direct imaging of mNG::IFT81 fluorescence was carried out revealing the existence of two parallel lines in mature and growing flagella. The base of both types of flagella is clearly visible on the bottom image.

**Fig. S2. SIM imaging in live cells reveals trafficking on two separate tracks.** (A) SIM images showing the presence of IFT trains on two tracks in cells expressing the mNG::IFT81 fusion protein. Fifteen images per plane per channel (five phases, three angles) were acquired to perform the SIM image. (B) Temporal projection of images coming from Video S5 in cells expressing the GFP::IFT52 fusion protein showing the presence of IFT trains on two tracks.

Areas in rectangles have been zoomed to show the two tracks. However, temporal resolution is not sufficient to determine the orientation of trafficking.

**Fig. S3. Bidirectional IFT trafficking takes place on two tracks in live trypanosomes**

**expressing GFP::IFT52.** (A) Individual images from Video S7 showing the presence of two tracks for IFT in the flagellum. The IFT pool at the base is out of the plane of focus. The left (green) and right (magenta) tracks were defined after orientating the cell with the posterior end on top of the image and the flagellum on the left-hand side. (B) Still images from Video S7 of live trypanosomes expressing GFP::IFT52 imaged at high-resolution. Green and magenta arrowheads indicate trains on the left and right tracks with lighter arrowheads pointing at anterograde trains and darker arrowheads showing retrograde trains. (C) Kymograph analysis of the same cell showing the left (green), the right (magenta) and the merged images. Scale bars are 2  $\mu\text{m}$  for length (horizontal bar) and 2 seconds for time (vertical bar). (D) Dot plot of the frequency of anterograde IFT trains visible on the left (green) and the right (magenta) track and the sum of both (cyan). (E) Dot plot but for the speed of anterograde trains.

**Video S1.** Three-dimensional view of wild-type trypanosomes analysed by FIB-SEM with the stack of original data where several cells are visible with all typical organelles including the flagellum.

**Video S2.** Individual flagella of the stack from Video S1 are shown in different colours and the IFT trains are shown in red. The volume is then rotated in all dimensions to visualise the positioning of IFT trains.

**Video S3.** Live imaging of a cell expressing mNG::IFT81 showing robust bidirectional IFT.

**Video S4.** Live imaging by SIM of a cell expressing mNG::IFT81 showing the existence of two tracks for IFT trafficking. Fifteen images per plane per channel (five phases, three angles) were acquired to perform the SIM image.

**Video S5.** Live imaging by SIM of a cell expressing GFP::IFT52 showing the existence of two tracks for IFT trafficking. Time-series were acquired for a total of 14 seconds. Although the spatial resolution allows the distinction of two tracks, the time resolution is not sufficient to discriminate individual IFT trains on them.

**Video S6.** Live imaging by high-resolution microscopy using a 1.57 NA objective of a cell expressing mNG::IFT81. Bidirectional IFT trafficking is visible on two distinct tracks. The spatial resolution allows the distinction of two tracks and the time resolution permits the discrimination of individual IFT trains on each of them.

**Video S7.** Live imaging by high-resolution microscopy using a 1.49 NA objective of a cell expressing GFP::IFT52. Bidirectional IFT trafficking is visible on two distinct tracks. The spatial resolution allows the distinction of two tracks and the time resolution permits the discrimination of individual IFT trains on each of them.

**Video S8.** Live imaging by high-resolution microscopy using a 1.57 NA objective of a cell expressing mNG::IFT81. Focusing on the distal tip reveals the transit and turnaround of IFT material during the conversion of anterograde to retrograde trains.

**Video S9.** Live imaging by high-resolution microscopy using a 1.49 NA objective of a cell expressing GFP::IFT52. Focusing on the distal tip reveals the transit and turnaround of IFT material during the conversion of anterograde to retrograde trains.

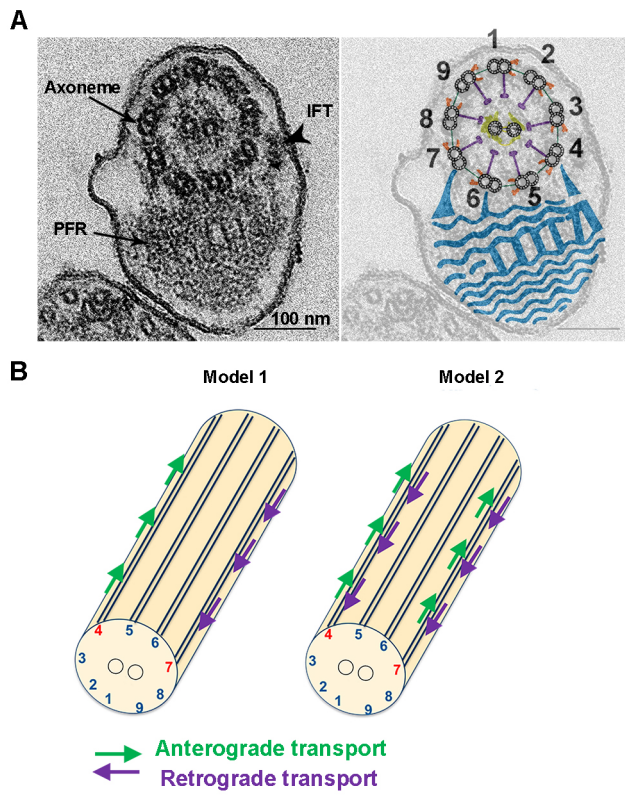


Figure 1

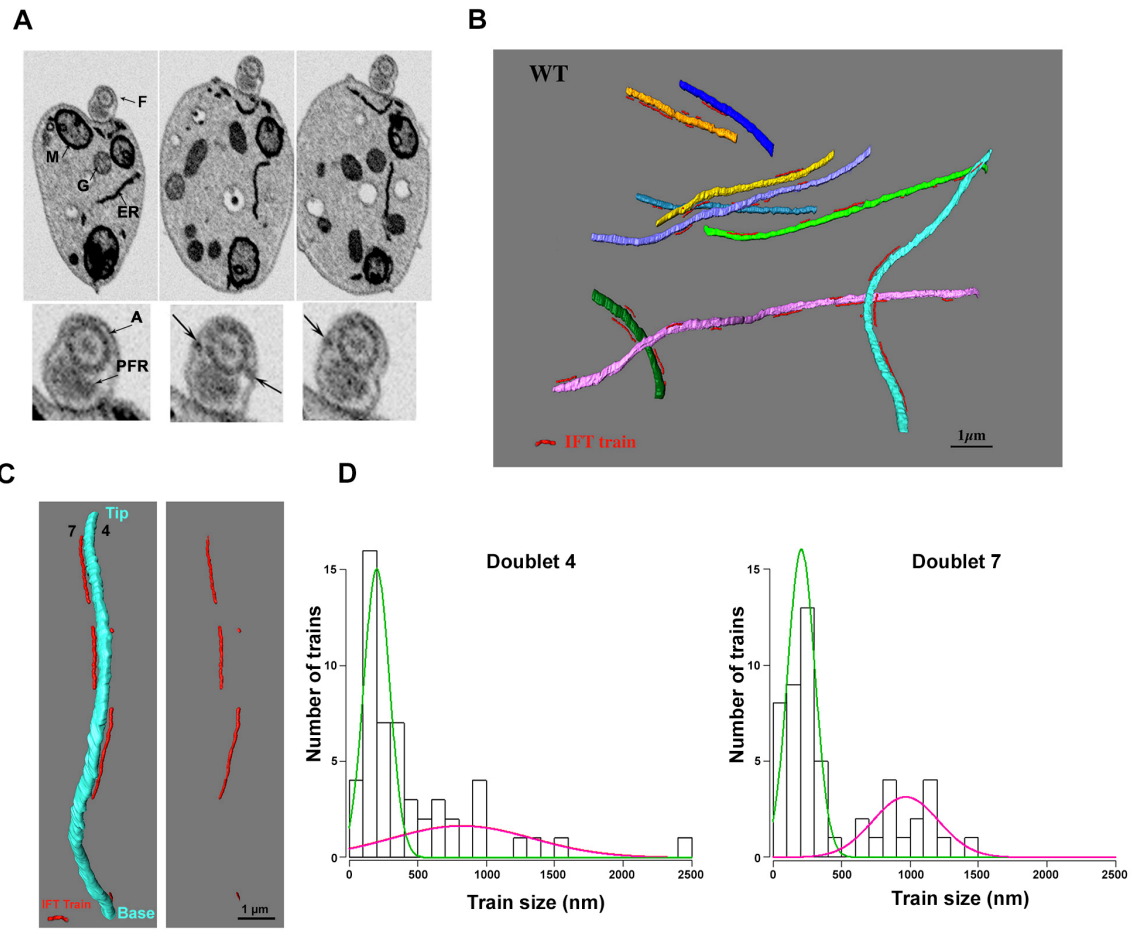


Figure 2

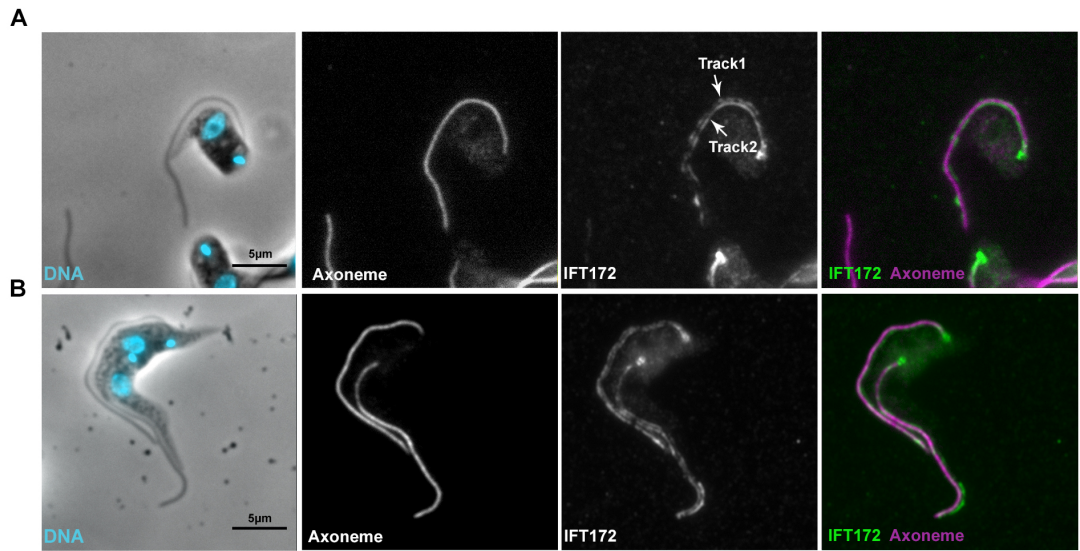


Figure 3

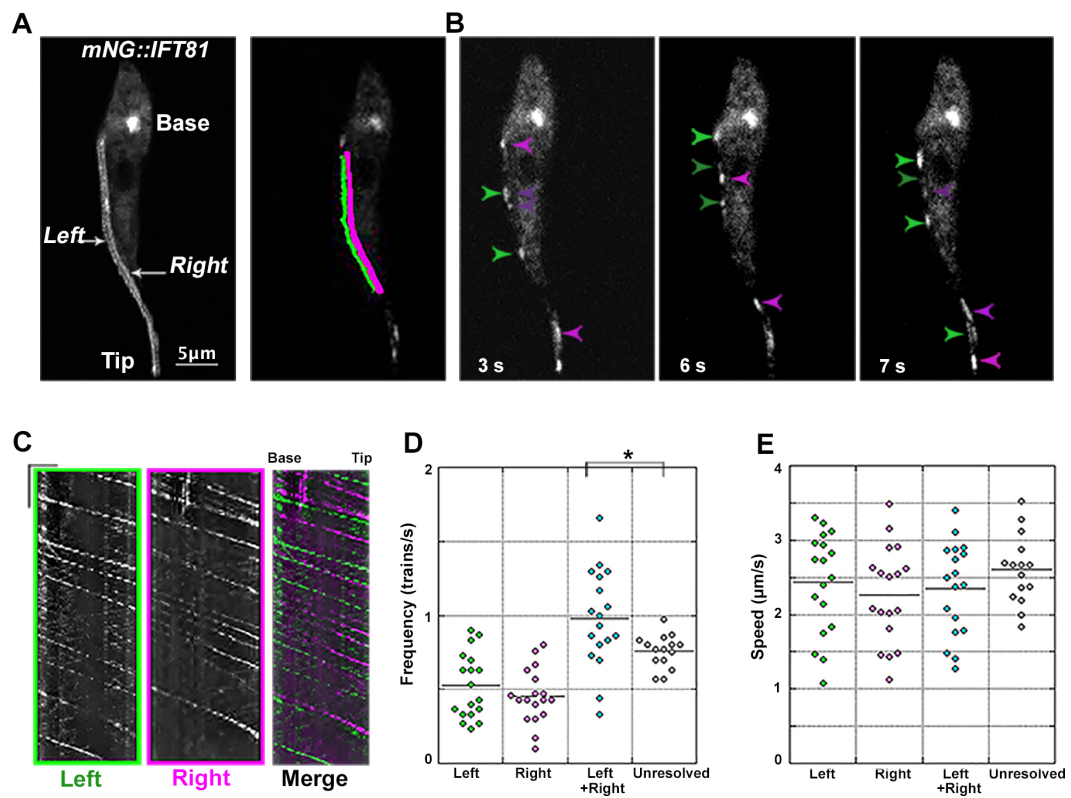


Figure 4

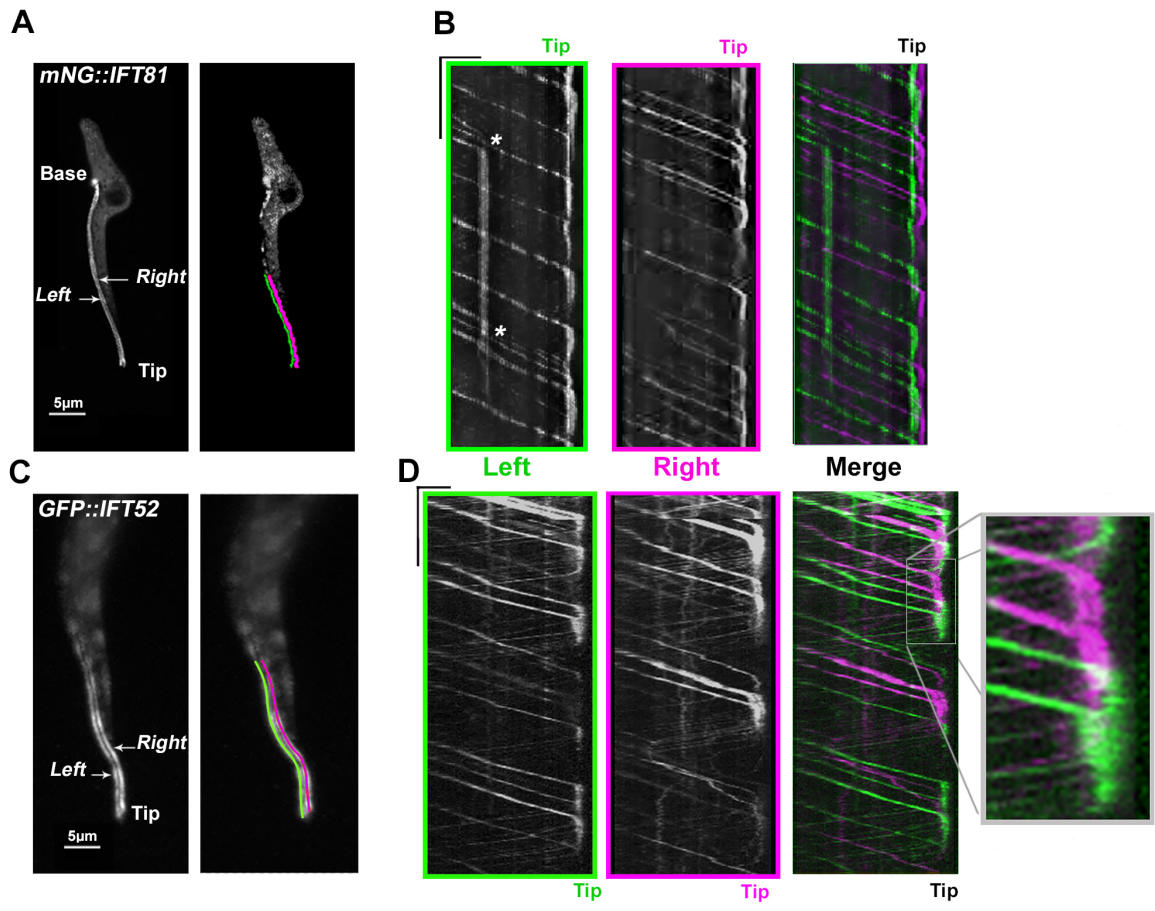


Figure 5

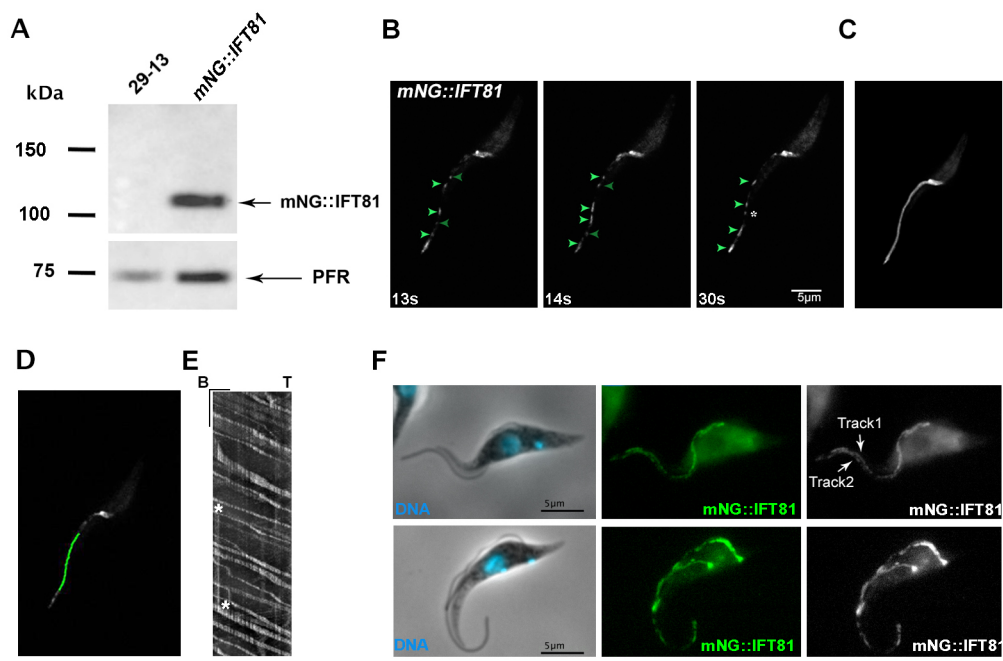


Figure S1

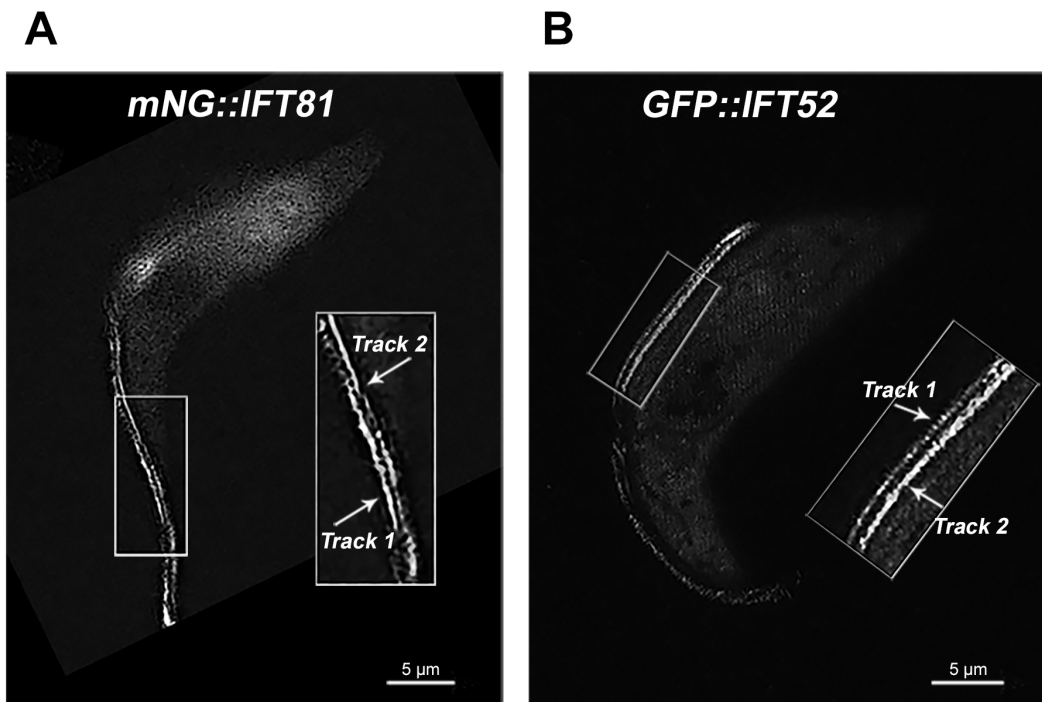


Figure S2

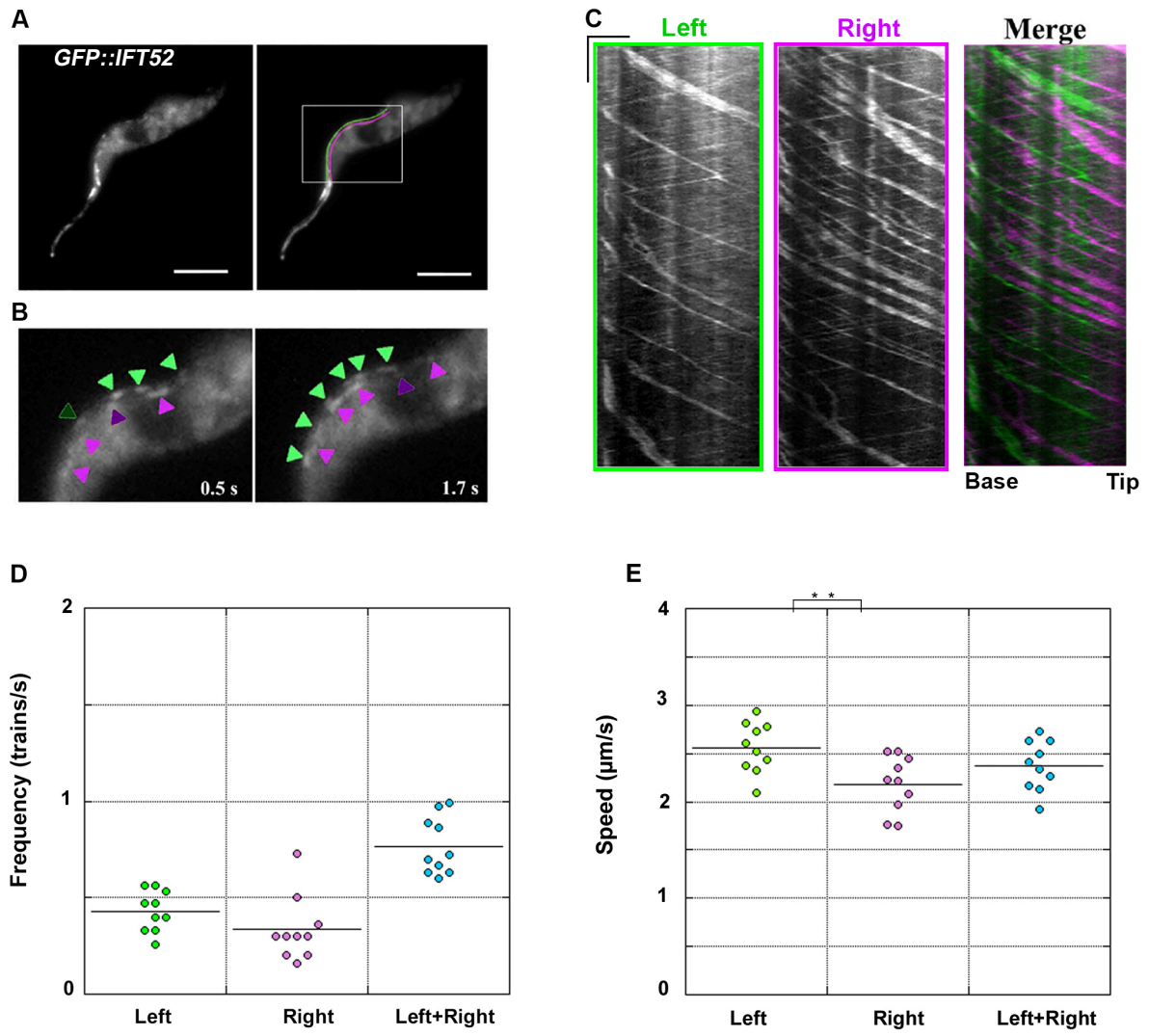


Figure S3



## ***Results***

## II. Flagellum length control in trypanosomes.

---

### 1) Summary

Eukaryotic cilia and flagella are composed of more than 600 proteins that need to be timely transported and incorporated at the right place in the flagellum (Subota, Julkowska et al. 2014). IFT is the key process involved in flagellum construction as it is associated to protein transport at the distal tip of the organelle. Laetitia Vincensini *et al.* have investigated the incorporation in growing flagella of different skeletal components of the axoneme such as dynein arm intermediate chain (DNAI1) and Radial spoke protein 3 (RSP3). Incorporation of the membrane-associated protein Arginine Kinase 3 (AK3) was also investigated in both growing and mature flagella in procyclic parasites in culture (Subota, Julkowska et al. 2014). By using inducible expression of epitope-tagged labelled proteins and FRAP (Fluorescence Recovery After Photobleaching) approaches, they demonstrated the existence of at least two routes for flagellar protein incorporation. Structural proteins were mostly added at the distal tip, with little or no turnover in full-length flagella, while membrane proteins were indifferently incorporated in new and old flagella with a rapid turnover.

As said above, IFT is not necessary to maintain flagellum length in trypanosomes (Fort, Bonnefoy et al. 2016) suggesting a high stability of tubulin and the absence of assembly-disassembly turnover at the distal tip. To confirm this hypothesis, I investigated the turnover of the outer dynein arm heavy chain B (DHCODAB) fused to mNeonGreen by FRAP experiments. After photo bleaching of the distal tip of mature flagella, I followed the fluorescence recovery every 5 minutes during 45 minutes (n=14). During this period, I was not able to detect any fluorescence recovery suggesting an absence of turnover of DHCODAB at the distal tip of mature

flagella. Dynein arms are firmly attached to the microtubules of the axoneme and their absence of turnover reflects the stability of mature flagellum. Therefore, if there is no turnover of tubulin-associated proteins, it is likely that there will be no turnover of axonemal tubulin. This observation supports the idea that the length of the mature flagellum in *T. brucei* procyclic cells in culture is fixed.

Canonical models proposed to explain flagellum length control are based on dynamic assembly and disassembly activity at the distal tip of the organelle, involving the IFT machinery for tubulin transport. In a second manuscript, we propose a new “grow and lock” model that could be more relevant to explain flagellum length control in stable flagella. In this model, we propose that the flagellum grows at a constant rate until it is locked at a given length. First, we have studied the distribution of fluorescent IFT proteins in the flagellum of cultured parasites at different phases of elongation and compared growing and mature flagella. We have demonstrated that IFT protein concentration per unit of length remains constant during flagellum elongation. These data revealed that IFT are recruited in parallel to flagellum elongation, which is compatible with the reported linear growth rate (Bastin, MacRae et al. 1999). The evaluation of IFT particle speed and frequency showed that IFT trafficking is constant during both elongation and maintenance of flagella. In the IFT-associated kinesin 2 motor RNAi mutant, Benjamin Morga (previous post-doc in the lab) observed a reduction of IFT frequency accompanied by the emergence of shorter cells with shorter flagella. By reducing IFT trafficking, we decreased the flagellum growth rate resulting in the assembly of shorter flagella in agreement with the “grow and lock” model. Conventional models such as the limiting pool model could explain the production of shorter flagella, especially in mother cells. However we showed the tubulin soluble was not exhausted and was at least equivalent, if is not more abundant, compared to control conditions. Moreover, the length of the new flagellum still increased after cell division until it became fixed, before the cell produced a new flagellum during the next cell cycle. To evaluate the importance of the timing of cell division and flagellum maturation, we have chemically blocked cell division using teniposide, an inhibitor of topoisomerase II. This led to an increase of new flagellum elongation, but never beyond the length of the parental one. Then we have used FLAM8 as a marker whose high concentration reflects the state of flagellum

## **Results**

maturation. We have demonstrated that flagellum elongation after teniposide treatment is followed by maturation and acquisition of a strong FLAM8 signal explaining why the new flagellum length does not exceed the length of the old one. Finally we have deinduced *KIN2A2B*<sup>RNAi</sup> after 6 days of induction, this is accompanied by a 2-fold augmentation of IFT trafficking. Despite this augmentation the old flagellum did not grow further confirming the locking of the old flagellum. In this experiment the ability of *KIN2A2B*<sup>RNAi</sup> cells to assemble fairly long new flagella that grow beyond the short cell body demonstrates that flagellum length is not controlled by the cell body.



**Flagellar incorporation of proteins follows at least two different routes in trypanosomes**

Article accepted in *Biology of the Cell*

Laetitia Vincensini, Thierry Blisnick, Eloïse Bertiaux, Sebastian Hutchinson, Christina Georgikou, Cher-Pheng Ooi and Philippe Bastin.

## ***Results***

# Flagellar incorporation of proteins follows at least two different routes in trypanosomes

Laetitia Vincensini<sup>2</sup>, Thierry Blisnick, Eloïse Bertiaux, Sebastian Hutchinson, Christina Georgikou, Cher-Pheng Ooi<sup>3</sup> and Philippe Bastin<sup>1</sup>

Trypanosome Cell Biology Unit, Institut Pasteur & INSERM U1201, Paris 75015, France

**Background Information.** Eukaryotic cilia and flagella are sophisticated organelles composed of several hundreds of proteins that need to be incorporated at the right time and the right place during assembly.

**Results.** Two methods were used to investigate this process in the model protist *Trypanosoma brucei*: inducible expression of epitope-tagged labelled proteins and fluorescence recovery after photobleaching of fluorescent fusion proteins. This revealed that skeletal components of the radial spokes (RSP3), the central pair (PF16) and the outer dynein arms (DNAI1) are incorporated at the distal end of the growing flagellum. They display low or even no visible turnover in mature flagella, a finding further confirmed by monitoring a heavy chain of the outer dynein arm. In contrast, the membrane-associated protein arginine kinase 3 (AK3) showed rapid turnover in both growing and mature flagella, without particular polarity and independently of intraflagellar transport.

**Conclusion.** These results demonstrate different modes of incorporation for structural and membrane-associated proteins in flagella.

**Significance.** The existence of two distinct modes for incorporation of proteins in growing flagella suggests the existence of different targeting machineries. Moreover, the absence of turnover of structural elements supports the view that the length of the mature flagellum in trypanosomes is not modified after assembly.



Additional supporting information may be found in the online version of this article at the publisher's web-site

## Introduction

Cilia and flagella are ubiquitous organelles whose architecture is highly conserved, from protists to mammals. The distinction between cilia and flagella is mostly historical, as both organelles display a common architecture: cilia and flagella elongate their microtubules from a basal body forming a cylindrical

structure termed the axoneme, composed of nine doublets of microtubules. Most motile cilia exhibit a 9+2 structure, in which the axoneme surrounds a central pair of single microtubules. There are a few exceptions however, most strikingly the motile 9+0 cilia of the embryonic node [Nonaka et al., 1998] and the atypical spermatozoa of insects [Mencarelli et al., 2008]. Various microtubule-associated appendages are involved in ciliary beating. Some generate the force necessary for motility such as outer dynein arms and inner dynein arms, whereas others regulate motor activity such as radial spokes and central pair projections. On the contrary, primary cilia have a 9+0 axoneme, lack dynein arms and do not appear to be motile. Defects in flagellum assembly or function have been linked to an increasing number of genetic diseases collectively termed ciliopathies,

<sup>1</sup>To whom correspondence should be addressed (email: pbastin@pasteur.fr)

<sup>2</sup>Current address: Sorbonne Universités, UPMC, INSERM, CNRS, Centre d'Immunologie et des Maladies Infectieuses, U1135, ERL8255, 91 Bd de l'hôpital, 75013 Paris, France.

<sup>3</sup>Current address: Department of Life Sciences, Sir Alexander Fleming Building, Imperial College-South Kensington, London SW7 2AZ, United Kingdom.

**Key words:** Arginine kinase, Axoneme, Cilia and flagella, Outer dynein arms, Organelle assembly.

**Abbreviations:** AK3, arginine kinase 3; DRC, dynein regulatory complex; IFA, immunofluorescence assay; IFT, intraflagellar transport; PFR, paraflagellar rod; RNAi, RNA interference; RSP, radial spoke protein.

such as primary ciliary dyskinesia, polycystic kidney disease, retinitis pigmentosa or the Bardet–Biedl syndrome [Huber and Cormier-Daire, 2012; Reiter and Leroux, 2017].

Cilia and flagella are complex organelles, composed of over 500 proteins [Pazour et al., 2005; Smith et al., 2005; Broadhead et al., 2006; Oberholzer et al., 2011; Subota et al., 2014], that must be incorporated into the flagellar axoneme, membrane or matrix. Cilia and flagella constitute a distinct compartment, as their content is separated from the rest of the cytoplasm by a barrier, or ciliary gate, positioned between the transition zone and the plasma membrane [Reiter et al., 2012]. Since the cilium lacks ribosomes, its proteins must be synthesised in the cytoplasm prior to entry and incorporation into the organelle. This raises the issue of protein targeting and incorporation to the organelle during both construction and maintenance.

Intraflagellar transport (IFT) is a key process involved in flagellar construction. First identified in the green alga *Chlamydomonas reinhardtii* [Kozminski et al., 1993], it refers to the bidirectional transport of protein complexes along the axoneme, from the basal body to the distal tip of the axoneme and vice versa, powered by the action of kinesin motors in the anterograde direction and dynein motor in the retrograde direction [Ishikawa and Marshall, 2011]. IFT has since been shown to be conserved and essential for the assembly of almost all eukaryotic flagella [Hao and Scholey, 2009], and inhibition of IFT prevents flagellum assembly in most organisms studied so far [Kozminski et al., 1995; Nonaka et al., 1998; Brown et al., 1999; Han et al., 2003; Kohl et al., 2003]. The canonical model for flagellum assembly proposes that flagellar components are transported by IFT to the distal tip of the flagellum, which is the site of construction of the organelle [Craft et al., 2015]. Yet so far distal incorporation during flagellum construction has been formally demonstrated for relatively few structural proteins: alpha tubulin and the radial spoke protein (RSP)3 in *Chlamydomonas* [Johnson and Rosenbaum, 1992], and the PFR2 and KMP11 proteins in *Trypanosoma brucei* [Bastin et al., 1999a; Zhou et al., 2015]. In *Chlamydomonas*, analysis of dikaryons between wild-type and strains with various defects in structural elements, or with a tagged version of a given protein, revealed various profiles: addition at the distal end for tubulin, RSP3 [Johnson and Rosenbaum, 1992], the inner dynein arm subunit

p28 [Piperno et al., 1996], the central pair protein PF6 [Lechtreck et al., 2013] or the dynein regulatory complex (DRC) subunit 4 [Bower et al., 2013]. By contrast, proximal incorporation was observed for the docking complex of the outer dynein arm [Owa et al., 2014], and intercalation of the IC69 component was reported for the outer dynein arm [Piperno et al., 1996]. Lateral diffusion has also been reported for the membrane protein Smoothened [Milenkovic et al., 2009]. More recently proximal incorporation was demonstrated for the components of the associated flagellum attachment zone in *T. brucei* [Sunter et al., 2015; Zhou et al., 2015]. The mode of incorporation could depend on the type of protein and on its final location.

In order to investigate the site of incorporation of various flagellar proteins and their dynamics, we turned to the protist *T. brucei*, the etiological agent of sleeping sickness in Africa that is a very amenable model for studying cilium biology [Vincensini et al., 2011]. It possesses a single flagellum that remains present throughout the cell cycle and is composed of a typical 9+2 axoneme with central pair, dynein arms and radial spokes [Langousis and Hill, 2014], which is flanked by a lattice-like structure called the paraflagellar rod (PFR) [Portman and Gull, 2010]. The trypanosome assembles its new flagellum while maintaining the existing one, offering the opportunity to compare in the same cell an elongating flagellum with a flagellum undergoing maintenance. Moreover, the axoneme contains specific subdomains identified with unique proteins such as FLAM6 (restricted to the proximal part) and FLAM8 (only present at the distal tip) [Subota et al., 2014]. This restricted protein localisation has also been reported in other eukaryotes including humans [Fliegeauf et al., 2005; Yagi et al., 2009]. Since multiple reverse genetics and imaging tools are available, trypanosomes are perfectly suited to study protein incorporation and turnover [Julkowska and Bastin, 2009; Oberholzer et al., 2009].

Here, we investigated the mode of addition to the growing flagellum of three proteins belonging to distinct elements of the axoneme (radial spokes, central pair, outer dynein arms) and of a membrane protein, using two experimental setups based either on rapid inducible expression of epitope-tagged versions of flagellar proteins, or on photobleaching experiments. The results reveal the existence of different modes

## Assembly of flagellar components

of incorporation in both the old and the new flagellum, and highlight slow or no dynamics for structural proteins compared to the membrane protein that was studied.

### Results

**Assembly of radial spoke and central pair proteins**  
RSP3 incorporation into the growing flagellum of *Chlamydomonas* has been unambiguously shown to be distal [Johnson and Rosenbaum, 1992]. Hence, we decided to first focus on this well-characterised protein to confirm that its mode of incorporation is indeed conserved in *T. brucei*. RSP3 is conserved in trypanosomes and its knockdown leads to the absence of radial spokes accompanied by a pronounced motility phenotype [Ralston et al., 2006]. Flagellar incorporation of RSP3 was investigated using a strain expressing a Ty1-tagged version of the RSP3 protein (N-terminal tagging) under the control of a tetracycline inducible trypanosome promoter. The plasmid was transfected in a cell line constitutively expressing the tet-repressor, so that the promoter is silent under normal culture conditions, but can be rapidly activated upon addition of tetracycline [Wirtz and Clayton, 1995; Bastin et al., 1999a; Sunter et al., 2015].

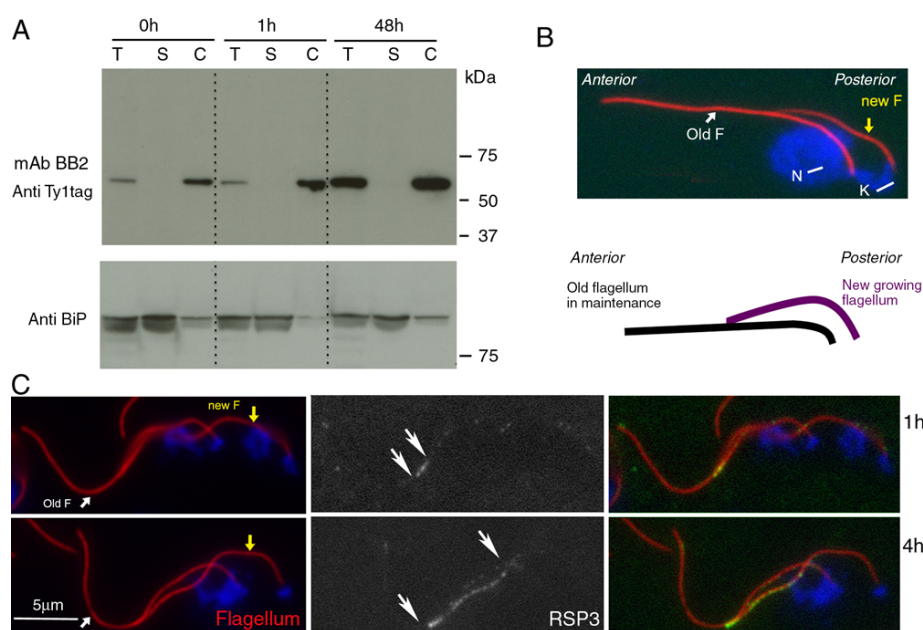
This system allows the visualisation of recently synthesised proteins and the monitoring of their location during flagellum construction. Since the old flagellum is maintained while the new one is assembled, it is possible to monitor the fate of newly synthesised proteins within both flagella, and thus assess protein turnover in the mature flagellum. The strain displayed normal growth rate, unaltered by the addition of tetracycline, showing that the epitope-tagged protein is not toxic (data not shown). Western blotting with the Ty1 epitope tag specific monoclonal antibody BB2 was used to assess the incorporation of the tagged protein to the axoneme. Samples were treated with 1% NP40 to separate a cytoskeleton and a soluble fraction [Robinson et al., 1991]. In non-induced cells, the level of TY1::RSP3 was low but detectable, indicating a slight leakiness of the system as previously reported [Wirtz and Clayton, 1995]. Cells were induced for one hour by addition of tetracycline, leading to an increase in the amount of tagged protein (Figure 1A). The TY1::RSP3 protein fractionates in the cytoskeletal fraction (lanes C), confirming its in-

corporation to the axoneme. As observed for other axoneme or PFR proteins [Bastin et al., 1998; Baron et al., 2007; Kabututu et al., 2010; Ralston et al., 2011], the soluble pool turned out to be either absent or below detection level. However, these cells are not synchronised and the existence of a soluble pool during a brief phase of the cell cycle cannot be formally excluded. These results validate the strain as inducible, with expression kinetics compatible with flagellar assembly that takes 4–5 h in cultured trypanosomes [Sherwin and Gull, 1989; Bastin et al., 1999a]. In our experimental setup, the expression of the TY1::RSP3-tagged protein can be induced in just an hour, implying that its localisation provides a marker of recently synthesised proteins. As the pool of soluble flagellar proteins is low, newly synthesised proteins should also represent recently assembled material.

In order to determine the site of incorporation of RSP3, cells were induced with tetracycline, and TY1::RSP3 localisation was monitored over time by IFA. Cells were treated with 1% Nonidet prior to methanol fixation, in order to solubilise the cytoplasm and non-incorporated material. The remaining cytoskeletons were double labelled with BB2 to visualise the newly incorporated tagged RSP3, and with mAb25, an axoneme marker [Pradel et al., 2006]. Observations were focused on bi-flagellated cells, in which the new assembling flagellum can be distinguished from the old flagellum based on its posterior position and its shorter length (Figure 1B) [Sherwin and Gull, 1989]. Short incubations with tetracycline (1 h) lead to expression of the fusion protein that was mostly localised at the distal tip of the new flagellum (Figure 1C, top panel). This profile was reproduced after 1 h 30 min of growth in the presence of tetracycline, where quantification revealed that more than 95% of the cells exhibited this staining profile ( $n = 53$ ). The remaining cells possessed a short flagellum that was fully stained, presumably because its assembly was initiated during the induction period (Figure 1C, left panel). The length of the labelled segment increased with the duration of growth in the presence of tetracycline, in agreement with flagellar elongation rate. The length of the new flagellum segment showing bright positive signal was measured to  $3.9 \pm 0.3 \mu\text{m}$  (induction for 1 h,  $n = 45$ ),  $4.6 \pm 0.3 \mu\text{m}$  (1h30,  $n = 53$ ) and  $7.1 \pm 0.5 \mu\text{m}$  (2h30,  $n = 35$ ), in good agreement with an elongation rate of  $3.6 \mu\text{m}$

**Figure 1 | The RSP3 is incorporated at the distal tip of the flagellum**

(A) Western blot showing inducible expression of Ty1::RSP3 upon tetracycline induction. Total (T), soluble (S) and cytoskeletal (C) protein extracts of non-induced cells (0 h), and cells induced for 1 and 48 h were prepared. The membrane was incubated with the BB2 monoclonal antibody directed against the Ty1 tag to detect the Ty1::RSP3 fusion protein (top panel), or the anti-BiP as a loading and fractionation control (bottom panel). (B) In bi-flagellated cells, the new assembling flagellum is posterior to the cell and shorter than the old flagellum in maintenance. Cells were fixed in methanol and stained with the Mab25 antibody to detect the axoneme (red) and with DAPI (blue). F, flagellum; N, nucleus; K, kinetoplast. (C) 1 h-induced and 4 h-induced Ty1::RSP3 cells were treated with 1% NP40 prior to methanol fixation, stained with the Mab25 antibody to detect the axoneme (red, left panels) and the BB2 antibody to detect Ty1::RSP3 (green, middle panels) then counterstained with DAPI (blue). Sites of incorporation of newly synthesised proteins are indicated with long white arrows. Yellow arrow, new flagellum; white arrow, old flagellum. Scale bar: 5  $\mu$ m.



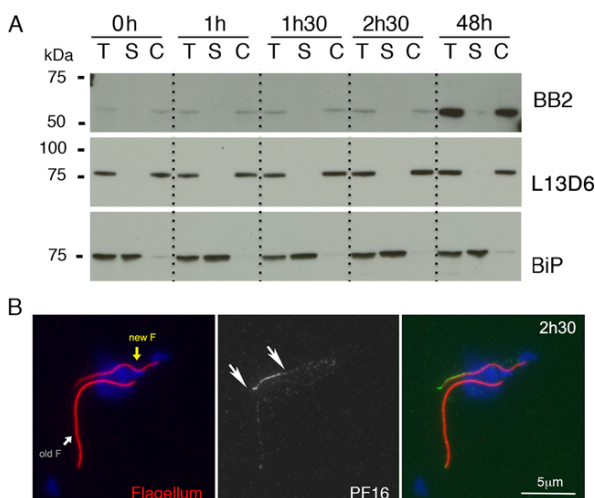
per hour [Bastin et al., 1999a]. After 4 h of growth in the presence of tetracycline, a large segment of the distal part of long flagella was stained (Figure 1C, bottom panels). In all cases, the signal is resistant to detergent, showing that the tagged protein is indeed incorporated in the axoneme. These data support the view that RSPs are added to the distal end of the growing flagellum in trypanosomes.

We next wondered whether a protein located within a different sub-region of the axoneme could undergo a different mode of incorporation. We therefore investigated PF16, a well-characterised protein of the central pair [Smith and Lefebvre, 1996; Sapiro et al., 2002; Branche et al., 2006; Ralston et al., 2006], whose central position is more distant from the microtubule doublets that carry IFT particles.

The same approach was used to generate an inducible cell line expressing Ty1-tagged PF16 upon addition of tetracycline. The strain displayed normal growth rate, unaltered by the addition of tetracycline, suggesting that the tagged protein is not toxic (data not shown). Expression was first monitored by Western blotting, using the Ty1 tag specific antibody BB2 (Figure 2A). In non-induced cells, a low amount of tagged PF16 is visible, but upon tetracycline addition, the level of the protein increases slowly and reaches much higher levels after the cells have been induced for over 48 h. The protein is restricted to the cytoskeletal fraction and is not detected within the soluble fraction. These results validate the strain as inducible, with kinetics acceptable for investigation of protein localisation during flagellum construction.

**Figure 2 | The central pair protein PF16 is incorporated at the distal tip of the flagellum**

(A) Western blot showing inducible expression of PF16 upon tetracycline induction. Total (T), soluble (S) and cytoskeletal (C) protein extracts of non-induced cells, and cells induced for 1, 1.5, 2.5 and 48 h were prepared. The membrane was incubated with the BB2 antibody directed against the Ty1 tag to detect the PF16::Ty1 fusion protein (top panel), the L13D6 antibody to detect the PFR (middle panel) or the anti-BiP (bottom panel), as loading and fractionation controls. (B) 2.5-hr-induced *PF16::Ty1* cells were treated with 1% NP40 prior to methanol fixation, stained with the Mab25 antibody to detect the axoneme (red, left panel) and the BB2 antibody to detect Ty1::PF16 (green, middle panels) then counterstained with DAPI (blue, left and right panels). The site of incorporation of newly synthesised proteins is indicated with long white arrows. A weak homogenous signal can be seen on the old flagellum and corresponds to a low level of expression of PF16::Ty1 due to a slight leakiness of the inducible system as also observed on the Western blot. Yellow arrow, new flagellum; white arrow, old flagellum. Scale bar: 5  $\mu$ m.



In order to determine the site of incorporation of PF16, cells were induced with tetracycline for 1–3 h, and Ty1::PF16 expression was monitored over time by IFA. Cells were treated with 1% Nonidet prior to methanol fixation, in order to confirm axonemal incorporation. Slides were analysed by IFA double labelled with BB2, to visualise the newly incorporated tagged PF16, and with the flagellar marker mAb25. Short incubations with tetracycline (1 h and 1 h 30 min) did not lead to detectable expression

of Ty1::PF16 (data not shown). After 2 h 30 min of induction, the fusion protein was detected at the distal tip of the new flagellum (Figure 2B). Moreover, this signal was resistant to detergent, showing that the protein is indeed incorporated in the axoneme. A weak signal could be detected in the old flagellum, corresponding to a low level of expression of Ty1::PF16 due to a slight leakiness of the inducible system (as also observed on the Western blot), but it did not show a particular polarity (Figure 2B). These results demonstrate that central pair proteins are added to the distal end of the elongating flagella, as observed for radial spokes.

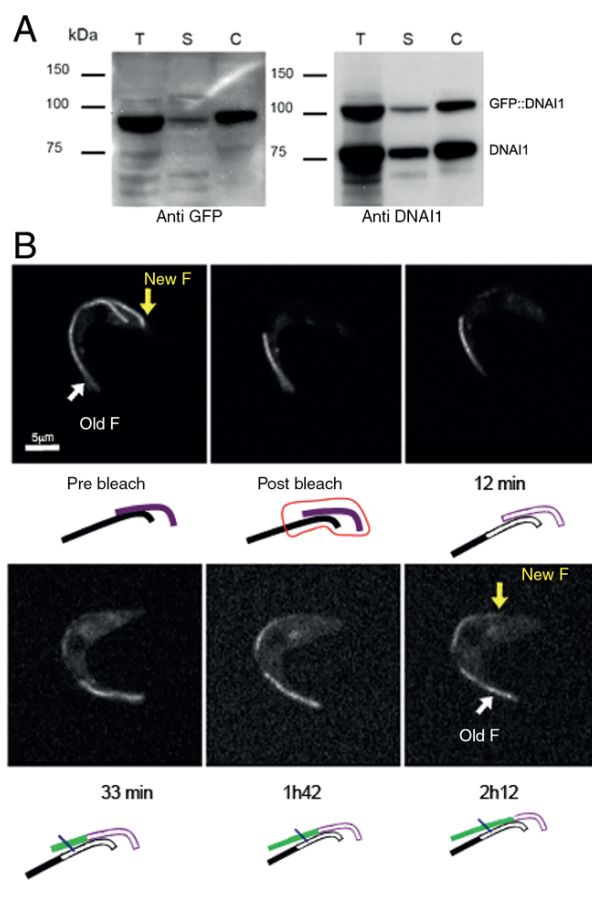
**Photobleaching analysis of a dynein arm component during flagellum construction and maintenance**

We next investigated the incorporation of a component of the outer dynein arm, the dynein intermediate chain 1 (DNAI1), which is located in the periphery of the axoneme [Branche et al., 2006]. We developed a cell line where DNAI1 is endogenously tagged with GFP for photobleaching analysis. Western blotting analysis was performed with an anti-GFP, or with a mouse anti-DNAI1 polyclonal antibody [Duquesnoy et al., 2009] on total protein samples, cytoskeletal and detergent-soluble fractions (Figure 3A). The fusion protein was detected with both antibodies, whereas the untagged endogenous DNAI1 only reacted with the anti-DNAI1 antibody. This revealed that the fluorescent version represents about half of the endogenous one. Both proteins showed the same distribution profile with more material in the cytoskeletal fraction than in the soluble fraction (Figure 3A) as previously observed [Duquesnoy et al., 2009]. Live video-microscopy showed that, as expected, the protein is constitutively expressed and localises to both old and new flagella (Figure 3B).

DNAI1 flagellar incorporation and dynamics were investigated using fluorescence recovery after photobleaching (FRAP). In bi-flagellated cells, the fluorescent signal was bleached in both flagella and fluorescence recovery was monitored simultaneously in the mature and in the elongating flagellum. We decided to photobleach the new flagellum in its entirety but only half of the old flagellum, hence leaving a positive signal to control for bleaching due to laser exposure and to facilitate cell detection. Evolution of the fluorescent signal was monitored for up to 2 h. In

**Figure 3 | The outer dynein arm protein DNAI1 undergoes both distal incorporation and intercalation**

FRAP analysis of trypanosomes expressing the GFP::DNAI1 fusion protein. **(A)** Western blot showing expression of GFP::DNAI1. Total (T), soluble (S) and cytoskeletal (C) protein extracts were prepared. The membrane was incubated with the anti-GFP antibody that detects only the GFP::DNAI1 fusion protein (left panel) and then with the anti-DNAI1 antibody that detects both the endogenous DNAI1 protein and the GFP::DNAI1 fusion protein (right panel). **(B)** The new flagellum and the proximal part of the old flagellum were bleached with a brief laser pulse (framed area) and recovery was monitored upon acquisition of an image every 3 min, for up to 2 h. Pre-bleach situation: old and new flagella are equally positive for GFP::DNAI1. Post-bleach situation: only the second half of the old flagellum remains positive. Recovery of fluorescent signals is shown at the indicated times. Cartoons under each panel show the situation for old (black) and new (purple) flagella. Closed and open segments are GFP positive and negative, respectively. Recovered signal is shown in green. Yellow arrow, new flagellum; white arrow, old flagellum. Scale bar: 5  $\mu$ m.



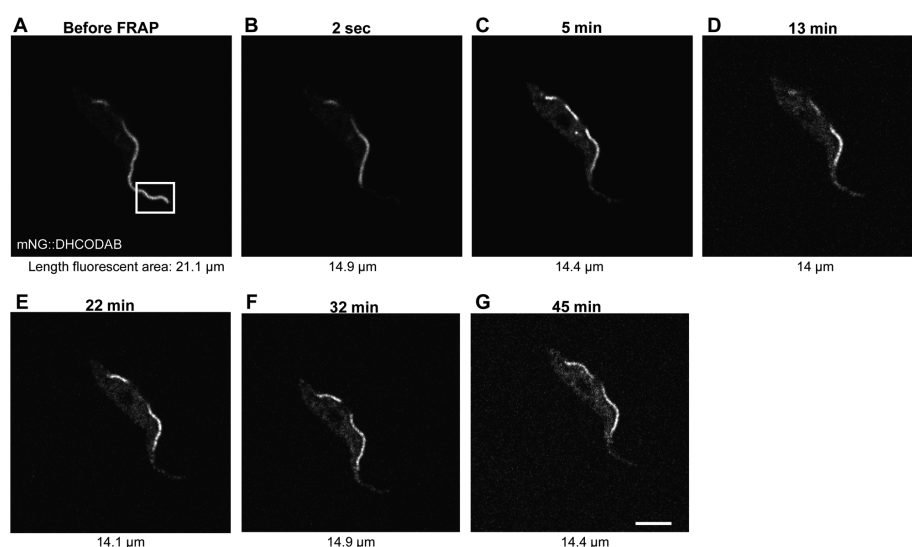
all cases, no recovery was detected in the old flagellum (Figure 3B). By contrast, a fluorescent signal became detectable in the new flagellum from half an hour after photobleaching (Figure 3B, time 33 minutes). It was mostly present towards the distal tip, but some signal was also detected towards the proximal part (Figure 3B). A clear gradient was visible at later time points with stronger signal at the distal tip (Figure 3B). The new flagellum showed signs of conspicuous elongation during the course of the experiment and so the bright signal corresponds to the incorporation of new GFP::DNAI1 proteins on the growing axoneme. Presence of a positive (albeit less bright) signal in the adjacent proximal region that was already assembled before the bleach could reflect either turnover of material that had already been incorporated or completion of the assembly by an intercalation process. This suggests a clear difference in protein dynamic between the new flagellum and the old flagellum where no turnover is observed.

However, turnover could still occur at the distal end of the mature flagellum, that is known to be highly dynamic in some species such as *Chlamydomonas* [Marshall and Rosenbaum, 2001], or *C. elegans* [Hao et al., 2011]. To investigate whether dynein turnover may occur in the distal portion of the flagellum of *T. brucei*, the fluorescent signal was bleached at the distal tip of the flagellum in cells expressing GFP::DNAI1, and fluorescence recovery was monitored. No recovery could be detected at the distal tip (Supplementary Figure 1). This experiment was reproduced using a cell line expressing the dynein heavy chain ODA-B fused to mNeonGreen following *in situ* tagging at the 5' end of the gene [Shen et al., 2001]. The distal end of the mature flagellum was bleached (Figure 4A) and recovery was monitored over 45 min (Figures 4B–4G). Again, no recovery was observed. These results demonstrate that both the heavy and the intermediate dynein chains undergo little or no turn over at the distal tip of the flagellum, supporting the view that, once assembled, mature trypanosome flagella do not modify their length [Ooi and Bastin, 2013].

Overall these results show that the structural proteins of the axoneme studied so far mostly follow a distal pattern of incorporation, with a slight variation for the outer dynein arm DNAI1 protein that appears to also undergo intercalation or turnover at the proximal part of the elongating flagellum.

**Figure 4 | The outer dynein arm heavy chain B does not show visible turnover in the mature flagellum**

FRAP analysis of trypanosomes expressing the GFP::DHCODAB fusion protein. The distal end of the flagellum was bleached with a brief laser pulse (framed area) and recovery was monitored upon acquisition of a series of 20 images at each of the indicated time points. This is a typical example out of 14 cells from two different experiments. **(A)** Pre-bleach situation: the flagellum is positive along its length. Darker areas correspond to regions that are not in the focal plane. **(B)** Post-bleach situation: only the proximal part of the flagellum remains positive. The length of the fluorescent portion has been measured and is indicated at the bottom of each image. **(C–G)** The fluorescent signal is shown at the indicated times. No recovery could be detected in the flagellum. The thin fluorescent portion corresponds to the anterior end of the cell body and not the flagellum. Scale bar: 5  $\mu\text{m}$ .


**The flagellum membrane-associated protein AK3 shows fast and non-polarised incorporation in growing or mature flagella**

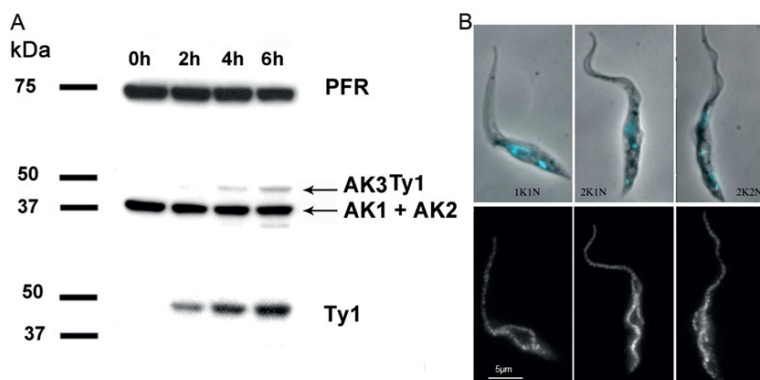
A recent study indicated that flagellar proteins display diverse dynamic behaviours depending on their flagellar localisation [Subota et al., 2014]. To investigate this phenomenon, we turned towards a novel flagellum membrane protein called arginine kinase 3 (AK3) [Oberholzer et al., 2011; Voncken et al., 2013; Subota et al., 2014; Ooi et al., 2015]. In contrast to structural axonemal proteins, detergent extraction localised AK3 exclusively to the soluble fraction and IFA data unambiguously revealed that AK3 co-localises with the flagellum membrane and wraps around all flagellar structural elements such as the axoneme and the PFR [Subota et al., 2014]. The staining is distinct from that observed for intraflagellar proteins and is sensitive to detergent treatment [Subota et al., 2014]. This staining profile is very similar to that observed for the flagellar membrane proteins calflagins [Maric et al., 2011]. The *T. brucei*

genome contains three genes encoding closely related proteins for arginine kinase that differ in their N- or C-termini sequences [Miranda et al., 2009]. These sequences are responsible for differential locations: AK1 is in the cytosol, AK2 is in the glycosomes and AK3 is in the flagellum membrane [Voncken et al., 2013; Ooi et al., 2015]. RNA interference (RNAi) silencing leads to rapid disappearance of AK3 in both old and new flagella in less than 4 h, corresponding to one third of the duration of the cell cycle. This disappearance did not show a particular polarity in IFA experiments, suggesting that AK3 might move rapidly in the flagellum membrane [Subota et al., 2014].

An inducible strain expressing AK3::Ty1 under the control of the tetracycline repressor was generated in an *ak3*<sup>-/-</sup> knockout strain: the tagged protein being expressed in a negative genetic background, there is no competition with the endogenous AK3 protein. Tetracycline-inducible expression was confirmed by Western blotting, using the anti-Ty1 tag

**Figure 5 | The flagellum membrane AK3 shows fast and non-polarised incorporation in growing and mature flagella**

(A) Western blot showing inducible expression of AK3::Ty1 upon tetracycline induction. Total protein extracts of non-induced cells, and cells induced for 2 and 4 h were prepared. The membrane was incubated with the BB2 antibody directed against the Ty1 tag, to detect the AK3::Ty1 fusion protein (bottom panel), the anti-AK antibody (middle panel) and the L13D6 antibody (top panel) to detect the PFR as a loading control. (B) 30-min-induced AK3::Ty1 cells were subjected to PFA fixation, and stained with the BB2 antibody to detect AK3::Ty1 (green) then counterstained with DAPI. Cells are shown at different time points of the cell cycle (1K1N, 2K1N, 2K2N). Scale bar: 5  $\mu$ m.



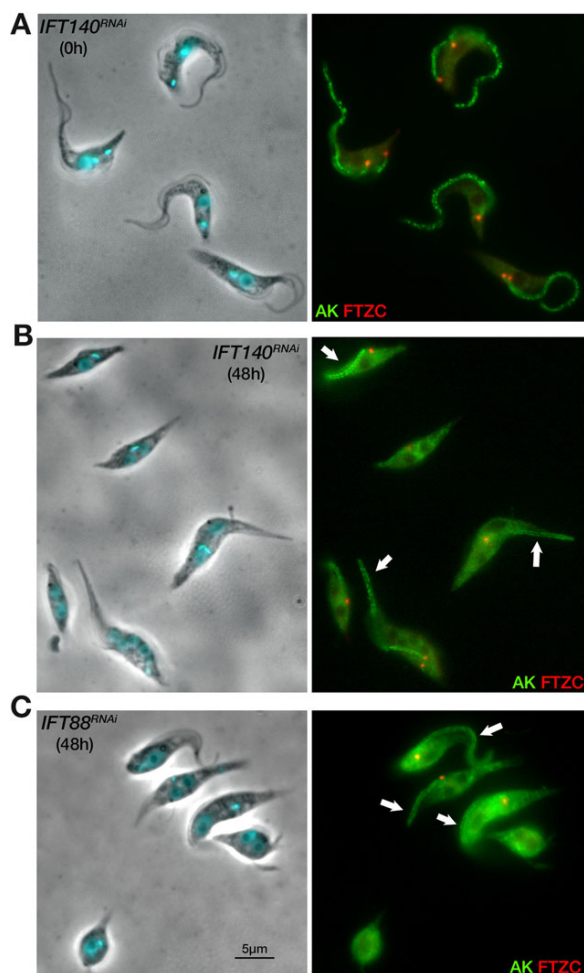
BB2 antibody and the anti-AK polyclonal antibody (Figure 5A). In non-induced cells, no AK3::Ty1 is detectable, neither by BB2 nor by the anti-AK antiserum. Upon tetracycline addition, the level of the tagged protein increases rapidly as confirmed by detection with both BB2 and the anti-AK antiserum, which detects both AK1/AK2 proteins (these two co-migrate at  $\sim$ 40 kDa) and the tagged AK3 protein. These results validate the strain as inducible, with fast kinetics compatible with flagellar dynamics.

Induction experiments were then analysed by IFA with either the BB2 or the anti-AK antibody. Upon 30 min of induction, both flagella were equally labelled, with no significant difference in intensity between them (Figure 5B). This was consistently observed no matter the length of the new flagellum (Figure 5B). Neither a particular polarity nor a gradient could be observed. These results were reproduced using a cell line expressing the Ty1-tagged version of AK3 in a background where both AK3 endogenous alleles were still present, showing that these distribution profiles are not explained by the fact that AK3 is absent from the mature flagella before induction (data not shown). These results illustrate fast turn over in both flagella, and the possibility of rapid exchange between the two flagella could also be considered.

IFT has long been postulated to transport flagellar components within the organelle and recent work has shown that several proteins rely on IFT to be maintained at their correct location in the flagellum [Fort et al., 2016]. The possible contribution of IFT to the flagellar incorporation of AK3 was investigated using two tetracycline-inducible RNAi strains: *IFT88<sup>RNAi</sup>* and *IFT140<sup>RNAi</sup>* in which respectively anterograde and retrograde transport are inhibited upon knock-down [Kohl et al., 2003; Absalon et al., 2008]. Cells were stained with the anti-AK antibody and an antibody against the flagellum transition zone component (FTZC), as marker of the base of the flagellum [Bringaud et al., 2000]. In non-induced conditions, the signal covered the flagellum membrane as expected (Figure 6A). Over the course of RNAi silencing, the amount of IFT is reduced and cells assemble shorter and shorter flagella. However, mature flagella that were assembled prior to initiation of RNAi remain present (Figures 6B and 6C), even though IFT is absent (*IFT88* knockdown), or arrested (*IFT140* knockdown) [Fort et al., 2016]. This system thus allows the investigation of the contribution of IFT to flagellar targeting of AK and its distribution within the flagellum. The AK signal was retained in all flagella of induced *IFT88<sup>RNAi</sup>* and *IFT140<sup>RNAi</sup>* cells (arrows on Figures 6B and 6C), no matter their length,

**Figure 6 | Entry and maintenance of AK3 in the flagellum does not rely on IFT**

*IFT140<sup>RNAi</sup>* and *IFT88<sup>RNAi</sup>* cells were grown in the absence of tetracycline (0 h, **A**) or in the presence of tetracycline for 48 h (**B and C**). Cells were stained with an anti-AK antibody and with the flagellum transition zone component (FTZC), as a marker of the base of the flagellum. The right panel shows the phase contrast image merge with DAPI (cyan) to reveal nuclear and kinetoplast DNA. The left panel shows the immunofluorescence images with the anti-AK (that detects all three AK proteins) in green and the anti-FTZC in red. Arrows indicate remaining flagella in the induced sample that all remain positive for arginine kinase. Note the increase of arginine kinase signal in the cytoplasm in induced samples. Scale bar: 5  $\mu$ m.



indicating that flagellar targeting of AK is probably independent of IFT. In cells lacking flagella, the signal for AK was significantly increased in the cytoplasm (Figures 6B and 6C). This could correspond to AK3 still being produced and accumulating there in the absence of flagellum, or it could represent an increase in the amount of AK1 and AK2 that have been located to the cytoplasm and to glycosomes, respectively [Voncken et al., 2013].

**Discussion**

This study revealed two distinct protein behaviours during flagellum construction and maintenance. Structural proteins are mostly added at the distal end of the elongating organelle with little (if any) turnover in mature flagella, whereas membrane proteins do not show a specific polarity during incorporation and exhibit a rapid turnover. Components of the radial spokes, the central pair and the dynein arms (RSP3, PF16 and DNAI1) are mainly assembled at the distal end of the growing *T. brucei* axoneme. This is in agreement with the established observation for PFR2, a major component of the PFR [Bastin et al., 1999a] and supports the view that this mode of incorporation is conserved for components of flagellar skeletal structures among eukaryotic species [Rosenbaum et al., 1969; Johnson and Rosenbaum, 1992; Lechtreck et al., 2013]. The approaches used here have the advantage of visualising addition of new subunits in elongating flagella, rather than in the dikaryon experiments where flagella are already assembled.

Distal assembly is compatible with IFT transport of components of the axoneme and the PFR. FRAP analyses in *Chlamydomonas* have convincingly demonstrated transport of alpha-tubulin, DRC components and PF16 in growing and mature flagella [Wren et al., 2013; Craft et al., 2015]. So far, IFT movement of axoneme or PFR proteins has not been shown directly in trypanosomes. Epitope- or YFP-tagged alpha-tubulin fails to incorporate into flagellar microtubules, hence hampering direct analysis [Bastin et al., 1996; Sheriff et al., 2014]. Here, monitoring of the elongating flagellum after photobleaching of the GFP::DNAI1 signal failed to reveal IFT-type movement. This could be explained by technical reasons if the amount of DNAI1 per IFT train was too low to be detected, or if the association of the cargo to the

IFT train complex interfered with the ability of GFP to fluoresce.

Alternatively, outer dynein arms might not rely on IFT for transport in the trypanosome flagellum. In *Chlamydomonas*, analysis of dikaryons between dynein arm and IFT mutants suggested that inner dynein arms, but not outer dynein arms, require a functional IFT kinesin for correct incorporation [Piperno et al., 1996]. However, further work has shown that outer dynein arm addition was dependent on IFT46 [Hou et al., 2007] and the IFT-associated adaptor protein ODA16 [Ahmed et al., 2008]. These data support a contribution of IFT, but visualisation of the way ODA components move within the flagellum will be needed to formally prove whether they are transported by IFT or by other means. For example, the distal protein EB1 is added at the distal end of axonemal microtubules independently of IFT [Harris et al., 2016].

Transport of flagellar precursors was suggested in the *PFR2<sup>RNAi</sup>* mutant that fails to assemble a normal PFR [Bastin et al., 1998] in which other PFR proteins are found at the distal end of the flagellum where they accumulate over the course of organelle assembly. This material is not incorporated in any structure and is lost after cell division [Bastin et al., 1999b]. However, formal evidence of IFT-like movement of PFR precursors is still lacking and the possibility of diffusion [Ye et al., 2013], or the use of other types of motor systems [Demonchy et al., 2009] cannot be ruled out.

Although distal incorporation of structural axoneme proteins was the major trend in both series of experiments (inducible expression of tagged proteins and FRAP experiments), some signal was detected towards the proximal part of the assembling flagellum for DNAI1, often visible as a gradient starting from the distal region. One could imagine that the majority of the material destined for incorporation is delivered at the distal tip to be associated to “naked”, recently elongated microtubule segments but that some material is released from the IFT train prior to reaching the tip of the flagellum. These proteins would serve for completion of the assembly or for turnover. This hypothesis is supported by the relative structural disorganisation found in the terminal portion of the new flagellum of *T. brucei* perhaps because assembly of all subcomponents is not complete [Hoog et al., 2014]. In this context, it should be

pointed out that in *Chlamydomonas*, DRC4 can dissociate from IFT trains at various sites along the flagellum and not always at the distal tip [Wren et al., 2013].

The situation turned out to be very different for the membrane-associated flagellar protein AK3, where no polarity could be detected during assembly of the flagellum. AK3 is found all along the flagellum membrane without any specific association to a defined substructure [Subota et al., 2014]. It is likely associated to the membrane by prenylation, as suggested by the presence of a typical flagellum-targeting signal at its amino-terminus [Ooi et al., 2015] similar to that found in calflagins [Godsel and Engman, 1999; Maric et al., 2011]. These proteins presumably associate first to the cell body membrane and then to the flagellum membrane [Emmer et al., 2009]. Although direct trafficking studies of calflagins have not been reported, these proteins likely reach the flagellum by its base and then could either diffuse within the organelle, or be associated or transported by systems yet to discover. In cultured mammalian cells, two transmembrane proteins (the somatostatin receptor 3 and Smoothed, the Hedgehog transducer) appeared to diffuse freely within the primary cilium [Ye et al., 2013]. RNAi showed that all the AK3 flagellar protein pool is turned over in less than 4 h [Subota et al., 2014], which is less than half of the trypanosome cell cycle. This shows that the old flagellum is dynamic with regards to rapid replacement of at least certain membrane proteins. AK3 is a phosphagen shuttle and has been proposed to contribute to flagellum motility [Voncken et al., 2013; Ooi et al., 2015]. Since both flagella appear equally motile, the requirements for AK3 could be similar.

During half of their cell cycle, trypanosomes possess two basal bodies and two flagella, one undergoing construction and one that is already fully assembled [Sherwin and Gull, 1989]. The results reported here show that newly synthesised subunits for structural proteins are mostly targeted to the new flagellum with low amounts reaching the old flagellum. In mature flagella of *Chlamydomonas*, the degree of protein exchange turned out to be highly variable: some axonemal proteins hardly showed any turnover, whereas others were totally replaced during the life of the flagellum [Song and Dentler, 2001]. Protein exchange requires the existence of a soluble pool of material that could not be detected in the

## Assembly of flagellar components

case of PFR [Bastin et al., 1998] or DRC proteins [Kabutu et al., 2010; Ralston et al., 2011], but exists in significant amounts for the dynein component LC1 [Ralston et al., 2011], and to a lesser extent for the inner dynein arm component 5 [Wei et al., 2014] and for DNAI1 [Duquesnoy et al., 2009]. A large soluble pool might not be necessary providing that mRNA is available and that translation produces protein that is immediately used for turnover. Analysis of mRNA content at different cell cycle stages from trypanosomes that had been synchronised by elutriation revealed that many flagellar genes are up-regulated during flagellum synthesis [Archer et al., 2011]. Moreover, the timing of the expression peaks reflects that of flagellum construction: transcripts for basal body and IFT proteins emerge first, followed by those for axonemal proteins and ultimately those for PFR proteins [Morga and Bastin, 2013].

Finally, the absence of turnover of both the heavy and the intermediate dynein chains supports the view that the length of the mature flagellum in trypanosomes is fixed [Ooi and Bastin, 2013]. This finding explains that absence or arrest of IFT in mature flagella had no effect on their length, contrarily to the growing flagellum [Fort et al., 2016]. This means that the control of flagellum length is different compared to what has been described for *Chlamydomonas*, where flagellar length is regulated by a dynamic balance of assembly (relying on IFT for continuous delivery of tubulin) and disassembly at the distal end [Marshall and Rosenbaum, 2001].

## Materials and methods

### Trypanosome cell line and culture

For inducible expression, procyclic trypanosome cell lines were generated from the PTH cell line, a derivative of strain 427 that constitutively expresses the tet-repressor [Bastin et al., 1999a]. *IFT88<sup>RNAi</sup>* [Kohl et al., 2003] and *IFT140<sup>RNAi</sup>* [Absalon et al., 2008] strain have been described previously. They were cultured in SDM-79 [Brun and Schonenberger, 1979] supplemented with hemin and 10 % foetal bovine serum, with the exception of the inducible cell line expressing the AK3::Ty1 protein that was grown in SDM79 supplemented with 20 mM glycerol [Ooi et al., 2015]. The AnTat1.1 strain was used for expression of mNeonGreen::DHCODAB. Long primer PCR transfections were performed in bloodstream form parasites cultured in HMI-11 medium prior to differentiation into procyclic stage parasites. Bloodstream pleomorphic parasites were differentiated by addition of 5  $\mu$ M 8-pCPT-2-O-methyl-5-AMP to 10<sup>5</sup> parasites per ml in 10 ml of HMI-11. Parasites were cultured for 48 h to induce stumpy formation followed by transfer to SDM-79 medium supplemented with 20 mM glycerol and 6 mM cis-aconitate at

10<sup>6</sup> parasites per ml and transferred to a 27°C incubator for 72 h, after which time cells were cultured in SDM-79 supplemented with 20 mM glycerol. Cell numbers in culture was determined using the Z2 cell counter (Beckman Coulter).

### Expression of Ty1 and fluorescent fusion proteins

Expression of Ty1-tagged flagellar proteins was achieved with the pHD430 plasmid that contains the full gene sequence fused to the Ty1 tag in 5' (RSP3) or 3' (PF16) positions, under the control of the tetracycline-inducible EP promoter [Bastin et al., 1999a]. All the sequence fragments were chemically synthesised by GeneCust Europe and sub-cloned into the pHD430 vector. For the generation of cell lines expressing these Ty1 fusion proteins, linearised pHD430 vectors were nucleofected into PTH cells that express the tetracycline-repressor by targeting the inverted spacer of the ribosomal DNA that is supposed to be silent [Wirtz and Clayton, 1995]. For endogenous tagging of DNAI1, the first 400 bp of the gene were cloned in the pPCPFRGF-PDHC1b vector [Blisnick et al., 2014] and integrated in the genome following linearisation within the *DNAI1* sequence. For *in situ* tagging of DHC-ODAB (Tb927.11.3250), primers matching the p2675mNeonGreenIFT81 plasmid were designed with 80 bp extensions covering the last 80 bp of the 5'UTR sequence (CGT GTC CGT AGG TGG AAC GAT TAA GCA ACG AGA GGA GTT ACG TAA ATC AAA CAA GCA AAC TAA GGA AAG GAA CCC CGC CTA AAG TCG AGG AGG TTG A) and the first 80 bp of the *DHC-ODAB* coding sequence ((TTT AAC CCG GTA ATG ATG CGC TGC TCA AGC CAC TGA ACA CGC CTA TCG ACG GGT GCC TCT TCC TTG TCG CCC TTC GCC ATG TCA AGT GGG TCC TGG TTA G), hence amplifying the puromycin drug resistance cassette, the splicing sequence, a Ty-1 tag and the mNeonGreen sequence. Transfections were carried out using Nucleofector<sup>®</sup> technology [Burkard et al., 2007]. Transgenic cell lines were selected in medium supplemented with phleomycin (2.5  $\mu$ g/ml) or puromycin (1  $\mu$ g/ml) where appropriate.

### Tetracycline induction time course

Tetracycline induction was carried out at a concentration of 1  $\mu$ g/ml. Cells were grown in culture to  $\sim 10^7$  cells/ml in SDM79 or SDMG medium prior to commencement of the experiment. Non-induced cells were split into separate flasks corresponding to the number of time points and induction was initiated in a staggered manner. Upon addition of tetracycline (Sigma) to the flask for time 0, cells were harvested for Western blotting or immunofluorescence assays (IFAs).

### Immunoblot analysis

Samples were boiled in Laemmli buffer (2 $\times$  stock: 0.5 M Tris pH 6.8 containing 20% glycerol, 4% dithiothreitol, 4% SDS, Bromo-phenol blue) before SDS-PAGE separation, loading 40  $\mu$ g of total cell protein per lane. The Criterion system (Biorad) was used for electrophoresis. Proteins were transferred to polyvinylidene difluoride membranes (Hybond-P from Amersham) in the Criterion blotter (Biorad) for 45 min at 100 V constant in TG buffer (10 $\times$  stock: 0.25 mM Tris pH 8.3, 1.92 mM glycine). The membrane was blocked overnight with 5% skimmed milk in PBS and incubated with primary antibodies diluted in 1% milk and 0.1% Tween20 in PBS for 1 h. Membrane

washes were performed with 0.2% Tween20 in PBS. Species-specific secondary antibodies coupled to horseradish peroxidase (GE Healthcare) were diluted 1/20,000 in 1% milk and 0.1% Tween20 in PBS and incubated with the membranes for 1 h. Final detection was carried out by using an ECL kit according to manufacturer's instructions (Amersham) and exposure of Hyperfilm-ECL (Amersham). Antibodies against the endoplasmic reticulum component BiP [Bangs et al., 1993] or against the paraflagellar proteins [Kohl et al., 1999] were used as loading controls.

#### Indirect IFA

Cultured parasites were washed twice in SDM79 medium without serum and spread on poly-L-lysine coated slides (Menzel-Gläser) before fixation. For methanol fixation, parasites were air dried and fixed in methanol at  $-20^{\circ}\text{C}$  for 5 min followed by a rehydration step for 15 min in PBS. For PFA fixation, parasites were left to settle on slides, rinsed in PBS before being incubated for 30 min at room temperature with a 4% PFA solution in PBS at pH 7. After a permeabilisation step with 0.1% Nonidet P-40 (Fluka) in PBS, samples were blocked for 1 h with 1% BSA in PBS. To extract the cytoskeleton and solubilise cytoplasmic contents, the cells were left to settle on poly-L-lysine coated slides for 10 min, rinsed in PBS and treated for 7 s with 1% NP40 in PEM buffer (0.1 M PIPES pH 6.9, 2 mM EGTA, 1 mM  $\text{MgSO}_4$ ). After thorough washes, the samples were fixed in methanol before being processed.

For immunodetection, slides were incubated with the appropriate dilution of the first antibody in 0.1% BSA in PBS for 1 h. Mab25 recognises the axonemal protein TbSAXO1 [Dacheux et al., 2012] and was used as a marker of the axoneme [Pradel et al., 2006], whereas BB2 served to detect the Ty1 tag [Bastin et al., 1996]. After three 5-min washes, species and subclass-specific secondary antibodies coupled to the appropriate fluorochrome (Alexa 488, Cy3 or Cy5; Jackson ImmunoResearch) were diluted 1/400 in PBS containing 0.1% BSA and were applied for 1 h. After washing as above, cells were stained with a 1  $\mu\text{g}/\text{ml}$  solution of the DNA-dye DAPI (Roche) and mounted with the ProLong antifade reagent (Invitrogen). Slides were analysed with a DMR microscope (Leica) and images captured with a CoolSnap HQ camera (Roper Scientific). Image acquisition was controlled using ImageJ and images were taken with the threshold set at maximum. Subsequent normalisation of signals was carried out by parallel manipulation of brightness and contrast against controls, and images were superimposed using Photoshop CC.

#### FRAP analysis

The expression of GFP::DNAI1 was first observed directly with a DMI4000 Leica microscope using a mercury bulb for excitation to verify correct protein expression and localisation. For FRAP analysis of cells expressing GDP::DNAI1, a Zeiss inverted microscope (Axiovert 200) equipped with an oil immersion objective (magnification  $\times 63$  with a 1.4 numerical aperture) and a spinning disk confocal head (CSU22, Yokogawa) was used [Buisson et al., 2013]. Images were acquired using Volocity software with an EMCCD camera (C-9100, Hamamatsu) operating in streaming mode. A sample was taken directly from the culture grown at  $6\text{--}8 \times 10^6$  cells/ml and trapped between slide and

coverslip. The samples were kept at  $27^{\circ}\text{C}$  using a fast response mini-stage temperature controller. Time-lapse sequences were acquired to analyse GFP signal recovery after photobleaching. Movies were taken using a time lapse of 3 min. Exposure time was 0.8 s per frame (binning was  $1 \times 1$  pixels). In the case of cells expressing mNeonGreen::DHC-ODAB, the same settings were used except that the microscope was equipped with a  $100\times$  objective (1.4 numerical aperture). In this case, eight cells were identified per series and their position recorded before photobleaching. Sequences of 20 s were filmed for each with an exposure time of 0.1 s per frame. Time lapse varied between 5 and 13 min.

#### Author contribution

L.V. and P.B. conceived and designed the experiments; L.V., T.B., E.B., S.H., C.P.O and C.G. performed the experiments; L.V. and P.B. wrote the manuscript. T.B. prepared the figures, and all the authors commented on the manuscript.

#### Funding

L.V. was supported by a Roux post-doctoral fellowship from the Institut Pasteur. E.B. is supported by fellowships from French National Ministry for Research and Technology (doctoral school CDV515) and from La Fondation pour la Recherche Médicale (FDT20170436836). S. H. is funded by Roux post-doctoral fellowship from the Institut Pasteur. This work is funded by ANR grants (11-BSV8-016 and 14-CE35-0009-01), by a French Government Investissement d'Avenir programme, Laboratoire d'Excellence "Integrative Biology of Emerging Infectious Diseases" (ANR-10-LABX-62-IBEID) and by La Fondation pour la Recherche Médicale (Equipe FRM DEQ20150734356). The funders had no role in the study design, data collection and analysis, decision to publish or preparation of the manuscript.

#### Acknowledgements

We thank Derrick Robinson (Bordeaux) for providing the Mab25 antibody. We thank the UTechS-PBI (Imagopole) France-BioImaging infrastructure, supported by the French National Research Agency (ANR10-INSB-04-01, Investments for the Future), for advice and access to the microscopy systems and Jean-Yves Tinevez for training and valuable advice.

#### Conflict of interest statement

The authors have declared no conflict of interest.

## References

- Absalon, S., Blisnick, T., Kohl, L., Toutirais, G., Dore, G., Julkowska, D., Tavenet, A. and Bastin, P. (2008) Intraflagellar transport and functional analysis of genes required for flagellum formation in trypanosomes. *Mol. Biol. Cell* **19**, 929–944
- Ahmed, N.T., Gao, C., Lucker, B.F., Cole, D.G. and Mitchell, D.R. (2008) ODA16 aids axonemal outer row dynein assembly through an interaction with the intraflagellar transport machinery. *J. Cell Biol.* **183**, 313–322
- Archer, S.K., Inchaustegui, D., Queiroz, R. and Clayton, C. (2011) The cell cycle regulated transcriptome of *Trypanosoma brucei*. *PLoS One* **6**, e18425
- Bangs, J.D., Uyetake, L., Brickman, M.J., Balber, A.E. and Boothroyd, J.C. (1993) Molecular cloning and cellular localization of a BiP homologue in *Trypanosoma brucei*. Divergent ER retention signals in a lower eukaryote. *J. Cell Sci.* **105**(Pt 4), 1101–1113
- Baron, D.M., Ralston, K.S., Kabututu, Z.P. and Hill, K.L. (2007) Functional genomics in *Trypanosoma brucei* identifies evolutionarily conserved components of motile flagella. *J. Cell Sci.* **120**, 478–491
- Bastin, P., Bagherzadeh, Z., Matthews, K.R. and Gull, K. (1996) A novel epitope tag system to study protein targeting and organelle biogenesis in *Trypanosoma brucei*. *Mol. Biochem. Parasitol.* **77**, 235–239
- Bastin, P., MacRae, T.H., Francis, S.B., Matthews, K.R. and Gull, K. (1999a) Flagellar morphogenesis: protein targeting and assembly in the paraflagellar rod of trypanosomes. *Mol. Cell. Biol.* **19**, 8191–8200
- Bastin, P., Pullen, T.J., Sherwin, T. and Gull, K. (1999b) Protein transport and flagellum assembly dynamics revealed by analysis of the paralysed trypanosome mutant *snl-1*. *J. Cell Sci.* **112**(Pt 21), 3769–3777
- Bastin, P., Sherwin, T. and Gull, K. (1998) Paraflagellar rod is vital for trypanosome motility. *Nature* **391**, 548
- Blisnick, T., Buisson, J., Absalon, S., Marie, A., Cayet, N. and Bastin, P. (2014) The intraflagellar transport dynein complex of trypanosomes is made of a heterodimer of dynein heavy chains and of light and intermediate chains of distinct functions. *Mol. Biol. Cell* **25**, 2620–2633
- Bower, R., Tritschler, D., Vanderwaal, K., Perrone, C.A., Mueller, J., Fox, L., Sale, W.S. and Porter, M.E. (2013) The N-DRC forms a conserved biochemical complex that maintains outer doublet alignment and limits microtubule sliding in motile axonemes. *Mol. Biol. Cell* **24**, 1134–1152
- Branche, C., Kohl, L., Toutirais, G., Buisson, J., Cosson, J. and Bastin, P. (2006) Conserved and specific functions of axoneme components in trypanosome motility. *J. Cell Sci.* **119**, 3443–3455
- Bringaud, F., Robinson, D.R., Barradeau, S., Biteau, N., Baltz, D. and Baltz, T. (2000) Characterization and disruption of a new *Trypanosoma brucei* repetitive flagellum protein, using double-stranded RNA inhibition. *Mol. Biochem. Parasitol.* **111**, 283–297
- Broadhead, R., Dawe, H.R., Farr, H., Griffiths, S., Hart, S.R., Portman, N., Shaw, M.K., Ginger, M.L., Gaskell, S.J., McKean, P.G. and Gull, K. (2006) Flagellar motility is required for the viability of the bloodstream trypanosome. *Nature* **440**, 224–227
- Brown, J.M., Marsala, C., Kosoy, R. and Gaertig, J. (1999) Kinesin-II is preferentially targeted to assembling cilia and is required for ciliogenesis and normal cytokinesis in *Tetrahymena*. *Mol. Biol. Cell* **10**, 3081–3096
- Brun, R. and Schonenberger. (1979) Cultivation and in vitro cloning or procyclic culture forms of *Trypanosoma brucei* in a semi-defined medium. Short communication. *Acta Trop.* **36**, 289–292
- Buisson, J., Chenouard, N., Lagache, T., Blisnick, T., Olivo-Marin, J.C. and Bastin, P. (2013) Intraflagellar transport proteins cycle between the flagellum and its base. *J. Cell Sci.* **126**, 327–338
- Burkard, G., Fragoso, C.M. and Roditi, I. (2007) Highly efficient stable transformation of bloodstream forms of *Trypanosoma brucei*. *Mol. Biochem. Parasitol.* **153**, 220–223
- Craft, J.M., Harris, J.A., Hyman, S., Kner, P. and Lechtreck, K.F. (2015) Tubulin transport by IFT is upregulated during ciliary growth by a cilium-autonomous mechanism. *J. Cell Biol.* **208**, 223–237
- Dacheux, D., Landrein, N., Thonnus, M., Gilbert, G., Sahin, A., Wodrich, H., Robinson, D.R. and Bonhivers, M. (2012) A MAP6-related protein is present in protozoa and is involved in flagellum motility. *PLoS One* **7**, e31344
- Demonchy, R., Blisnick, T., Deprez, C., Toutirais, G., Lousset, C., Marande, W., Grellier, P., Bastin, P. and Kohl, L. (2009) Kinesin 9 family members perform separate functions in the trypanosome flagellum. *J. Cell Biol.* **187**, 615–622
- Duquesnoy, P., Escudier, E., Vincensini, L., Freshour, J., Bridoux, A.M., Coste, A., Deschildre, A., de Blic, J., Legendre, M., Montantin, G., Tenreiro, H., Vojtek, A.M., Lousset, C., Clement, A., Escalier, D., Bastin, P., Mitchell, D.R. and Amselem, S. (2009) Loss-of-function mutations in the human ortholog of *Chlamydomonas reinhardtii* ODA7 disrupt dynein arm assembly and cause primary ciliary dyskinesia. *Am. J. Hum. Genet.* **85**, 890–896
- Emmer, B.T., Souther, C., Toriello, K.M., Olson, C.L., Epting, C.L. and Engman, D.M. (2009) Identification of a palmitoyl acyltransferase required for protein sorting to the flagellar membrane. *J. Cell Sci.* **122**, 867–874
- Fliegauf, M., Olbrich, H., Horvath, J., Wildhaber, J.H., Zariwala, M.A., Kennedy, M., Knowles, M.R. and Omran, H. (2005) Mislocalization of DNAH5 and DNAH9 in respiratory cells from patients with primary ciliary dyskinesia. *Am. J. Respir. Crit. Care Med.* **171**, 1343–1349
- Fort, C., Bonnefoy, S., Kohl, L. and Bastin, P. (2016) Intraflagellar transport is required for the maintenance of the trypanosome flagellum composition but not its length. *J. Cell Sci.* **129**, 3026–3041
- Godsel, L.M. and Engman, D.M. (1999) Flagellar protein localization mediated by a calcium-myristoyl/palmitoyl switch mechanism. *EMBO J.* **18**, 2057–2065
- Han, Y.G., Kwok, B.H. and Kernan, M.J. (2003) Intraflagellar transport is required in *Drosophila* to differentiate sensory cilia but not sperm. *Curr. Biol.* **13**, 1679–1686
- Hao, L. and Scholey, J.M. (2009) Intraflagellar transport at a glance. *J. Cell Sci.* **122**, 889–892
- Hao, L., Thein, M., Brust-Mascher, I., Civelekoglu-Scholey, G., Lu, Y., Acar, S., Prevo, B., Shaham, S. and Scholey, J.M. (2011) Intraflagellar transport delivers tubulin isotypes to sensory cilium middle and distal segments. *Nat. Cell Biol.* **13**, 790–798
- Harris, J.A., Liu, Y., Yang, P., Kner, P. and Lechtreck, K.F. (2016) Single-particle imaging reveals intraflagellar transport-independent transport and accumulation of EB1 in *Chlamydomonas* flagella. *Mol. Biol. Cell* **27**, 295–307
- Hoog, J.L., Lacomble, S., O'Toole, E.T., Hoenger, A., McIntosh, J.R. and Gull, K. (2014) Modes of flagellar assembly in *Chlamydomonas reinhardtii* and *Trypanosoma brucei*. *eLife* **3**, e01479
- Hou, Y., Qin, H., Follit, J.A., Pazour, G.J., Rosenbaum, J.L. and Witman, G.B. (2007) Functional analysis of an individual IFT protein: IFT46 is required for transport of outer dynein arms into flagella. *J. Cell Biol.* **176**, 653–665
- Huber, C. and Cormier-Daire, V. (2012) Ciliary disorder of the skeleton. *Am. J. Med. Genet. C Semin. Med. Genet.* **160C**, 165–174
- Ishikawa, H. and Marshall, W.F. (2011) Ciliogenesis: building the cell's antenna. *Nat. Rev. Mol. Cell Biol.* **12**, 222–234
- Johnson, K.A. and Rosenbaum, J.L. (1992) Polarity of flagellar assembly in *Chlamydomonas*. *J. Cell Biol.* **119**, 1605–1611

- Julkowska, D. and Bastin, P. (2009) Tools for analyzing intraflagellar transport in trypanosomes. *Methods Cell Biol.* **93**, 59–80
- Kabututu, Z.P., Thayer, M., Melehan, J.H. and Hill, K.L. (2010) CMF70 is a subunit of the dynein regulatory complex. *J. Cell Sci.* **123**, 3587–3595
- Kohl, L., Robinson, D. and Bastin, P. (2003) Novel roles for the flagellum in cell morphogenesis and cytokinesis of trypanosomes. *EMBO J.* **22**, 5336–5346
- Kohl, L., Sherwin, T. and Gull, K. (1999) Assembly of the paraflagellar rod and the flagellum attachment zone complex during the *Trypanosoma brucei* cell cycle. *J. Eukaryot. Microbiol.* **46**, 105–109
- Kozminski, K.G., Beech, P.L. and Rosenbaum, J.L. (1995) The *Chlamydomonas* kinesin-like protein FLA10 is involved in motility associated with the flagellar membrane. *J. Cell Biol.* **131**, 1517–1527
- Kozminski, K.G., Johnson, K.A., Forscher, P. and Rosenbaum, J.L. (1993) A motility in the eukaryotic flagellum unrelated to flagellar beating. *Proc. Natl. Acad. Sci. U.S.A.* **90**, 5519–5523
- Langousis, G. and Hill, K.L. (2014) Motility and more: the flagellum of *Trypanosoma brucei*. *Nature reviews. Microbiology* **12**, 505–518
- Lehtreck, K.F., Gould, T.J. and Witman, G.B. (2013) Flagellar central pair assembly in *Chlamydomonas reinhardtii*. *Cilia* **2**, 15
- Maric, D., McGwire, B.S., Buchanan, K.T., Olson, C.L., Emmer, B.T., Epting, C.L. and Engman, D.M. (2011) Molecular determinants of ciliary membrane localization of *Trypanosoma cruzi* flagellar calcium-binding protein. *J. Biol. Chem.* **286**, 33109–33117
- Marshall, W.F. and Rosenbaum, J.L. (2001) Intraflagellar transport balances continuous turnover of outer doublet microtubules: implications for flagellar length control. *J. Cell Biol.* **155**, 405–414
- Mencarelli, C., Lupetti, P. and Dallai, R. (2008) New insights into the cell biology of insect axonemes. *Int. Rev. Cell Mol. Biol.* **268**, 95–145
- Milenkovic, L., Scott, M.P. and Rohatgi, R. (2009) Lateral transport of Smoothed from the plasma membrane to the membrane of the cilium. *J. Cell Biol.* **187**, 365–374
- Miranda, M.R., Bouvier, L.A., Canepa, G.E. and Pereira, C.A. (2009) Subcellular localization of *Trypanosoma cruzi* arginine kinase. *Parasitology* **136**, 1201–1207
- Morga, B. and Bastin, P. (2013) Getting to the heart of intraflagellar transport using *Trypanosoma* and *Chlamydomonas* models: the strength is in their differences. *Cilia*, in press
- Nonaka, S., Tanaka, Y., Okada, Y., Takeda, S., Harada, A., Kanai, Y., Kido, M. and Hirokawa, N. (1998) Randomization of left-right asymmetry due to loss of nodal cilia generating leftward flow of extraembryonic fluid in mice lacking KIF3B motor protein. *Cell* **95**, 829–837
- Oberholzer, M., Langousis, G., Nguyen, H.T., Saada, E.A., Shimogawa, M.M., Jonsson, Z.O., Nguyen, S.M., Wohlschlegel, J.A. and Hill, K.L. (2011) Independent analysis of the flagellum surface and matrix proteomes provides insight into flagellum signaling in mammalian-infectious *Trypanosoma brucei*. *Mol. Cell. Proteom.* **10**, M111 010538
- Oberholzer, M., Lopez, M.A., Ralston, K.S. and Hill, K.L. (2009) Approaches for functional analysis of flagellar proteins in African trypanosomes. *Methods Cell Biol.* **93**, 21–57
- Ooi, C.P. and Bastin, P. (2013) More than meets the eye: understanding *Trypanosoma brucei* morphology in the tsetse. *Front. Cell. Infect. Microbiol.* **3**, 1–12
- Ooi, C.P., Rotureau, B., Gribaldo, S., Georgikou, C., Julkowska, D., Blisnick, T., Perrot, S., Subota, I. and Bastin, P. (2015) The flagellar arginine kinase in *Trypanosoma brucei* is important for infection in Tsetse flies. *PLoS One* **10**, e0133676
- Owa, M., Furuta, A., Usukura, J., Arisaka, F., King, S.M., Witman, G.B., Kamiya, R. and Wakabayashi, K. (2014) Cooperative binding of the outer arm-docking complex underlies the regular arrangement of outer arm dynein in the axoneme. *Proc. Natl. Acad. Sci. U.S.A.* **111**, 9461–9466
- Pazour, G.J., Agrin, N., Leszyk, J. and Witman, G.B. (2005) Proteomic analysis of a eukaryotic cilium. *J. Cell Biol.* **170**, 103–113
- Piperno, G., Mead, K. and Henderson, S. (1996) Inner dynein arms but not outer dynein arms require the activity of kinesin homologue protein KHP1(FLA10) to reach the distal part of flagella in *Chlamydomonas*. *J. Cell Biol.* **133**, 371–379
- Portman, N. and Gull, K. (2010) The paraflagellar rod of kinetoplastid parasites: from structure to components and function. *Int. J. Parasitol.* **40**, 135–148
- Pradel, L.C., Bonhivers, M., Landrein, N. and Robinson, D.R. (2006) NIMA-related kinase TbNRKC is involved in basal body separation in *Trypanosoma brucei*. *J. Cell Sci.* **119**, 1852–1863
- Ralston, K.S., Kisalu, N.K. and Hill, K.L. (2011) Structure-function analysis of dynein light chain 1 identifies viable motility mutants in bloodstream-form *Trypanosoma brucei*. *Eukaryot. Cell* **10**, 884–894
- Ralston, K.S., Lerner, A.G., Diener, D.R. and Hill, K.L. (2006) Flagellar motility contributes to cytokinesis in *Trypanosoma brucei* and is modulated by an evolutionarily conserved dynein regulatory system. *Eukaryot. Cell* **5**, 696–711
- Reiter, J.F., Blacque, O.E. and Leroux, M.R. (2012) The base of the cilium: roles for transition fibres and the transition zone in ciliary formation, maintenance and compartmentalization. *EMBO Rep.* **13**, 608–618
- Reiter, J.F. and Leroux, M.R. (2017) Genes and molecular pathways underpinning ciliopathies. *Nat. Rev. Mol. Cell Biol.* **18**, 533–547
- Robinson, D., Beattie, P., Sherwin, T. and Gull, K. (1991) Microtubules, tubulin, and microtubule-associated proteins of trypanosomes. *Methods Enzymol.* **196**, 285–299
- Rosenbaum, J.L., Moulder, J.E. and Ringo, D.L. (1969) Flagellar elongation and shortening in *Chlamydomonas*. The use of cycloheximide and colchicine to study the synthesis and assembly of flagellar proteins. *J. Cell Biol.* **41**, 600–619
- Sapiro, R., Kostetskii, I., Olds-Clarke, P., Gerton, G.L., Radice, G.L. and Strauss, I.J. (2002) Male infertility, impaired sperm motility, and hydrocephalus in mice deficient in sperm-associated antigen 6. *Mol. Cell. Biol.* **22**, 6298–6305
- Shen, S., Arhin, G.K., Ullu, E. and Tschudi, C. (2001) In vivo epitope tagging of *Trypanosoma brucei* genes using a one step PCR-based strategy. *Mol. Biochem. Parasitol.* **113**, 171–173
- Sheriff, O., Lim, L.F. and He, C.Y. (2014) Tracking the biogenesis and inheritance of subpellicular microtubule in *Trypanosoma brucei* with inducible YFP- $\alpha$ -tubulin. *BioMed Res. Int.* **2014**, 893272
- Sherwin, T. and Gull, K. (1989) The cell division cycle of *Trypanosoma brucei*: timing of event markers and cytoskeletal modulations. *Philos. Trans. R. Soc. Lond. B Biol. Sci.* **323**, 573–588
- Smith, E.F. and Lefebvre, P.A. (1996) PF16 encodes a protein with armadillo repeats and localizes to a single microtubule of the central apparatus in *Chlamydomonas* flagella. *J. Cell Biol.* **132**, 359–370
- Smith, J.C., Northey, J.G., Garg, J., Pearlman, R.E. and Siu, K.W. (2005) Robust method for proteome analysis by MS/MS using an entire translated genome: demonstration on the ciliome of *Tetrahymena thermophila*. *J. Proteome Res.* **4**, 909–919
- Song, L. and Dentler, W.L. (2001) Flagellar protein dynamics in *Chlamydomonas*. *J. Biol. Chem.* **276**, 29754–29763
- Subota, I., Julkowska, D., Vincensini, L., Reeg, N., Buisson, J., Blisnick, T., Huet, D., Perrot, S., Santi-Rocca, J., Duchateau, M., Houdel, V., Rousselle, J.C., Cayet, N., Namane, A., Chamot-Rooke, J. and Bastin, P. (2014) Proteomic analysis of intact flagella of procyclic *Trypanosoma brucei* cells identifies novel flagellar proteins with unique sub-localization and dynamics. *Mol. Cell. Proteom.* **13**, 1769–1786
- Sunter, J.D., Varga, V., Dean, S. and Gull, K. (2015) A dynamic coordination of flagellum and cytoplasmic cytoskeleton assembly

- specifies cell morphogenesis in trypanosomes. *J. Cell Sci.* **15**, 1580–1594
- Vincensini, L., Blisnick, T. and Bastin, P. (2011) 1001 model organisms to study cilia and flagella. *Biol. Cell* **103**, 109–130
- Voncken, F., Gao, F., Wadforth, C., Harley, M. and Colasante, C. (2013) The phosphoarginine energy-buffering system of *trypanosoma brucei* involves multiple arginine kinase isoforms with different subcellular locations. *PLoS One* **8**, e65908
- Wei, Y., Hu, H., Lun, Z.R. and Li, Z. (2014) Centrin3 in trypanosomes maintains the stability of a flagellar inner-arm dynein for cell motility. *Nat. Commun.* **5**, 4060
- Wirtz, E. and Clayton, C. (1995) Inducible gene expression in trypanosomes mediated by a prokaryotic repressor. *Science* **268**, 1179–1183
- Wren, K.N., Craft, J.M., Tritschler, D., Schauer, A., Patel, D.K., Smith, E.F., Porter, M.E., Kner, P. and Lehtreck, K.F. (2013) A differential cargo-loading model of ciliary length regulation by IFT. *Curr. Biol.* **23**, 2463–2471
- Yagi, T., Uematsu, K., Liu, Z. and Kamiya, R. (2009) Identification of dyneins that localize exclusively to the proximal portion of *Chlamydomonas* flagella. *J. Cell Sci.* **122**, 1306–1314
- Ye, F., Breslow, D.K., Koslover, E.F., Spakowitz, A.J., Nelson, W.J. and Nachury, M.V. (2013) Single molecule imaging reveals a major role for diffusion in the exploration of ciliary space by signaling receptors. *eLife* **2**, e00654
- Zhou, Q., Hu, H., He, C.Y. and Li, Z. (2015) Assembly and maintenance of the flagellum attachment zone filament in *Trypanosoma brucei*. *J. Cell Sci.* **128**, 2361–2372

---

Received: 11 September 2017; Accepted: 19 October 2017; Accepted article online: 16 November 2017



**Control of flagellum length by a “grow-and-lock” model.**

Article submitted to Current Biology.

Eloïse Bertiaux, Benjamin Morga, Thierry Blisnick, Brice Rotureau & Philippe Bastin.



## Control of flagellum length by a grow-and-lock model

Eloïse Bertiaux<sup>1,2,4</sup>, Benjamin Morga<sup>1,3,4</sup>, Thierry Blisnick<sup>1</sup>, Brice Rotureau<sup>1</sup> & Philippe Bastin<sup>1,5</sup>

<sup>1</sup>Trypanosome Cell Biology Unit, Institut Pasteur & INSERM U1201, 25, rue du Docteur Roux, 75015 Paris, France.

<sup>2</sup>Université Pierre et Marie Curie Paris 6, Cellule Pasteur-UPMC, 25 rue du Docteur Roux, 75015 Paris, France

<sup>3</sup> Present address: Laboratoire de Génétique et Pathologie des Mollusques Marins, Station de La Tremblade - Ronce Les Bains - 17390 La Tremblade, France

<sup>4</sup> Equal contribution

<sup>5</sup> Lead contact: [pbastin@pasteur.fr](mailto:pbastin@pasteur.fr)

## SUMMARY

Several cell types such as photoreceptors and spermatozoa possess very stable cilia and flagella, a feature also encountered in numerous protists. We tested an original model for the control of flagellum length in such cells, using *Trypanosoma brucei* as an experimental system. The grow-and-lock model proposes that the flagellum elongates at a linear rate and that a locking event takes place in a timely defined manner preventing further elongation or shortening. We show that the total amount of IFT material increases during flagellum elongation, ensuring a constant concentration per unit of length and the ability to provide a constant delivery of precursors in agreement with a linear growth rate. Reducing the IFT rate by RNAi knockdown of the IFT kinesin motors slows down the growth rate and results in the assembly of shorter flagella. The flagellum is locked after cell division in an irreversible process and even subsequent increase in the IFT rate does not lead to further elongation. Other models (limitation by the soluble pool of tubulin, equilibrium between assembly and disassembly rates, or morphogenetic control) fail to explain the experimental data. The locking event is associated to the addition of the FLAM8 molecular marker at the distal end of the flagellum and is initiated prior cell division, leading to an arrest of elongation in the daughter cell. These results provide support for the grow-and-lock model as a new paradigm for the control of organelle length.

Keywords: cilia and flagella; ciliogenesis; organelle length; microtubules; intraflagellar transport; trypanosome; photoreceptor; spermatozoa

## INTRODUCTION

Cilia and flagella (interchangeable terms) are present at the surface of many eukaryotic cells from protists to humans where they are involved in a range of functions including motility, sensing or morphogenesis. Multiple types of ciliary organisations are encountered from one species to another, and also between different cells in the same organism. Striking variations have been noted in cilia composition, positioning or length, presumably reflecting an optimisation related to the function in a given cell type. The lifespan of cilia is also highly variable, from the transitory existence of some primary cilia to the very stable cilia or flagella of photoreceptors or spermatozoa that show little or no turnover of their microtubules.

Despite extensive variation, each cilium or flagellum exhibits a defined length, a process that has fascinated scientists for decades [1]. To decipher the mechanisms that control length, it is essential to understand how the organelle is constructed. Tubulin is delivered via Intraflagellar Transport (IFT) to the distal end of growing microtubules where incorporation takes place [2-4]. Absence of IFT prevents cilium construction in all organisms investigated so far [5]. The control of flagellum length has mostly been studied in the green algae *Chlamydomonas* [6], a member of the Archeoplastida group [7]. In this organism, flagellar microtubules are highly dynamic and exhibit constant disassembly at their plus end. In such a situation, IFT is essential not only for the construction but also for the maintenance of length [8]. Several models have been proposed to explain the control of length in this context, mainly as a balance between assembly and disassembly rates [6], with IFT being a central component [4, 8-11]. These models could function in other systems where cilia display significant microtubule turnover such as in *C. elegans* [12] but could not be applied in cells with more stable cilia.

In mammals, the mouse sperm flagellum relies on IFT for assembly but not for maintenance, and yet the sperm flagellum does not disassemble after maturation [13]. Another case is the connecting cilium of photoreceptors in the retina. These cells display very low turnover [14] and loss of IFT after assembly only impacts ciliary length after 2-3 weeks, possibly because the cell degenerates [15]. How is length control achieved in such conditions? Here, we propose a new model termed grow-and-lock where the organelle grows up to a stage where a signal blocks further elongation or shortening by inducing a modification that locks the structure in a stable (or mature) configuration. The organelle is now ready to perform its final function and does not need length monitoring. In theory, this model is compatible with any type of assembly rate but the easiest situation is to assume a linear growth rate. The moment when the flagellum is locked could be controlled at the level of the flagellum itself, thereby implying a way to measure length. A simpler option would be to link that event to another cellular process that is timely regulated, such as progression through the cell cycle or through cell differentiation. The locking event would lead to a modification of the organelle that makes its structural elements very stable whereas other components could remain dynamic. **Alternatively, it could prevent access of tubulin dimers and other components to the flagellum.** This simple model predicts that cells could produce flagella of different lengths by modulating the growth rate and/or the timing of the locking event.

Spermatozoa or photoreceptors do not lend easily to manipulation. By contrast, protists represent great model organisms, are amenable in the laboratory and several of them exhibit very stable flagella. Here, we selected the protist *Trypanosoma brucei* for the investigation of the grow-and-lock model for several reasons. First, its axoneme is very stable [16] and relies on IFT for construction [17, 18] but not for length maintenance [19], exactly like in spermatozoa or photoreceptors. IFT remains active after assembly to maintain other elements but not axoneme composition [19]. Second, when trypanosomes infect mammals or

tsetse flies, they progress through several stages of development during which they assemble flagella of different length [20-22] and composition [23]. This is reminiscent to what multicellular organisms do in different cell types and means that the system is flexible. Third, trypanosomes grow well in culture; they assemble their flagellum in a timely, reproducible and well-characterised manner [24-26]; they are amenable to reverse genetics and IFT has been exhaustively quantified [27].

In this study, we provide experimental evidence that supports each of the major predictions of the grow-and-lock model. **We show that results are not compatible with three other possible models: limited pool of soluble tubulin, equilibrium between assembly and disassembly and control by cell body length.** The growth rate of the trypanosome flagellar is linear thanks to the continuous recruitment of new IFT trains in the elongating flagellum and its reduction upon IFT kinesin knockdown results in the construction of shorter flagella. The locking event is controlled at the cell cycle level, is triggered prior cell division and is correlated to the addition of a unique marker protein. **The fact that the flagellum is locked is supported by the fact that increasing the IFT rate after maturation does not result in further elongation.** Blocking cell division allows for the construction of longer flagella that ultimately mature and reach exactly the same length as the flagellum assembled in the previous generation. The grow-and-lock model provides an opportunity to explain the control of flagellum length in cells with very stable organelles.

## RESULTS

### *IFT delivery remains constant during flagellum construction*

The simplest version of the grow-and-lock model is based on a linear growth rate. This is exactly the case of flagellum assembly in *T. brucei* as measured in culture [25] and during animal infection [28]. This implies a constant delivery of tubulin by IFT no matter the stage of elongation. So far, IFT has only been quantified in mature flagella of *T. brucei* at the procyclic stage maintained in culture [27, 29]. Here, IFT trafficking was examined in the elongating flagellum and compared to the mature flagellum that remains present during the cell cycle, providing an ideal control [24]. This was carried out in live procyclic trypanosomes that express a fusion protein between the fluorescent Tandem Tomato protein (TdT)[30] and the IFT-B protein IFT81, upon endogenous tagging in the *IFT81* locus [31]. In addition to the bright signal at the base, a succession of motile spots was detected all along the length of the flagellum moving in either anterograde or retrograde direction in cells with a single flagellum (Video 1, Fig. 1A1) or in those assembling the new one, hence possessing two flagella (Videos 2-4, Fig. 1 A2-4). **A summary of flagellum elongation during the trypanosome cell cycle is presented at Figure S1A.** At first glance, IFT behaviour looked quite similar in both growing and mature flagella (Fig. 1A). The total amount of fluorescence emitted by the TdT::IFT81 protein **in the flagellar compartment** was quantified by using the first image of each movie. Plotting the ratio between the total amount of fluorescence in the new flagellum and that in the old one versus the length of the growing flagellum demonstrated a linear correlation between these two parameters (Fig. 1C). This data shows that IFT proteins are progressively recruited to the flagellum as it elongates. **This means that the IFT amount increases linearly with length hence IFT density per unit of length of length remains constant during elongation.**

Next, kymograph analysis [27] was carried out to quantify IFT rates and frequencies in cells with one (Fig. 1A1 and Fig. 1B1) or two flagella at different steps of elongation (Fig. 1A2-4 and Fig 1B2-4). Kymograph observations revealed brighter individual tracks for anterograde transport and less intense tracks for retrograde transport as expected [27]. Both IFT speed (Fig. 1D) and frequency (Fig. 1E) were invariant during flagellum elongation (**Table 1**), supporting a constant delivery rate of material at the tip of the growing flagellum. We conclude that the IFT delivery rate remains constant during flagellum construction, which is in agreement with the reported linear growth rate [25, 28].

### ***Knockdown of IFT kinesins reduces frequency and speed of IFT and results in the assembly of short flagella***

The grow-and-lock model implies **that modulation** of the flagellum growth rate would impact on the final length reached by the organelle. To reduce IFT trafficking, we selected to deplete the expression of kinesin II, the IFT anterograde motor. The genome of *T. brucei* encodes two putative kinesin II proteins (Tb927.5.2090 and Tb927.11.13920) but no kinesin-associated protein (KAP) [32, 33]. Individual RNAi silencing of KIN2A or KIN2B did not result in a visible phenotype: cells assembled apparently normal flagella and grew normally in culture (data not shown), suggesting redundancy. Hence simultaneous knockdown of KIN2A and KIN2B was performed following stable transformation of trypanosomes with a plasmid expressing dsRNA of both *KIN2A* and *KIN2B* under the control of tetracycline-inducible promoters [34]. The efficiency of RNAi silencing in *KIN2A2B<sup>RNAi</sup>* cells was confirmed by western blotting using an antibody against KIN2B [33](Fig. S2). The signal for KIN2B dropped by at least 8-fold from day 1 and remained low for at least 6 days, confirming the efficiency of RNAi silencing (Fig. S2). The frequency and speed of IFT was examined upon transformation of *KIN2A2B<sup>RNAi</sup>* cells with the reporter construct described

above allowing endogenous tagging of IFT81 with TdTomato. Trypanosomes were grown in induced or non-induced conditions and IFT was measured in live unflagellated cells upon kymograph analysis. In control cells, bright anterograde trains were frequently observed, trafficking from the base to the tip of the flagellum where they were transformed to retrograde trains (Fig. S3A & Video 5). Kymograph analysis revealed that the average anterograde speed was  $1.7 \pm 0.5 \mu\text{m} \cdot \text{s}^{-1}$  ( $n=159$  trains from 10 separate cells) and the mean frequency was  $0.64 \text{ train} \cdot \text{s}^{-1}$  (Fig. S3B & **Table 2**). RNAi-induced cells looked different, the signal at the base of the flagellum appeared brighter and adopted a more elongated shape compared to that in control cells (Fig. S3C). The train frequency was reduced to  $0.37 \cdot \text{s}^{-1}$  ( $n=95$ ) after one day of induction, and down to  $0.25 \cdot \text{s}^{-1}$  after 4 to 6 days in RNAi conditions ( $n=125$ )(Video 6)(**Table 2**). This is visible on the kymograph with fewer traces in induced cells (Fig. S3D) compared to control ones (Fig. S3B). In addition, IFT trains travelled more slowly when kinesin expression was knocked down:  $1.4 \mu\text{m} \cdot \text{s}^{-1}$  at days 4 or 6 instead of  $1.9 \mu\text{m} \cdot \text{s}^{-1}$  at day 0 (Fig. S3D)(**Table 2**). We conclude that the joint depletion of KIN2A and KIN2B expression efficiently reduced IFT delivery in the flagellum.

The observed 3-fold reduction in IFT train frequency should result in a significant reduction in the flagellum growth rate that should consequently allow testing the impact of this parameter on the grow-and-lock model. Monitoring the culture by microscopy during the course of RNAi indicated the presence of smaller cells with a shorter flagellum (Fig. 2A). To quantify this reduction, cells were fixed, processed for immunofluorescence assay (IFA) using the axonemal marker Mab25 and DAPI for DNA staining, and the length of the flagellum was measured. Cells that possessed a single flagellum were first examined. In non-induced samples, the length of the axoneme was on average  $\sim 20 \mu\text{m}$ , as expected [24]. However, the length of the flagellum was shorter during the course of RNAi induction, down to  $\sim 9 \mu\text{m}$  at

day 4. **Despite the large dispersion, this difference was statistically significant** (Fig. 2B). Flagellum length remained in that range over the next two days of induction (Fig. 2B), and up to 11 days after having triggered kinesin knockdown (not shown). In control non-induced samples, analysis by scanning electron microscopy revealed the typical elongated trypanosome shape with the flagellum attached to the cell body (Fig. 2C). By contrast, flagellum length was clearly shorter in induced cells that displayed a shorter cell body (Fig. 2D), in agreement with the role of the flagellum in governing trypanosome morphogenesis [17].

The flagellum can be shorter because it is made too short, hence reflecting a defect in construction as predicted by the grow-and-lock model, but it could also be the case because it shortens after construction. To discriminate between these two possibilities, trypanosomes at a late stage of the cell cycle were investigated. These cells can easily be recognised because they possess two nuclei [24]. In control non-induced cells, the length of the new flagellum was  $\sim 15 \mu\text{m}$  whereas that of the old flagellum was  $\sim 20 \mu\text{m}$  (Fig. 3A, grey symbols on Fig. 3B) as expected because construction is not completed before cell division [24, 35]. This was confirmed by scanning electron microscopy of dividing cells: when the cleavage furrow was visible, the length of the new flagellum was shorter than that of the old one (Fig. 3C). In induced *KIN2A2B<sup>RNAi</sup>* cells, the average length of the new flagellum was around  $7 \mu\text{m}$ , for all induction times examined and **that difference was statistically significant** (Fig. 3A, black symbols on Fig. 3B). Analysis by scanning electron microscopy revealed that the new flagellum is much shorter and that the daughter cell is smaller (Fig. 3D) compared to the non-induced cells (Fig. 3C). This implies that the new flagellum is made too short when the cell is about to divide and supports the first postulate of the “grow and lock model”: reducing the growth rate impacts on the length of the flagellum.

*Presence of soluble tubulin does not support the limited cytoplasmic pool model*

The shorter flagellum length could also be explained if the amount of soluble tubulin was more limited, for example because of the shorter cell size. In this were true, regulation of flagellum length could be explained by the model of the limiting pool of cytoplasmic components [36]. To challenge this model, the amount of soluble tubulin was determined using cell fractionation in detergent to separate a cytoskeletal and a soluble fraction [37]. Analysis non-induced *KIN2A2B<sup>RNAi</sup>* cells demonstrated the existence of a low-abundance pool of soluble tubulin (Fig. S4) in agreement with previous studies [38]. A similar (possibly even more abundant) pool of soluble tubulin was found in *KIN2A2B<sup>RNAi</sup>* cells after RNAi knockdown (Fig. S4). We conclude that the amount of soluble tubulin is not the limiting factor that would cause flagella to be shorter in *KIN2A2B<sup>RNAi</sup>* cells after RNAi knockdown.

*Evidence for flagellum locking after cell division is not compatible with the balance-point model*

The grow-and-lock model implies that the mature flagellum is locked in a stable state that prevents further elongation or shortening. Although this is supported by the maintenance of flagellum length in the absence of IFT [19], the presence of a shorter mature flagellum of *KIN2A2B<sup>RNAi</sup>* cells offers the possibility to bring more direct evidence. *KIN2A2B<sup>RNAi</sup>* cells were grown in RNAi conditions for 6 days, resulting in the presence of short flagella as observed above. Tetracycline was washed out, leading to expression of fresh KIN2A and KIN2B and restoring IFT (Fig. 4A). The return of IFT trafficking in old and new flagella was monitored in live cells by the presence of a fusion protein between mNeonGreen [39] and IFT81 expressed from the endogenous *IFT81*

locus [40]. After 16 hours without tetracycline, the frequency of IFT is increased by ~2-fold in both the new and the mature flagellum (Table 2). This was confirmed by immunofluorescence staining with an anti-IFT172 antibody that revealed close to normal signal in both flagella (Fig. 4B). This shows that new IFT proteins have access to the mature flagellum in addition to the new one.

The length of each flagellum was measured using the Mab25 axonemal staining in induced and “de-induced” conditions. In induced conditions, the average length of the old flagellum was  $14.2 \pm 4.1 \mu\text{m}$  (black squares, Fig. 4C) whereas that of the new one was  $8.25 \pm 3.1 \mu\text{m}$  (black circles, Fig. 4C), as previously observed (Fig. 3B). Strikingly, the length of the old flagellum remained unchanged at  $13.9 \pm 4.08 \mu\text{m}$  (grey squares, Fig. 4C). This demonstrates that a 2-fold increase in IFT cannot rescue flagellum length after maturation. We interpret this result as evidence that the mature flagellum is locked. This also proves that the balance point model between assembly and disassembly does not apply to this type of flagellum since this model would predict an elongation of the flagellum upon increase of the IFT frequency [9].

The *T. brucei* flagellum is attached to the cell body via a sophisticated cytoskeletal network [41] and this could provide an original way to control flagellum length. This hypothesis is somehow contradicted by the fact that mutants with defects in the adhesion machinery assemble detached flagella of apparently normal length [42-46]. However, these flagella are completely detached from the cell body with the exception of the anchoring via the flagellar pocket and might be regulated differently compared to *KIN2A2B<sup>RNAi</sup>* cells where the short flagella are properly attached to the cell body. The “de-induction” experiment provides a way to challenge this model directly because at the time of tetracycline wash out, cells exhibit a short cell body. If this is a limiting factor, it should prevent further elongation of the new flagellum since it is formed on a

short cell body. Measurements of the length of the new flagellum in de-induced cells contradicted this model. Indeed, the length of the new flagellum was  $11.7 \pm 3.9 \mu\text{m}$  instead of  $8.25 \pm 3.1 \mu\text{m}$  (Fig. 4C, grey circles). Examining the ratio between the length of the new and the old flagellum revealed further interesting observations (Fig. 4D, grey circles). In close to one third of de-induced cells (16/55), the new flagellum was longer than the mature one; something that was never observed in induced *KIN2A2B<sup>RNAi</sup>* cells (Fig. 4D, black circles) or in control cells [26]. Several of these cells grew flagella that extended well beyond the cell body (Fig. S5). We conclude that flagellum length is not controlled by the size of the cell body.

#### *The locking event is initiated prior cell division*

Having brought further evidence for flagellum locking, we next investigated the second postulate of the grow-and-lock model. It says that a timely controlled event should lead to a modification that locks the flagellum and prevents further elongation or shortening. Since flagellum assembly is intimately linked with the progression through the cell cycle in trypanosomes as in other protists [24, 47, 48], we propose that the locking event is controlled by a cell cycle-dependent mechanism rather than at the flagellum level. When a procyclic trypanosome divides, the new flagellum has reached ~80% of the length of the old flagellum meaning that elongation continues up to 20  $\mu\text{m}$  in the daughter cell inheriting that flagellum. Post-division elongation has been experimentally proven but not quantified so far [49] and the events leading to its arrest are unknown. Arrest of flagellum growth could happen instantly or could be triggered by a specific signal that would be effective after a lag phase. In the first hypothesis (sharp arrest), flagellum elongation would be blocked when the flagellum becomes mature at some point after cell division. In the second hypothesis (delayed arrest), the signal leading to flagellum locking could happen prior or after cell division.

Whilst measuring the length of the new flagellum in *KIN2A2B<sup>RNAi</sup>* cells (7  $\mu\text{m}$ , see above), we noticed that the old flagellum of the same cells was almost twice longer (12  $\mu\text{m}$ , black symbols, Fig. 3B), but albeit shorter than normal (20  $\mu\text{m}$ ). This could be explained by the first hypothesis if the flagellum keeps its slow growth rate after cell division until the locking event occurs. But it could also be explained with the second model if the locking signal is triggered before division and blocks flagellum elongation later on. Therefore, this result does not discriminate between the two hypotheses.

To tease apart the mechanism responsible for the locking of the flagellum, cell division was inhibited. **If the locking event takes place after division, it should be possible to restore normal flagellum length since flagellum growth should continue unabated. If it were initiated before cell division, only limited growth would be possible after activation of the signal.** *KIN2A2B<sup>RNAi</sup>* cells were grown in the presence of 10 mM teniposide, a drug that interferes with mitochondrial DNA segregation but neither with basal body duplication nor with flagellum elongation [50]. This resulted in the expected arrest of cell division **that is clearly visible** on the growth curve (Fig. S6). *KIN2A2B<sup>RNAi</sup>* cells induced for 5 days were incubated in the presence of 10 mM teniposide. After incubation, cells were fixed and processed for IFA with the axonemal marker Mab25 whilst DNA was stained with DAPI. In controls without teniposide, the mitochondrial DNA segregated normally and cells progressed to the typical pattern with 2 kinetoplasts and 2 nuclei preceding cell division (Fig. 5A, top panels). By contrast, kinetoplasts failed to fully segregate in the presence of teniposide (Fig. 5A, bottom panels, **white arrow**), inhibiting cell division. In the absence of teniposide, the ratio between the length of the new and the old flagellum in induced *KIN2A2B<sup>RNAi</sup>* cells was about 60% (Fig. 5B, light grey), in agreement with previous measurements (Fig. 3B). Remarkably, **after 16 hours of incubation with teniposide**, the ratio was close to 100%, meaning that the length of the new flagellum had reached the length

of the old flagellum at  $\sim 12 \mu\text{m}$  but had failed to reach the normal  $20 \mu\text{m}$  (Fig. 5B, dark grey, left bars). **However, this short length could be due to slow elongation and not to a locking event.** *KIN2A2B<sup>RNAi</sup>* cells were therefore incubated for 24 hours in the presence of teniposide. These extra 8 hours in teniposide did not result in an increase of new flagellum length that remained stuck at  $12 \mu\text{m}$  (Fig. 5A, bottom panels & Fig. 5B, dark grey, right bars). We conclude that the signal for the locking event is triggered prior cell division and impacts elongation definitely.

One could consider that *KIN2A2B<sup>RNAi</sup>* cells behave differently than wild-type cells for whatever reasons (shorter flagellum length, shorter cell size, reduced motility) and this might not reflect the normal situation. Therefore, we analysed the impact of an inhibition of cell division in wild-type cells. If the model is true, blocking cell division should result in an increase of the new flagellum from 80% (**length of the new flagellum in wild-type cells**) to 100% of the length of the old flagellum. In the absence of teniposide, the ratio between new and old flagella in cells about to divide was close to 80% as expected [26, 35](Fig. S7A, top panels and S7B, light grey bars). After incubation with teniposide, the length of the new flagellum reached that of the old flagellum but did not elongate further (Fig. S7A, bottom panels and S7B, dark grey bars). **We conclude that when cytokinesis is blocked upon inhibition of mitochondrial DNA segregation, the signal that locks flagellum length is still present. This shows that this signal is triggered prior to cell division.**

#### *A molecular marker to monitor flagellum maturation*

The last element of the grow-and-lock model implies that a modification of the flagellum takes place preventing further elongation. The data above indicate this must be progressive since it is initiated prior cell division and leads to an elongation arrest only after

division. We therefore searched for candidate molecules that accumulate towards the late phase of flagellum elongation and could serve as markers for flagellum maturation. The FLAM8 protein appeared as an attractive candidate. It is a large protein (3,075 amino acids) of unknown function that was discovered in a proteomic study of purified trypanosome flagella [35]. FLAM8 is abundant at the distal tip of mature flagella and detected in very low concentrations at the first stages of flagellum construction. However, its amount increases during elongation to reach 40% of that of the old flagellum just prior cell division [35]. It means that a significant increase must happen after cell division, which is compatible with the findings above.

If FLAM8 is indeed a marker of flagellum maturation, it should accumulate in the new flagellum of teniposide-treated cells. Therefore, cell division was inhibited using teniposide in induced *KIN2A2B<sup>RNAi</sup>* cells exactly as above. Cells were fixed and stained by IFA with an anti-FLAM8 antibody, the Mab25 antibody as an axonemal marker, and DAPI to label DNA. When induced *KIN2A2B<sup>RNAi</sup>* cells were not treated with teniposide, FLAM8 was abundant at the tip of the old flagellum, but was present in very low amounts or below detection level in the new flagellum (Fig. 6A, top panels). By contrast, in cells treated with teniposide for 24 hours, the new flagellum had elongated further as described above and the FLAM8 signal at its tip was much brighter and looked similar to that at the tip of the mature flagellum (Fig 6A, bottom panels). A circular region of interest was defined around the tip of the new and the old flagella and the total amount of fluorescence was quantified. In untreated induced *KIN2A2B<sup>RNAi</sup>* cells at an advanced step of their cell cycle, the ratio of FLAM8 signal intensities between the new and the old flagellum was close to 60% (Fig. 6B, light grey). However, for induced cells treated with teniposide (where the new flagellum reached the length of the old flagellum), the FLAM8 ratio increased to 100% (Fig. 6B, dark grey). **This difference was statistically significant.**

We conclude that maturation of the new flagellum is initiated towards the end of the cell cycle and has an impact in the daughter cell after division. When cytokinesis is inhibited, maturation is triggered but because flagellum elongation is slower in induced *KIN2A2B<sup>RNAi</sup>* cells due to the reduced IFT trafficking, the locking event took place too early, therefore preventing the new flagellum to reach the normal length of 20  $\mu\text{m}$ . **We conclude that** these results support the last point of the grow-and-lock model that implied that the mature flagellum should be different from the elongating flagellum.

## DISCUSSION

In the grow-and-lock model proposed here, the flagellum shows a linear growth rate until a signal triggers a modification that blocks further elongation or shortening (Fig. 7A). The flagellum is now ready for its final function and its length is not modified anymore. In such a model, a cell can produce a shorter flagellum either by a slower growth rate (Fig. 7A, magenta curve) or by an earlier initiation of the locking event (Fig. 7B, magenta). Conversely, a longer flagellum can be constructed using a faster growth rate (Fig. 7A, green curve) or by delaying the timing of maturation (Fig. 7B, green). One could also consider that both parameters can be shifted together to achieve a different length. **In this manuscript, we have exploited the *KIN2A2B<sup>RNAi</sup>* cells that assemble shorter flagella to provide experimental evidence for the grow-and-lock model. First, we have shown that the mature flagellum is indeed locked since it does not elongate despite an increase of 2-fold in IFT trafficking in the de-induction experiment. This result adds up to the fact that the mature flagellum does not shorten in the absence of IFT [19]. We also reveal that FLAM8 can be considered as a molecular marker of mature flagella present at the distal end of the axoneme and whose high concentration reflects the state of maturation independent of the length of the flagellum. Second, we have shown that the signal for the locking event takes place prior cell division. Indeed, blocking mitochondrial DNA segregation with teniposide and hence cell division allows the flagellum of *KIN2A2B<sup>RNAi</sup>* cells to elongate for a few microns but is followed by maturation and acquisition of a strong FLAM8 signal. Rising the incubation time in teniposide from 16 to 24 hours did not result in further increase in flagellum length, showing that it is definitely locked. Finally, a reduction of IFT frequency leads to a slower growth rate and results in the formation of a shorter flagellum, as predicted by the model (Fig. 7).**

**Importantly, the experiments reported here do not support other possible models for length control. First, the presence of a soluble pool of tubulin in control cells and in induced *KIN2A2B<sup>RNAi</sup>* cells that exhibit short flagella does not support the model based on control of flagellum length by a depletion of the pool of components [36]. Second, the fact that the short mature flagellum does not elongate despite a 2-fold augmentation of IFT trafficking in de-induced *KIN2A2B<sup>RNAi</sup>* cells contradicts the balance point-model [9]. Third, the ability of *KIN2A2B<sup>RNAi</sup>* cells to assemble fairly long new flagella that grow beyond the short cell body demonstrates that a control via the cytoskeletal attachment zone system [41] cannot explain the results either.**

**By contrast, the grow-and-lock model is so far the only one that is compatible with the experimental data. The principle is fairly simple since it relies on a linear growth rate and a locking event initiated prior cell division. There is no need to modulate the construction rate but this requires a sufficient supply of IFT proteins to ensure a regular increase of IFT trains in the flagellum and maintain a constant delivery rate of tubulin. This is in agreement with the fact that the amount of IFT proteins in the cell body largely exceeds that in the flagellum [18, 27, 51]. Moreover, the amount of *IFT* gene transcripts increases during flagellum assembly, followed closely by mRNA from genes coding for axonemal proteins [52, 53]. Examination of mouse photoreceptors during differentiation also indicates a significant amount of IFT proteins in the cell body in addition to the cilium [15, 54].**

Here, we have shown that the event leading to the maturation of the flagellum is linked to the cell cycle timing and is triggered prior trypanosome division. This could also be the case of multiple protists where flagella are assembled during nuclear mitosis whilst maintaining flagella assembled in the previous generation(s) [24, 47, 48, 55]. The signal being activated before cell division, the cell commits to flagellum maturation even if it practically takes place only in the daughter cell. However, it is not directly controlled by cell division,

since its inhibition by the teniposide treatment still allows maturation to occur, as well as elongation arrest.

This model has potential for cilia and flagella that do not disassemble their microtubules after assembly and maturation. Locking the length of the axoneme in a mature state could have significant advantages for cellular functions. Protein turnover costs energy and this would dispense the cell of a potentially costly maintenance process. A maybe more significant advantage may be found in the fact that cilia and flagella are central elements in the morphogenesis of the three cell types discussed here. In trypanosomes, the flagellum is attached along the length of the cell body from the onset of assembly. Some stages even use a flagella connector to position the new flagellum alongside the existing one [56]. The flagellum actually guides cell morphogenesis and defines the axis of cytokinesis [17, 44]. In spermatozoa, the axoneme of the flagellum is fully elongated before the cascade of morphogenetic events leading the emergence of the typical elongated shape of the cell body. These occur in a precise manner and are articulated around the flagellum [13, 57]. In photoreceptors, the large outer segment develops from the cilium [58] and is actually derived from the fusion of ectosomes that originated from it [59]. In all three situations, one could imagine the requirement of a stable axoneme both to ensure correct morphogenesis and to fulfil specific cell function after complete differentiation.

**Locking the mature flagellum could help the cell to discriminate the new flagellum (that elongates) from the mature flagellum (that does not). Recent evidence indicates that the two flagella differ not only by their length but also by their content [35, 60]. This could be particularly helpful during differentiation steps where the new flagellum could perform a different function in the daughter cell [22, 23]. The situation is very different from the green algae *Chlamydomonas* that contains two flagella of normally equivalent length. When only one of them is severed, the remaining ones**

**shortens while the severed one starts to grow again up to a point where both flagella grow at the same rate [61]. This implies an exchange of information between the two flagella, something that was not observed in *T. brucei* where the two flagella function independently.**

What could be the nature of the locking event that prevents further elongation of axoneme microtubules so stable? Several hypotheses can be put forward. First, the addition of a cap at the tip of microtubule doublets could be sufficient to prevent further assembly or disassembly. The identification of the distal tip FLAM8 protein as a marker of maturation goes along this line but it does not necessarily mean that this protein inhibits elongation. So far, a cap structure has not been detected on electron micrographs of *T. brucei* procyclic flagella [62] but the morphology of the axoneme tip looks very different between growing and mature flagella: whilst it looks disorganised in elongating flagella with some microtubule doublets very close to the central pair and others further away and in contact with the membrane, it is nicely and regularly structured in mature ones [63]. A cap at the tip could also protect against the action of the depolymerising kinesin 13 that has been connected to flagellum length control in the related protists *Leishmania major* [64] or *Giardia intestinalis* [65] but whose contribution appears minor in *T. brucei* [66]. A second possibility is the level of some post-translational modifications of tubulin that could alter the dynamics of microtubules. For example, the tip of the growing flagellum contains a large amount of tyrosinated tubulin that is not detected in the mature flagellum [67]. One could imagine that exhaustive detyrosination protects the axoneme from disassembly. By contrast, the totality of trypanosome tubulin being acetylated, a direct role of tubulin acetylation sounds unlikely [68]. **Finally, the locking event could take place at the level of the base of the flagellum, for example by preventing access of fresh tubulin to the mature organelle. However, the de-induction experiment revealed that new IFT proteins were able to enter the mature**

**flagellum, showing that access remained available, at least for this category of proteins. Yet, this was not accompanied by an increase in flagellum length. The membrane protein arginine kinase 3 also has access to the mature flagellum since RNAi experiments showed it undergoes complete turnover in four hours [35]. Nevertheless, it remains to be seen if tubulin itself can access the old flagellum. Due to the failure of tagged tubulin to incorporate trypanosome microtubules [69, 70], it is not technically feasible to address this question.**

The maturation/locking could be reversible in case the organelle needs to be modified, for example during a differentiation process [71], **as recently demonstrated in the related parasite *Trypanosoma congolense* where shortening of the flagellum takes place during the transition between a free-swimming stage to an attached stage in culture conditions [72].** One could imagine that a structural cap is removed or that some post-translational modifications of tubulin are reverted, for example via the action of specific enzymes [73]. In mammalian cells, cilia are usually assembled after mitosis (or meiosis) in the so-called G0 phase of the cell cycle. If post-translational modifications are involved, the enzyme in charge could be expressed from this time point to progressively act on microtubules and finally inhibit assembly. **Intriguingly, a “decapitation” process removes the distal end of the primary cilium in mouse embryonic fibroblasts as well as a large amount of IFT-B proteins before the organelle is resorbed [74].**

Timing information for the locking event could come from the process of cell differentiation. We note that in both spermatozoa and photoreceptors, assembly of the cilium is one of the first steps in morphological differentiation [13, 59]. Alternatively, the timing of maturation could be controlled at the level of the flagellum once it reaches a certain length, via a length sensor. **This possibility remains open via the time-of-flight model whereby a**

sensing molecule traffics in association with IFT proteins and undergoes some modification in the flagellum. As the flagellum elongates the time spent for a trip increases and the proportion of modified sensor could become high enough to trigger the locking event. This model had been tested in *Chlamydomonas* but was not supported by experimental evidence in this organism [75]. **In induced *KIN2A2B<sup>RNAi</sup>* cells, the speed of IFT is reduced by ~30%, meaning that the time spent in the flagellum increases, what could trigger a premature locking event when the flagellum reaches 70% of the theoretical length. The length of the mature flagellum in induced *KIN2A2B<sup>RNAi</sup>* cells is compatible with this result. The grow-and-lock model could therefore function with a length sensor system, as proposed in other organisms with more dynamic flagella [3, 76].** This simple model could therefore be suitable for different types of cilia and flagella with different options for the control of the growth rate and for both the mode and the timing of maturation of the organelle.

## **ACKNOWLEDGEMENTS**

We acknowledge Derrick Robinson (Bordeaux, France), Paul McKean (Lancaster, UK) and Robert Lee Douglas (Berkeley, USA) for generous gifts of antibodies and Linda Kohl (Paris, France) for critical reading of the manuscript. We thank Adeline Mallet for the mNG::IFT81 cell line. We are thankful to the Ultrastructural BioImaging Plateforme for providing access to their equipment. E.B. is supported by fellowships from French National Ministry for Research and Technology (doctoral school CDV515) and from La Fondation pour la Recherche Médicale (FRM) (FDT20170436836). B.M. was supported by a Roux post-doctoral fellowship from the Institut Pasteur. This work is funded by ANR grants (11-BSV8-016 and 14-CE35-0009-01), by a French Government Investissement d’Avenir programme, Laboratoire d’Excellence “Integrative Biology of Emerging Infectious Diseases” (ANR-10-LABX-62-IBEID) and by La Fondation pour la Recherche Médicale (Equipe FRM DEQ20150734356). The funders had no role in the study design, data collection and analysis, decision to publish or preparation of the manuscript.

## **AUTHOR CONTRIBUTIONS**

E.B., B.M., B.R. & P.B. conceived and designed the experiments; E.B., B.M. and T.B. performed the experiments; T.B. prepared the figures, E.B. and P.B. wrote the manuscript. All authors commented on the manuscript.

## **DECLARATION OF INTEREST**

The authors declare no competing financial interests.

## REFERENCES

1. Broekhuis, J.R., Leong, W.Y., and Jansen, G. (2013). Regulation of cilium length and intraflagellar transport. *International review of cell and molecular biology* 303, 101-138.
2. Kozminski, K.G., Johnson, K.A., Forscher, P., and Rosenbaum, J.L. (1993). A motility in the eukaryotic flagellum unrelated to flagellar beating. *Proc Natl Acad Sci U S A* 90, 5519-5523.
3. Wren, K.N., Craft, J.M., Tritschler, D., Schauer, A., Patel, D.K., Smith, E.F., Porter, M.E., Kner, P., and Lehtreck, K.F. (2013). A differential cargo-loading model of ciliary length regulation by IFT. *Current biology : CB* 23, 2463-2471.
4. Craft, J.M., Harris, J.A., Hyman, S., Kner, P., and Lehtreck, K.F. (2015). Tubulin transport by IFT is upregulated during ciliary growth by a cilium-autonomous mechanism. *J Cell Biol* 208, 223-237.
5. Prevo, B., Scholey, J.M., and Peterman, E.J.G. (2017). Intraflagellar transport: mechanisms of motor action, cooperation, and cargo delivery. *FEBS J* 284, 2905-2931.
6. Ludington, W.B., Ishikawa, H., Serebrenik, Y.V., Ritter, A., Hernandez-Lopez, R.A., Gunzenhauser, J., Kannegaard, E., and Marshall, W.F. (2015). A systematic comparison of mathematical models for inherent measurement of ciliary length: how a cell can measure length and volume. *Biophys J* 108, 1361-1379.
7. Adl, S.M., Simpson, A.G., Lane, C.E., Lukes, J., Bass, D., Bowser, S.S., Brown, M.W., Burki, F., Dunthorn, M., Hampl, V., et al. (2012). The revised classification of eukaryotes. *J Eukaryot Microbiol* 59, 429-493.
8. Marshall, W.F., and Rosenbaum, J.L. (2001). Intraflagellar transport balances continuous turnover of outer doublet microtubules: implications for flagellar length control. *J Cell Biol* 155, 405-414.
9. Engel, B.D., Ludington, W.B., and Marshall, W.F. (2009). Intraflagellar transport particle size scales inversely with flagellar length: revisiting the balance-point length control model. *J Cell Biol* 187, 81-89.
10. Liang, Y., Pang, Y., Wu, Q., Hu, Z., Han, X., Xu, Y., Deng, H., and Pan, J. (2014). FLA8/KIF3B phosphorylation regulates kinesin-II interaction with IFT-B to control IFT entry and turnaround. *Developmental cell* 30, 585-597.
11. Chien, A., Shih, S.M., Bower, R., Tritschler, D., Porter, M.E., and Yildiz, A. (2017). Dynamics of the IFT machinery at the ciliary tip. *eLife* 6.
12. Hao, L., Thein, M., Brust-Mascher, I., Civelekoglu-Scholey, G., Lu, Y., Acar, S., Prevo, B., Shaham, S., and Scholey, J.M. (2011). Intraflagellar transport delivers tubulin isoforms to sensory cilium middle and distal segments. *Nature cell biology* 13, 790-798.
13. San Agustin, J.T., Pazour, G.J., and Witman, G.B. (2015). Intraflagellar transport is essential for mammalian spermiogenesis but is absent in mature sperm. *Molecular biology of the cell* 26, 4358-4372.
14. Besharse, J.C., and Hollyfield, J.G. (1979). Turnover of mouse photoreceptor outer segments in constant light and darkness. *Invest Ophthalmol Vis Sci* 18, 1019-1024.
15. Jiang, L., Wei, Y., Ronquillo, C.C., Marc, R.E., Yoder, B.K., Frederick, J.M., and Baehr, W. (2015). Heterotrimeric kinesin-2 (KIF3) mediates transition zone and axoneme formation of mouse photoreceptors. *J Biol Chem* 290, 12765-12778.

16. Vincensini, L., Blisnick, T., Bertiaux, E., Hutchinson, S., Georgikou, C., Ooi, C.P., and Bastin, P. (2017). Flagellar incorporation of proteins follows at least two different routes in trypanosomes. *Biol Cell*.
17. Kohl, L., Robinson, D., and Bastin, P. (2003). Novel roles for the flagellum in cell morphogenesis and cytokinesis of trypanosomes. *Embo J* 22, 5336-5346.
18. Absalon, S., Blisnick, T., Kohl, L., Toutirais, G., Dore, G., Julkowska, D., Tavenet, A., and Bastin, P. (2008). Intraflagellar transport and functional analysis of genes required for flagellum formation in trypanosomes. *Molecular biology of the cell* 19, 929-944.
19. Fort, C., Bonnefoy, S., Kohl, L., and Bastin, P. (2016). Intraflagellar transport is required for the maintenance of the trypanosome flagellum composition but not its length. *Journal of cell science* 129, 3026-3041.
20. Rotureau, B., Subota, I., and Bastin, P. (2011). Molecular bases of cytoskeleton plasticity during the *Trypanosoma brucei* parasite cycle. *Cell Microbiol* 13, 705-716.
21. Van Den Abbeele, J., Claes, Y., van Bockstaele, D., Le Ray, D., and Coosemans, M. (1999). *Trypanosoma brucei* spp. development in the tsetse fly: characterization of the post-mesocyclic stages in the foregut and proboscis. *Parasitology* 118, 469-478.
22. Sharma, R., Peacock, L., Gluenz, E., Gull, K., Gibson, W., and Carrington, M. (2008). Asymmetric cell division as a route to reduction in cell length and change in cell morphology in trypanosomes. *Protist* 159, 137-151.
23. Rotureau, B., Subota, I., Buisson, J., and Bastin, P. (2012). A new asymmetric division contributes to the continuous production of infective trypanosomes in the tsetse fly. *Development* 139, 1842-1850.
24. Sherwin, T., and Gull, K. (1989). The cell division cycle of *Trypanosoma brucei brucei*: timing of event markers and cytoskeletal modulations. *Philos Trans R Soc Lond B Biol Sci* 323, 573-588.
25. Bastin, P., MacRae, T.H., Francis, S.B., Matthews, K.R., and Gull, K. (1999). Flagellar morphogenesis: protein targeting and assembly in the paraflagellar rod of trypanosomes. *Mol Cell Biol* 19, 8191-8200.
26. Robinson, D.R., Sherwin, T., Ploubidou, A., Byard, E.H., and Gull, K. (1995). Microtubule polarity and dynamics in the control of organelle positioning, segregation, and cytokinesis in the trypanosome cell cycle. *J Cell Biol* 128, 1163-1172.
27. Buisson, J., Chenouard, N., Lagache, T., Blisnick, T., Olivo-Marin, J.C., and Bastin, P. (2013). Intraflagellar transport proteins cycle between the flagellum and its base. *Journal of cell science* 126, 327-338.
28. Tyler, K.M., Matthews, K.R., and Gull, K. (2001). Anisomorphic cell division by African trypanosomes. *Protist* 152, 367-378.
29. Huet, D., Blisnick, T., Perrot, S., and Bastin, P. (2014). The GTPase IFT27 is involved in both anterograde and retrograde intraflagellar transport. *eLife* 3, e02419.
30. Shaner, N.C., Campbell, R.E., Steinbach, P.A., Giepmans, B.N., Palmer, A.E., and Tsien, R.Y. (2004). Improved monomeric red, orange and yellow fluorescent proteins derived from *Discosoma* sp. red fluorescent protein. *Nature biotechnology* 22, 1567-1572.
31. Bhogaraju, S., Cajanek, L., Fort, C., Blisnick, T., Weber, K., Taschner, M., Mizuno, N., Lamla, S., Bastin, P., Nigg, E.A., et al. (2013). Molecular basis of tubulin transport within the cilium by IFT74 and IFT81. *Science* 341, 1009-1012.
32. Julkowska, D., and Bastin, P. (2009). Tools for analyzing intraflagellar transport in trypanosomes. *Methods Cell Biol* 93, 59-80.

33. Douglas, R., Haltiwanger, B., Wu, H., Jeng, R., Mancuso, J., Cande, Z., and Welch, M. (2018). Trypanosomes have divergent kinesin-2 proteins that function differentially in IFT, cell division, and motility. *BioRxiv*.
34. Wang, Z., Morris, J.C., Drew, M.E., and Englund, P.T. (2000). Inhibition of trypanosoma brucei gene expression by RNA interference using an integratable vector with opposing T7 promoters. *J Biol Chem* 275, 40174-40179.
35. Subota, I., Julkowska, D., Vincensini, L., Reeg, N., Buisson, J., Blisnick, T., Huet, D., Perrot, S., Santi-Rocca, J., Duchateau, M., et al. (2014). Proteomic analysis of intact flagella of procyclic Trypanosoma brucei cells identifies novel flagellar proteins with unique sub-localization and dynamics. *Molecular & cellular proteomics : MCP* 13, 1769-1786.
36. Goehring, N.W., and Hyman, A.A. (2012). Organelle growth control through limiting pools of cytoplasmic components. *Current biology : CB* 22, R330-339.
37. Robinson, D., Beattie, P., Sherwin, T., and Gull, K. (1991). Microtubules, tubulin, and microtubule-associated proteins of trypanosomes. *Methods in enzymology* 196, 285-299.
38. Schneider, A., Sherwin, T., Sasse, R., Russell, D.G., Gull, K., and Seebeck, T. (1987). Subpellicular and flagellar microtubules of Trypanosoma brucei brucei contain the same alpha-tubulin isoforms. *J Cell Biol* 104, 431-438.
39. Shaner, N.C., Lambert, G.G., Chammas, A., Ni, Y., Cranfill, P.J., Baird, M.A., Sell, B.R., Allen, J.R., Day, R.N., Israelsson, M., et al. (2013). A bright monomeric green fluorescent protein derived from Branchiostoma lanceolatum. *Nat Methods* 10, 407-409.
40. Bertiaux, E., Mallet, A., Fort, C., Blisnick, T., Bonnefoy, S., Jung, J., Lemos, M., Vaughan, S., Marco, S., Trépout, S., et al. (2018). Bidirectional intraflagellar transport is restricted to only two microtubule doublets in the trypanosome flagellum. *BioRxiv*.
41. Sunter, J.D., and Gull, K. (2016). The Flagellum Attachment Zone: 'The Cellular Ruler' of Trypanosome Morphology. *Trends in parasitology*.
42. LaCount, D.J., Barrett, B., and Donelson, J.E. (2002). Trypanosoma brucei FLA1 is required for flagellum attachment and cytokinesis. *J Biol Chem* 277, 17580-17588.
43. Rotureau, B., Blisnick, T., Subota, I., Julkowska, D., Cayet, N., Perrot, S., and Bastin, P. (2014). Flagellar adhesion in Trypanosoma brucei relies on interactions between different skeletal structures in the flagellum and cell body. *Journal of cell science* 127, 204-215.
44. Zhou, Q., Liu, B., Sun, Y., and He, C.Y. (2011). A coiled-coil- and C2-domain-containing protein is required for FAZ assembly and cell morphology in Trypanosoma brucei. *Journal of cell science* 124, 3848-3858.
45. Sun, S.Y., Wang, C., Yuan, Y.A., and He, C.Y. (2013). An intracellular membrane junction consisting of flagellum adhesion glycoproteins links flagellum biogenesis to cell morphogenesis in Trypanosoma brucei. *Journal of cell science* 126, 520-531.
46. Sunter, J.D., Benz, C., Andre, J., Whipple, S., McKean, P.G., Gull, K., Ginger, M.L., and Lukes, J. (2015). Modulation of flagellum attachment zone protein FLAM3 and regulation of the cell shape in Trypanosoma brucei life cycle transitions. *Journal of cell science* 128, 3117-3130.
47. Dawson, S.C., and House, S.A. (2010). Life with eight flagella: flagellar assembly and division in Giardia. *Curr Opin Microbiol* 13, 480-490.
48. Noel, C., Gerbod, D., Delgado-Viscogliosi, P., Fast, N.M., Younes, A.B., Chose, O., Roseto, A., Capron, M., and Viscogliosi, E. (2003). Morphogenesis during division and griseofulvin-induced changes of the microtubular cytoskeleton in the parasitic protist, Trichomonas vaginalis. *Parasitol Res* 89, 487-494.

49. Farr, H., and Gull, K. (2009). Functional studies of an evolutionarily conserved, cytochrome b5 domain protein reveal a specific role in axonemal organisation and the general phenomenon of post-division axonemal growth in trypanosomes. *Cell motility and the cytoskeleton* *66*, 24-35.
50. Robinson, D.R., and Gull, K. (1991). Basal body movements as a mechanism for mitochondrial genome segregation in the trypanosome cell cycle. *Nature* *352*, 731-733.
51. Franklin, J.B., and Ullu, E. (2010). Biochemical analysis of PIFTC3, the *Trypanosoma brucei* orthologue of nematode DYF-13, reveals interactions with established and putative intraflagellar transport components. *Mol Microbiol* *78*, 173-186.
52. Morga, B., and Bastin, P. (2013). Getting to the heart of intraflagellar transport using *Trypanosoma* and *Chlamydomonas* models: the strength is in their differences. *Cilia* *2*, 16.
53. Archer, S.K., Inchaustegui, D., Queiroz, R., and Clayton, C. (2011). The cell cycle regulated transcriptome of *Trypanosoma brucei*. *PloS one* *6*, e18425.
54. Pazour, G.J., Baker, S.A., Deane, J.A., Cole, D.G., Dickert, B.L., Rosenbaum, J.L., Witman, G.B., and Besharse, J.C. (2002). The intraflagellar transport protein, IFT88, is essential for vertebrate photoreceptor assembly and maintenance. *J Cell Biol* *157*, 103-113.
55. Wheeler, R.J., Gluenz, E., and Gull, K. (2011). The cell cycle of *Leishmania*: morphogenetic events and their implications for parasite biology. *Mol Microbiol* *79*, 647-662.
56. Moreira-Leite, F.F., Sherwin, T., Kohl, L., and Gull, K. (2001). A trypanosome structure involved in transmitting cytoplasmic information during cell division. *Science* *294*, 610-612.
57. Leblond, C.P., and Clermont, Y. (1952). Definition of the stages of the cycle of the seminiferous epithelium in the rat. *Ann N Y Acad Sci* *55*, 548-573.
58. Molday, R.S., and Moritz, O.L. (2015). Photoreceptors at a glance. *Journal of cell science* *128*, 4039-4045.
59. Salinas, R.Y., Pearing, J.N., Ding, J.D., Spencer, W.J., Hao, Y., and Arshavsky, V.Y. (2017). Photoreceptor discs form through peripherin-dependent suppression of ciliary ectosome release. *J Cell Biol* *216*, 1489-1499.
60. Bonnefoy, S., Watson, C.M., Kernohan, K.D., Lemos, M., Hutchinson, S., Poulter, J.A., Crinnion, L.A., O'Callaghan, C., Hirst, R.A., Rutman, A., et al. (2018). Biallelic Mutations in LRRC56 encoding a protein associated with intraflagellar transport, cause mucociliary clearance and laterality defects. *BioRxiv*.
61. Rosenbaum, J.L., Moulder, J.E., and Ringo, D.L. (1969). Flagellar elongation and shortening in *Chlamydomonas*. The use of cycloheximide and colchicine to study the synthesis and assembly of flagellar proteins. *J Cell Biol* *41*, 600-619.
62. Woolley, D., Gadelha, C., and Gull, K. (2006). Evidence for a sliding-resistance at the tip of the trypanosome flagellum. *Cell motility and the cytoskeleton* *63*, 741-746.
63. Höög, J.L., Lacomble, S., O'Toole, E.T., Hoenger, A., McIntosh, J.R., and Gull, K. (2014). Modes of flagellar assembly in *Chlamydomonas reinhardtii* and *Trypanosoma brucei*. *eLife* *3*, e01479.
64. Blaineau, C., Tessier, M., Dubessay, P., Tasse, L., Crobu, L., Pages, M., and Bastien, P. (2007). A novel microtubule-depolymerizing kinesin involved in length control of a eukaryotic flagellum. *Current biology : CB* *17*, 778-782.
65. Dawson, S.C., Sagolla, M.S., Mancuso, J.J., Woessner, D.J., House, S.A., Fritz-Laylin, L., and Cande, W.Z. (2007). Kinesin-13 regulates flagellar, interphase, and mitotic microtubule dynamics in *Giardia intestinalis*. *Eukaryotic cell* *6*, 2354-2364.

66. Chan, K.Y., and Ersfeld, K. (2010). The role of the Kinesin-13 family protein TbKif13-2 in flagellar length control of *Trypanosoma brucei*. *Mol Biochem Parasitol* *174*, 137-140.
67. Sherwin, T., Schneider, A., Sasse, R., Seebeck, T., and Gull, K. (1987). Distinct localization and cell cycle dependence of COOH terminally tyrosinolated alpha-tubulin in the microtubules of *Trypanosoma brucei brucei*. *J Cell Biol* *104*, 439-446.
68. Schneider, A., Plessmann, U., and Weber, K. (1997). Subpellicular and flagellar microtubules of *Trypanosoma brucei* are extensively glutamylated. *Journal of cell science* *110 (Pt 4)*, 431-437.
69. Bastin, P., Bagherzadeh, Z., Matthews, K.R., and Gull, K. (1996). A novel epitope tag system to study protein targeting and organelle biogenesis in *Trypanosoma brucei*. *Mol Biochem Parasitol* *77*, 235-239.
70. Sheriff, O., Lim, L.F., and He, C.Y. (2014). Tracking the biogenesis and inheritance of subpellicular microtubule in *Trypanosoma brucei* with inducible YFP-alpha-tubulin. *BioMed research international* *2014*, 893272.
71. Ooi, C.P., and Bastin, P. (2013). More than meets the eye: understanding *Trypanosoma brucei* morphology in the tsetse. *Frontiers in cellular and infection microbiology* *3*, 1-12.
72. Peacock, L., Kay, C., Bailey, M., and Gibson, W. (2018). Shape-shifting trypanosomes: Flagellar shortening followed by asymmetric division in *Trypanosoma congolense* from the tsetse proventriculus. *PLoS Pathog* *14*, e1007043.
73. Gadadhar, S., Bodakuntla, S., Natarajan, K., and Janke, C. (2017). The tubulin code at a glance. *Journal of cell science* *130*, 1347-1353.
74. Phua, S.C., Chiba, S., Suzuki, M., Su, E., Roberson, E.C., Pusapati, G.V., Setou, M., Rohatgi, R., Reiter, J.F., Ikegami, K., et al. (2017). Dynamic Remodeling of Membrane Composition Drives Cell Cycle through Primary Cilia Excision. *Cell* *168*, 264-279 e215.
75. Ishikawa, H., and Marshall, W.F. (2017). Testing the time-of-flight model for flagellar length sensing. *Molecular biology of the cell* *28*, 3447-3456.
76. Cao, M., Meng, D., Wang, L., Bei, S., Snell, W.J., and Pan, J. (2013). Activation loop phosphorylation of a protein kinase is a molecular marker of organelle size that dynamically reports flagellar length. *Proc Natl Acad Sci U S A* *110*, 12337-12342.
77. Le Ray, D., Barry, J.D., Easton, C., and Vickerman, K. (1977). First tsetse fly transmission of the "AnTat" serodeme of *Trypanosoma brucei*. *Ann Soc Belg Med Trop* *57*, 369-381.
78. Brun, R., and Schonenberger (1979). Cultivation and in vitro cloning or procyclic culture forms of *Trypanosoma brucei* in a semi-defined medium. Short communication. *Acta tropica* *36*, 289-292.
79. Wirtz, E., Leal, S., Ochatt, C., and Cross, G.A. (1999). A tightly regulated inducible expression system for conditional gene knock-outs and dominant-negative genetics in *Trypanosoma brucei*. *Mol Biochem Parasitol* *99*, 89-101.
80. Redmond, S., Vadivelu, J., and Field, M.C. (2003). RNAi: an automated web-based tool for the selection of RNAi targets in *Trypanosoma brucei*. *Mol Biochem Parasitol* *128*, 115-118.
81. Kelly, S., Reed, J., Kramer, S., Ellis, L., Webb, H., Sunter, J., Salje, J., Marinsek, N., Gull, K., Wickstead, B., et al. (2007). Functional genomics in *Trypanosoma brucei*: a collection of vectors for the expression of tagged proteins from endogenous and ectopic gene loci. *Mol Biochem Parasitol* *154*, 103-109.

82. Burkard, G., Fragoso, C.M., and Roditi, I. (2007). Highly efficient stable transformation of bloodstream forms of *Trypanosoma brucei*. *Mol Biochem Parasitol* 153, 220-223.
83. Absalon, S., Kohl, L., Branche, C., Blisnick, T., Toutirais, G., Rusconi, F., Cosson, J., Bonhivers, M., Robinson, D., and Bastin, P. (2007). Basal body positioning is controlled by flagellum formation in *Trypanosoma brucei*. *PloS one* 2, e437.
84. Pradel, L.C., Bonhivers, M., Landrein, N., and Robinson, D.R. (2006). NIMA-related kinase TbNRKC is involved in basal body separation in *Trypanosoma brucei*. *Journal of cell science* 119, 1852-1863.
85. Chenouard, N., Buisson, J., Bloch, I., Bastin, P., and Olivo-Marin, J.C. (2010). Curvelet analysis of kymograph for tracking bi-directional particles in fluorescence microscopy images. *International Conference on Image Processing*, in press.
86. Subota, I., Rotureau, B., Blisnick, T., Ngwabyt, S., Durand-Dubief, M., Engstler, M., and Bastin, P. (2011). ALBA proteins are stage regulated during trypanosome development in the tsetse fly and participate in differentiation. *Molecular biology of the cell* 22, 4205-4219.
87. Woods, A., Sherwin, T., Sasse, R., MacRae, T.H., Baines, A.J., and Gull, K. (1989). Definition of individual components within the cytoskeleton of *Trypanosoma brucei* by a library of monoclonal antibodies. *Journal of cell science* 93, 491-500.
88. Adhiambo, C., Blisnick, T., Toutirais, G., Delannoy, E., and Bastin, P. (2009). A novel function for the atypical small G protein Rab-like 5 in the assembly of the trypanosome flagellum. *Journal of cell science* 122, 834-841.

## FIGURE LEGENDS

### **Figure 1. IFT trafficking during flagellum construction is compatible with a linear growth rate**

(A) Still images of AnTat1.1E cells expressing a TdTomato::IFT81 from the endogenous locus. Subpanel 1 shows a cell with a single flagellum (Video S1) and subpanels 2-4 show cells at successive stages of flagellum construction (Videos S2-S4). Orange and white arrowheads indicate the new and the old flagellum, respectively. (B) Kymographs extracted from the corresponding videos where the X axis corresponds to flagellum length (horizontal scale bar, 2  $\mu\text{m}$ ) and the Y axis represents the elapsed time (vertical bar, 1s). (C) The ratio between the total TdT::IFT81 fluorescence intensity in the new and the old flagellum was calculated and plotted according to the length of the new flagellum. A linear correlation curve is indicated together with its  $R^2$  coefficient. (D) The ratio between IFT rates (anterograde transport, magenta circles; retrograde transport, green circles) in the new flagellum and the old flagellum from the same cell was calculated and plotted according to the length of the new flagellum. Retrograde transport is more difficult to detect and data were only incorporated when the signal was sufficiently reliable. (E) Quantification of the ratio between the IFT frequency (anterograde transport, magenta circles; retrograde transport, green circles) in the new flagellum and the old flagellum in the same cell was calculated and plotted versus the length of the new flagellum. See Table 1 for total number of trains analysed.

### **Figure 2. Reduction of IFT train frequency impacts on flagellum length in *KIN2A2B<sup>RNAi</sup>* cells.**

(A) IFA of non-induced *KIN2A2B<sup>RNAi</sup>* cells, or cells induced for 3 or 6 days as indicated, fixed in methanol, and stained with the Mab25 antibody to detect the axoneme (white). The top

panels show the phase-contrast image merged with DAPI (blue) and Mab25 signal (white). Scale bar: 10 $\mu$ m. The bottom panels show Mab25 staining (white) merged with DAPI (blue). (B) Dot plot showing flagellum length during the course of RNAi induction of *KIN2A2B<sup>RNAi</sup>* cells including 100 uni-flagellated cells for each time point. The mean values are indicated with a bold segment. **Statistically significant differences are indicated with two stars (p<0.0001).** (C-D) Scanning electron microscopy analysis of a non-induced *KIN2A2B<sup>RNAi</sup>* cell showing the typical trypanosome shape and length (C) and of two induced *KIN2A2B<sup>RNAi</sup>* cells for 6 days with shorter flagella (D).

**Figure 3. The new flagellum is built shorter upon reduction of IFT train frequency in *KIN2A2B<sup>RNAi</sup>* cells.**

(A) IFA images of non-induced and 6-day induced *KIN2A2B<sup>RNAi</sup>* cells obtained after methanol fixation and staining with the Mab25 antibody labeling the axoneme (white). The top panels show the phase-contrast images merged with DAPI (cyan) and the Mab25 axonemal marker (red) and the bottom ones show the Mab25 signal (white) merged with DAPI (cyan). Scale bar: 10 $\mu$ m. (B) Dot plot showing the length of old and new flagella during the course of RNAi induction of *KIN2A2B<sup>RNAi</sup>* measured in cells possessing 2 kinetoplasts and 2 nuclei (n= 50 for each time point). The mean values are indicated with a bold segment. **Statistically significant differences are indicated with one (p<0.001) or two stars (p<0.0001).** (C) Scanning electron microscopy pictures of non-induced (C) and induced *KIN2A2B<sup>RNAi</sup>* cells after 6 days (D). The purple arrow indicates the cleavage furrow. Orange and white arrowheads show the new and the old flagellum, respectively.

**Figure 4. De-induction of RNAi leads to an increase of IFT trafficking in *KIN2A2B<sup>RNAi</sup>* cells but has no impact on the length of the mature flagellum.**

(A) Schematic representation of the de-induction experiment. *KIN2A2B<sup>RNAi</sup>* cells were grown in RNAi conditions for 6 days before extensive washings to remove tetracycline and returned to culture with (control) or without tetracycline (de-induced) for 16 hours. (B) IFA pictures of a de-induced *KIN2A2B<sup>RNAi</sup>* cell undergoing cytokinesis, stained with the anti-IFT172 antibody and with the Mab25 antibody targeting the axoneme as indicated. The first image shows phase contrast and DAPI staining (cyan). The merged panel contains DAPI (cyan), Mab25 (white) and IFT172 (magenta) signals. Scale bar: 5 $\mu$ m. (C) Dot plot showing the length of old and new flagella in *KIN2A2B<sup>RNAi</sup>* cells that were grown in RNAi conditions (left, black symbols) and in de-induced cells for 16 hours (grey symbols). This was measured in cells possessing 2 kinetoplasts and 2 nuclei (n=54 for induced cells and n=49 for de-induced cells). (D) Dot plot representing the ratio between the length of the new flagellum and that of the old flagellum. The mean values are indicated with a bold segment. Statistically significant differences are indicated with two stars (p<0.0001).

**Figure 5. Inhibition of cell division impacts flagellar length.**

(A) IFA pictures of 6-day induced *KIN2A2B<sup>RNAi</sup>* cells that were left untreated (top panels) or treated for 24 hours with teniposide (bottom panels), stained with the Mab25 antibody targeting the axoneme (white) and DAPI labeling DNA (cyan). The left panels show the phase-contrast image merged with DAPI (cyan) and Mab25 signal (white). The right panels show the Mab25 signal (white) and DAPI (cyan). Orange and white arrowheads show the new and the old flagellum, respectively. The white arrow shows the bridge linking the kinetoplasts after treatment with teniposide. Scale bar: 5 $\mu$ m. (B) Ratio between the length of the new flagellum and the old flagellum for 6-day induced *KIN2A2B<sup>RNAi</sup>* cells treated (dark bars) or not (white bars) with teniposide during **16 (left, one experiment) or 24 (right, three**

**independent experiments with standard deviation)** hours. For the 16 hour-experiment, n=40 for teniposide-treated cells and n=62 for the untreated control. For the 24 hour-experiment, n=112 for teniposide-treated cells and n=163 for the untreated control. **Statistically significant differences are indicated with two stars ( $p < 0.0001$ ).**

**Figure 6. The event leading to flagellum maturation is triggered prior cell division.**

(A) IFA pictures of 6 day-induced *KIN2A2B*<sup>RNAi</sup> cells non-treated or treated for 24 hours with teniposide, fixed in methanol and stained using the Mab25 antibody to detect the axoneme (white), the anti-FLAM8 (magenta) and DAPI (cyan). The left panels show the phase-contrast image merged with DAPI (cyan), the anti-FLAM8 (magenta) and Mab25 antibody (white). The right panels show the anti-FLAM8 signal only (white). Orange and white arrowheads show the new and the old flagellum, respectively. The white circles are centered on the FLAM8 signal. Scale bar: 5 $\mu$ m. (B) Ratios between the FLAM8 fluorescent signal intensity in the new and the old flagellum in 6 day-induced *KIN2AB*<sup>RNAi</sup> cells treated (n=109) or not (n=60) with teniposide during 24 hours. Two independent experiments are shown. **Statistically significant differences are indicated with two stars ( $p < 0.0001$ ).**

**Figure 7. The grow-and-lock model to explain the control of flagellum length in *T. brucei***

(A) A slower (magenta) or faster (green) growth rate allows the production of shorter or longer flagella without having to change the timing of the locking event. (B) The flagellum elongates with a linear growth rate until a point where it is locked (arrow) and shows neither assembly nor disassembly. Keeping the same growth rate but triggering the locking event earlier (magenta) or later (green) will result in the formation of shorter or longer flagella.

## STAR METHODS

### Plasmids, cell lines, and culture conditions

The pleomorphic strain *T. brucei* AnTat1.1E [77] was used for transformation with p2675TdTIFT81. Cells were cultured in SDM79 medium [78] supplemented with hemin, 10% fetal bovine serum and 10mM glycerol. All the other procyclic *T. brucei* cell lines were derivatives of the strain 427 and grown in SDM79 medium with hemin and 10% fetal bovine serum. All the cells were cultivated at 27°C. The 29–13 cell line expressing the T7 RNA polymerase and the tetracycline-repressor has been described previously [79]. For generation of the *KIN2A2B*<sup>RNAi</sup> cell line, a 489-nucleotide fragment of *KIN2A* (Tb927.11.13920) was amplified by PCR flanked by HindIII and XhoI sites and cloned in the compatible sites of the pZJM vector. The *KIN2B* (Tb 927.5.2090) fragment was generated by chemical synthesis by GeneCust Europe (Dudelange, Luxembourg). GeneCust cloned these fragment into the pZJM vector [34], allowing tetracycline-inducible expression of dsRNA generating RNAi upon transfection in the 29-13 recipient cell line. The dsRNA is expressed from two tetracycline-inducible T7 promoters facing each other in the pZJM vector. Primers were selected using the RNAit algorithm to ensure that the fragment lacked significant identity to other genes to avoid cross-RNAi [80]. For generation of the *KIN2A2B*<sup>RNAi</sup> expressing TdT::IFT81 cell line and AnTat1.1E expressing TdT::IFT81, the first 500 nucleotides of the *IFT81* gene (Gene DB number Tb927.10.2640) were chemically synthesised (GeneCust, Luxembourg) and cloned in frame with the TdTomato gene within the HindIII and ApaI sites of the p2675 vector [81]. The construct was linearised within the *IFT81* sequence with the enzyme XcmI and nucleofected [82] in the *KIN2A2B*<sup>RNAi</sup> or the AnTat1.1E cell line, leading to integration by homologous recombination in the *IFT81* endogenous locus and to expression of the full-length coding sequence of IFT81 fused to TdTomato. **To construct the**

**p2675mNeonGreenIFT81 plasmid, the *mNeonGreen* gene [39] was chemically synthesised (GeneCust, Luxembourg) with HindIII and ApaI site and cloned in the corresponding site of the p2675YFPIFT81 [31] to replace the *YFP* gene. The vector was linearised with XcmI and nucleofected in the *KIN2A2B<sup>RNAi</sup>* cell line as described above. Transfectants were grown in media with the appropriate antibiotic concentration and clonal populations were obtained by limited dilution.**

**For de-induction experiments, *KIN2A2B<sup>RNAi</sup>* cells were grown for 6 days in the presence of tetracycline and then washed in four times in SMD79 supplemented with serum and hemin before being returned to culture either in the presence of tetracycline (induced control) or in the absence of tetracycline (de-induced sample). For inhibition of cell division, teniposide (Sigma SML0609), a topoisomerase II inhibitor was dissolved in DMSO and added to trypanosome cultures at a final concentration of 200  $\mu$ M [50] during 24 hours (*KIN2A2B<sup>RNAi</sup>* strain) and 8 hours (wild-type strain). In the control flask, the same volume of DMSO was added (63  $\mu$ L).**

### **Scanning electron microscopy**

For scanning electron microscopy, samples were fixed overnight at 4°C with 2.5% glutaraldehyde in 0.1 M cacodylate buffer (pH 7.2) and post-fixed in 2% OsO<sub>4</sub> in the same buffer. After serial dehydration, samples were dried at the critical point and coated with platinum according to standard procedures [83]. Observations were made in a JEOL 7600F microscope.

### **Immunofluorescence and live cell imaging**

Cultured parasites were washed twice in SDM79 medium without serum or in Phosphate Buffer Saline (PBS), and spread directly onto poly-L-lysine coated slides. The slides were air-

dried for 10 min, fixed in methanol at  $-20^{\circ}\text{C}$  for 30 s and rehydrated for 10 min in PBS. For immuno-detection, slides were incubated with primary antibodies diluted in PBS with 0.1% Bovine Serum Albumin (BSA) for 1 h at  $37^{\circ}\text{C}$ . Three washes of 10 min were performed and the secondary antibody diluted in PBS with 0.1% BSA was added to the slides. After an incubation of 45 min at  $37^{\circ}\text{C}$ , slides were washed three times in PBS for 10 min and DAPI ( $2\ \mu\text{g}/\mu\text{l}$ ) was added. Slides were mounted with coverslips using ProLong antifade reagent (Invitrogen). The antibodies used were the Mab25 monoclonal antibody recognising TbSAXO1, a protein found all along the trypanosome axoneme [84], an anti-IFT172 mouse monoclonal antibody diluted at 1/200 [18], an anti-FLAM8 rabbit polyclonal 1/500 (kind gift of Paul McKean, Lancaster University, UK). Subclass-specific secondary antibodies coupled to Alexa 488 and Cy3 (1/400; Jackson ImmunoResearch Laboratories, West Grove, PA) were used for double labelling. Sample observation was performed using a DMI4000 microscope equipped with a 100X NA 1.4 lens (Leica, Wetzlar, Germany) and images captured with an ORCA-03G Hamamatsu camera. Pictures were analyzed using ImageJ 1.47g13 software (National Institutes of Health, Bethesda, MD) and images were merged and superimposed using Adobe Photoshop CC. For fluorescence quantification, we have used the Raw Integrated Density values and removed the background at all these values. For live video microscopy, cells were covered with a coverslip and observed directly with the DMI4000 microscope at room temperature. Videos were acquired using an Evolve 512 EMCCD Camera (Photometrics, Tucson, AZ), driven by the Metavue acquisition software (Molecular Probes, Sunnyvale, CA). IFT trafficking was recorded at 100 (AnTat1.1E expressing TdT::IFT81) or 250 (*KIN2A2B<sup>RNAi</sup>* expressing TdT::IFT81) milliseconds per frame during 30 seconds. Kymographs were extracted and analysed as described previously [27, 85]. **For length measurements, the Mab25 staining of the axoneme was taken as reference using ImageJ. Statistical analyses were done with Kaleidagraph v4.5.2 using ANOVA test with**

**Turkey HSD ( $\alpha=0.5$ ). Graphs were drawn using Kaleidagraph v4.5.2. All errors correspond to the standard deviation of the population.**

### **Western blot analysis**

Cells were washed in PBS and boiled in Laemmli loading buffer before SDS-PAGE separation, loading 20  $\mu\text{g}$  of total cell protein per lane. Proteins were transferred overnight at 25V at 4°C to polyvinylidene fluoride membranes (PVDF), then blocked with 5% skimmed milk in PBS-Tween 0.1% (PBST) and incubated with primary antibodies diluted in 1% milk and PBST. The anti-KIN2B (a kind gift of Robert L. Douglas, Berkeley)[33] serum was diluted 1/100. As loading controls, antibodies against ALBA proteins [86] diluted 1/500 were used. Three membrane washes were performed with PBST for 5 minutes. Species-specific secondary antibodies coupled to horseradish peroxidase (GE Healthcare) were diluted 1/20,000 in PBST containing 1% milk and incubated for 1 hour. Final detection was carried out using an enhanced chemoluminescence kit and a high performance chemoluminescence film according to manufacturer's instructions (Amersham, Piscataway, NJ).

**For fractionation in detergent, cells were washed twice in PBS by 5 minutes at 500 g and the pellet was incubated for 2 minutes in Nonidet P-40 1% in PEM buffer in the presence of protease inhibitors (Sigma P8340). After centrifugation for 2 minutes at full speed, the supernatant (soluble fraction) was separated from the pellet (cytoskeletal fraction). Cells without treatment were used as control (total extract). Samples were loaded on gel and treated as above for transfer on membranes. Tubulin was detected with the TAT-1 monoclonal antibody [87] and IFT22 that was used here as a soluble marker was detected with a mouse anti-IFT22 antiserum [88].**



## SUPPLEMENTAL INFORMATION

### Figure S1. Cartoons representing the trypanosome cell cycle in different conditions

(A) In wild-type conditions, a new flagellum elongates after duplication of the basal body. After mitosis, flagellum has grown to ~80% of its final length [24, 26]. One daughter cell inherits the old flagellum and the other one inherits the new flagellum after division. This one continues growing until it reaches the final length of 20  $\mu\text{m}$ . (B) In *KIN2A2B<sup>RNAi</sup>* cells, the new flagellum only reaches 7  $\mu\text{m}$  at the time of cell division but elongates up to 12  $\mu\text{m}$  until it matures in the next cell cycle. DNA is shown in dark blue whereas old and new flagella are shown in cyan and orange, respectively.

### Figure S2. RNAi efficiently targets KIN2B at the protein level.

Total protein samples of non-induced and induced *KIN2A2B<sup>RNAi</sup>* cells were prepared after the indicated number of days. Proteins were separated by SDS-PAGE, transferred to a PVDF membrane that was incubated with the anti-KIN2B (top picture) or the anti-ALBA that detects ALBA3 and ALBA4 as loading control (bottom picture).

### Figure S3. The frequency of IFT trains is reduced in *KIN2A2B<sup>RNAi</sup>* cells.

Live imaging of a non-induced (A) and a 6-day induced *KIN2A2B<sup>RNAi</sup>* cell (B) expressing the TdT::IFT81 from its endogenous locus. Still images from Video S5 (A) and S6 (B) at the indicated time points showing the movement of IFT trains. White arrowheads indicate the successive position of anterograde IFT trains. Kymograph analyses from non-induced (C) and induced cells (D) show clear anterograde IFT traces that are highlighted in color. Note the difference in frequency between non-induced and induced cells. Horizontal scale bar is 2 $\mu\text{m}$  and vertical scale bar is 2s.

**Figure S4. A soluble pool of tubulin is available.**

Samples from *KIN2A2B<sup>RNAi</sup>* cells grown in non-induced or induced conditions for 8 days were run on gel, transferred to membranes and incubated with the indicated antibodies. Total protein samples, detergent-soluble and cytoskeletal fractions were analysed. Tubulin was detected with the TAT-1 monoclonal antibody whereas IFT22 (soluble marker) was detected with a mouse anti-IFT22 antiserum [88]. Tubulin is detected in the soluble pool in all conditions. Since the cytoskeletal pool is comparatively more abundant [38], a higher amount of protein was loaded to analyse the soluble pool alone (right panel). This confirmed the presence of a soluble pool of tubulin in both non-induced and induced conditions.

**Figure S5. De-induction of RNAi in *KIN2A2B<sup>RNAi</sup>* cells leads to the formation of longer new flagella that extend beyond the cell body.**

IFA pictures of a de-induced *KIN2A2B<sup>RNAi</sup>* cell undergoing cytokinesis, stained with the Mab25 antibody targeting the axoneme. The first image shows phase contrast and DAPI staining (cyan) and the second one shows the axoneme staining (white). White and orange arrowheads indicate the old and the new flagellum, respectively.

**Figure S6. Teniposide blocks cell proliferation.**

Growth curve of wild-type cells untreated (grey continuous line) or treated with teniposide for 24h (grey dotted line) and 6 day-induced *KIN2A2B<sup>RNAi</sup>* cells untreated (cyan continuous line) or treated with teniposide (purple dotted line).

**Figure S7. Inhibition of cell division and flagellum growth in wild-type cells**

(A) IFA pictures of or wild-type cells that were left untreated (top panels) or treated for 24 hours with teniposide (bottom panels), stained with the Mab25 antibody targeting the axoneme (white) and DAPI labeling DNA (cyan). The left panels show the phase-contrast image merged with DAPI (cyan) and Mab25 signal (white). The right panels show the Mab25 signal (white) and DAPI (cyan). Orange and white arrowheads show the new and the old flagellum, respectively. The white arrows show the bridge linking the kinetoplasts after treatment with teniposide. Scale bar: 5µm. (B) Ratios between the length of the new flagellum and the old flagellum for wild-type cells treated (dark bars, n=150) or not (white bars, n=180) with teniposide during 8 hours. The results are shown for three independent experiments. **Statistically significant differences are indicated with two stars (p<0.0001).**

## **Supplementary Videos**

### **Video S1: Visualisation of TdT::IFT81 in AnTat1.1E cells.**

TdT::IFT81 is found inside the trypanosome flagellum where it travels by IFT. Live procyclic, wild-type *T. brucei* cell transfected with TdT::IFT81 observed by time-lapse epifluorescence microscopy using a DMI4000 microscope at room temperature. Frames were taken every 100 ms for 30 s by an Evolve 512 EMCCD Camera. Example of a cell with a single flagellum.

### **Video S2: Visualisation of TdT::IFT81 in AnTat1.1E cells.**

Same as Video S1 but example of a cell with two flagella, the new one being at early phase of assembly.

### **Video S3: Visualisation of TdT::IFT81 in 1.1E cells.**

Same as Video S1 but example of a cell with two flagella, the new one being at an intermediate phase of assembly.

**Video S4: Visualisation of TdT::IFT81 in AnTat1.1E cells.**

Same as Video S1 but example of a cell with two flagella, the new one being at a late phase of assembly.

**Video S5: Visualisation of TdT::IFT81 in *KIN2A2B<sup>RNAi</sup>* cells.**

This is an example of a non-induced cell showing robust IFT. IFT proteins are found at the base of the flagellum and as motile trains trafficking both ways in the flagellum.

**Video S6: Visualisation of TdT::IFT81 in *KIN2A2B<sup>RNAi</sup>* cells.**

This is an example of a cell induced for 6 days where the frequency of IFT is much reduced whereas the total amount of IFT protein at the base is significantly increased.

**Table 1 IFT speed and frequency in growing and mature flagella of AnTat1E cells expressing TdT::IFT81.** The number of measured trains is given in parentheses. Since retrograde trains are more difficult to detect, only non-ambiguous ones were used for analysis, hence the reduced number. **There are no statistically significant differences for all parameters between unflagellated and biflagellated cells with the exception of the speed of anterograde trains in the old flagellum of biflagellated cells compared to the new one (p=0.06).**

		Uniflagellated cells	Biflagellated cells	
			New F	Old F
Speed ( $\mu\text{m}\cdot\text{sec}^{-1}$ )	Anterograde	$1.65 \pm 0.36$ (329)	$1.63 \pm 0.40$ (396)	$1.9 \pm 0.53$ (419)
	Retrograde	$5.09 \pm 0.86$ (297)	$5.29 \pm 0.60$ (284)	$5.38 \pm 1.0$ (261)
Frequency ( $\text{trains}\cdot\text{sec}^{-1}$ )	Anterograde	$1.13 \pm 0.21$	$1.00 \pm 0.22$	$1.04 \pm 0.33$
	Retrograde	$1.59 \pm 0.28$	$1.78 \pm 0.84$	$1.7 \pm 0.63$

**Table 2. IFT anterograde speed and frequency in the *KIN2A2B<sup>RNAi</sup>* cell line in various conditions**

<b>Conditions</b>	<b>Frequency (train.sec<sup>-1</sup>)</b>	<b>Speed (µm sec<sup>-1</sup>)</b>	<b>Trains</b>
<b>No tetracycline</b>	<b>0.63 ± 0.08</b>	<b>1.78 ± 0.51</b>	<b>159</b>
<b>1-day induction</b>	<b>0.38 ± 0.06</b>	<b>1.91 ± 0.64</b>	<b>95</b>
<b>4-day induction</b>	<b>0.28 ± 0.09</b>	<b>1.32 ± 0.65</b>	<b>62</b>
<b>6-day induction</b>	<b>0.25 ± 0.07</b>	<b>1.40 ± 0.59</b>	<b>63</b>
<b>De-induced (OF)</b>	<b>0.38 ± 0.11</b>	<b>-</b>	<b>161</b>
<b>De-induced (NF)</b>	<b>0.50 ± 0.13</b>	<b>-</b>	<b>239</b>

**In the case of conventional tetracycline induction of RNAi, only cells possessing a single flagellum was used for the analysis. In the case of the de-induction experiment, only cells with two nuclei and two flagella were measured. IFT speed was not measured in these experiments. OF, old flagella; NF, new flagella.**

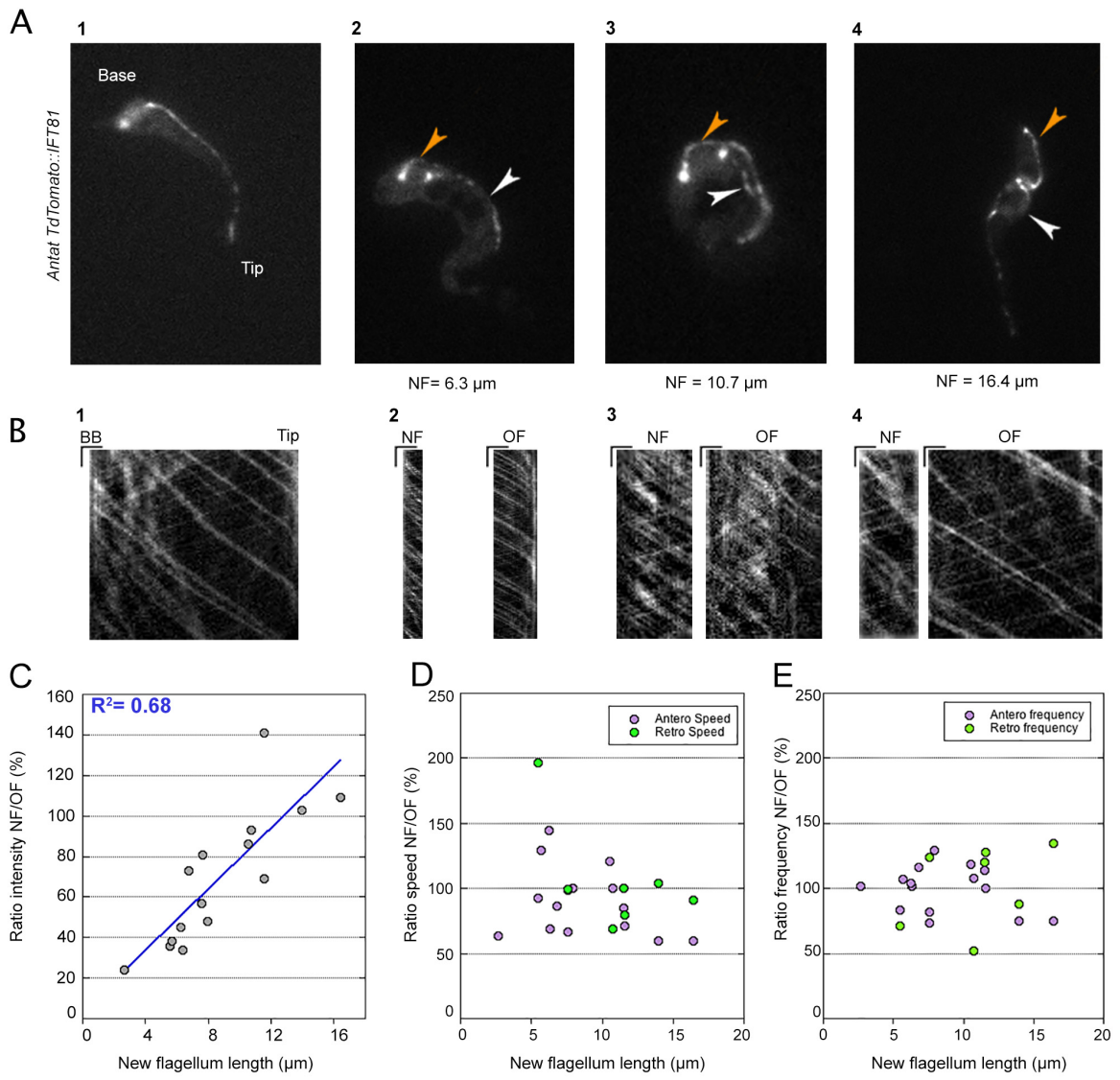


Figure 1

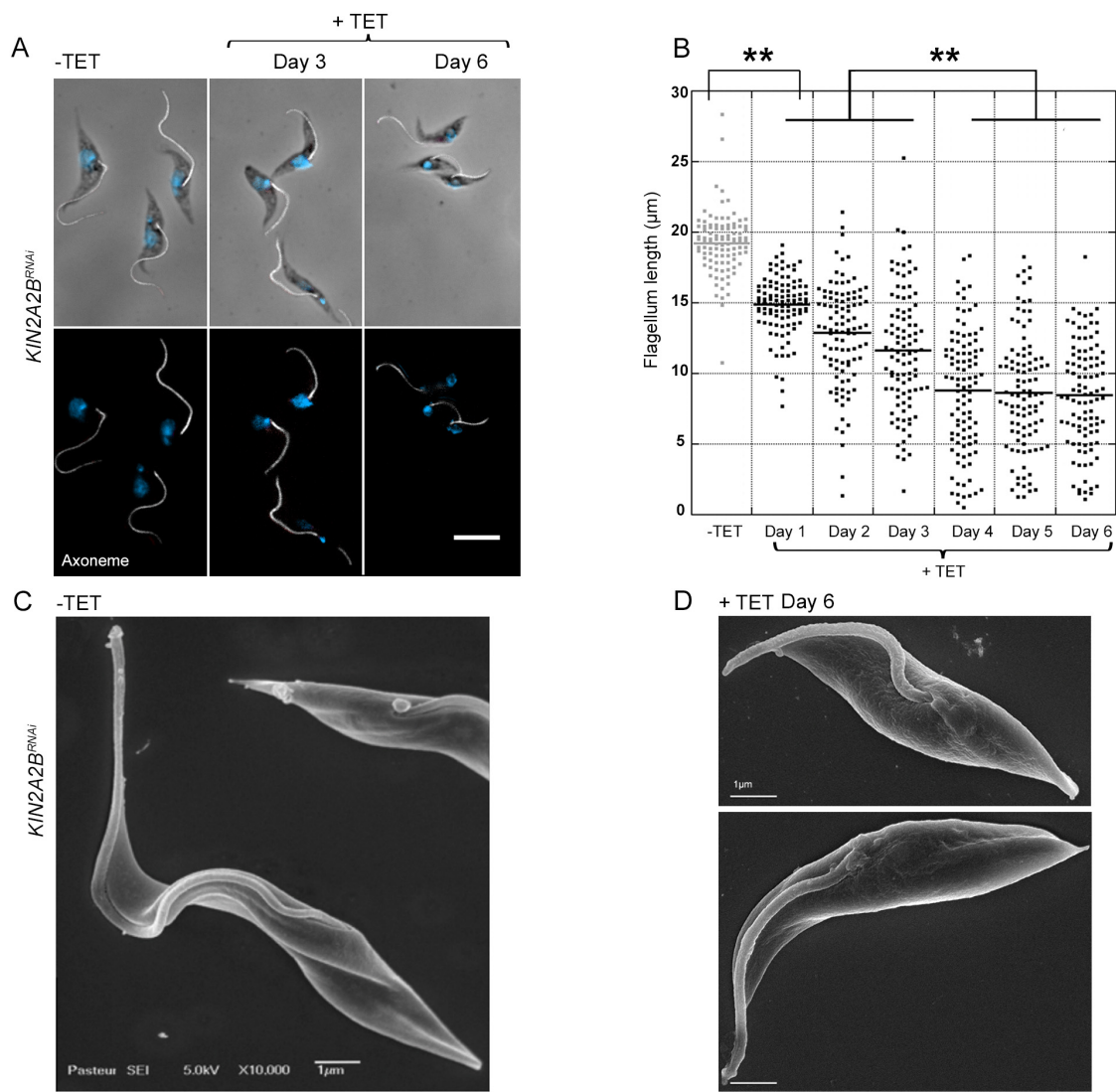


Figure 2

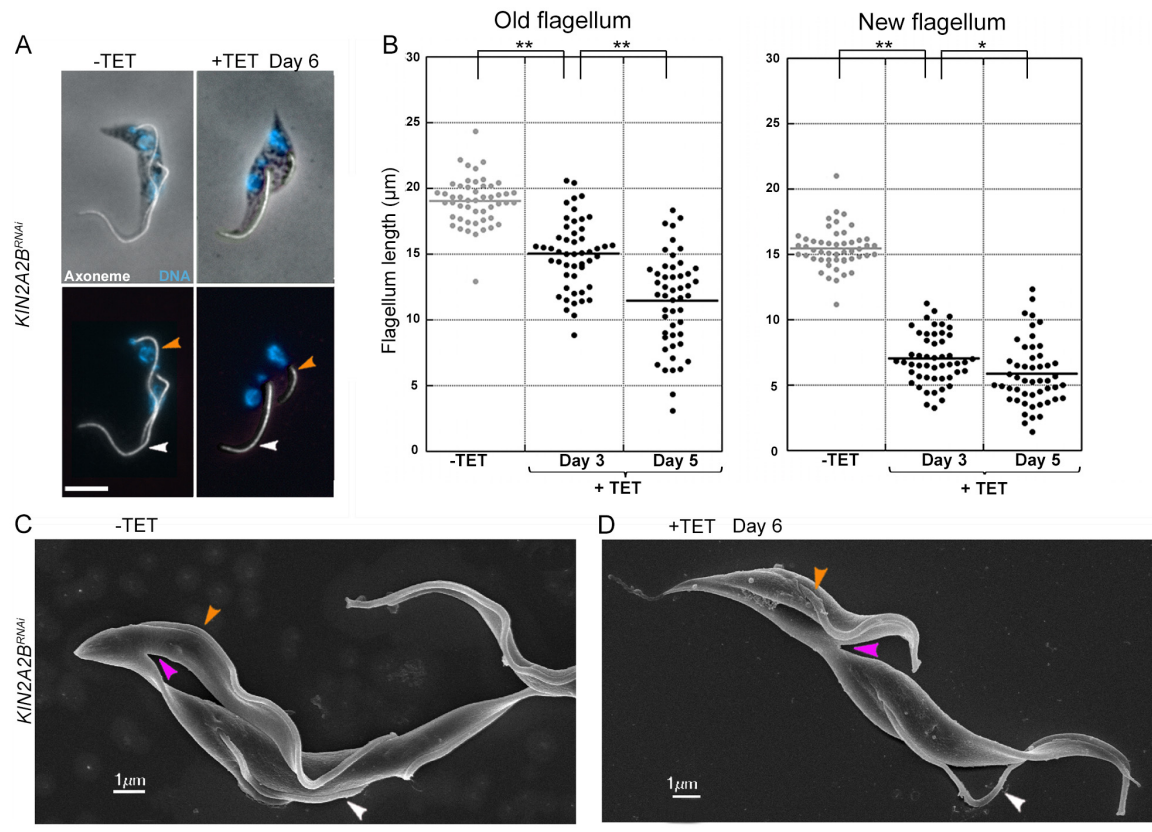


Figure 3

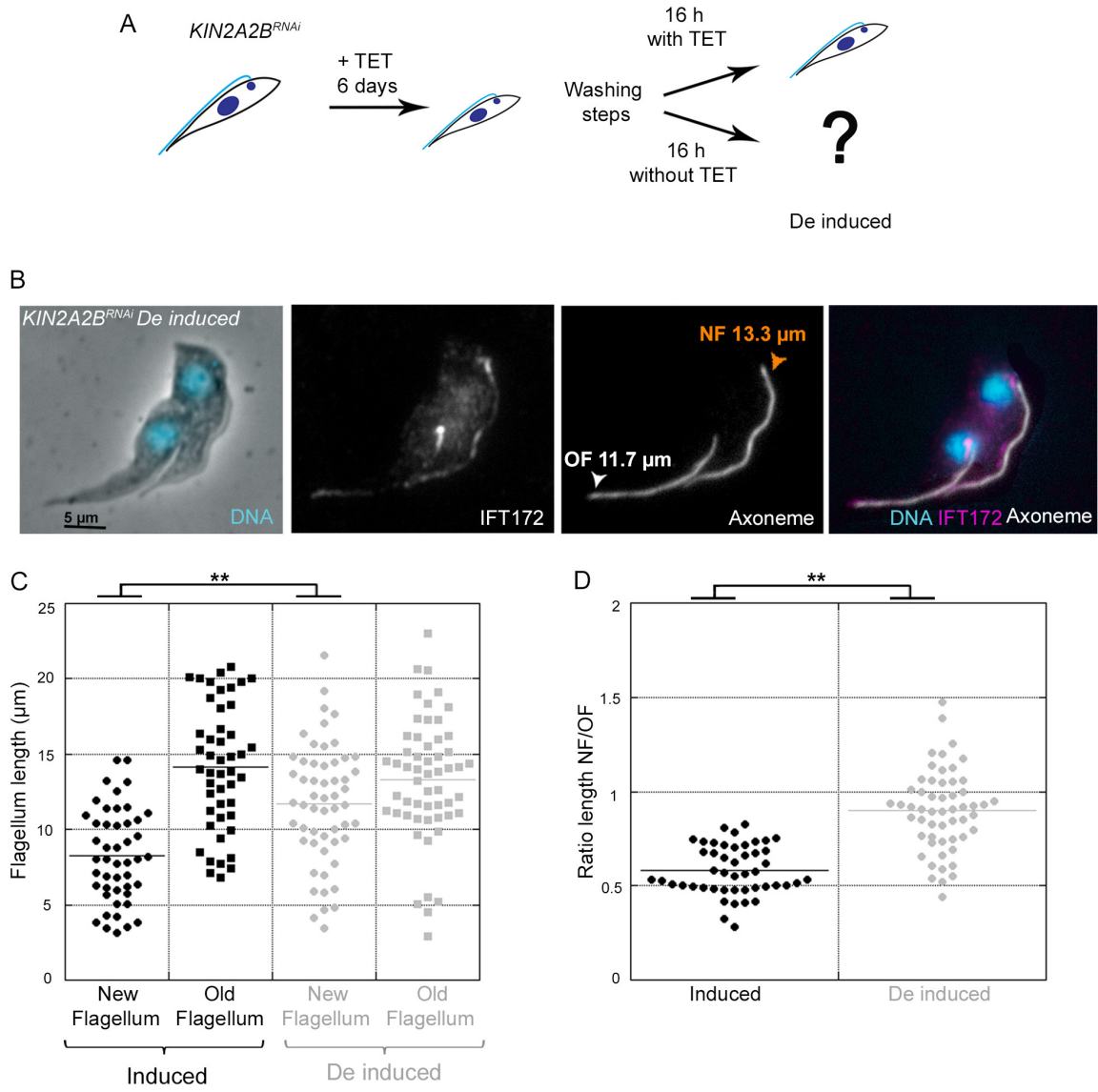


Figure 4

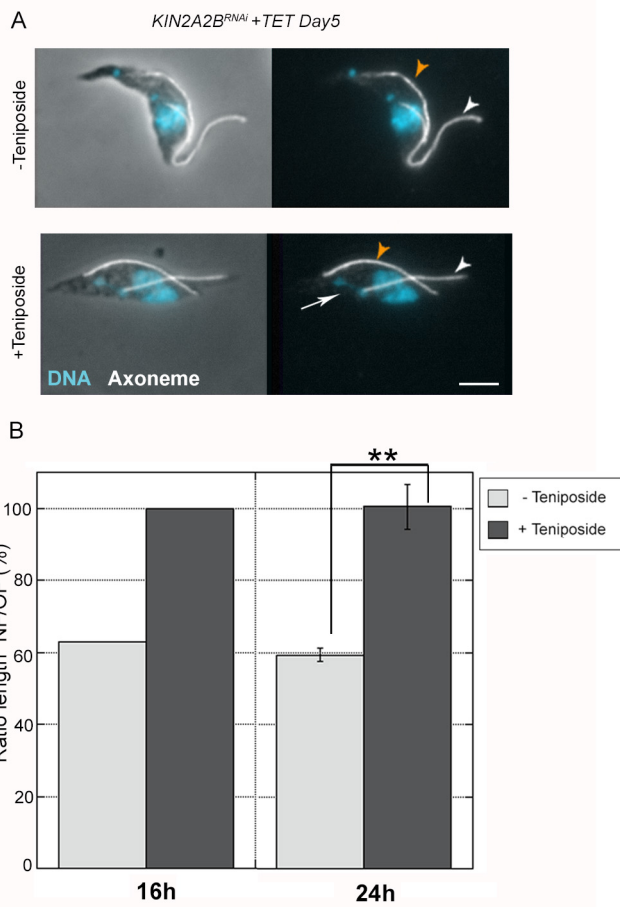


Figure 5

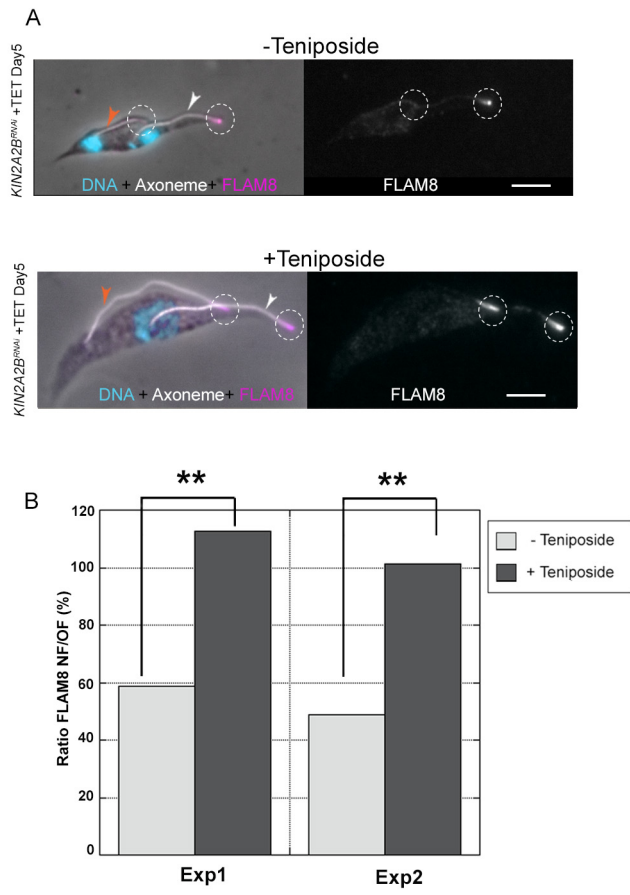


Figure 6

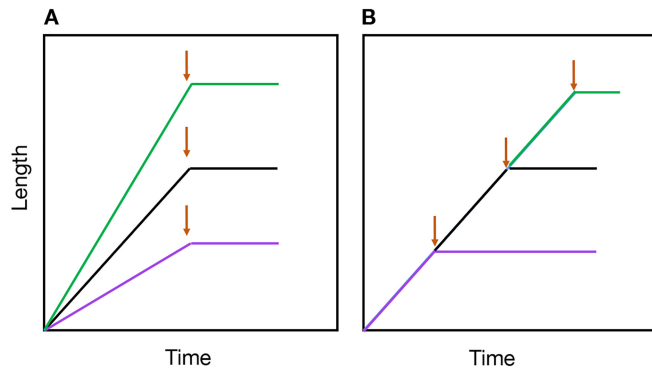


Figure 7

Figure 7

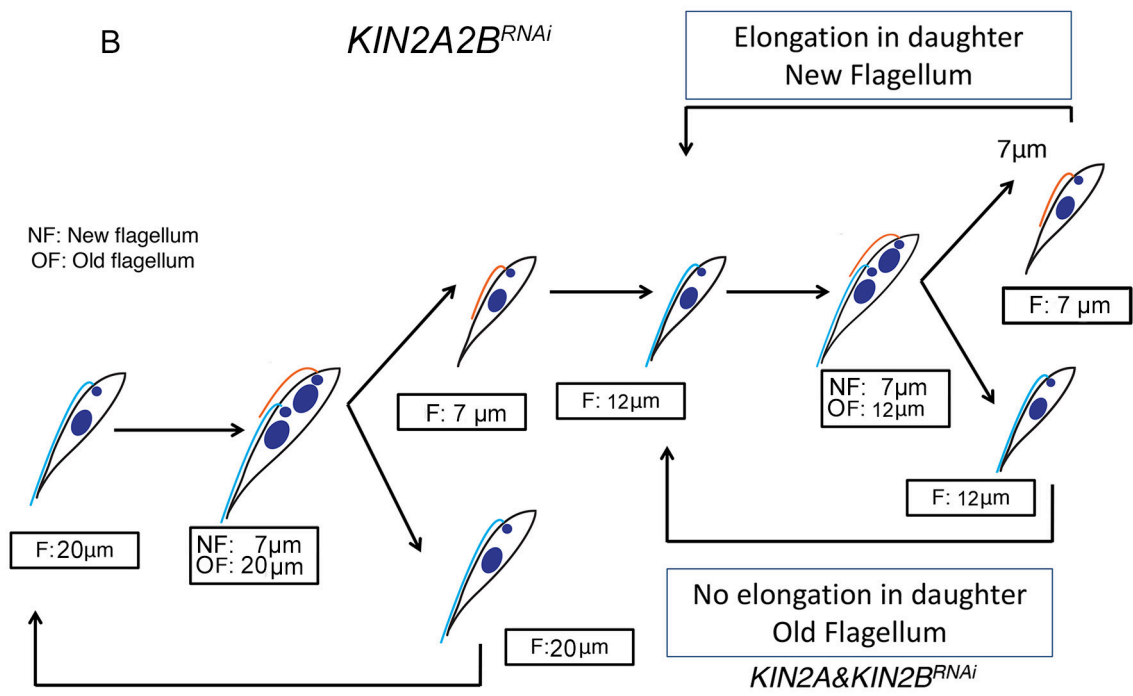
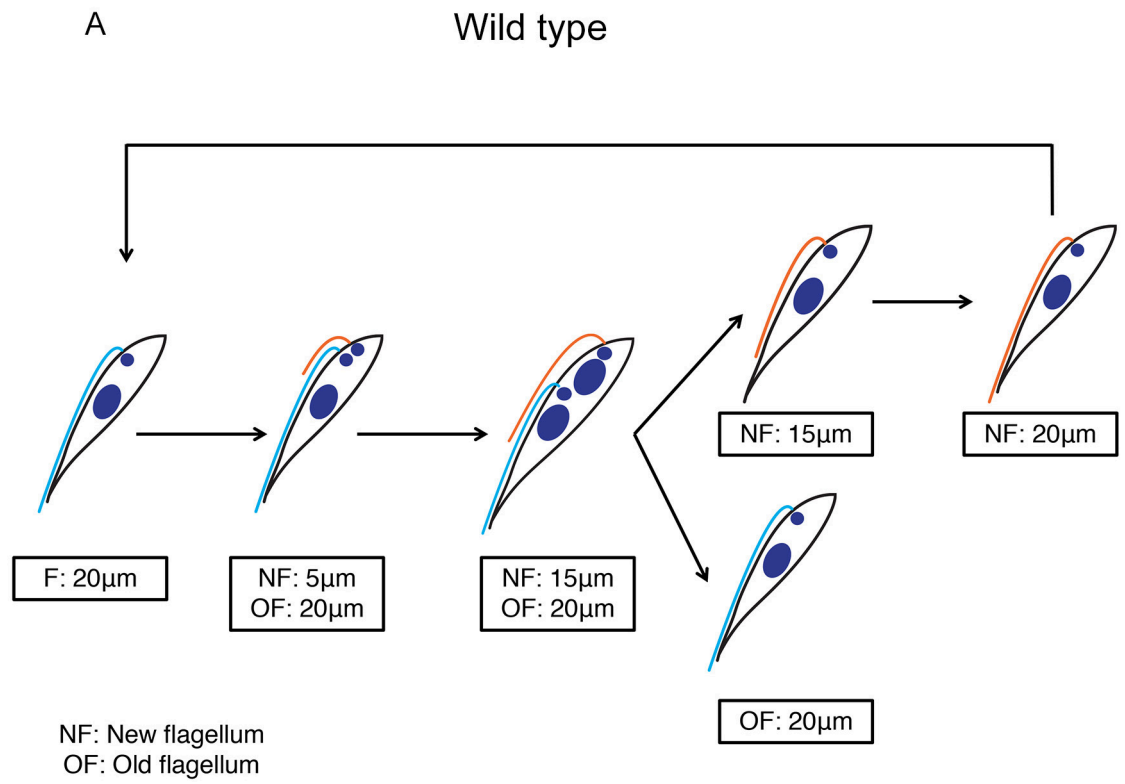


Figure S1

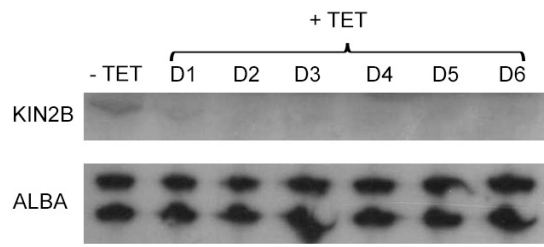


Figure S2

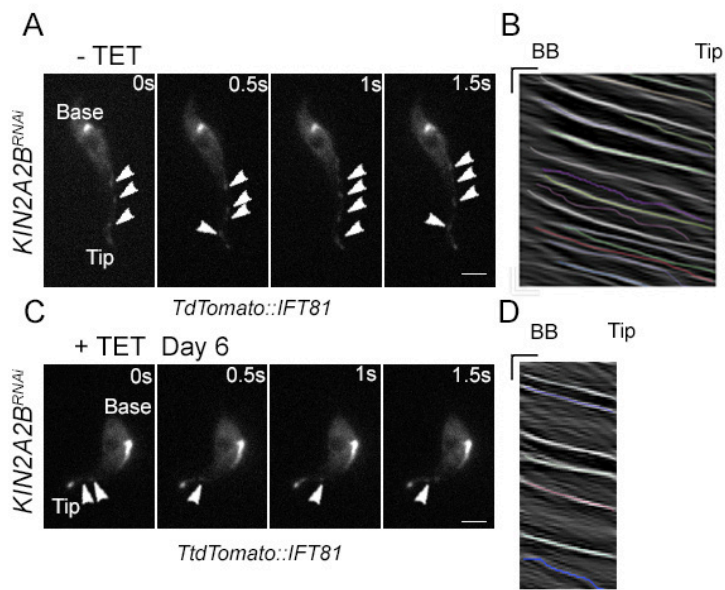


Figure S3

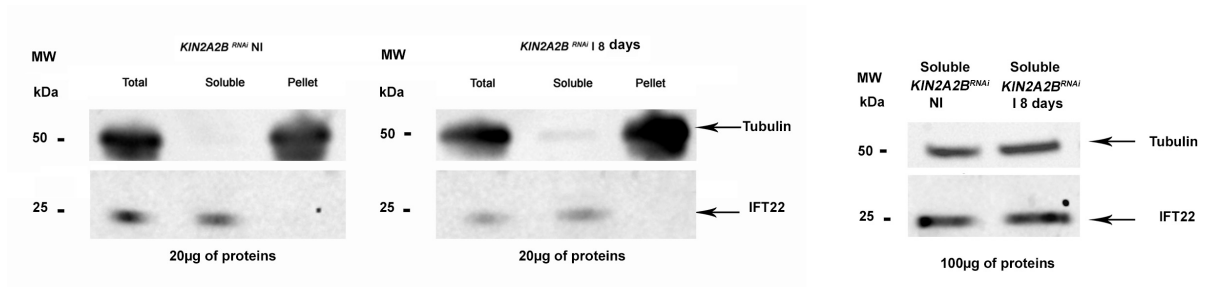


Figure S4

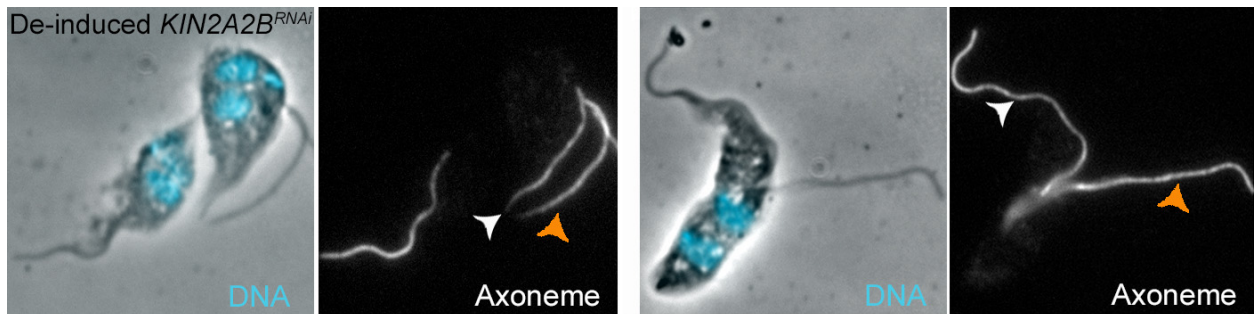


Figure S5.

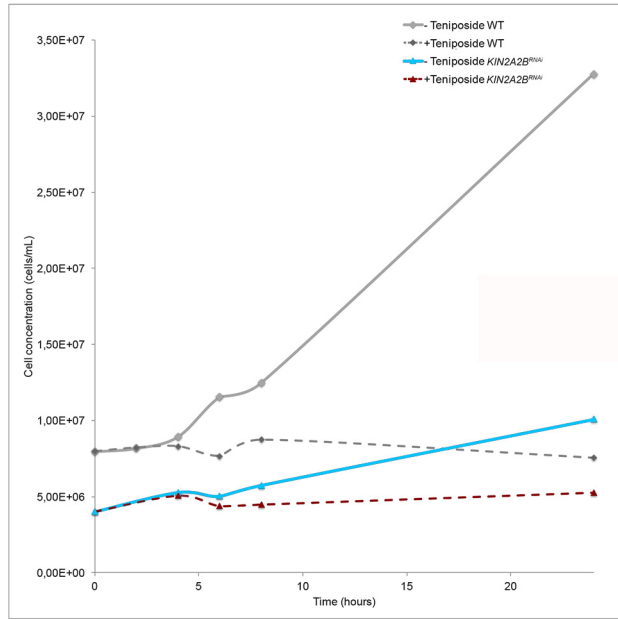


Figure S6

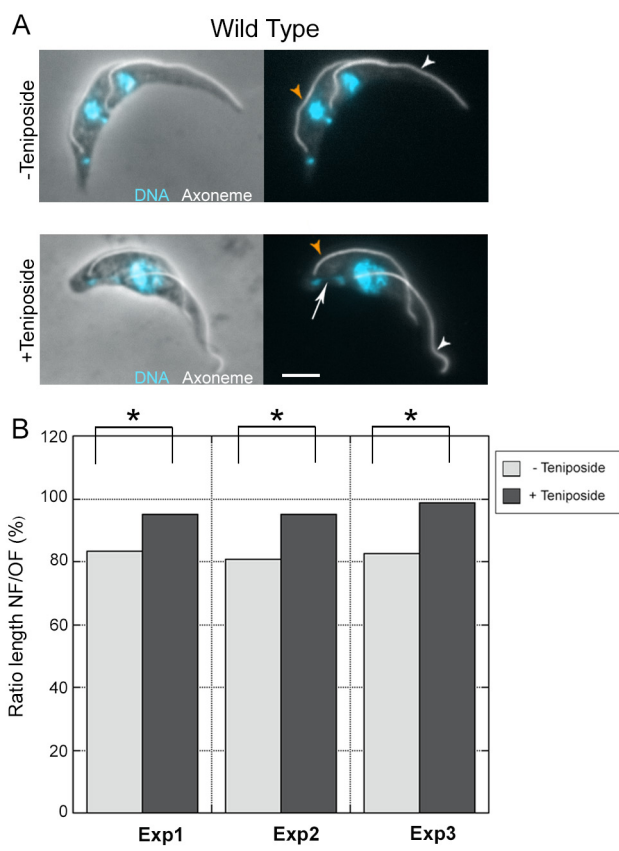


Figure S7



## ***Results***

### III. Production of flagella with different length during the trypanosome parasite cycle.

---

#### 1) Introduction

During its complex parasite cycle, *T. brucei* successively transforms into several developmental stages that exhibit flagella of different lengths and are accompanied with drastic cell morphology modifications (Rotureau, Subota et al. 2011). The morphological variations are thought to reflect specific functional requirements. Some cells with long flagella, such as the long mesocyclic trypomastigote, are known to migrate over long distances to reach the proventriculus in the tsetse. Proliferative cell division occurs in procyclic and attached epimastigote forms where the new daughter cells are morphologically similar to the parental cells. Some asymmetric divisions also occur at several phases of the parasite cycle producing very different daughter cells, such as the long proventricular dividing epimastigote that gives birth to one cell with a flagellum ten times shorter than the second one. So far, reduction of an existing flagellum to produce a shorter one has never been observed in *T. brucei*. Instead, it always constructs *de novo* a smaller organelle (Ooi and Bastin 2013). In the tsetse salivary glands, the “Epi-Trypo” asymmetric division generates two daughter cells. The cell inheriting the new flagellum adopts the trypomastigote conformation and is the precursor of the metacyclic infective form (Rotureau, Subota et al. 2012). It is the only known case where the new flagellum is longer than the old one. Despite these inter-stage variations, the flagellum length is always the same in a given stage.

We have seen that the “grow and lock” model can explain flagellum length control in cultured procyclic trypanosomes that always assemble flagella of the same length. During the asymmetric division in the tsetse proventriculus, a cell with a tiny flagellum is produced. What does control the flagellum length in this specific case? Could the “grow and lock” model apply here? Or is it an alternative system put in place? To answer these questions, we have examined the two different variables of the “grow and lock” model during the natural parasite cycle of *T. brucei*. Focusing on the production of the short flagellum of 3  $\mu\text{m}$ , we have evaluated whether a reduction of IFT train frequency could explain a slower flagellum growth rate. Second, we have searched whether flagellum maturation was taking place earlier to lock the flagellum at a shorter length.

## 2) Materials and methods

### Trypanosome cell lines and cultures

Derivatives of *T. brucei brucei* strain AnTat 1.1E PCF strain (Le Ray, Barry et al. 1977) were cultured at 27°C in SDM79 medium supplemented with hemin, 8mM of glycerol and 10% foetal calf serum (Brun and Schonemberger 1979). The 427 BSF was cultured in complete HMI-11 medium at 37°C in 5% CO<sub>2</sub> (Kooy, Hirumi et al. 1989). IFT imaging in live cells was carried out with a cell line expressing a TdTomato::IFT81 fusion produced from its endogenous locus in AnTat1.1E PCF cells. The first 500 nucleotides of the *IFT81* gene (Gene DB number Tb927.10.2640) were chemically synthesised (GeneCust, Luxembourg) and cloned in frame with the TdTomato gene within the HindIII and ApaI sites of the p2675 vector (Kelly, Reed et al. 2007). The construct was linearized within the *IFT81* sequence with the enzyme XcmI and nucleofected in the AnTat1.1E PCF cell line, leading to integration by homologous recombination in the *IFT81* endogenous locus and to the expression of the full-length coding sequence of IFT81 fused to TdTomato.

### Tsetse fly maintenance, infection and dissection

Tsetse flies (*Glossina morsitans morsitans*) were maintained, infected and dissected at the Institut Pasteur as previously described (Rotureau, Subota et al. 2011). Teneral males were collected 24 to 48 h post-eclosion and fed through a silicone membrane with  $6-9 \times 10^6$  parasites/ml in SDM-79 medium supplemented with 10% FCS, 8mM glycerol and 10mM glutathione for their first meal (MacLeod, Maudlin et al. 2007). Flies were infected with the *T. brucei brucei* AnTat 1.1E wild type (Le Ray, Barry et al. 1977) and AnTat 1.1E IFT81::TdT strains. Flies were then maintained in Roubaud cages for one month at 27°C and 50% humidity and fed three times a week with mechanically defibrinated sheep blood. Flies were starved for at least 48h before being individually dissected 28 days after ingestion of the infected meal. In our colony conditions, the average midgut infection rates usually obtained with AnTat WT strain are 50-60% in the midgut and 10-15% in the salivary glands. Salivary glands were first rapidly dissected into a drop of PBS or culture medium. The whole tsetse alimentary tract was then dissected and arranged lengthways for assessing the parasite presence. The proventriculus and anterior midgut were physically separated from the posterior midgut in a distinct PBS drop. Tissues were dilacerated to allow parasites to spread in PBS; parasites were recovered and treated for further experiments no more than 15 minutes after dissection.

### Immunofluorescence

Cultured parasites were washed twice in PBS and spread directly into poly-L-lysine coated slides. The slides with cultured parasites or parasites isolated from tsetse flies were air-dried for 10 min, fixed in methanol at -20°C for 30 s and rehydrated for 10 min in PBS. For immunodetection, slides were incubated with primary antibodies diluted in PBS with 0.1% Bovine Serum Albumin (BSA) for 1 h at 37°C in humid chamber. Three washes of 10 min were performed and the secondary antibody diluted in PBS with 0.1% BSA was added on the slides. After an incubation of 45 min, slides were washed three times in PBS for 10 min and DAPI (4',6-diamidino-2-

phenylindole) (2 µg/µl) was added to stain DNA. Slides were finally mounted with coverslips using ProLong antifade reagent (Invitrogen). The antibodies used were the Mab25 mouse monoclonal antibody recognizing TbSAXO1, a protein found all along the trypanosome axoneme (Pradel, Bonhivers et al. 2006, Dacheux, Landrein et al. 2012), an anti-IFT172 mouse monoclonal antibody diluted at 1/200 (Absalon, Blisnick et al. 2008), an anti-IFT22 mouse polyclonal antiserum diluted at 1/200 (Adhiambo, Blisnick et al. 2009), an anti-FLAM8 rabbit polyclonal antibody diluted at 1/500 (kind gift of Paul Mc Kean, Lancaster University). Subclass-specific secondary antibodies coupled to Alexa 488 and Cy3 (1/400; Jackson ImmunoResearch Laboratories, West Grove, PA) were used for double labelling. Sample observation was performed using a DMI4000 microscope equipped with a 100X NA 1.4 objective (Leica, Wetzlar, Germany) and images were captured with a ORCA-03G Hamamatsu camera. Pictures were analysed using the ImageJ 1.47g13 software (National Institutes of Health, Bethesda, MD). For presentation purposes and only after analysis, images were merged using Photoshop CS6 (Adobe).

### **Live imaging of parasites isolated from tsetse fly**

Fly dissections were performed in SDM-79 medium. The midgut, proventriculus and salivary glands were rapidly separated in different drops. After a visual inspection to confirm the presence of parasite, each organ was kept in 15µL of SDM-79 medium supplemented with serum in Eppendorf tubes. To increase parasite density 6 organs were pooled in each tube and dilacerated. A SDM-79 solution containing 4% Agar was heat-liquefied and progressively cooled for being mixed with the medium containing the freshly isolated parasites (1:1). For live video microscopy, the solution was spread on a slide, covered with a coverslip and rapidly observed at room temperature under a DMI4000 microscope. Videos were acquired using an Evolve 512 EMCCD Camera (Photometrics, Tucson, AZ) driven by the Metaview acquisition software (Molecular Probes, Sunnyvale, CA). IFT trafficking was recorded at 100 ms per frame during 30 seconds. Kymographs were extracted and analysed using Quia

software as described previously (N Chenouard 2010, Buisson, Chenouard et al. 2013).

### **FRAP analysis**

For FRAP analysis of cells expressing Tdt::IFT81, an Axiovert 200 inverted microscope (Zeiss) equipped with an oil immersion objective (magnification x100 with 1.4 numerical aperture) and a spinning disk confocal head (CSU22, Yokogawa) was used (Buisson, Chenouard et al. 2013). Movies were acquired using Volocity software with an EMCCD camera (C-9100, Hamamatsu) operating in streaming mode. The samples were kept at 27°C using a thermo-controlled chamber. Sequences of 30 s were acquired at an exposure time of 0.1 s per frame.

### **Inhibition of cell division**

Flies were dissected in SDM-79 medium and after visual inspection; three positive proventriculi were pooled and resuspended in 500 µL of SDM-79 supplemented with hemin, 10% fetal bovine serum and 10mM glycerol in 24-wells plates. For inhibiting cell division, teniposide (Sigma SML0609), a topoisomerase II inhibitor was dissolved in DMSO and added to isolated parasites from tsetse flies at a final concentration of 10 mM for 24 hours (Robinson and Gull 1991). In the control wells, the same volume of DMSO alone was added (6.3µL). Parasites were spread on poly-lysine slides and allowed to sediment for 30 minutes at 27°C before fixed and processed treated for immunofluorescence.

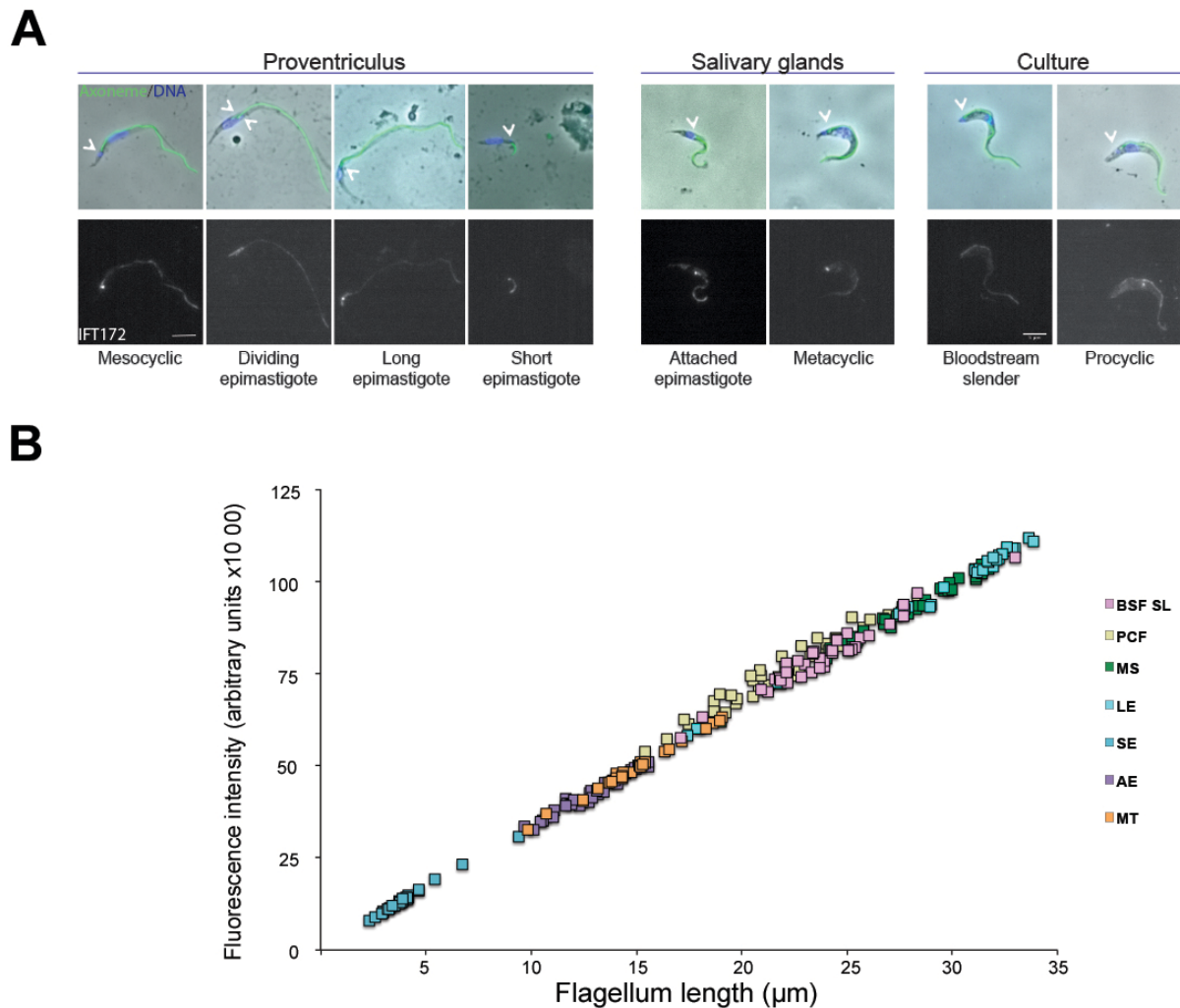


**Figure 1: Variation of IFT172 distribution during the *T. brucei* parasite cycle.**

**(A)** Parasites isolated from tsetse flies or grown in culture were fixed in methanol and stained with the Mab25 antibody to detect the axoneme (green) and the anti-IFT172 antibody (white). The top panels show the phase-contrast images merged with DAPI (blue) and Mab25 signals (green). The bottom ones show the IFT172 fluorescent signal (white). Scale bar: 5µm. Arrowheads indicate kinetoplast positions **(B)** Quantification of the total amount of IFT172 fluorescent signal normalized to the flagellum length in the flagellum of each stage of the parasite cycle. The ROI was defined by the axonemal marker and used to measure the flagellum length. The fluorescence intensity directly reflects the total amount of IFT172 proteins present in the flagellum compartment per flagellum length unit. n=35 cells per stage. BSF SL: Slender bloodstream from slender, PCF: Procyclic form, MS: mesocyclic, LE: Long epimastigote, SE: Short epimastigote, AE: Attached epimastigote, MT: Metacyclic.

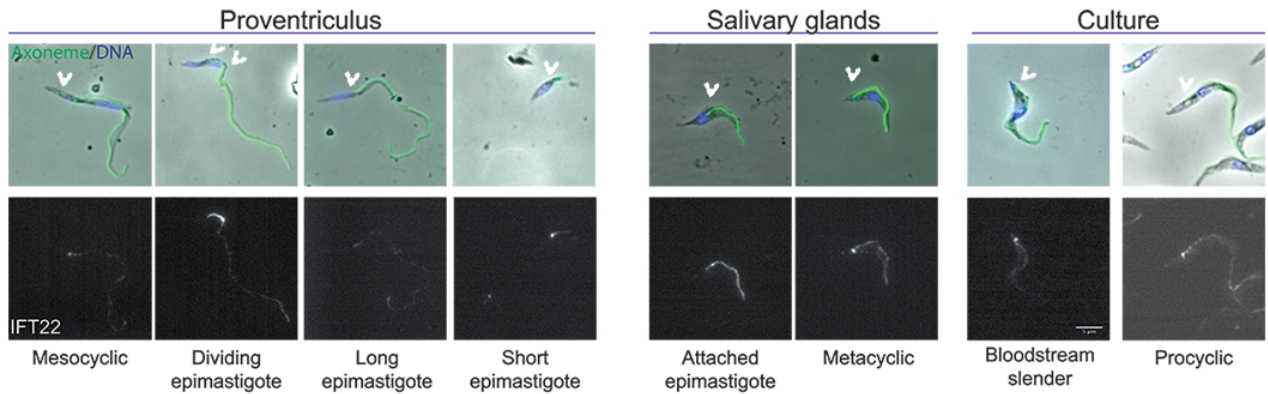
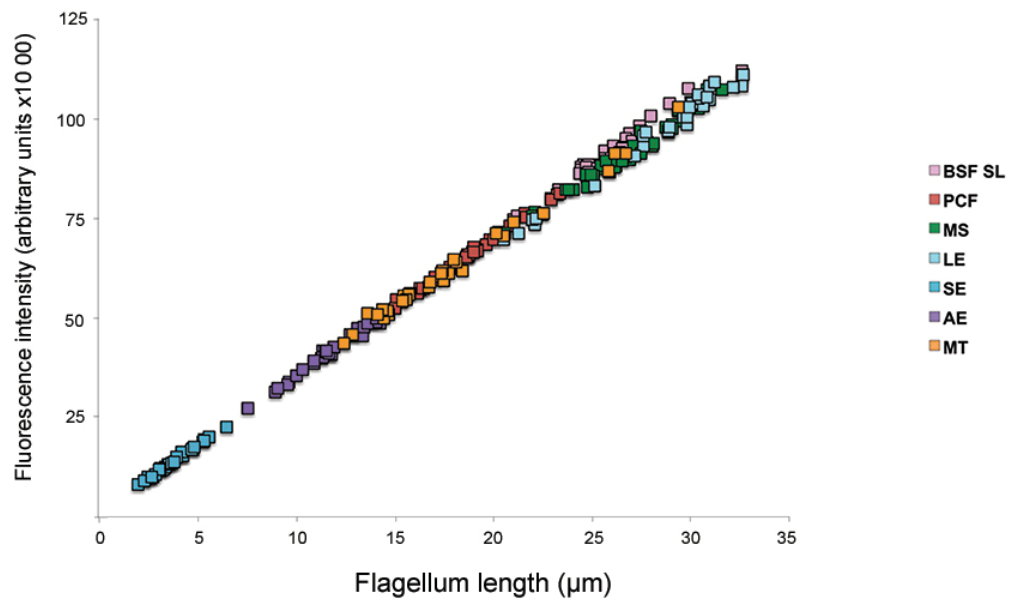
### **3) Results**

#### **The IFT concentration remains constant in the flagellum during the entire parasite cycle**

In procyclic trypanosomes in culture, we have demonstrated that IFT proteins are progressively recruited during the flagellum growth, in such a way that the concentration of IFT proteins per unit length remains constant. To evaluate whether the IFT amount in a given flagellum correlates with its length in other parasite cycle stages, we have first studied the distribution of IFT proteins in fixed cells. IFAs with antibodies raised against IFT172 (Figure 1A) (Absalon, Blisnick et al. 2008) or IFT22/RABL5 (Figure 2A) (Adhiambo, Blisnick et al. 2009) were performed on both cultured parasites and parasites isolated from tsetse flies, in combination with the axonemal marker Mab25 (Pradel, Bonhivers et al. 2006). For all parasite stages, IFT proteins were present as a succession of spots all along the length of the flagellum, with a brighter signal at the base present in almost all stages except in short epimastigotes. To quantify the total amount of IFT22 and IFT172 proteins per flagellum, a region of interest (ROI) was defined using the Mab25 axonemal marker. The total amount of fluorescence, corresponding to the total amount of IFT proteins present in the flagellum, was plotted against flagellum length. For both IFT proteins, a direct correlation between the total amount of IFT proteins and the length of the corresponding flagellum was found (Figure 1B and 2B). These data demonstrate that the IFT protein concentration is constant in the flagella of all stages of the parasite cycle, in agreement with our previous data obtained in procyclic parasites in culture.

#### **IFT trafficking remains constant during all the parasite cycle**

The methanol fixation classically used for IFA could have led to a loss of material and therefore biased the results (Absalon, Blisnick et al. 2008). Moreover, IFA only provides “static” information whereas IFT is a dynamic process. To circumvent these

**A****B**

## Figure 2: Variation of IFT22 distribution during the *T. brucei* parasite cycle

**(A)** Parasites isolated from tsetse flies or grown in culture were fixed in methanol and stained with the Mab25 antibody to detect the axoneme (green) and the anti-IFT22 antibody (white). The top panels show the phase-contrast images merged with DAPI (blue) and Mab25 signal (green). The bottom panels show the IFT22 fluorescent signal (white). Scale bar: 5 μm. Arrowheads indicate kinetoplast positions

**(B)** Quantification of the total amount of IFT22 fluorescent signal normalized to the flagellum length in the flagellum of each stage of the parasite cycle. The ROI was defined by the axonemal marker and used to measure the flagellum length. The fluorescence intensity directly reflects the total amount of IFT22 proteins present in the flagellum compartment per flagellum. n=35 cells per stage. BSF SL: Slender bloodstream from slender, PCF: Procyclic form, MS: mesocyclic, LE: Long epimastigote, SE: Short epimastigote, AE: Attached epimastigote, MT: Metacyclic.

## Results

potential issues, the distribution of IFT proteins was examined in live trypanosomes expressing a fusion protein composed of the IFT-B protein IFT81 coupled to the red fluorescent Tandem Tomato protein (TdT). This fusion protein was expressed upon endogenous tagging under the control of the 3' untranslated region (UTR) of the *IFT81* gene (Bhogaraju, Cajanek et al. 2013). IFT was recorded in live trypanosomes at different stages of the parasite cycle. IFT trafficking was detected in all of them (Figure 3A). Unfortunately and despite numerous attempts, the difficulty to immobilise parasites prevented us from recording exploitable movies for kymograph analysis in most stages. This was especially true for the highly motile long epimastigote cells that were still able to move through the agar network. For this reason, we first focused our study on the procyclic and mesocyclic trypomastigote stages found in the tsetse midgut that bear a long flagellum of 20-30 $\mu\text{m}$ . Next, we have recorded IFT in the short and barely mobile epimastigote cells from the tsetse proventriculus that possess a flagellum of about 3  $\mu\text{m}$ . This allowed us to compare IFT trafficking in flagella with naturally very different lengths.

In fixed samples, IFT proteins were present as a succession of spots all along the length of the flagellum. Because fixation may have altered IFT distribution, the total amounts of TdT::IFT81 in short epimastigote and mesocyclic / procyclic flagella were quantified in living cells by using the first image of each movie, and plotted according to flagellum length. This confirmed the direct correlation between these two parameters (Figure 3B), in agreement with the IFA data showing that IFT protein concentration increases in parallel to flagellum length.

Although the total amount of IFT proteins appeared proportional to the length of the flagellum, a reduction of IFT speed and frequency could still have an impact on the flagellum growth rate and could not be excluded. Therefore, this was investigated in details and TdT::IFT trafficking was detected between the base and the tip of the flagellum in both directions in all cell types examined. Kymograph analyses were carried out to quantify IFT rates and frequencies in cells with a long (procyclic and mesocyclic forms) or a short flagellum (short epimastigote). In the flagellum of short epimastigote cells, the anterograde trains travelled at 2.4  $\pm$  1.3  $\mu\text{m}\cdot\text{sec}^{-1}$  and

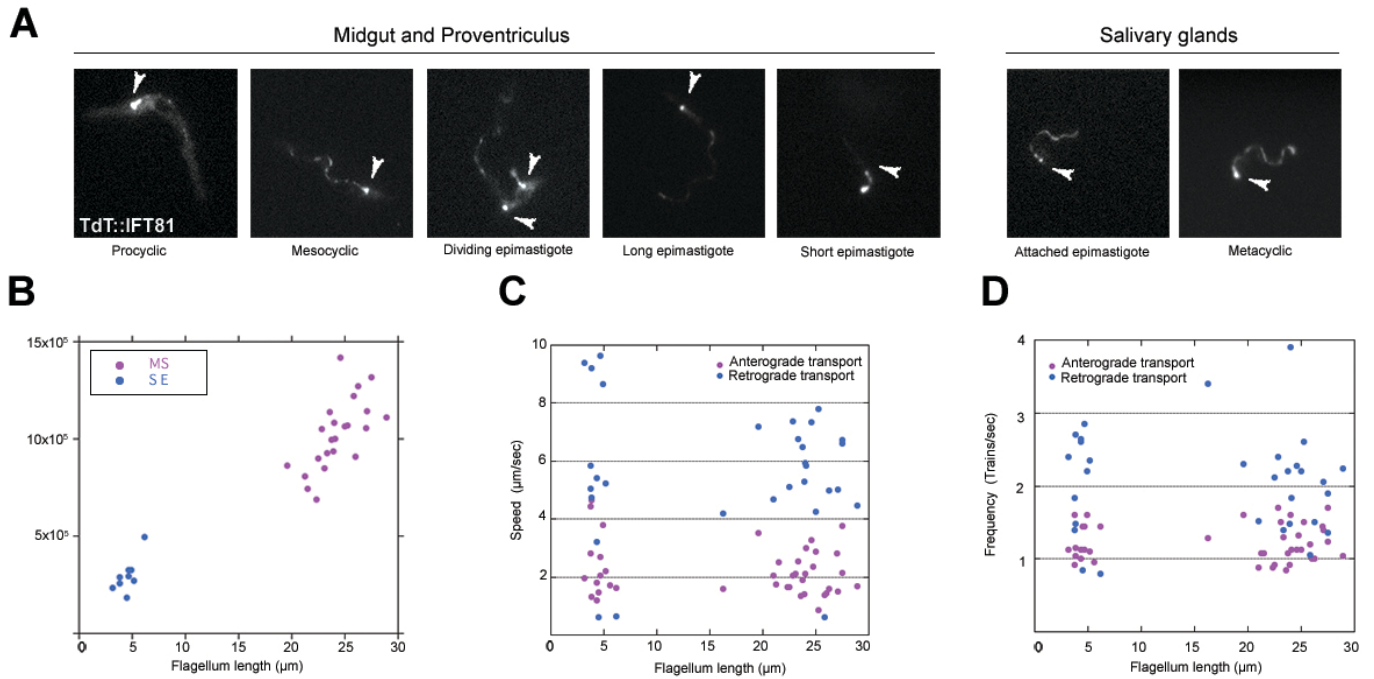


**Figure 3: Variation of the IFT81 trafficking during the *T. brucei* parasite cycle.**

(A) Still images extracted from movies of AnTat1.1E cells expressing a TdTomato::IFT81 from the endogenous locus at the indicated stages of the parasite cycle in the tsetse fly. Arrowheads indicate the base of the flagellum. (B) The total TdTomato::IFT81 fluorescence intensity in flagella of short epimastigote and long trypomastigote mesocyclic cells was calculated and plotted according to the length of the corresponding flagella. MS: Mesocyclic; SE: Short epimastigote. (C) The IFT particle speeds (anterograde transport, magenta circles; retrograde transport, blue circles) in the flagella of short epimastigote and long trypomastigote mesocyclic cells were calculated and plotted according to the respective length of the flagella. Retrograde transport is more difficult to detect and data were therefore only incorporated when the signal was sufficiently intense and reliable. (D) The IFT particle frequencies (anterograde transport, magenta circles; retrograde transport, blue circles) in the flagellum of short epimastigotes and long trypomastigote mesocyclic cells were calculated and plotted according to the respective length of the flagella.

retrograde trains at  $5.6 \pm 3.1 \mu\text{m}\cdot\text{sec}^{-1}$  (Figure 3C). In the flagellum of mesocyclic / procyclic trypomastigote cells, the anterograde trains travelled at  $2.1 \pm 0.7 \mu\text{m}\cdot\text{sec}^{-1}$  and retrograde trains at  $5.6 \pm 1.7 \mu\text{m}\cdot\text{sec}^{-1}$ . Next the IFT frequency was evaluated: in the short epimastigote flagellum, the frequency of anterograde trains was  $1.2 \pm 0.4$  trains/sec and  $2.0 \pm 0.7$  trains/sec for retrograde trains (Figure 3D). In the mesocyclic / procyclic trypomastigote flagellum the anterograde frequency was  $1.22 \pm 0.3$  trains/sec and the retrograde frequency was  $2.1 \pm 0.1$  trains/sec. Therefore, the anterograde and retrograde IFT speeds appeared equivalent in long (mesocyclic / procyclic) and short (short epimastigote) flagella, meaning that there is no modification of the IFT speed and frequency that could explain the difference between these two stages. These values were slightly higher to the TdT::IFT81 speeds measured in cultured procyclic parasites and to GFP::IFT52 speeds obtained in previous studies (Buisson, Chenouard et al. 2013) possibly because of the temperature increase after mixing the cell medium with hot liquid agar. However, the retrograde frequency was lower compared to that obtained for GFP::IFT52 (3.31 train/sec) (Buisson, Chenouard et al. 2013), but the latter quantifications were performed by overexpressing a different IFT protein (IFT52) with a different fluorophore (GFP) and in a different strain (427).

In conclusion, these results show that IFT speeds and frequencies are equivalent in cells with long and short flagella, no matter their length. In total, the IFT delivery appears to be constant and its modulation cannot explain how *T. brucei* changes its flagellum length.

### **IFT protein repartition is different in short epimastigote flagella**

By immunofluorescence as well as in live cells, IFT proteins were found as a discreet spots along the flagellum and concentrated at the base of the flagellum in procyclic and bloodstream forms in culture (Figure 4A). Using methanol fixation to study the IFT profile in parasite isolated from tsetse flies, we have noticed a lower abundance

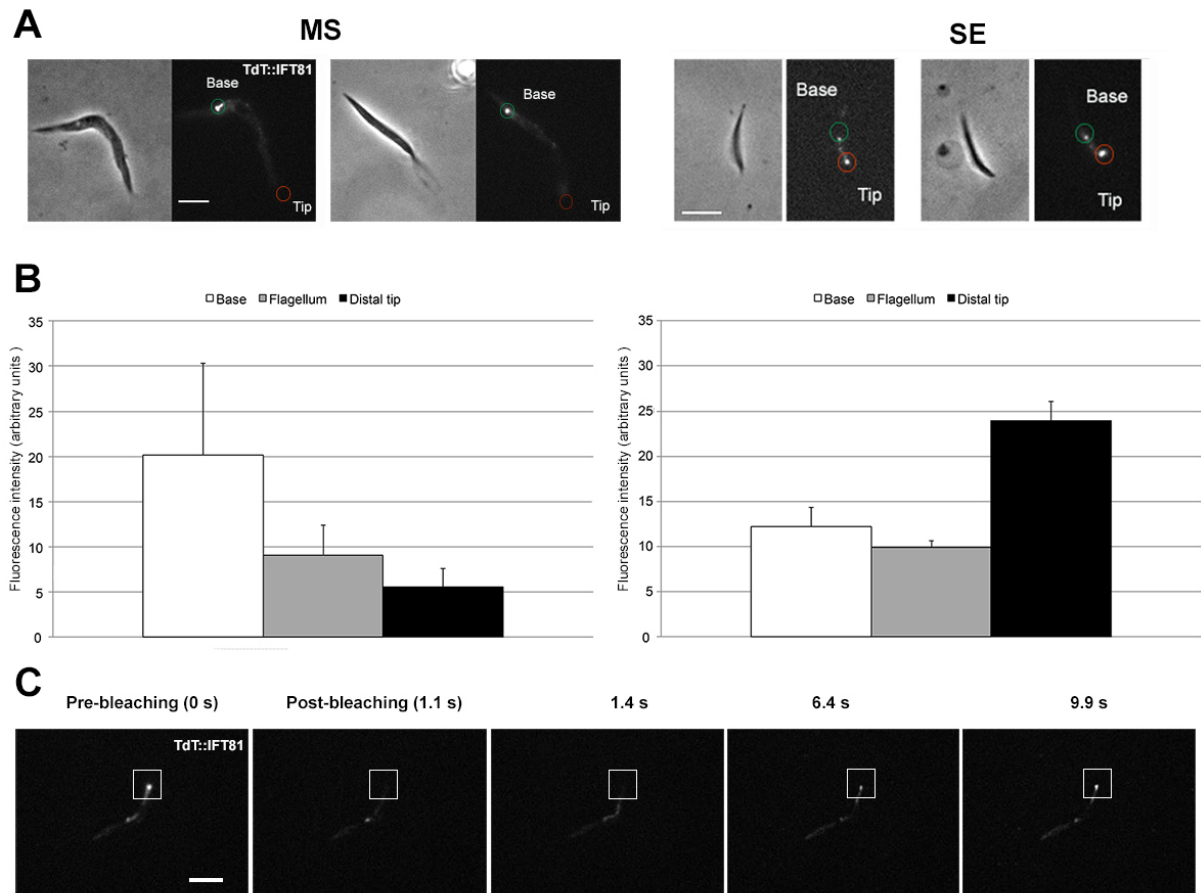


**Figure 4: Focus on the IFT81 pool at the distal tip of short epimastigote flagella.**

**(A)** Still images of AnTat1.1E cells expressing a TdTomato-tagged version of IFT81 and isolated from a tsetse fly and showing the existence of an IFT pool at the flagellum base in the mesocyclic stage (Green circle) and at the flagellum tip in the short epimastigote (Red circle). MS: Mesocyclic, SE: Short epimastigote Scale bar: 5  $\mu\text{m}$  **(B)** Quantifications of the TdT::IFT81 mean fluorescence intensities at the base, in the middle region, and the tip of flagella in procyclic cells (n=22 left plot) and in short epimastigote cells (n=17 right plot). **(C)** FRAP analysis in a SE of trypanosomes expressing the TdT::IFT81 fusion protein. The distal end of the flagellum was bleached with a brief laser pulse and the fluorescence recovery was monitored during 20 sec. Pre-bleach situation: the IFT pool is present at the distal tip. Post-bleach situation: the IFT pool is black. The fluorescent signal is shown at the indicated times. Rapid recovery could be detected at the distal tip. Scale bar: 3 $\mu\text{m}$ .

of the IFT pool at the flagellum base of short epimastigotes compared to the other stages. Intriguingly, we have also noticed the existence of an IFT pool at the distal end of these short flagella in live cells (Figure 4A). To validate these observations, we have quantified the TdT::IFT81 fluorescent signal at the base, along the flagellum and at the distal tip in procyclic cells (n= 22) and in short epimastigote cells (n=17). This result confirms the presence of an IFT pool at the distal tip of the short epimastigote flagellum (Figure 4B). This material could actively participate to the IFT process or simply be inactive, for example being there to facilitate the future flagellum elongation in the salivary glands to produce the attached epimastigotes with a longer flagellum. However, using FRAP analysis, we have observed a rapid fluorescence recovery at the distal tip of these short flagella (n=7) demonstrating that the IFT pool was actively participating to the IFT process (Figure 4C).

### **Modulation of FLAM8 concentration is not responsible for flagellum length control in short epimastigote.**

In the “grow and lock” model, we have proposed that a modification of the flagellum could take place to prevent further elongation once it has reached its expected length. We reasoned that the timing of this locking event could be different for each stage of the parasite cycle in order to produce a shorter or a longer flagellum by blocking its elongation earlier or later. Using FLAM8 as a marker of flagellum maturation, we have evaluated whether a faster maturation of the flagellum in the short epimastigote could explain why this flagellum does not reach the same length as the one in the long epimastigote sibling. To do so, cells isolated from tsetse flies were fixed and stained by IFA with an anti-FLAM8 antibody, the Mab25 antibody as axonemal marker and DAPI to label DNA. In all stages of the parasite cycle in the tsetse fly, it was present at the distal tip of the flagellum except in metacyclic stages where FLAM8 was sparsely distributed all along the flagellum (Figure 5A). We used an axonemal marker to define a region of interest along the flagellum in all stages for quantifying all the fluorescence associated to the anti-FLAM8 staining. The total amount of fluorescence was quantified and a direct correlation with flagellum length

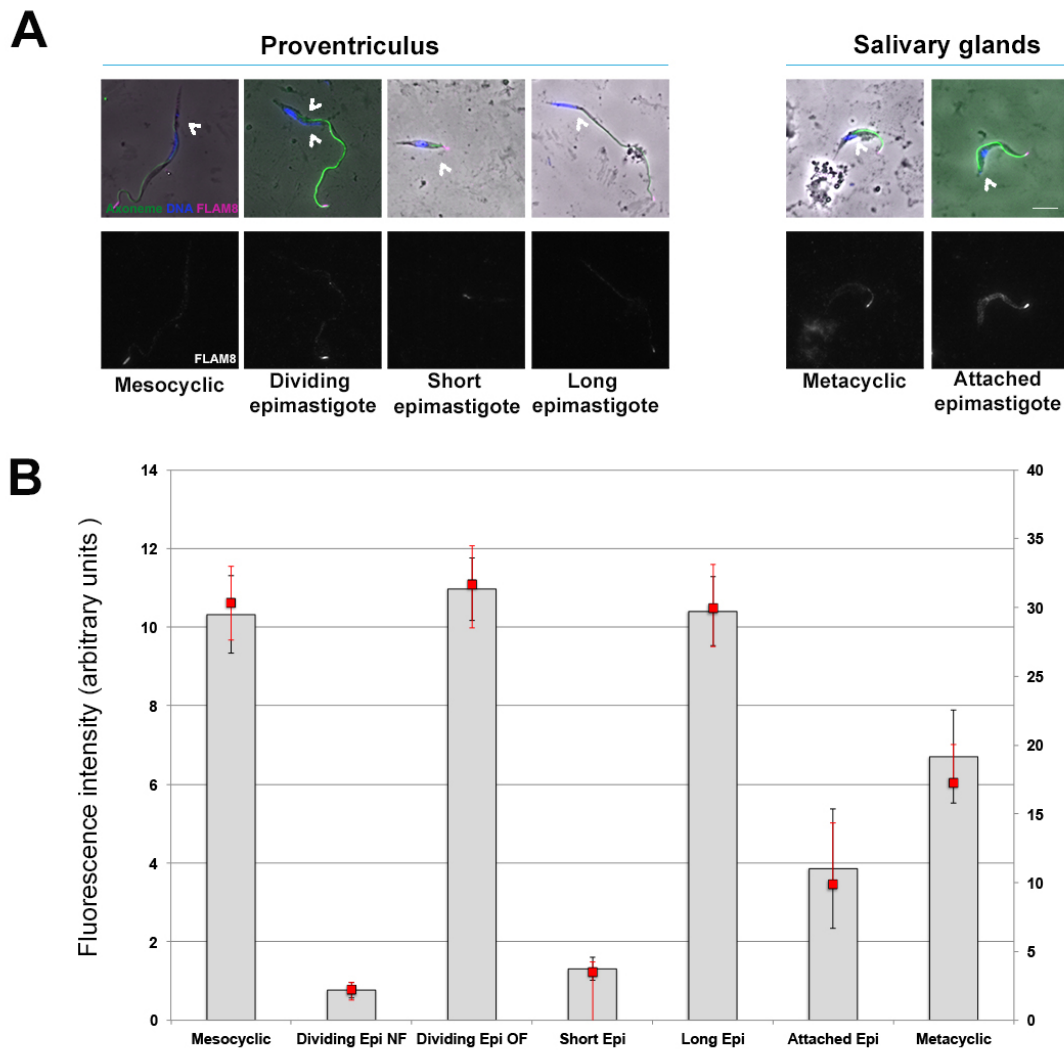


**Figure 5: Variations of FLAM8 expression during the *T. brucei* parasite cycle**

**(A)** Parasites isolated from tsetse flies were fixed in methanol and stained with the Mab25 antibody to detect the axoneme (green) and the anti-FLAM8 (magenta). The top panel shows the phase-contrast images merged with the DAPI (DNA in blue) Mab25 antibody (axoneme in green) and anti-FLAM8 antibody (FLAM8 in magenta) images. The bottom panel only shows the FLAM8 signal (white). Arrowheads indicate kinetoplast positions Scale bar: 5μm **(B)** Quantification of the fluorescence intensity corresponding to the FLAM8 amount in the ROI defined by the axonemal marker in the flagellum (left axis) associated to the flagellum length (right axis, red dots) in each stage of the parasite cycle. n=35 cells per stage.

was demonstrated (Figure 5B). This shows that the flagellum of the short epimastigotes does not mature faster or at least that it does not acquire this marker earlier.

### **Cell division timing contributes to the control of flagellum length.**

In the “grow and lock” model, the timing of cell division is linked to the locking event. To address whether a modification of the timing of cell division could explain the production of flagella with different length in the context of the natural cyclical development of trypanosomes, we chemically induced a cell division arrest in parasites isolated from the tsetse proventriculi and evaluated its impact on flagellum elongation. Cells were maintained for 24 hours in the presence of 10mM teniposide, a drug that interferes with mitochondrial DNA segregation but neither with basal body duplication nor with flagellum elongation (Robinson and Gull 1991). Then, we scrutinized the impact of this cell division arrest on both flagella of dividing epimastigotes by IFA using DAPI to stain DNA and the axonemal marker Mab25 (Figure 6). In dividing epimastigote cells treated with teniposide, the new flagellum had a length of  $3.2 \pm 1.2 \mu\text{m}$  and the old one of  $27.95 \pm 3.54 \mu\text{m}$  ( $n= 17$ ). These values were comparable to those from previous studies obtained in flies infected with wild type parasites (Van Den Abbeele, Claes et al. 1999, Sharma, Peacock et al. 2008, Rotureau, Subota et al. 2011).

The exact duration of this asymmetric division is currently not known. Based on data available for cultured PCF and BSF, we can reasonably estimate that the asymmetric division is completed between 6 and 12 hours. This means that 24 hours of teniposide treatment is likely to be sufficient to efficiently block the asymmetric division. However, despite an apparent delay in elongation, the flagellum of short epimastigotes never exceeded  $3 \mu\text{m}$  (Figure 6A), suggesting that the short flagellum could be already blocked or that the elements necessary for its elongation are not available anymore.

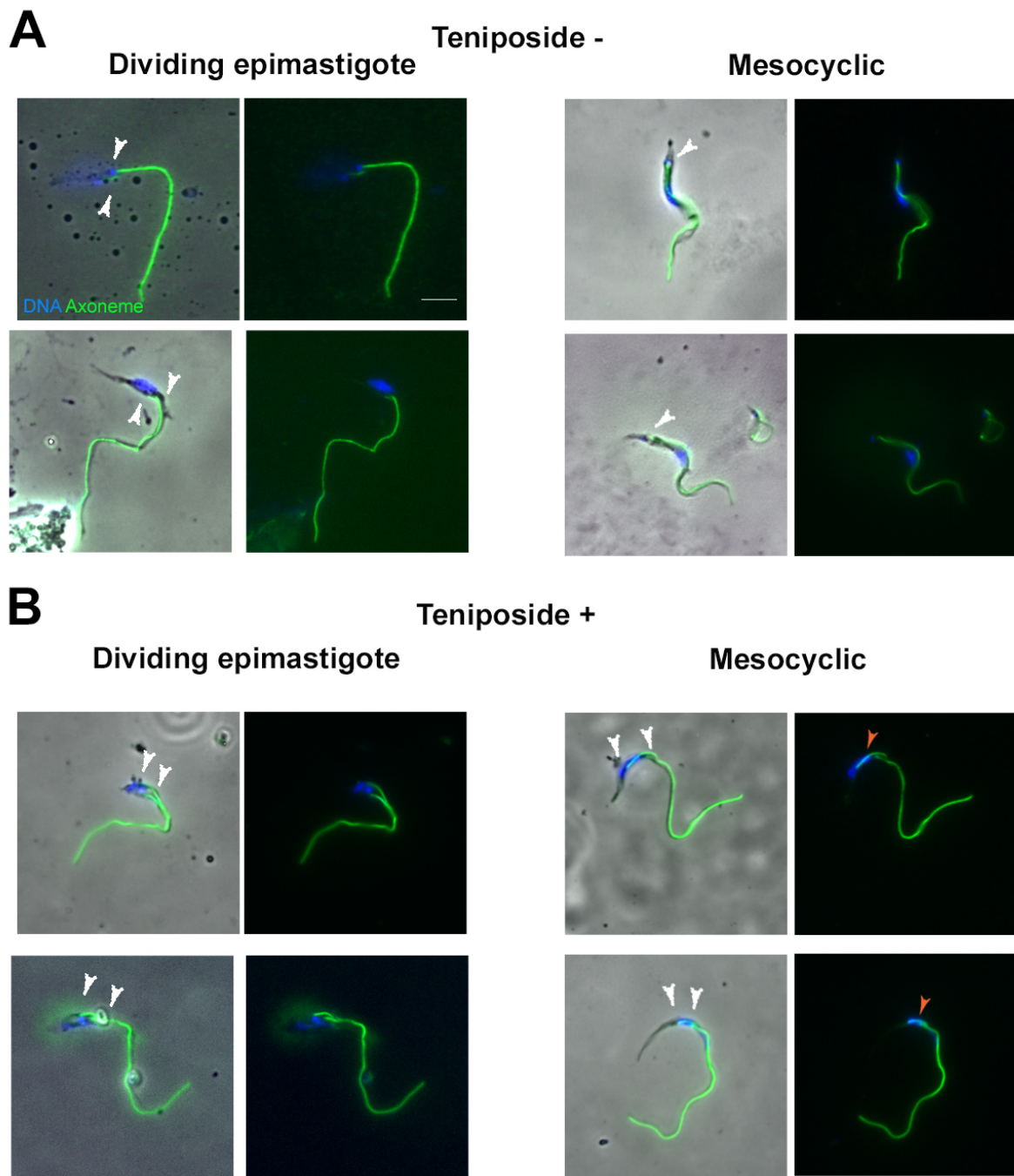


**Figure 6: Effects of the cell division blocking in proventricular trypanosome stages.**

Parasites isolated from tsetse proventriculi were treated or not with teniposide for 24 hours and fixed in methanol and stained with the Mab25 antibody to detect the axoneme (green) and DAPI to stain DNA. The top panels shows untreated cells and the bottom ones cells treated with teniposide. The orange arrowhead shows a new flagellum at the posterior end of a long trypomastigote mesocyclic. Arrowheads indicate kinetoplast positions. Scale bar: 5  $\mu$ m

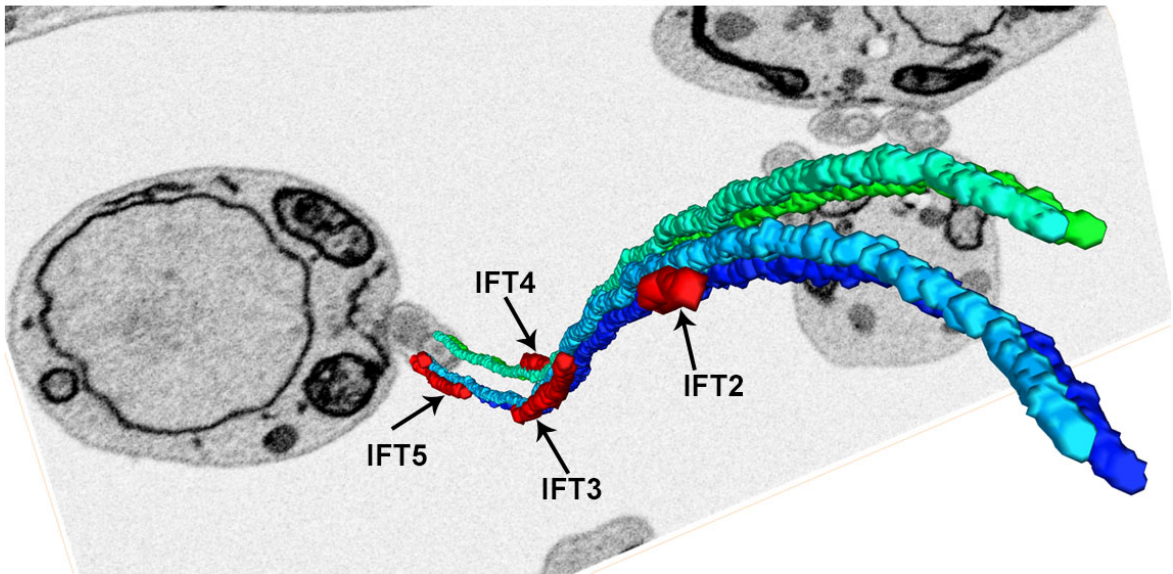
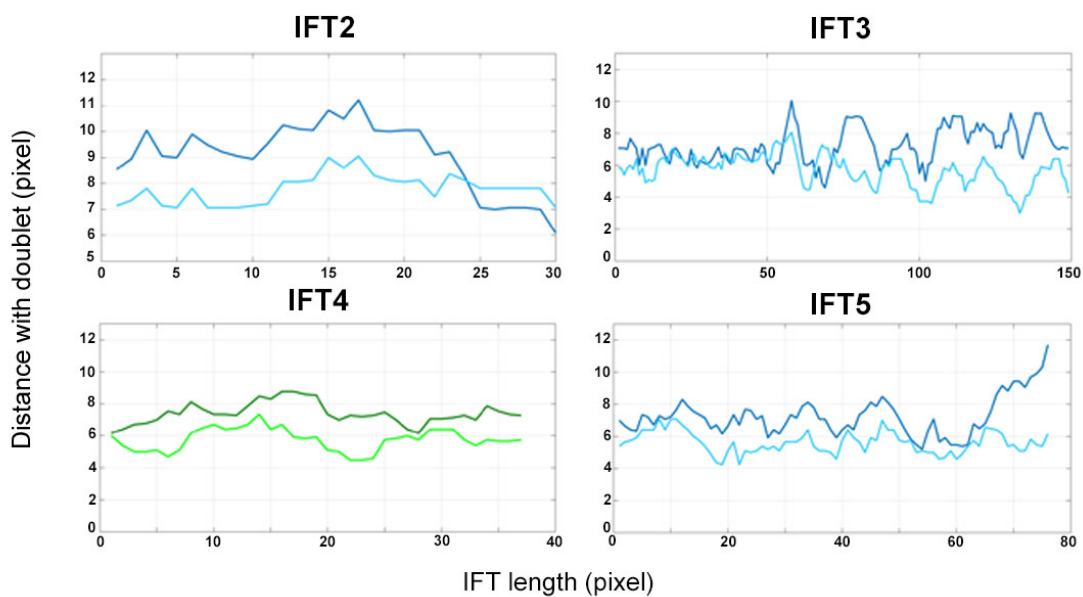
## **Results**

Strikingly, we observed the unexpected emergence of a new flagellum at the surface of long mesocyclic trypomastigote parasites (Figure 6B). During the parasite cycle, the long mesocyclic trypomastigotes migrate from the posterior midgut to the proventriculus and differentiate into long epimastigotes almost concomitantly to the initiation of the asymmetric division. During this differentiation, the emergence of the new flagellum was described to start in parallel to nucleus migration toward the posterior pole of the cell (Sharma, Peacock et al. 2008). From our observations, the emergence of a new flagellum in mesocyclic trypomastigote cells could mean that a short new flagellum is already present to these cells or that the treatment induced duplication of basal body followed by flagellum growth. Using an axonemal marker, we have measured the length of both new and old flagella in these teniposide-treated trypomastigote cells: the length of the new flagellum was on average  $6.2 \pm 2.8 \mu\text{m}$  ( $n= 24$ ) a value that was higher than the average flagellum length in short epimastigotes. Surprisingly, the length of the old flagellum was shorter ( $21.4 \pm 4.5 \mu\text{m}$ ) than that untreated cells ( $28\text{-}30\mu\text{m}$ ) (Rotureau, Subota et al. 2011). The significance of these unexpected results will be addressed on the general discussion of the manuscript.





# Discussion

**A****B**

**Figure 32: Determination of the exact position of IFT trains along trypanosome axoneme.**

**(A)** Axonemal microtubule doublets reconstructed after FIB-SEM. Each microtubule doublet is shown with a different colour (Dark green: doublet 3, Light green: doublet 4, Light blue: doublet 7 and Dark blue: doublet 8) and IFT trains are presented in red. **(B)** Graphics showing distance in pixel between the center of the skeleton of the IFT train and of the doublets along IFT train length. IFT trains are systematically closer to doublets 4 and 7. Analysis performed by Sylvain Trépout.

# I. IFT on specific doublets

---

## 1) Why do IFT trains travel only on specific doublets?

In the first manuscript, we have confirmed and extended previous TEM data, by using FIB-SEM analysis that showed that IFT trains are restricted to doublets 3-4 and 7-8 of the *T. brucei* axoneme. FIB-SEM is a technique with a powerful z-resolution but x- and y- resolutions are limited compared to classical transmission electron microscopy. Limitations in x-y made it difficult to discriminate doublets 3 from 4 and 7 from 8 (Manuscript 1). So, are IFT trains travelling on 2 or 4 doublets? Some preliminary individual 3D-reconstructions of these four doublets (3/4/7 and 8) in few flagella where they could unambiguously be discriminated support the view that IFT trains are restricted only to doublets 4 and 7 (Figure 32) (Sylvain Trépout, unpublished data). Whatever the scenario, IFT train distribution in the trypanosome axoneme is different compared to the other model organism *Chlamydomonas*, where a CLEM study combining TIRF and 3D-electron microscopy demonstrated that IFT trains travel at least on 7 out of the 9 doublets (Figure 33) (Stepanek and Pigino 2016). This means that IFT trains could be differentially distributed according to the type of cilia / flagella.

So far, IFT trains have not been characterised in detail with electron microscopy in other organisms. Therefore, it remains unknown whether one of the two scenarios would be relevant to other types of cilia / flagella or whether distinct situations could be considered. Moreover, due to the resolution limit of conventional light microscopy, it is not possible to distinguish the number of tracks used by IFT trains in most of these model organisms.

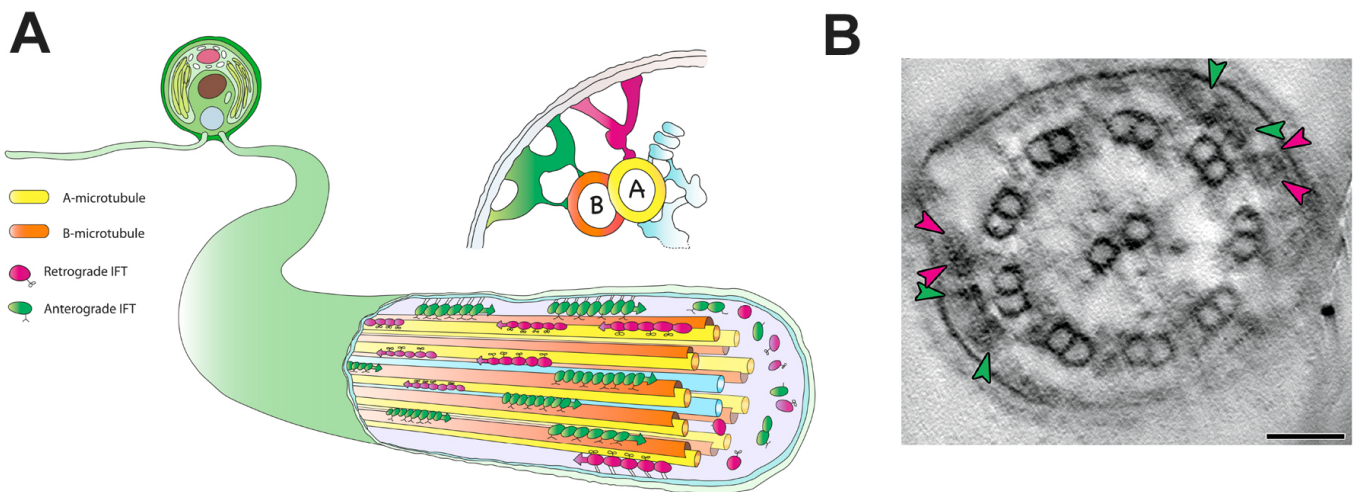


**Figure 33: IFT transport takes place on most microtubule doublets of the axoneme in *Chlamydomonas*.**

**(A)** Schematic representation of IFT in *Chlamydomonas* cilium. Anterograde IFT trains (green), move from the cell body to the ciliary tip along the B tubule (bright yellow) of the microtubule doublets, whereas retrograde IFT trains (red) move along the A tubule (orange). Each microtubule doublet can be used as a bidirectional doubletrack railway. **(B)** Cross-sectional picture showing anterograde (green arrow) and retrograde (pink arrow) trains on several doublet microtubules. Scale bar: 50nm (Right panel) (Stepanek and Pigino 2016).

## Discussion

In view of the two available examples, we can raise the question whether the distribution of IFT trains distribution around the axoneme is species-dependent or if the situation is even more complex and IFT trains repartition could be different on the same organism depending on the cilia / flagella type. In the first case, control would be at the genetic level, whereas in the second one, it would require distinct modulation per cell type. In the human body where a large diversity of cilia and flagella is present, are IFT trains positioned on the same microtubule doublets in sperm flagella and olfactory cilia for example? Due to the difficulty to access to ciliated human cells, the use of model organisms can be very informative. *T. brucei* is a particularly good model because using the same genome; it activates different programmes during its parasite cycle, where each stage is associated to a flagellum with different length and function (Rotureau, Subota et al. 2011) as this is the case for cilia found at the surface of different tissues in the human body.

Different flagella are assembled during the *T. brucei* life cycle, with variable length, composition and functions. In this context, the repartition of IFT trains might be different. For example, one could hypothesize that more tubulin need to be transported to the distal tip in order to construct longer flagella in proventricular mesocyclic trypomastigotes. This could be associated to IFT trafficking in more than two tracks in order to increase flagellum assembly rate. Based on the results obtained in this thesis, this scenario is unlikely in *T. brucei*. Indeed, we have demonstrated that IFT train frequency is invariant no matter the length of the flagellum. These analyses were carried out in standard imaging conditions; but we have demonstrated that the underestimation of IFT train frequency is not major (about 10%) (Manuscript 1).

Interestingly, preliminary electron microscopy data obtained in parasites present in the tsetse proventriculus showed that IFT trains could also be positioned in doublets 1 and 9. This has never been observed in cultured procyclic parasites (Figure 34B and C). Moreover in TEM sections of cultured bloodstream forms, the distribution of the IFT trains around the axoneme also differs from cultured procyclic form situation. Indeed, IFT trains of bloodstream form flagella are preferentially found in positions 4

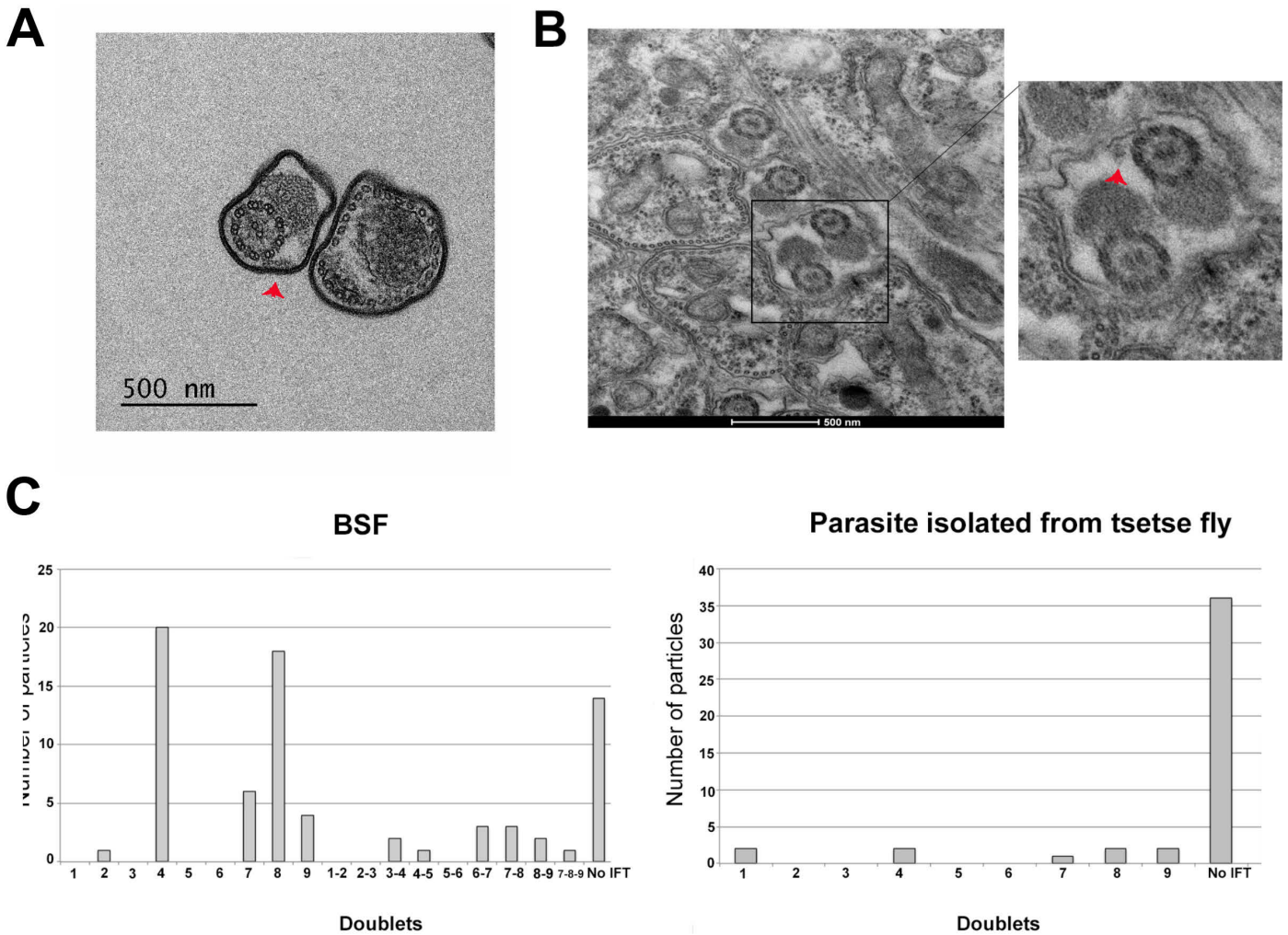


**Figure 34: IFT train localisation in flagella from cultured bloodstream and from proventricular parasites .**

**(A)** Transmission electron microscopy image of a cross section through a BSF axoneme (Cécile Fort). An IFT particle positioned on doublet 8 is indicated by the arrowhead. **(B)** Transmission electron microscopy images of axonemes from proventricular parasites *in situ*. The enlargement of the picture shows axoneme with IFT particle positioned on doublet 9 (Red arrowhead). **(C)** Graph showing the number of IFT particles found on the indicated doublet in flagella from BSF (n total= 95) and or from proventricular parasites (n total =45 flagella from 3 proventriculi).

and 8 (Figure 34A and C). In BSF flagellum sections, IFT trains have a different aspect; they look larger and more diffuse. This could be due to a difference in IFT train composition or assembly. These differences could impact on IFT train distribution and explain their localisation on doublet 8.

These observations suggest that IFT trains could be repositioned around the axoneme depending of the parasite stages while remaining associated to only two tracks. This can be investigated by using FIB-SEM analysis of parasites *in situ* in the proventriculus. Indeed, FIB-SEM analysis will first allow us to determine parasite stage that is not possible in classical TEM due to the population heterogeneity and then determine whether IFT train positioning on doublets 1 or 9 is always associated to the same parasite stage. Moreover, we would see if IFT trains are found exclusively on two microtubule doublets out of nine in all the situations or if IFT trains could use more than two tracks in some axonemes.

We cannot exclude that IFT train distribution looks different in several parasite stages because of technical issues. Indeed, these stages are less studied than cultured procyclic cells; therefore we do not have perspectives of fixation effects on IFT trains in these parasites. Our experiments showed that IFT trains can still traffic for about 200ms after addition of glutaraldehyde (J. Jung and M. Lemos, unpublished data). In theory, the train can still move by 0.4 $\mu$ m for anterograde and 1 $\mu$ m for retrograde trains. Since membrane composition is different between BSF, PCF and parasites isolated from tsetse fly, this could impact on the position of the train after fixation, for example if it fell off the microtubules. Repositioning of IFT trains around the axoneme could be constrained by the shape of the flagellum membrane. This could be significant at the distal tip of the attached epimastigotes that develop extensive membrane outgrowths to contact microvilli of tsetse salivary glands (Vickerman 1985). Because IFT trains are sandwiched between flagellum membrane and the axonemal microtubules, any membrane shape modifications could potentially impact IFT train positioning around the axoneme and in this case especially at the distal tip of the flagellum. An analysis in TEM or FIB-SEM of attached epimastigote flagella could be interesting to evaluate if IFT train positioning is modified or not. Flagellum



attachment looks different in BSF from PCF, what is reflected by their more elaborate beating pattern (Elmendorf, Dawson et al. 2003, Heddergott, Kruger et al. 2012). Could this have an impact on IFT positioning on doublet 8?

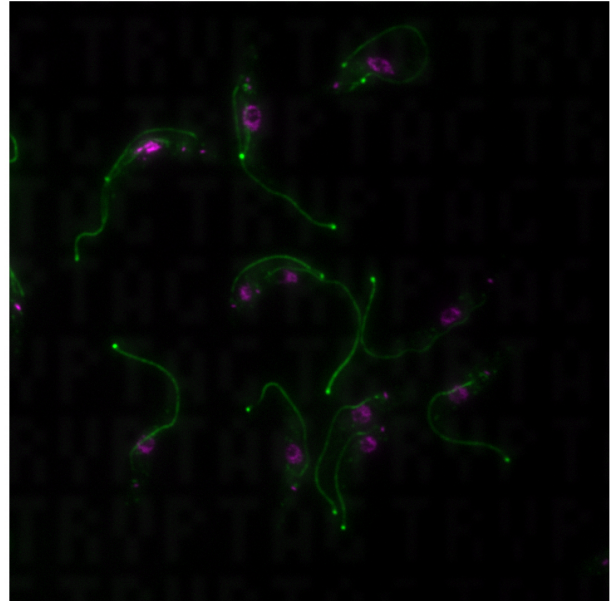
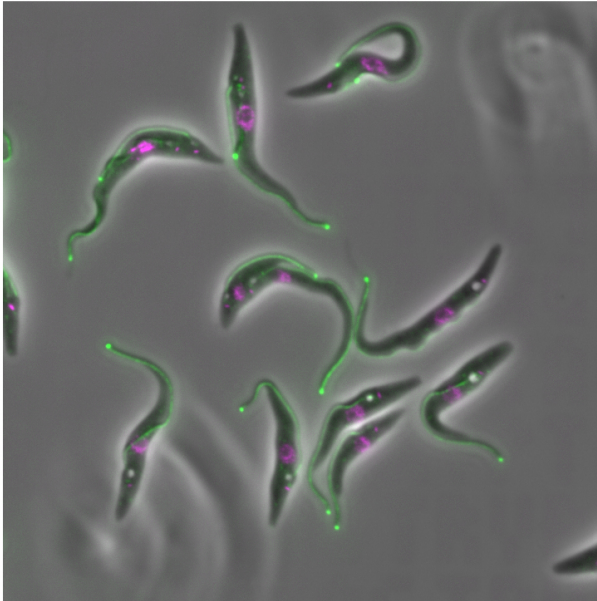
In humans, photoreceptor outer segments also present extensive plasma membrane outgrowths. It would be interesting to evaluate if IFT train distribution is different between the proximal region (present on the side of the inner segment) of the connecting cilium and the distal region in contact with plasma membrane outgrowths.

## **2) Why does IFT only use 2 of the 9 microtubule doublets?**

While in theory, nine microtubule doublets are available for IFT trafficking, why only few are used for IFT? In both cultured procyclic and bloodstream forms, IFT trains were never observed on positions 5 and 6, corresponding to the two doublets associated with the PFR. The absence of IFT on these doublets could be due to the presence of the PFR that would prevent interaction with the membrane. On the contrary, does the absence of IFT trains on the two doublets allow the construction of the PFR?

A first simple explanation could be that the access to these two doublets by IFT trains is physically blocked by the presence of the PFR preventing fixation of IFT motors and then their trafficking. On the contrary, we propose that the restriction of IFT trains to only two sets of doublets could liberate space for the construction of extra-axonemal structures such as the PFR. In sperm flagella, extra-axonemal structures are also found such as the fibrous sheath and the ring of mitochondria all around the axoneme (Fawcett 1975). These extra-axonemal structures are added latter on, when the axoneme is already constructed at the stage where IFT proteins start to disappear (San Agustin, Pazour et al. 2015). We propose that the arrest of IFT in mature sperm flagellum liberates space to add these extra-axonemal

**Kinesin, putative (Tb927.5.2410)**



**Kinesin, putative (Tb927.4.2730)**

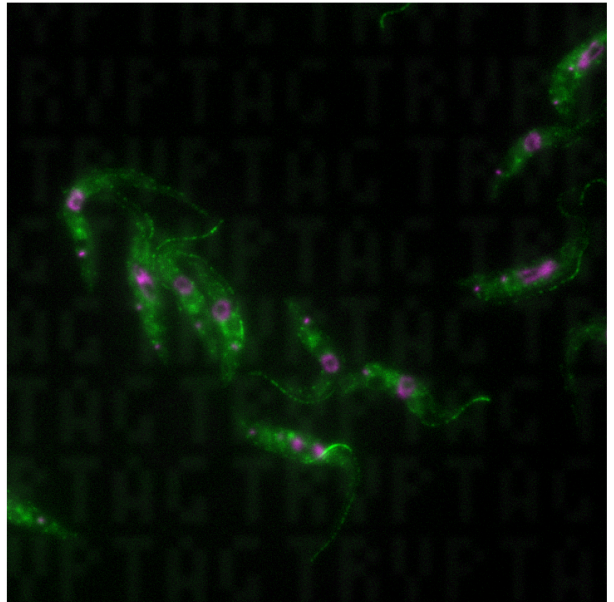
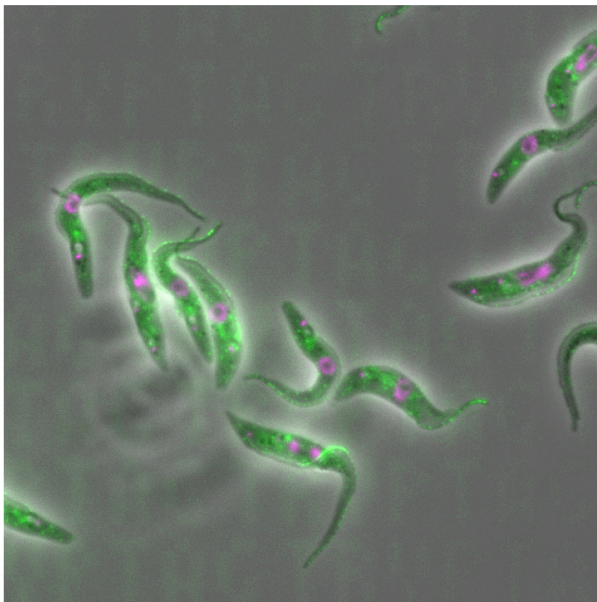


**Figure 35: Putative kinesins with flagellar localisation.**

Images extracted from TrypTag database. These examples show two putative kinesins presenting a flagellar localization that could be associated to other microtubule doublets than 4 and 7 (Dean, Sunter et al. 2017).

structures. In *Giardia*, extra axonemal structures are only detected in cytoplasmic portion of the axoneme, where IFT is absent (Elmendorf, Dawson et al. 2003).

As previously described, only two kinesins II (KIN2A and KIN2B) implicated in anterograde IFT are found in the trypanosome genome (Julkowska and Bastin 2009). However, there are more than forty genes encoding kinesins and only a few of them have been studied so far (Wickstead and Gull 2006). In the TrypTag database (a project to determine protein localisation for all trypanosome genes <http://tryptag.org/> (Dean, Sunter et al. 2017)), several different kinesins are also found to be localized in the flagellum but their functions are still unknown (Figure 35). These other kinesin motors could possibly walk along the axoneme using free doublets that are not already used for IFT. They could be implicated in transport of proteins involved in construction or in signalling pathways. For example, they could be essential to carry proteins from cell body to flagellar tip in response to external stimuli. The first contact between the attached epimastigote and the salivary gland epithelium could initiate the production of proteins necessary to create hemi-desmosome-like junctions. These proteins need to be transported to the distal tip of the flagellum and kinesin motors (not already implicated in IFT) could be implicated in this process.

In trypanosomes, KIF9B is a kinesin motor not associated to IFT but present in the axonemal region and at the base of the flagellum (Demonchy, Blisnick et al. 2009). It is a good candidate to be associated to microtubule doublets where no IFT trains are present. The *KIF9B<sup>RNAi</sup>* procyclic mutant was studied and exhibited spectacular defaults in PFR assembly (Demonchy, Blisnick et al. 2009). In this mutant, immunofluorescence using antibodies against PFR1 and PFR2 proteins produced a discontinuous signal, showing alternating regions of intense labelling with regions where the signal was negative (Figure 36A) (Demonchy, Blisnick et al. 2009). These results were confirmed by scanning and transmission electron microscopy. Flagella of *KIF9B<sup>RNAi</sup>* mutants present regions with one or more PFR-like structures alternating with sections containing only the axoneme (Figure 36B). PFR assembly takes place at the distal tip of the flagellum like axonemal proteins and its elongation

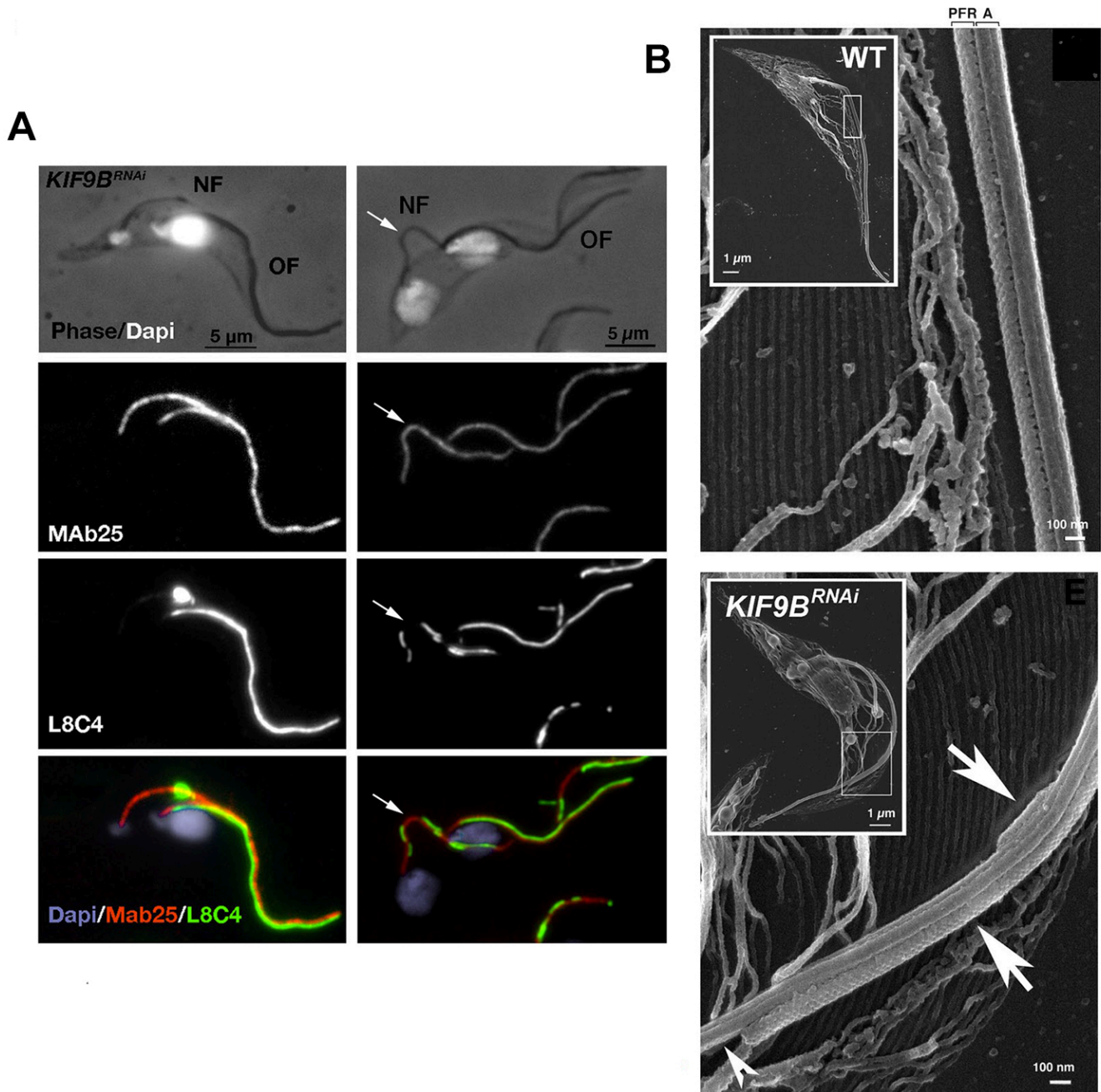


**Figure 36: KIF9B and the transport of PFR components in *T. brucei*.**

**(A)** Immunofluorescence pictures of *KIF9B<sup>RNAi</sup>* PCF cells induced for 48 hours. The old flagellum (OF) presents a normal axoneme (Mab25) and PFR (L8C4) labelling, whereas the new flagellum (NF) presents a normal axoneme but a disrupted PFR. Arrows show the detached flagellum. **(B)** Scanning electron micrograph of a WT cell (top panel) and a *KIF9B<sup>RNAi</sup>* PCF cell induced for 72 hours (bottom panel) extracted with cold Triton X-100. The white rectangle indicates the position of the magnified area. The arrows point PFR material, and the arrowhead shows a naked region of the axoneme (Démonchy, Blisnick et al. 2009)

follows that of the axoneme shortly (Bastin, MacRae et al. 1999). Therefore, PFR proteins could be cargoes of IFT trains, although no study has formally proved it yet. Therefore it was proposed that KIF9B could be implicated in the transport of PFR proteins toward the distal tip for assembly. However, no GFP::KIF9B trafficking was visible along the axoneme of live cells (Demonchy, Blisnick et al. 2009). Furthermore, unlike IFT proteins, KIF9B is resistant to detergent-treatment, suggesting a strong interaction with microtubules. Based on these results, it was proposed that KIF9B could be fixed along the axoneme possibly on doublet 5-6 and to progressively drag PFR proteins to the distal tip.

In *T. brucei*, the IFT dynein RNAi mutants are characterised by the presence of dilated flagella full of IFT proteins (Blisnick, Buisson et al. 2014). Interestingly, kinesin motors do not accumulate in these dilated flagella. In *Chlamydomonas*, kinesin seems to return to the flagellum base by simple diffusion (Engel, Ludington et al. 2009, Chien, Shih et al. 2017). Alternatively, IFT kinesin motors are actively returned by retrograde transport in *C. elegans* (Prevo, Mangeol et al. 2015). The last option could be that kinesin goes back to the flagellum base independently of IFT and could be transported by other motors that would walk on the free microtubule doublets that are not already used by IFT.

In *T. brucei* procyclic cells, the flagella connector is a structure that links both flagella through skeletal fibers during new flagellum elongation. It was proposed that flagella connector fibers are present on doublets 7, 8 and 9 of the old flagellum and on doublets 3 and 4 of the new flagellum (Briggs, McKean et al. 2004, Hoog, Lacombe et al. 2016). Study of flagella connector composition has revealed the presence of kinesin motors (Varga, Moreira-Leite et al. 2017). It was proposed that these kinesins could be responsible for flagella connector movement along the old axoneme. In this context, these motors could walk on doublets 8 and 9, where there is no IFT but what about doublet 7? The presence of flagella connector does not seem to interfere with IFT. Indeed IFT trafficking in the old flagellum of cultured procyclic forms is not disrupted (Manuscript 3). This is possible because IFT motors only walk on a small



part of the microtubule (Kozminski, Beech et al. 1995) thus; the flagella connector could cohabit with IFT motors and use a different area of the microtubule. The flagella connector probably does not interfere with IFT in the new flagellum because it is only present at the distal tip where IFT trains stop anyway.

In bloodstream forms, the flagella connector is absent and the distal tip is embedded in a cell-body groove (Hughes, Towers et al. 2013). Furthermore IFT trains are found on different positions (doublets 7 and 8). Thus a tempting question would be the possible impact of flagella connector in IFT positioning? It would therefore be interesting to study the repartition of IFT trains in procyclic flagella connector mutants to evaluate whether the presence of flagella connector could restrict IFT positions around the axoneme. Moreover, during Epi-trypanosome asymmetric division the two flagella are not connected to each other (Rotureau, Subota et al. 2012). It could be also interesting to study whether IFT train distribution is different during this specific division to evaluate if the flagella connector could really have an impact on IFT positioning.

### **3) How does IFT only take place on specific microtubule doublets?**

In trypanosomes, there is no tubulin  $\alpha$  or  $\beta$  gene specifically dedicated to axonemal construction. The nine microtubule doublets are therefore made of the same tubulin proteins, so why are only two microtubule doublets out of nine are used for IFT? What differentiates them from the others? A possible explanation can be found by the fact that doublets 4 and 7 have a distinct molecular identity compared to the other doublets due to tubulin post-translational modifications or that proteins might associate specifically to doublets? Such biochemical information could be preferentially recognized by IFT motors and favour their interaction. On the contrary, specific biochemical information could prevent IFT train access to all the other doublets.



Tubulin is the main component of the axoneme and can undergo a large panel of post-translational modifications such as polyglycylation or polyglutamylation (L'Hernault and Rosenbaum 1985, Rudiger, Plessmann et al. 1995). Analyses of loss-of-function mutants of microtubule-modifying enzymes suggest that post-translational modifications are important for assembly, stability and function of the cilium (Janke 2014).

A recent study in mice fibroblasts showed that the anterograde trafficking of mNg::IFT88 was slowed down in absence of ciliary tubulin glutamylation (Hong, Wang et al. 2018). Additionally, the effect of tubulin polyglutamylation on the velocity of kinesin-2 has been tested *in vitro*. Using yeast tubulin fused to different human tubulin carboxy terminal tails (CTTs), it has been demonstrated that both short (3 glutamates) and long (10 glutamates) CCTs increased the velocity and the processivity of the kinesin-2 motors (Sirajuddin, Rice et al. 2014). In contrast, the recruitment and the processivity of kinesin-2 motors were reduced by tubulin tyrosination (Sirajuddin, Rice et al. 2014). We could propose that specific post-translational modifications on doublet 4 and 7 could favour IFT (polyglutamylation) fixation or in contrast prevent IFT fixation on the other doublets (tyrosination).

Glycylation enzymes are absent from the genome of *T. brucei* and mass spectrometry analysis demonstrated that glycylation was not detected in tubulin trypanosome (Schneider, Plessmann et al. 1997). Moreover, this study showed that trypanosome tubulin is extensively glutamylated, with variable numbers of glutamate residues added to both cytoplasmic and axonemal tubulin (Schneider, Plessmann et al. 1997). Glutamylases belong in Tyrosine ligase like proteins (TTLL) and the 7 genes are found *in T. brucei* genome (Casanova, de Monbrison et al. 2015).

During the construction of the new flagellum, the tip of the extended axoneme microtubules of *T. brucei* contains exclusively tyrosinated tubulin (Sherwin, Schneider et al. 1987). This post-translational modification could inhibit kinesin recruitment and IFT (Sirajuddin, Rice et al. 2014). Recently, the localisation of the seven TTLLs has

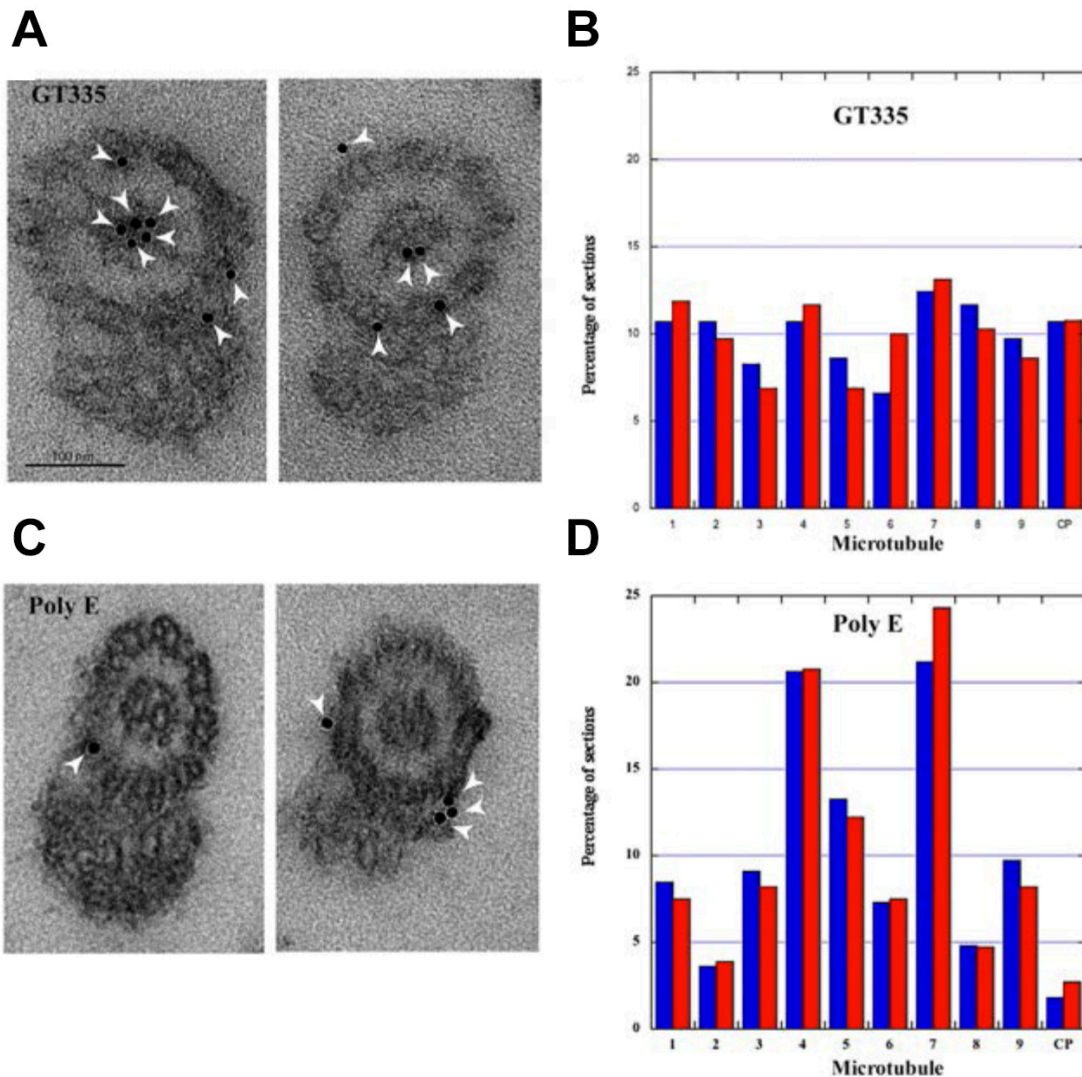


**Figure 37: Microtubules 4 and 7 are differentially polyglutamylated.**

**(A and C)** TEM micrographs of detergent-extracted cytoskeletons from wild-type procyclic trypanosomes post-embedded and immuno-gold stained with GT335 that detect all forms of glutamylated tubulin no matter the length of the chain **(A)** or with poly-E antibody that binds selectively to the polyglutamate chains longer than 3 residues **(C)**. Positions of gold beads are indicated with white arrowheads.

**(B and D)** Histograms showing the percentage of sections with gold particles on the 9 doublet microtubules and the central pair (CP) in samples stained with GT335 (n=290 flagellum cross sections) **(B)** or the poly-E antibody (n=165 flagellum cross-sections) **(D)**. Since more than one particle can be encountered on the same doublet, both the absolute number of gold particles (in red) and the event occurrence (positive signal no matter the number of particles (in blue) are represented. Results obtained by Cécile Fort.

been investigated and several were found to be located in the flagellum, especially TTLL4A that is concentrated at the distal tip of the growing flagellum (Elise Warter, unpublished data). Because of this localisation, TTLL4A is a strong candidate to rapidly glutamylate microtubules immediately after their polymerisation. Tubulin glutamylation achieved by TTLL4A could be specific to doublet 4 and 7. This could relieve tyrosine inhibition and allow access to IFT trains on these two doublets. Indeed the characterisation of polyglutamylation distribution in the trypanosome axoneme was performed in the lab, using immuno-gold detection with two antibodies: the GT335 monoclonal antibody that detect all forms of glutamylated tubulin no matter the length of the chain (Wolff, de Nechaud et al. 1992) and a poly-E anti-serum that binds selectively to the polyglutamate chains longer than 3 residues (Rogowski, Juge et al. 2009). While GT335 stained equally the nine doublets and the central pair (Figure 37A) (10% of the gold particles on each) (Figure 37B), the poly-E signal was overrepresented on doublets 4 and 7 (50% of the gold particles) (Figure 37C and 37D) (Cécile Fort *et al.*, Unpublished data). Based on this observation, microtubule doublets 4 and 7 are specifically polyglutamylated discriminating them from the other doublets. In contrast doublets appear indifferently tyrosinated during axoneme construction (Sherwin and Gull 1989). This could relieve tyrosination inhibition of IFT and favour interaction and traffic of kinesin IFT motors and explain the specific localisation of IFT trains on these two doublets.

The restriction of IFT trains on only two doublets out of nine could also be due to the presence of unique proteins on specific microtubule doublets conferring a particular identity to them a particular identity. These proteins could facilitate (on doublet 4 and 7) or prevent (all the other doublets) IFT train access. Few examples of protein association to specific doublets are known that could confer them their own identity. Doublets 4 and 7 are linked to the PFR by strong and bulky connectors. Using immunogold labelling, I17 protein (high molecular weight protein with unknown function) was shown to localize between the axoneme and the PFR (Imboden, Müller et al. 2009). I17 could be essential to determine the identity of doublet 4 or 7. Two other proteins CFAP43 and CFAP44 (WD repeats containing proteins important for

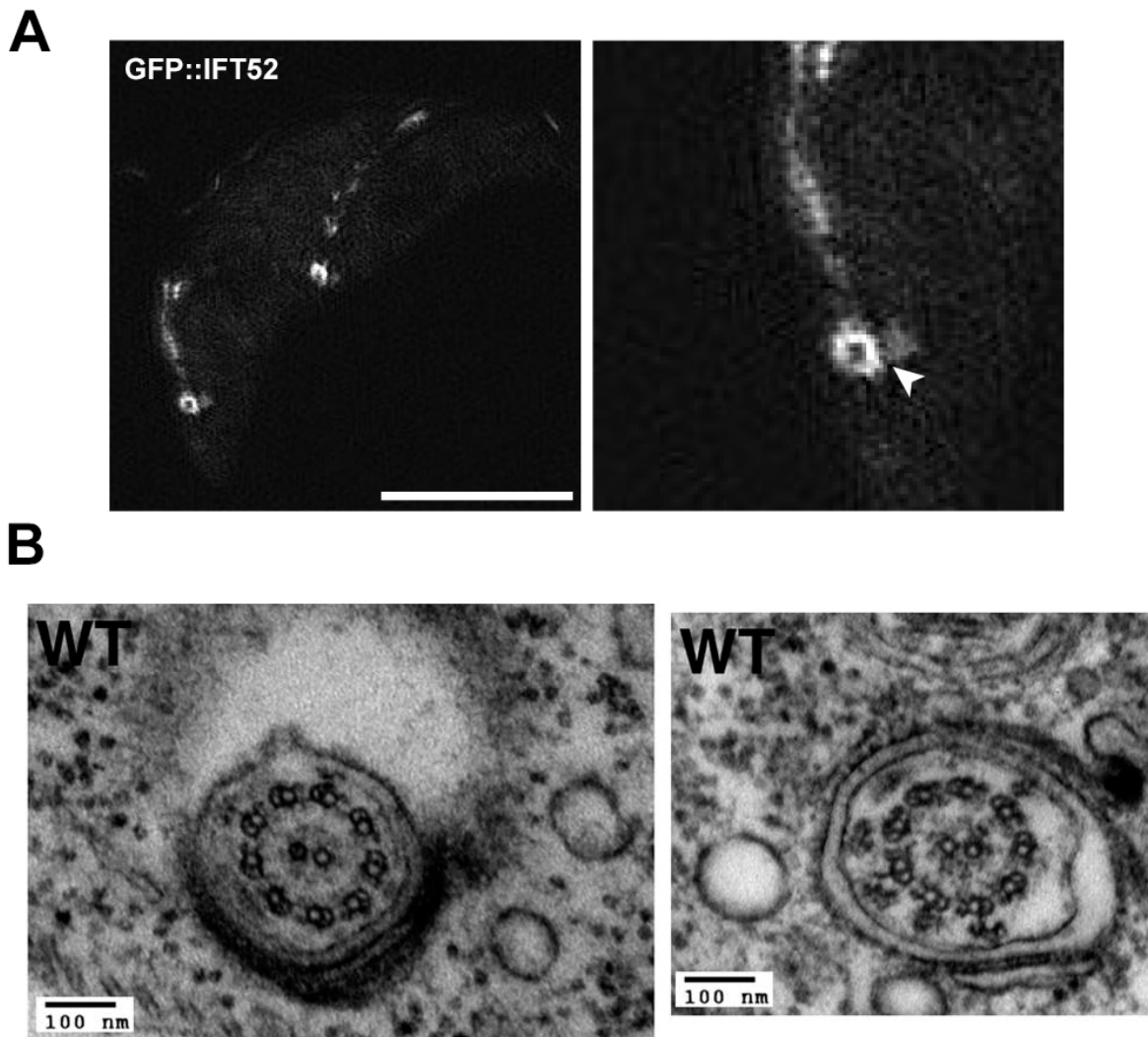


**Figure 38: IFT train repartition around the axoneme in the flagellar pocket of *T. brucei*.**

**(A)** Still images of cells expression GFP::IFT52 obtain in SIM showing that IFT proteins form a donut-like structure (pointed by the arrowhead) at the base of the flagellum. Scale bar: 5 $\mu$ m. Images obtained by Cécile Fort and Jean-Yves Tinevez.

**(B)** TEM pictures of WT trypanosome flagellar cross-sections close to the top of the flagellar pocket. Central pair and dynein arms are visible, but the PFR is not yet present. Abundant electron dense material similar to IFT particles can be seen close to most doublets (Absalon, Blisnick et al. 2008).

axonemal organisation) localized on doublet 5 and 6 and their presence could also determine doublet identity (Coutton, Vargas et al. 2018). Based on these two examples, we could propose that specific proteins could be associated to each doublet to distinguish them from each other.

In IFA and live cell studies of *T. brucei*, an IFT pool is observed at the base of the flagellum of all the different parasite stages except for the short epimastigote. TEM images of the transition zone of cultured procyclic cells show electron dense material between membrane and microtubules. These could correspond to IFT trains or IFT material (Trepout, Tassin et al. 2018) but the presence of Y-links does not facilitate the interpretation. This material is gone with detergent treatment demonstrating that it is probably not physically linked with microtubules (Vaughan and Gull 2015). Recent data obtained in the lab by super-resolution microscopy (SIM), have shown that IFT proteins are concentrated in a donut-like structure at the base of the flagellum (Figure 38A) (Cécile Fort, Jean-Yves Tynevez and Jamin Jung, unpublished data). These observations raise the question of the localisation of the IFT train assembly site. Are IFT trains assembled in the cytoplasm and then able to enter in the flagellar compartment? Or are IFT proteins first concentrated at the flagellum base before trains are assembled and injected in the axoneme? Does IFT-A and IFT-B assemble at the same place? A fluorescence resonance energy transfer (FRET) analysis using an IFT-A and IFT-B tagged proteins could elucidate the site of IFT train assembly. Using the same method, it could be possible to evaluate where IFT trains are attached to kinesin motors to initiate anterograde transport.

The donut-like distribution of IFT proteins at the flagellum base suggests that this material is associated to the nine microtubule doublets of the region. So, how trafficking could later be restricted to only on two microtubule doublets of the axoneme? We proposed the existence of a restricting system to explain the specific distribution of IFT trains on doublets 4 and 7. Are these modifications present all along the axoneme? Or are they present only at the flagellum base? And if there are



only present at the base at which level exactly? Transition zone? Transition fibres?  
Or the portion of axoneme without PFR?

In *T. brucei*, the transition zone is located in the flagellar pocket with the axoneme in its continuity. When the flagellum emerges from the flagellar pocket, the PFR is associated, meaning that the 9 microtubule doublets of the axoneme not already associated to the PFR are in theory available to link IFT train motors. In most of the TEM sections of the axoneme in this portion of the flagellar pocket region, there is no electron dense structures sandwiched between microtubules and flagellar membrane. In a few sections found close to the apex of the flagellar pocket, electron dense structures that look like IFT particles are detected, but all around the axoneme (Figure 38B) (Absalon, Blisnick et al. 2008).

The absence of electron dense material in this region could be due to the kinetics of fixation by glutaraldehyde. As said above, IFT trains need 200-300ms to stop after addition of the fixative (Jamin Jung and Moara Lemos, unpublished data). the majority of IFT anterograde trains travel with a speed of 2.4 $\mu$ m/sec (Buisson, Chenouard et al. 2013) and this region is 1.2 $\mu$ m in length (Trepout, Tassin et al. 2018). During this time lapse, IFT trains present in portion of axoneme in the flagellar pocket could leave this region and those being prepared in the transition zone could be blocked.

Electron dense material present in this regions are sensitive to detergent treatment (Vaughan and Gull 2015), an observation compatible with the fact that this material being IFT proteins or trains. If the electron dense material observed in the few TEM sections at the level of the flagellar pocket (Figure 38B) corresponds to IFT trains, it would mean that IFT trains are injected on most doublets of the axoneme before the addition of the PFR. The presence of the PFR would impose IFT train reorientation on doublets 4 and 7. However, this explanation does not explain why trains are absent from doublets 1,2 and 9. This raises the question of how an IFT train could “jump” from one microtubule to another. Alternatively, some IFT trains could already



be specifically associated to doublets 4 and 7 and all the other IFT trains present at this level are not fixed to the axoneme and are queuing to access on doublets 4 and 7. It could be interesting to study microtubule doublets identity at this level and check for example if the polyglutamylation profile is already specific on doublets 4 and 7 or not. Possibility to use transition zone enriched fractions as described by Dean et al. would facilitate this analysis (Dean, Moreira-Leite et al. 2016).

### **4) Why are only doublets 4 and 7 be modified?**

In the previous section, we have proposed several hypotheses to explain why IFT take place only on two specific doublets. This could be due to tubulin post-translational modifications, the presence of unique protein in microtubule doublets or a control at the base of the flagellum. This lead to another question: Why do only doublets 4 and 7 acquire this unique identity associated to IFT?

First, we can propose that doublets 4 and 7 already possess their own identities as soon as in the proximal region of the basal body. Each triplet of the basal body is associated to specific structures such as striated fibers or rootlets (Vaughan and Gull 2015). We can hypothesize that the specific identity of these microtubules is inherited at each basal body replication and facilitates their recognition by enzymes or proteins that modify axonemal microtubules and give them their specific identities. Second, the differential polyglutamylation profiles of the doublets 4 and 7 could be due to their proximity with the PFR. Indeed, the TTL(s) implicated in identifying IFT tracks could be localized at the PFR periphery. In these conditions, only doublets 4 and 7 would be accessible to the enzyme and therefore be strongly polyglutamylated. To validate this hypothesis, it will be interesting to study the pattern of axonemal glutamylation by immunogold in a calmodulin null mutant that has no PFR left (Ginger, Collingridge et al. 2013). If PFR presence mediates specific positioning of key enzymes are specifically positioned, its absence should result in a reduction of glutamylation on doublets 4 and 7, and in theory impact IFT train positioning. We note that the



calmodulin RNAi mutant has shorter flagellum, a phenotype associated to IFT frequency reduction.

Third, the axoneme is in close contact with the flagellum membrane. A specific distribution of membrane proteins or lipid rafts could also influence IFT distribution around the axoneme. Indeed, lipid-raft proteomic analyses revealed an over-representation of IFT proteins (Sharma, Olson et al. 2017). We could imagine that lipid-rafts are only present in the flagellar membrane along the doublet 4 and 7 (Tyler, Fridberg et al. 2009), inducing the positioning of IFT trains on these two doublets from the base of the flagellum. This brings the question as to how lipids would be preferentially organised.

### 5) How anterograde and retrograde trains avoid collisions?

In trypanosome flagella, anterograde trains move at different speeds. Fusion and fission events occur between anterograde particles but collisions were not observed between trains moving in opposite directions (Buisson, Chenouard et al. 2013). Further analyses using total internal reflection fluorescence microscopy (TIRF) in *Chlamydomonas* flagella confirmed the existence of interactions between anterograde trains but also demonstrated the existence of interactions between retrograde trains (Stepanek and Pigino 2016). Fusion events were typically observed as a faster train caught up with a slower one moving in the same direction, resulting in both progressing together at the faster speed (Buisson, Chenouard et al. 2013). On *T. brucei* flagellum sections, short electron dense fibres linking IFT particles to the axoneme microtubules are sometimes visible (Absalon, Blisnick et al. 2008). We think that these links could correspond to the IFT motor but they do not seem to be preferentially associated with specific doublets (3 or 4 and 7 or 8) or to any tubules (A or B). However, TEM sectioning does not allow discrimination of train identity (retrograde, anterograde). IFT motors could correspond to kinesin or dynein and



since anterograde and retrograde trains are found on both tracks, all possibilities could be observed in a section. CLEM approaches are currently the only option to determine train identity as well as their precise position on the axoneme. In view of the recent results obtained in *Chlamydomonas*, we can propose that the anterograde transport takes place on the B-tubule and the retrograde one on the A-tubule. This is currently investigated in the lab (Adeline Mallet).

In studies where polyglutamylation profile of ciliary microtubules was modified, the anterograde transport and kinesin motors were impacted (O'Hagan, Piasecki et al. 2011, Hong, Wang et al. 2018). The GT335 antibody stains only B-tubules of *Chlamydomonas* axonemes (Lechtreck and Geimer 2000). We can propose that the B-tubule could also be differentially glutamylated in trypanosomes, favouring interaction with the IFT kinesin motors implicated in anterograde transport. On the way back, dynein motors could specifically bind the A-tubule due to the presence of specific modifications that could attract them. In contrast the presence of proteins at the distal tip of the axoneme or specific modifications on the B-tubule could prevent dynein fixation. One other option may be to consider whether anterograde trains continuously travel on the B-tubule, and when they reach the end of the flagellum, the A-tubule is the only one available and dynein walks on it by default. In these conditions each type of transport would occur along a specific tubule, preventing collisions between trains running in opposite directions.



## II. Flagellum length control

---

Currently, the most popular model for flagellum length control is based on the existence of a dynamic assembly and disassembly of tubulin at the distal tip of the organelle, involving the IFT machinery for tubulin transport. In *T. brucei*, it was demonstrated that IFT is required for the construction but not for flagellum length maintenance (Fort, Bonnefoy et al. 2016). Here, we have proposed the new “grow and lock model that could be more relevant for stable flagella. This new model raises several questions especially concerning the regulation of flagellum growth and the nature of the locking event.

### 1) What could regulate flagellum growth?

We have shown a direct correlation between the total amount of IFT signal within a flagellum and its length, with the exception of the short flagellum of dividing epimastigote cells where the new flagellum contains more IFT material in an accumulation at the distal end. Analysis of the *KIN2A2B<sup>RNAi</sup>* cell line in knockdown conditions suggests that the growth rate is controlled by active IFT transport in the growing flagellum. But in wild-type conditions, what controls the growth rate? The simplest explanation would be that the cell produces the right amount of IFT proteins at the synthesis level. However, the situation is more complex than that because IFT proteins are also abundant in the cytoplasm in addition to the flagellum, as shown by immunofluorescence experiments using antibodies against various IFT proteins and motors (Huet, Blisnick et al. 2014). In *Chlamydomonas*, cell fractionation revealed a 20- to 50-fold excess of IFT protein in the cell body compared to the flagellum (Ahmed, Gao et al. 2008) and in mammalian cells, immunofluorescence analyses showed the presence a large cell body pool for many IFT proteins (Follit, Xu et al. 2009).



To gain further insights about the control of IFT proteins, Jamin Jung in our lab has deleted one allele of the *IFT172* gene and examined the distribution of the protein. Western blots confirmed a diminution of 50% of the IFT172 signal but IFA revealed that the total signal in the flagellum and its base remained unchanged, in contrast to the cytoplasmic signal that was reduced (J. Jung et al., unpublished data). This implies that the concentration of IFT proteins is regulated at the level of the flagellum itself. A similar conclusion was reached by Silva *et al.* who depleted the amount of IFT22/RABL5 by RNAi in *Chlamydomonas* (Silva, Huang et al. 2012). This raises the question whether the correlation between IFT amount and flagellum length is passive or active, i.e. which one controls the other one? The knockdown of both kinesins supports an active control of length by the actual IFT train frequency in the flagellum but this has not been observed during the life cycle where the frequency is the same in all life cycle stages that could be examined.

At first sight, these results suggest that the flagellum growth rate is likely to be constant in all life cycle stages and that the only adjustment for controlling flagellum length used *in vivo* would be at the level of the timing of the locking event. However, this assumption is only valid in case the loading of IFT trains with tubulin is constant. In *Chlamydomonas*, large differences in loading have been observed between growing and mature flagella (Craft, Harris et al. 2015). Therefore, one could propose that the growth rate is controlled by tubulin loading and delivery at the distal end of the flagellum. As said above, it has not been possible so far to visualise fluorescent tubulin in trypanosomes and the hypothesis cannot currently be challenged.

## 2) What could be the mechanism(s) responsible for flagellum locking?

Our experimental evidence indicates that the axoneme of procyclic trypanosomes does not undergo turnover once it has matured. We could propose four mechanisms for flagellum locking: (1) axoneme modifications, (2) membrane



availability as a limiting factor, (3) modification of flagellar compartment accessibility or (4) modification of IFT train conformation. These different mechanisms could act independently or in synergy.

First, one could consider that the axoneme microtubules in the mature flagellum are heavily modified by post-translational modifications that prevent further elongation or shortening. Post-translational modifications of tubulin are known for ensuring high stability to the ciliary axoneme (Janke 2014). Acetylation is known to be important for stabilizing microtubules and indeed the deacetylation of axonemal tubulin by histone deacetylase 6 (HDAC6) promotes the disassembly of primary cilia (Pugacheva, Jablonski et al. 2007). The trypanosome axoneme is acetylated in parallel to its construction (Sasse and Gull 1988) and the acetylation of axonemal tubulin at the distal tip could prevent disassembly but it cannot explain the arrest of flagellum growth. However this sounds unlikely because mass-spectrometry showed that the entirety of flagellar  $\alpha$ -tubulin was acetylated (Schneider, Sherwin et al. 1987). To study the impact of tubulin acetylation in flagellum locking, we could develop and study an acetyl-transferase inducible RNAi mutant or overexpress the enzyme and evaluate the impact of the loss of flagellum acetylation in flagellum construction and length control. This would require a way to target the enzyme specifically to the flagellum to avoid interfering with microtubules in the corset.

Then, the addition of several glycine residues to C-terminal tail of tubulin has been proposed to be essential for controlling the length of primary cilia (Gadadhar, Dadi et al. 2017). However, glycylation has not been detected in trypanosomes samples neither by mass-spectrometry nor by antibodies (Schneider, Sherwin et al. 1987).

Tubulin polyglutamylation by generating multiple negative charges to the tubulin dimers may facilitates and regulates association with other proteins and therefore be involved in axoneme stabilisation in addition to modulating IFT trafficking. Whatever the type of possible tubulin post-translational modifications, we could propose to compare their profile in the new and the old flagellum. Indeed, doing immunofluorescence or western blot with specific antibodies of tubulin glutamylation or mass-spectrometry analysis could allow us to highlight specific profiles associated

### Cation/proton antiporter (Tb927.11.840.1)

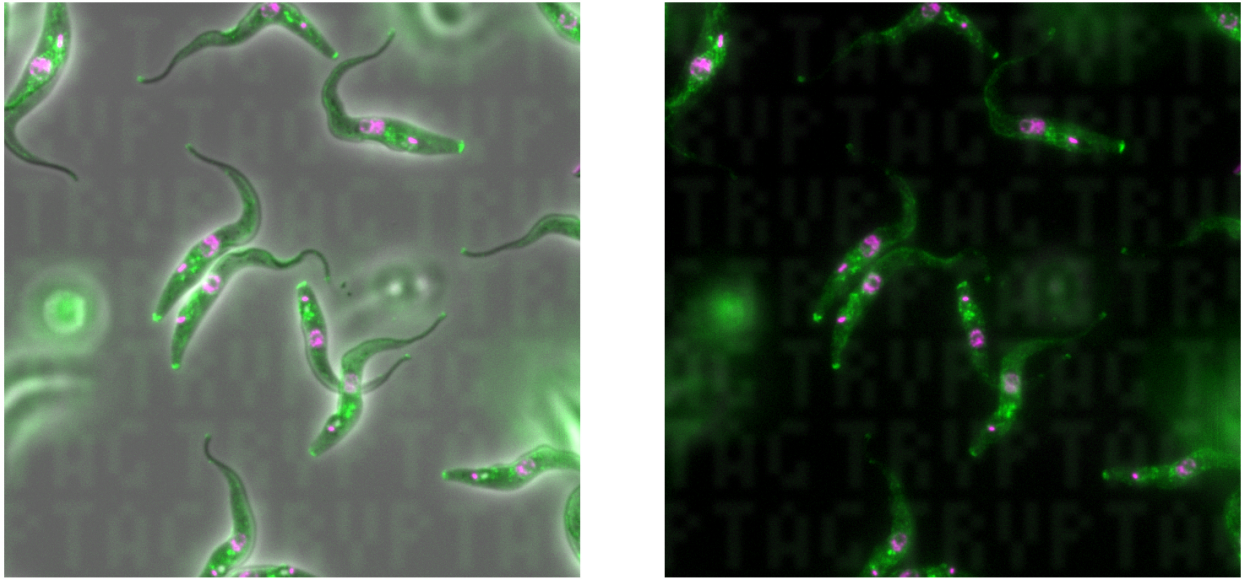


**Figure 39: Protein candidate for microtubule capping.**

Images extracted from Tryptag database. This example show one candidate protein presenting a flagellar tip and posterior end localization that could be associated to microtubule capping (Dean, Sunter et al. 2017).

to the flagellum status. For the moment it is not possible to separate new and old flagella, which prevent the realisation of this experiment.

The axoneme could be modified by the presence of microtubule capping proteins that would prevent tubulin assembly and disassembly. Such as capping proteins could be expressed at the final step of flagellum assembly and be transported to the distal tip to bind the (+) end of axonemal microtubules. FLAM8 is localized at the tip of the flagellum and is recruited in parallel to flagellum elongation. FLAM8 looks like a good candidate to function as cap for axonemal microtubules in the mature flagellum. However flagellum length looks normal, in both null and RNAi mutants of FLAM8 (Estefania Calvo Alvarez and Serge Bonnefoy, Unpublished data), demonstrating that FLAM8 does not lock the mature flagellum. Electron microscopy examination of the distal tip of the *T. brucei* flagellum does not indicate a clear structure at this level. However, the tip of the growing flagellum looks less organised than that of the mature flagellum (Hoog, Lacomble et al. 2014). These structural differences could reflect axoneme stabilisation and locking in the mature flagellum.

In the TrypTag database (Dean, Sunter et al. 2017) several unknown proteins localise to the tip of the flagellum and could represent good candidates to lock the axoneme by stabilising the (+) end of axonemal microtubules. For example the cation / proton antiporter encoded by gene Tb927.11.840.1 (Figure 39), is present at the distal tip of the old flagellum and in the posterior end of the cell where tubulin polymerisation occurs. This protein could be associated to the (+) end of microtubules and stabilised them.

Second, the other major component of the flagellum is its membrane. We could propose that flagellum length could be restricted by availability of membrane components. In *BILBO1<sup>RNAi</sup>* mutants (BILBO1 is a protein of the flagellar pocket collar), the flagellar pocket is absent and flagella are made too short (Bonhivers, Nowacki et al. 2008). We have evaluated the IFT trafficking in this strain after BILBO1 knockdown and IFT was still active (Data not shown). This demonstrates



that the construction of the shorter flagellum is not due to a defect in IFT trafficking. We propose that it could be due to a lower abundance of flagellar membrane components that will induce the production of shorter flagellum. Indeed, the absence of a flagellar pocket blocks endocytosis and exocytosis, which are essential to produce the flagellar membrane (Bonhivers, Nowacki et al. 2008). In these conditions the axoneme cannot grow further. This suggests that flagellum length depends on availability of flagellum membrane components. In wild-type conditions, flagellum membrane could also be the limiting factor if a fixed amount of flagellar membrane components are produced and could control flagellum length.

Third, the locking event could be associated to the flagellum base. All the elements necessary for flagellum elongation need to transit through the selective “flagellum gateway” at the transition zone. Therefore, one could imagine that specific modification of the flagellum base could prevent new flagellar components from entering the flagellum compartment and consequently lock the flagellum to a precise length. Finally the locking event could be at the level of the IFT trains if for instance the CH domain is modified and cannot transport tubulin. In both cases, this implies that there is no disassembly of the flagellum.

### **3) Could the “grow and lock” model apply to other stages of the *T. brucei* parasite cycle?**

The “grow and lock” model was based on the study of cultured procyclic trypanosomes. These cells construct flagella that ultimately always exhibit the same length (20  $\mu\text{m}$ ). BSF and attached epimastigotes (Epi-Epi division) also construct new flagella with always the same final length suggesting that the “grow and lock” model could also be relevant in these stages that possess flagellum with a final length of 24 $\mu\text{m}$  and 12 $\mu\text{m}$  respectively. However, this may not necessarily be the case in some other parasite stages as discussed here, such as the proventricular



dividing epimastigote that produces a new flagellum ten times shorter than the old one.

Could the “grow and lock” model explain formation of the very short new flagellum of the dividing epimastigote? The first possible explanation is a slower growth rate, as shown *in vitro* with the *KIN2A2B*<sup>RNAi</sup> following the reduction of IFT frequency. A lower abundance of IFT trains in the flagellum and / or to a reduced IFT frequency. This is not compatible with IFA results and monitoring of TdT::IFT81 concentration in live cells, which showed that IFT protein recruitment and train frequency in the short epimastigote flagellum are equivalent to what was observed in longer flagella. A modification of train loading could be responsible for the shorter flagellum but as said above we cannot visualise fluorescent tubulin, so this hypothesis cannot be challenged for the moment. Determination of the quantity of soluble tubulin also looks very difficult, since these dividing cells cannot be purified.

The second adjustment parameter of the “grow and lock” model is the timing of the division and of flagellum maturation. Possibly the short flagellum grows normally but the cell divides prematurely. To investigate this possibility, cells were treated with teniposide. Despite a long incubation, the new flagellum showed no sign of elongation. This indicates that the new flagellum could already be locked preventing further elongation. Is this associated to earlier flagellum maturation? This latter hypothesis was tested by using FLAM8 as a marker for flagellum maturation. We have quantified the total amount of fluorescence associated to the anti-FLAM8 antibody but we always observed weak signal at the distal tip of short epimastigote flagella compare to the old one. As previously said, flagellum length looks normal in both null and RNAi mutants of FLAM8 (Estefania Calvo Alvarez and Serge Bonnefoy, Unpublished data). This questions the relevance of using FLAM8 as a marker for flagellum maturation. It does not mean that the new flagellum of short epimastigote cells is not locked but rather calls for a search of new markers for maturation as discussed above.



## 4) Could other models explain flagellum length control?

We have seen that the “grow and lock” model could be relevant but it is worth also considering other models. First, reduced elongation could be due to the presence of a limiting pool of tubulin. Once all the blocks have been used, IFT trains would travel empty and could not contribute to flagellum elongation. In this case, the cells would not need to regulate IFT trafficking to modulate their flagellum length. Unfortunately, we cannot yet directly visualise tubulin incorporation due to the failure of tagged tubulin to incorporate trypanosome microtubules (Bastin, MacRae et al. 1999, Sheriff, Lim et al. 2014). Moreover, we can neither specifically isolate short epimastigotes from tsetse flies to evaluate the presence of a soluble pool of tubulin at this stage.

Second, a higher tubulin disassembly rate could be responsible for the production of shorter flagella. Indeed, if the disassembly rate is faster than the growth rate this could result in the production of shorter flagella. In trypanosomes, neo-synthesized tubulin is tyrosinated, and IFA performed on cultured procyclic cells with the YL1/2 antibody directed against tyrosinated tubulin highlights the tip of the new flagellum (Sherwin and Gull 1989). This was also observed at the distal tip of short epimastigotes (Rotureau, Subota et al. 2011) showing that tubulin was newly incorporated in these flagella. In this context tubulin incorporation that is not accompanied by flagellum elongation is arguing in favour of a high turnover.

In *Giardia* and *Leishmania*, the kinesin-13 (KIF13) protein is concentrated at the distal tip of the flagellum and possesses a depolymerising microtubule activity. Its overexpression in *Leishmania* produces flagellar shortening whereas its knockdown in *T. brucei* generates longer flagella (Blaineau, Tessier et al. 2007). However, another study of *KIF13<sup>RNAi</sup>* at the procyclic stage failed to reproduce this phenotype (Klaus Ersfeld data). KIF13 could be essential to regulate flagellum length but mostly in the short epimastigote. Overexpression at the distal tip of the short epimastigote



could prevent further elongation and explain the production of this short flagellum. In the future, it will be interesting to inactivate that gene and to evaluate the impact on flagellum formation in dividing epimastigote. Monitoring expression of a fluorescent version could also be informative, for example if the concentration at the distal tip of the new flagellum of dividing epimastigote was higher.

### 5) Discovery of a new stage during the parasite cycle.

During the parasite cycle, long mesocyclic trypomastigotes migrate from the posterior midgut to the proventriculus, differentiate into long epimastigotes almost concomitantly to the initiation of an asymmetric division (Vickerman 1985, Sharma, Peacock et al. 2008). During this differentiation, the emergence of the new flagellum was described to start in parallel to nucleus migration toward the posterior pole of the cell (Sharma, Peacock et al. 2008). Strikingly, after teniposide treatment of parasites isolated from tsetse flies, we have observed the emergence of a new flagellum in long mesocyclic trypomastigotes. This means that either the treatment induces a duplication of the basal bodies or that a new flagellum was already present before cell differentiation into epimastigotes and that basal bodies had *a fortiori* duplicated before nucleus migration. This second hypothesis was confirmed by FIB-SEM analysis of some proventricular parasites where 63% of mesocyclic trypomastigotes were presenting a short new flagellum that did not extend beyond the flagellar pocket (in total n=22) (Moara Lemos, unpublished data). This is supported by IFA data using the anti-FTZC antibody as a marker of the transition zone and the anti-IFT22 antibody revealing the presence of two spots at the base and consequently two transition zones in mesocyclic stage (Data not shown). These results demonstrate that generation of the new flagellum of the dividing proventricular epimastigote already initiates in mesocyclic trypomastigotes, i.e. earlier than previously described (Sharma, Peacock et al. 2008). This means that the new flagellum is maintained in a



short length conformation for longer periods than expected, which is an additional argument for the existence of a specific mechanisms implicated to restrict its length.

## **6) Flagellum length control during Epi-trypo division.**

Another asymmetric division occurs in the tsetse salivary glands to produce the infective metacyclic form. In contrast to the dividing epimastigote, this asymmetric division (Epi-Trypo) is characterised by the production of a new flagellum that is longer than the old one (Rotureau, Subota et al. 2012). So far, we did not investigate this division due to the difficulty to obtain a sufficient number of infected salivary glands and to the relatively low abundance of these Epi-Trypo dividing cells in infected salivary glands. Therefore, all the hypotheses previously discussed remain open to explain flagellum length control in this asymmetric division.

First, a longer flagellum could be produced by an increase of the flagellum growth rate or by a delay of the locking event in association to cell division or flagellum maturation, allowing the new flagellum to grow longer. The increase of flagellum growth rate could be associated to a modification of IFT protein availability during flagellum construction. The production of a higher amount of IFT proteins would therefore be associated to the construction of a longer flagellum. Second, the production of higher initial amounts of flagellar components could also explain the construction of a new longer flagellum, arguing for the limiting pool model. The validity of this model relies on the timing of cell division. Third based on the “balance point” model, a diminution of tubulin disassembly rate at the distal tip and / or a higher axonemal stability could also explain the production of longer flagella.



### III. Conclusion and perspectives.

---

In a recent paper, IFT-based tubulin transport has been attenuated by altering the tubulin binding sites in IFT81 and IFT74. Despite a strong reduction in transported tubulin rates, the length of the axoneme was only moderately reduced. The authors propose that ~ 80% of the axonemal tubulin content could enter the flagellum by simple diffusion and that IFT trains would rather be important to concentrate the tubulin in the flagellar compartment as well as to favour its polymerization {Harris, <https://doi.org/10.1101/268573>}. This important discovery raises the question of the role of IFT in axoneme construction and in length control.

IFT could be important to transport other axonemal components than tubulin especially those present as a large complexes such as Radial Spokes or Outer Dynein Arms (Qin, Diener et al. 2004). Moreover, IFT trains could be essential to transport tubulin-capping proteins at the distal tip of the flagellum. If these proteins were important to lock the flagellum at its final length, they would need to be transported rapidly at the distal tip and this could be achieved by IFT. Due to the inter-species differences on IFT observed especially between *Chlamydomonas* and *T. brucei*, it could be important to implement the experiment made by Harris *et al.* in other model organisms as well as to evaluate the role of tubulin diffusion in the axoneme construction and if IFT is only implicated in the import of material in flagellar compartment by crossing the ciliary gateway of the transition zone.

In human, flagella and cilia are present at the surface of different tissues and exhibit specific structural and functional characteristics. Some ciliopathies are associated to mutation in the same *IFT* genes but phenotypes are different. For example, Sensenbrenner syndrome is a ciliopathy associated to mutations in at least *IFT122* and *IFT43* genes and patient present only skeletal anomalies and live almost normally. While Bardet-Biedl syndrome is associated to mutations in the same



## ***Discussion***

genes, multiple organs are affected resulting in more severe pathology (Halbritter, Bizet et al. 2013). Finally, Jeune syndrome presents very severe symptoms mostly fatal in the first years of life (Beales, Bland et al. 2007). In these three ciliopathies IFT genes are affected but the type of mutation is different and the impact in cilia and flagella and their function is variable. This reveals that IFT and IFT proteins have not necessarily the same role in all the cilia present in human body. This diversity is likely to be also true at the level of the control of ciliary length. Studies in *Chlamydomonas* have brought great insights in the comprehension of cilia and flagella, particularly for IFT but they do not really take into account the diversity of these organelles. Our work on trypanosomes brings a new look by showing the diversity of IFT trafficking and proposing a new model for flagellum length control. The “grow and lock” model could explain length control in the stable flagellum of sperm cells. The model could also be significant for primary cilia that are disassembled following a decapitation (Phua, Chiba et al. 2017) during the cell cycle, in case would be a reversible locking. This highlights the importance to study a diversity of model organisms (Vincensini, Blisnick et al. 2011) and remind us to not consider that mechanisms and models proposed in one organism are valid for all the other situations.





# References

## ***References***

## 1) Text references

Absalon, S., T. Blisnick, M. Bonhivers, L. Kohl, N. Cayet, G. Toutirais, J. Buisson, D. Robinson and P. Bastin (2008). "Flagellum elongation is required for correct structure, orientation and function of the flagellar pocket in *Trypanosoma brucei*." J Cell Sci **121**(Pt 22): 3704-3716.

Absalon, S., T. Blisnick, L. Kohl, G. Toutirais, G. Dore, D. Julkowska, A. Tavenet and P. Bastin (2008). "Intraflagellar transport and functional analysis of genes required for flagellum formation in trypanosomes." Mol Biol Cell **19**(3): 929-944.

Absalon, S., L. Kohl, C. Branche, T. Blisnick, G. Toutirais, F. Rusconi, J. Cosson, M. Bonhivers, D. Robinson and P. Bastin (2007). "Basal body positioning is controlled by flagellum formation in *Trypanosoma brucei*." PLoS One **2**(5): e437.

Adhiambo, C., T. Blisnick, G. Toutirais, E. Delannoy and P. Bastin (2009). "A novel function for the atypical small G protein Rab-like 5 in the assembly of the trypanosome flagellum." J Cell Sci **122**(Pt 6): 834-841.

Adhiambo, C., J. D. Forney, D. J. Asai and J. H. LeBowitz (2005). "The two cytoplasmic dynein-2 isoforms in *Leishmania mexicana* perform separate functions." Mol Biochem Parasitol **143**(2): 216-225.

Afzelius, B. A. (1976). "A human syndrome caused by immotile cilia." Science **193**(4250): 317-319.

Ahmed, N. T., C. Gao, B. F. Lucker, D. G. Cole and D. R. Mitchell (2008). "ODA16 aids axonemal outer row dynein assembly through an interaction with the intraflagellar transport machinery." J Cell Biol **183**(2): 313-322.

Albisetti, A., C. Florimond, N. Landrein, K. Vidilaseris, M. Eggenspieler, J. Lesigang, G. Dong, D. R. Robinson and M. Bonhivers (2017). "Interaction between the flagellar pocket collar and the hook complex via a novel microtubule-binding protein in *Trypanosoma brucei*." PLoS Pathog **13**(11): e1006710.

Angelopoulos, E. (1970). "Pellicular microtubules in the family Trypanosomatidae." J Protozool **17**(1): 39-51.

## References

Avidor-Reiss, T., A. M. Maer, E. Koundakjian, A. Polyanovsky, T. Keil, S. Subramaniam and C. S. Zuker (2004). "Decoding cilia function: defining specialized genes required for compartmentalized cilia biogenesis." Cell **117**(4): 527-539.

Baccetti, B. (1986). "Evolutionary trends in sperm structure." Comp Biochem Physiol A Comp Physiol **85**(1): 29-36.

Baker, N., H. P. de Koning, P. Maser and D. Horn (2013). "Drug resistance in African trypanosomiasis: the melarsoprol and pentamidine story." Trends Parasitol **29**(3): 110-118.

Balyeidhusa, A. S., F. A. Kironde and J. C. Enyaru (2012). "Apparent lack of a domestic animal reservoir in Gambiense sleeping sickness in northwest Uganda." Vet Parasitol **187**(1-2): 157-167.

Banizs, B., M. M. Pike, C. L. Millican, W. B. Ferguson, P. Komlosi, J. Sheetz, P. D. Bell, E. M. Schwiebert and B. K. Yoder (2005). "Dysfunctional cilia lead to altered ependyma and choroid plexus function, and result in the formation of hydrocephalus." Development **132**(23): 5329-5339.

Barr, M. M. and P. W. Sternberg (1999). "A polycystic kidney-disease gene homologue required for male mating behaviour in *C. elegans*." Nature **401**(6751): 386-389.

Barsel, S. E., D. E. Wexler and P. A. Lefebvre (1988). "Genetic analysis of long-flagella mutants of *Chlamydomonas reinhardtii*." Genetics **118**(4): 637-648.

Bastin, P., Z. Bagherzadeh, K. R. Matthews and K. Gull (1996). "A novel epitope tag system to study protein targeting and organelle biogenesis in *Trypanosoma brucei*." Mol Biochem Parasitol **77**(2): 235-239.

Bastin, P., T. H. MacRae, S. B. Francis, K. R. Matthews and K. Gull (1999). "Flagellar morphogenesis: protein targeting and assembly in the paraflagellar rod of trypanosomes." Mol Cell Biol **19**(12): 8191-8200.

Bastin, P., T. Sherwin and K. Gull (1998). "Paraflagellar rod is vital for trypanosome motility." Nature **391**(6667): 548.

Beales, P. L., E. Bland, J. L. Tobin, C. Bacchelli, B. Tuysuz, J. Hill, S. Rix, C. G. Pearson, M. Kai, J. Hartley, C. Johnson, M. Irving, N. Elcioglu, M. Winey, M. Tada

## References

and P. J. Scambler (2007). "IFT80, which encodes a conserved intraflagellar transport protein, is mutated in Jeune asphyxiating thoracic dystrophy." *Nat Genet* **39**(6): 727-729.

Benchimol, M., B. Piva, L. Campanati and W. de Souza (2004). "Visualization of the funis of *Giardia lamblia* by high-resolution field emission scanning electron microscopy--new insights." *J Struct Biol* **147**(2): 102-115.

Berriman, M., E. Ghedin, C. Hertz-Fowler, G. Blandin, H. Renauld, D. C. Bartholomeu, N. J. Lennard, E. Caler, N. E. Hamlin, B. Haas, U. Bohme, L. Hannick, M. A. Aslett, J. Shallom, L. Marcello, L. Hou, B. Wickstead, U. C. Alsmark, C. Arrowsmith, R. J. Atkin, A. J. Barron, F. Bringaud, K. Brooks, M. Carrington, I. Cherevach, T. J. Chillingworth, C. Churcher, L. N. Clark, C. H. Corton, A. Cronin, R. M. Davies, J. Doggett, A. Djikeng, T. Feldblyum, M. C. Field, A. Fraser, I. Goodhead, Z. Hance, D. Harper, B. R. Harris, H. Hauser, J. Hostetler, A. Ivens, K. Jagels, D. Johnson, J. Johnson, K. Jones, A. X. Kerhornou, H. Koo, N. Larke, S. Landfear, C. Larkin, V. Leech, A. Line, A. Lord, A. Macleod, P. J. Mooney, S. Moule, D. M. Martin, G. W. Morgan, K. Mungall, H. Norbertczak, D. Ormond, G. Pai, C. S. Peacock, J. Peterson, M. A. Quail, E. Rabinowitsch, M. A. Rajandream, C. Reitter, S. L. Salzberg, M. Sanders, S. Schobel, S. Sharp, M. Simmonds, A. J. Simpson, L. Tallon, C. M. Turner, A. Tait, A. R. Tivey, S. Van Aken, D. Walker, D. Wanless, S. Wang, B. White, O. White, S. Whitehead, J. Woodward, J. Wortman, M. D. Adams, T. M. Embley, K. Gull, E. Ullu, J. D. Barry, A. H. Fairlamb, F. Opperdoes, B. G. Barrell, J. E. Donelson, N. Hall, C. M. Fraser, S. E. Melville and N. M. El-Sayed (2005). "The genome of the African trypanosome *Trypanosoma brucei*." *Science* **309**(5733): 416-422.

Berthier, D., S. F. Breniere, R. Bras-Goncalves, J. L. Lemesre, V. Jamonneau, P. Solano, V. Lejon, S. Thevenon and B. Bucheton (2016). "Tolerance to Trypanosomatids: A Threat, or a Key for Disease Elimination?" *Trends Parasitol* **32**(2): 157-168.

Bhogaraju, S., L. Cajanek, C. Fort, T. Blisnick, K. Weber, M. Taschner, N. Mizuno, S. Lamla, P. Bastin, E. A. Nigg and E. Lorentzen (2013). "Molecular basis of tubulin transport within the cilium by IFT74 and IFT81." *Science* **341**(6149): 1009-1012.

Blaineau, C., M. Tessier, P. Dubessay, L. Tasse, L. Crobu, M. Pages and P. Bastien (2007). "A novel microtubule-depolymerizing kinesin involved in length control of a eukaryotic flagellum." *Curr Biol* **17**(9): 778-782.

Blisnick, T., J. Buisson, S. Absalon, A. Marie, N. Cayet and P. Bastin (2014). "The intraflagellar transport dynein complex of trypanosomes is made of a heterodimer of

## References

dynein heavy chains and of light and intermediate chains of distinct functions." Mol Biol Cell **25**(17): 2620-2633.

Bonhivers, M., S. Nowacki, N. Landrein and D. R. Robinson (2008). "Biogenesis of the trypanosome endo-exocytotic organelle is cytoskeleton mediated." PLoS Biol **6**(5): e105.

Brancati, F., M. Iannicelli, L. Travaglini, A. Mazzotta, E. Bertini, E. Boltshauser, S. D'Arrigo, F. Emma, E. Fazzi, R. Gallizzi, M. Gentile, D. Loncarevic, V. Mejaski-Bosnjak, C. Pantaleoni, L. Rigoli, C. D. Salpietro, S. Signorini, G. R. Stringini, A. Verloes, D. Zablocka, B. Dallapiccola, J. G. Gleeson, E. M. Valente and J. S. G. International (2009). "MKS3/TMEM67 mutations are a major cause of COACH Syndrome, a Joubert Syndrome related disorder with liver involvement." Hum Mutat **30**(2): E432-442.

Branche, C., L. Kohl, G. Toutirais, J. Buisson, J. Cosson and P. Bastin (2006). "Conserved and specific functions of axoneme components in trypanosome motility." J Cell Sci **119**(Pt 16): 3443-3455.

Brazelton, W. J., C. D. Amundsen, C. D. Silflow and P. A. Lefebvre (2001). "The bld1 mutation identifies the Chlamydomonas osm-6 homolog as a gene required for flagellar assembly." Curr Biol **11**(20): 1591-1594.

Briggs, L. J., P. G. McKean, A. Baines, F. Moreira-Leite, J. Davidge, S. Vaughan and K. Gull (2004). "The flagella connector of Trypanosoma brucei: an unusual mobile transmembrane junction." J Cell Sci **117**(Pt 9): 1641-1651.

Broadhead, R., H. R. Dawe, H. Farr, S. Griffiths, S. R. Hart, N. Portman, M. K. Shaw, M. L. Ginger, S. J. Gaskell, P. G. McKean and K. Gull (2006). "Flagellar motility is required for the viability of the bloodstream trypanosome." Nature **440**(7081): 224-227.

Brown, J. M. and G. B. Witman (2014). "Cilia and Diseases." Bioscience **64**(12): 1126-1137.

Bruce, D. (1895). Preliminary report on the tsetse fly disease or nagana in Zululand.

Brun, R., J. Blum, F. Chappuis and C. Burri (2010). "Human African trypanosomiasis." Lancet **375**(9709): 148-159.

## References

- Brun, R. and Schonemberger (1979). "Cultivation and in vitro cloning or procyclic culture forms of *Trypanosoma brucei* in a semi-defined medium. Short communication." Acta Trop **36**(3): 289-292.
- Buisson, J., N. Chenouard, T. Lagache, T. Blisnick, J. C. Olivo-Marin and P. Bastin (2013). "Intraflagellar transport proteins cycle between the flagellum and its base." J Cell Sci **126**(Pt 1): 327-338.
- Butikofer, P., S. Ruepp, M. Boschung and I. Roditi (1997). "'GPEET' procyclin is the major surface protein of procyclic culture forms of *Trypanosoma brucei brucei* strain 427." Biochem J **326** ( Pt 2): 415-423.
- Caljon, G., N. Van Reet, C. De Trez, M. Vermeersch, D. Perez-Morga and J. Van Den Abbeele (2016). "The Dermis as a Delivery Site of *Trypanosoma brucei* for Tsetse Flies." PLoS Pathog **12**(7): e1005744.
- Callaini, G., W. G. Whitfield and M. G. Riparbelli (1997). "Centriole and centrosome dynamics during the embryonic cell cycles that follow the formation of the cellular blastoderm in *Drosophila*." Exp Cell Res **234**(1): 183-190.
- Calvert, P. D., K. J. Strissel, W. E. Schiesser, E. N. Pugh, Jr. and V. Y. Arshavsky (2006). "Light-driven translocation of signaling proteins in vertebrate photoreceptors." Trends Cell Biol **16**(11): 560-568.
- Capewell, P., C. Cren-Travaille, F. Marchesi, P. Johnston, C. Clucas, R. A. Benson, T. A. Gorman, E. Calvo-Alvarez, A. Crouzols, G. Jouvion, V. Jamonneau, W. Weir, M. L. Stevenson, K. O'Neill, A. Cooper, N. K. Swar, B. Bucheton, D. M. Ngoyi, P. Garside, B. Rotureau and A. MacLeod (2016). "The skin is a significant but overlooked anatomical reservoir for vector-borne African trypanosomes." Elife **5**.
- Casanova, M., F. de Monbrison, J. van Dijk, C. Janke, M. Pages and P. Bastien (2015). "Characterisation of polyglutamylases in trypanosomatids." Int J Parasitol **45**(2-3): 121-132.
- Cavalier-Smith, T. (1974). "Basal body and flagellar development during the vegetative cell cycle and the sexual cycle of *Chlamydomonas reinhardtii*." J Cell Sci **16**(3): 529-556.
- Chapman, A. B. and R. W. Schrier (1991). "Pathogenesis of hypertension in autosomal dominant polycystic kidney disease." Semin Nephrol **11**(6): 653-660.

## References

- Checchi, F., J. A. Filipe, M. P. Barrett and D. Chandramohan (2008). "The natural progression of Gambiense sleeping sickness: what is the evidence?" PLoS Negl Trop Dis **2**(12): e303.
- Chien, A., S. M. Shih, R. Bower, D. Tritschler, M. E. Porter and A. Yildiz (2017). "Dynamics of the IFT machinery at the ciliary tip." Elife **6**.
- Chilvers, M. (2003). "Ciliary beat pattern is associated with specific ultrastructural defects in primary ciliary dyskinesia." Journal of Allergy and Clinical Immunology **112**(3): 518-524.
- Chretien, D., B. Buendia, S. D. Fuller and E. Karsenti (1997). "Reconstruction of the centrosome cycle from cryoelectron micrographs." J Struct Biol **120**(2): 117-133.
- Clayton, C. E. (1999). "Genetic manipulation of kinetoplastida." Parasitol Today **15**(9): 372-378.
- Cole, D. G., S. W. Chinn, K. P. Wedaman, K. Hall, T. Vuong and J. M. Scholey (1993). "Novel heterotrimeric kinesin-related protein purified from sea urchin eggs." Nature **366**(6452): 268-270.
- Cole, D. G., D. R. Diener, A. L. Himelblau, P. L. Beech, J. C. Fuster and J. L. Rosenbaum (1998). "Chlamydomonas kinesin-II-dependent intraflagellar transport (IFT): IFT particles contain proteins required for ciliary assembly in *Caenorhabditis elegans* sensory neurons." J Cell Biol **141**(4): 993-1008.
- Collet, J., C. A. Spike, E. A. Lundquist, J. E. Shaw and R. K. Herman (1998). "Analysis of *osm-6*, a gene that affects sensory cilium structure and sensory neuron function in *Caenorhabditis elegans*." Genetics **148**(1): 187-200.
- Cooper, R., A. R. de Jesus and G. A. Cross (1993). "Deletion of an immunodominant *Trypanosoma cruzi* surface glycoprotein disrupts flagellum-cell adhesion." J Cell Biol **122**(1): 149-156.
- Cortellino, S., C. Wang, B. Wang, M. R. Bassi, E. Caretti, D. Champeval, A. Calmont, M. Jarnik, J. Burch, K. S. Zaret, L. Larue and A. Bellacosa (2009). "Defective ciliogenesis, embryonic lethality and severe impairment of the Sonic Hedgehog pathway caused by inactivation of the mouse complex A intraflagellar transport gene *lft122/Wdr10*, partially overlapping with the DNA repair gene *Med1/Mbd4*." Dev Biol **325**(1): 225-237.

## References

Coutton, C., A. S. Vargas, A. Amiri-Yekta, Z. E. Kherraf, S. F. Ben Mustapha, P. Le Tanno, C. Wambergue-Legrand, T. Karaouzene, G. Martinez, S. Crouzy, A. Daneshpour, S. H. Hosseini, V. Mitchell, L. Halouani, O. Marrakchi, M. Makni, H. Latrous, M. Kharouf, J. F. Deleuze, A. Boland, S. Hennebicq, V. Satre, P. S. Jouk, N. Thierry-Mieg, B. Conne, D. Dacheux, N. Landrein, A. Schmitt, L. Stouvenel, P. Lores, E. El Khouri, S. P. Bottari, J. Faure, J. P. Wolf, K. Pernet-Gallay, J. Escoffier, H. Gourabi, D. R. Robinson, S. Nef, E. Dulioust, R. Zouari, M. Bonhivers, A. Toure, C. Arnoult and P. F. Ray (2018). "Mutations in CFAP43 and CFAP44 cause male infertility and flagellum defects in *Trypanosoma* and human." Nat Commun **9**(1): 686.

Craft, J. M., J. A. Harris, S. Hyman, P. Kner and K. F. Lehtreck (2015). "Tubulin transport by IFT is upregulated during ciliary growth by a cilium-autonomous mechanism." J Cell Biol **208**(2): 223-237.

Craige, B., C. C. Tsao, D. R. Diener, Y. Hou, K. F. Lehtreck, J. L. Rosenbaum and G. B. Witman (2010). "CEP290 tethers flagellar transition zone microtubules to the membrane and regulates flagellar protein content." J Cell Biol **190**(5): 927-940.

Cross, G. A. (1975). "Identification, purification and properties of clone-specific glycoprotein antigens constituting the surface coat of *Trypanosoma brucei*." Parasitology **71**(3): 393-417.

Crouse, J. A., V. S. Lopes, J. T. Sanagustin, B. T. Keady, D. S. Williams and G. J. Pazour (2014). "Distinct functions for IFT140 and IFT20 in opsin transport." Cytoskeleton (Hoboken) **71**(5): 302-310.

Dacheux, D., N. Landrein, M. Thonnus, G. Gilbert, A. Sahin, H. Wodrich, D. R. Robinson and M. Bonhivers (2012). "A MAP6-related protein is present in protozoa and is involved in flagellum motility." PLoS One **7**(2): e31344.

David Papermasrer, B. G. S., and Joseph C. Desharse (1985). "Vesicular Transport of Newly Synthesized Opsin fromn the Golgi Apparatus toward the Rod Outer Segment."

Dawe, H. R., H. Farr and K. Gull (2007). "Centriole/basal body morphogenesis and migration during ciliogenesis in animal cells." J Cell Sci **120**(Pt 1): 7-15.

de Kruijff, B. and R. A. Demel (1974). "Polyene antibiotic-sterol interactions in membranes of *Acholeplasma laidlawii* cells and lecithin liposomes. 3. Molecular structure of the polyene antibiotic-cholesterol complexes." Biochim Biophys Acta **339**(1): 57-70.

## References

- Dean, S., J. D. Sunter and R. J. Wheeler (2017). "TrypTag.org: A Trypanosome Genome-wide Protein Localisation Resource." Trends Parasitol **33**(2): 80-82.
- Deane, J. (2001). "Localization of IFT52 identifies BB transitional fibers as the docking site for IFT particles." Current Biology.
- Deane, J. A., D. G. Cole, E. S. Seeley, D. R. Diener and J. L. Rosenbaum (2001). "Localization of intraflagellar transport protein IFT52 identifies basal body transitional fibers as the docking site for IFT particles." Curr Biol **11**(20): 1586-1590.
- Demonchy, R., T. Blisnick, C. Deprez, G. Toutirais, C. Loussert, W. Marande, P. Grellier, P. Bastin and L. Kohl (2009). "Kinesin 9 family members perform separate functions in the trypanosome flagellum." J Cell Biol **187**(5): 615-622.
- den Hollander, A. I., R. K. Koenekoop, S. Yzer, I. Lopez, M. L. Arends, K. E. Voeselek, M. N. Zonneveld, T. M. Strom, T. Meitinger, H. G. Brunner, C. B. Hoyng, L. I. van den Born, K. Rohrschneider and F. P. Cremers (2006). "Mutations in the CEP290 (NPHP6) gene are a frequent cause of Leber congenital amaurosis." Am J Hum Genet **79**(3): 556-561.
- Dentler, W. (2005). "Intraflagellar transport (IFT) during assembly and disassembly of Chlamydomonas flagella." J Cell Biol **170**(4): 649-659.
- DiBella, L. M., M. Sakato, R. S. Patel-King, G. J. Pazour and S. M. King (2004). "The LC7 light chains of Chlamydomonas flagellar dyneins interact with components required for both motor assembly and regulation." Mol Biol Cell **15**(10): 4633-4646.
- Dishinger, J. F., H. L. Kee, P. M. Jenkins, S. Fan, T. W. Hurd, J. W. Hammond, Y. N. Truong, B. Margolis, J. R. Martens and K. J. Verhey (2010). "Ciliary entry of the kinesin-2 motor KIF17 is regulated by importin-beta2 and RanGTP." Nat Cell Biol **12**(7): 703-710.
- Dujardin, F. (1841). "Histoire naturelle des zoophytes infusoires, comprenant la physiologie et la classification de ces animaux. ." Roret, Paris **2 vol.pp.**
- Elmendorf, H. G., S. C. Dawson and J. M. McCaffery (2003). "The cytoskeleton of Giardia lamblia." International Journal for Parasitology **33**(1): 3-28.

## References

- Engel, B. D., W. B. Ludington and W. F. Marshall (2009). "Intraflagellar transport particle size scales inversely with flagellar length: revisiting the balance-point length control model." J Cell Biol **187**(1): 81-89.
- Engstler, M., T. Pfohl, S. Herminghaus, M. Boshart, G. Wiegertjes, N. Heddergott and P. Overath (2007). "Hydrodynamic flow-mediated protein sorting on the cell surface of trypanosomes." Cell **131**(3): 505-515.
- Fan, Z. C., R. H. Behal, S. Geimer, Z. Wang, S. M. Williamson, H. Zhang, D. G. Cole and H. Qin (2010). "Chlamydomonas IFT70/CrDYF-1 is a core component of IFT particle complex B and is required for flagellar assembly." Mol Biol Cell **21**(15): 2696-2706.
- Fawcett, D. W. (1975). "The mammalian spermatozoon." Dev Biol **44**(2): 394-436.
- Ferguson, M. A., S. W. Homans, R. A. Dwek and T. W. Rademacher (1988). "Glycosyl-phosphatidylinositol moiety that anchors *Trypanosoma brucei* variant surface glycoprotein to the membrane." Science **239**(4841 Pt 1): 753-759.
- Filice, F. P. (1952). Studies on the cytology and life history of a Giardia from the laboratory rat.
- Follit, J. A., R. A. Tuft, K. E. Fogarty and G. J. Pazour (2006). "The intraflagellar transport protein IFT20 is associated with the Golgi complex and is required for cilia assembly." Mol Biol Cell **17**(9): 3781-3792.
- Follit, J. A., F. Xu, B. T. Keady and G. J. Pazour (2009). "Characterization of mouse IFT complex B." Cell Motil Cytoskeleton **66**(8): 457-468.
- Fort, C., S. Bonnefoy, L. Kohl and P. Bastin (2016). "Intraflagellar transport is required for the maintenance of the trypanosome flagellum composition but not its length." J Cell Sci **129**(15): 3026-3041.
- Franco, J. R., P. P. Simarro, A. Diarra and J. G. Jannin (2014). "Epidemiology of human African trypanosomiasis." Clin Epidemiol **6**: 257-275.
- Friend, D. S. (1966). "The fine structure of *Giardia muris*." J Cell Biol **29**(2): 317-332.

## References

- Frolov, A. O. (1994). "[The classification of the morphological forms of flagellates in the family Trypanosomatidae]." Parazitologiya **28**(4): 261-269.
- Funabashi, T., Y. Katoh, S. Michisaka, M. Terada, M. Sugawa and K. Nakayama (2017). "Ciliary entry of KIF17 is dependent on its binding to the IFT-B complex via IFT46-IFT56 as well as on its nuclear localization signal." Mol Biol Cell **28**(5): 624-633.
- Gadadhar, S., H. Dadi, S. Bodakuntla, A. Schnitzler, I. Bieche, F. Rusconi and C. Janke (2017). "Tubulin glycylation controls primary cilia length." J Cell Biol **216**(9): 2701-2713.
- Gallo, J. M., E. Precigout and J. Schrevel (1988). "Subcellular sequestration of an antigenically unique beta-tubulin." Cell Motil Cytoskeleton **9**(2): 175-183.
- Garcia-Gonzalo, F. R. and J. F. Reiter (2017). "Open Sesame: How Transition Fibers and the Transition Zone Control Ciliary Composition." Cold Spring Harb Perspect Biol **9**(2).
- Gibbons, B. H., D. J. Asai, W. J. Tang, T. S. Hays and I. R. Gibbons (1994). "Phylogeny and expression of axonemal and cytoplasmic dynein genes in sea urchins." Mol Biol Cell **5**(1): 57-70.
- Gibbons, I. R. and A. J. Rowe (1965). "Dynein: A Protein with Adenosine Triphosphatase Activity from Cilia." Science **149**(3682): 424-426.
- Gilula, N. B. (1972). "THE CILIARY NECKLACE: A Ciliary Membrane Specialization." The Journal of Cell Biology **53**(2): 494-509.
- Ginger, M. L., P. W. Collingridge, R. W. Brown, R. Sproat, M. K. Shaw and K. Gull (2013). "Calmodulin is required for paraflagellar rod assembly and flagellum-cell body attachment in trypanosomes." Protist **164**(4): 528-540.
- Goehring, N. W. and A. A. Hyman (2012). "Organelle growth control through limiting pools of cytoplasmic components." Curr Biol **22**(9): R330-339.
- Goodenough, U. W. (1989). "Cyclic AMP enhances the sexual agglutinability of *Chlamydomonas flagella*." The Journal of Cell Biology **109**(1): 247-252.

## References

- Goodenough, U. W. and J. E. Heuser (1985). "Substructure of inner dynein arms, radial spokes, and the central pair/projection complex of cilia and flagella." J Cell Biol **100**(6): 2008-2018.
- Graser, S., Y. D. Stierhof, S. B. Lavoie, O. S. Gassner, S. Lamla, M. Le Clech and E. A. Nigg (2007). "Cep164, a novel centriole appendage protein required for primary cilium formation." J Cell Biol **179**(2): 321-330.
- Griffiths, S., N. Portman, P. R. Taylor, S. Gordon, M. L. Ginger and K. Gull (2007). "RNA interference mutant induction in vivo demonstrates the essential nature of trypanosome flagellar function during mammalian infection." Eukaryot Cell **6**(7): 1248-1250.
- Halbritter, J., A. A. Bizet, M. Schmidts, J. D. Porath, D. A. Braun, H. Y. Gee, A. M. McInerney-Leo, P. Krug, E. Filhol, E. E. Davis, R. Airik, P. G. Czarnecki, A. M. Lehman, P. Trnka, P. Nitschke, C. Bole-Feysot, M. Schueler, B. Knebelmann, S. Burtey, A. J. Szabo, K. Tory, P. J. Leo, B. Gardiner, F. A. McKenzie, A. Zankl, M. A. Brown, J. L. Hartley, E. R. Maher, C. Li, M. R. Leroux, P. J. Scambler, S. H. Zhan, S. J. Jones, H. Kayserili, B. Tuysuz, K. N. Moorani, A. Constantinescu, I. D. Krantz, B. S. Kaplan, J. V. Shah, U. K. Consortium, T. W. Hurd, D. Doherty, N. Katsanis, E. L. Duncan, E. A. Otto, P. L. Beales, H. M. Mitchison, S. Saunier and F. Hildebrandt (2013). "Defects in the IFT-B component IFT172 cause Jeune and Mainzer-Saldino syndromes in humans." Am J Hum Genet **93**(5): 915-925.
- Han, Y. G., B. H. Kwok and M. J. Kernan (2003). "Intraflagellar transport is required in Drosophila to differentiate sensory cilia but not sperm." Curr Biol **13**(19): 1679-1686.
- Hao, L., M. Thein, I. Brust-Mascher, G. Civelekoglu-Scholey, Y. Lu, S. Acar, B. Prevo, S. Shaham and J. M. Scholey (2011). "Intraflagellar transport delivers tubulin isotypes to sensory cilium middle and distal segments." Nat Cell Biol **13**(7): 790-798.
- Heddergott, N., T. Kruger, S. B. Babu, A. Wei, E. Stellamanns, S. Uppaluri, T. Pfohl, H. Stark and M. Engstler (2012). "Trypanosome motion represents an adaptation to the crowded environment of the vertebrate bloodstream." PLoS Pathog **8**(11): e1003023.
- Hill, K. L. (2003). "Biology and Mechanism of Trypanosome Cell Motility." Eukaryotic Cell **2**(2): 200-208.

## References

- Hong, S. R., C. L. Wang, Y. S. Huang, Y. C. Chang, Y. C. Chang, G. V. Pusapati, C. Y. Lin, N. Hsu, H. C. Cheng, Y. C. Chiang, W. E. Huang, N. C. Shaner, R. Rohatgi, T. Inoue and Y. C. Lin (2018). "Spatiotemporal manipulation of ciliary glutamylation reveals its roles in intraciliary trafficking and Hedgehog signaling." Nat Commun **9**(1): 1732.
- Hoog, J. L., S. Lacomble, C. Bouchet-Marquis, L. Briggs, K. Park, A. Hoenger and K. Gull (2016). "3D Architecture of the *Trypanosoma brucei* Flagella Connector, a Mobile Transmembrane Junction." PLoS Negl Trop Dis **10**(1): e0004312.
- Hoog, J. L., S. Lacomble, E. T. O'Toole, A. Hoenger, J. R. McIntosh and K. Gull (2014). "Modes of flagellar assembly in *Chlamydomonas reinhardtii* and *Trypanosoma brucei*." Elife **3**: e01479.
- Horn, D. (2014). "Antigenic variation in African trypanosomes." Mol Biochem Parasitol **195**(2): 123-129.
- Hou, Y., G. J. Pazour and G. B. Witman (2004). "A dynein light intermediate chain, D1bLIC, is required for retrograde intraflagellar transport." Mol Biol Cell **15**(10): 4382-4394.
- Hou, Y., H. Qin, J. A. Follit, G. J. Pazour, J. L. Rosenbaum and G. B. Witman (2007). "Functional analysis of an individual IFT protein: IFT46 is required for transport of outer dynein arms into flagella." J Cell Biol **176**(5): 653-665.
- Hsiao, Y. C., K. Tuz and R. J. Ferland (2012). "Trafficking in and to the primary cilium." Cilia **1**(1): 4.
- Huangfu, D., A. Liu, A. S. Rakeman, N. S. Murcia, L. Niswander and K. V. Anderson (2003). "Hedgehog signalling in the mouse requires intraflagellar transport proteins." Nature **426**(6962): 83-87.
- Huet, D., T. Blisnick, S. Perrot and P. Bastin (2014). "The GTPase IFT27 is involved in both anterograde and retrograde intraflagellar transport." Elife **3**: e02419.
- Hughes, L., K. Towers, T. Starborg, K. Gull and S. Vaughan (2013). "A cell-body groove housing the new flagellum tip suggests an adaptation of cellular morphogenesis for parasitism in the bloodstream form of *Trypanosoma brucei*." J Cell Sci **126**(Pt 24): 5748-5757.

## References

Hughes, L. C., K. S. Ralston, K. L. Hill and Z. H. Zhou (2012). "Three-dimensional structure of the Trypanosome flagellum suggests that the paraflagellar rod functions as a biomechanical spring." PLoS One **7**(1): e25700.

Hunnicutt, G. R. (1990). "Cell body and flagellar agglutinins in *Chlamydomonas reinhardtii*: the cell body plasma membrane is a reservoir for agglutinins whose migration to the flagella is regulated by a functional barrier." The Journal of Cell Biology **111**(4): 1605-1616.

Imboden, M., N. Müller, A. Hemphill, R. Mattioli and T. Seebeck (2009). "Repetitive proteins from the flagellar cytoskeleton of African trypanosomes are diagnostically useful antigens." Parasitology **110**(03): 249.

Informal Expert Group on Gambiense, H. A. T. R., P. Buscher, J. M. Bart, M. Boelaert, B. Bucheton, G. Cecchi, N. Chitnis, D. Courtin, L. M. Figueiredo, J. R. Franco, P. Grebaut, E. Hasker, H. Ilboudo, V. Jamonneau, M. Koffi, V. Lejon, A. MacLeod, J. Masumu, E. Matovu, R. Mattioli, H. Noyes, A. Picado, K. S. Rock, B. Rotureau, G. Simo, S. Thevenon, S. Trindade, P. Truc and N. Van Reet (2018). "Do Cryptic Reservoirs Threaten Gambiense-Sleeping Sickness Elimination?" Trends Parasitol **34**(3): 197-207.

Inglis, P. N., O. E. Blacque and M. R. Leroux (2009). "Functional genomics of intraflagellar transport-associated proteins in *C. elegans*." Methods Cell Biol **93**: 267-304.

Ishikawa, H., T. Ide, T. Yagi, X. Jiang, M. Hirono, H. Sasaki, H. Yanagisawa, K. A. Wemmer, D. Y. Stainier, H. Qin, R. Kamiya and W. F. Marshall (2014). "TTC26/DYF13 is an intraflagellar transport protein required for transport of motility-related proteins into flagella." Elife **3**: e01566.

Ishikawa, H., A. Kubo, S. Tsukita and S. Tsukita (2005). "Odf2-deficient mother centrioles lack distal/subdistal appendages and the ability to generate primary cilia." Nat Cell Biol **7**(5): 517-524.

Ishikawa, H. and W. F. Marshall (2017). "Testing the time-of-flight model for flagellar length sensing." Mol Biol Cell **28**(23): 3447-3456.

Janke, C. (2014). "The tubulin code: molecular components, readout mechanisms, and functions." J Cell Biol **206**(4): 461-472.

## References

- Johnson, K. A. and J. L. Rosenbaum (1992). "Polarity of flagellar assembly in *Chlamydomonas*." J Cell Biol **119**(6): 1605-1611.
- Jospeh, H. (1903). Beitrage zur Flimmerzellen-und Centrosomafrage. Institut der Universität Wien und der Zoologischen Station in Triest.
- Julkowska, D. and P. Bastin (2009). "Tools for Analyzing Intraflagellar Transport in Trypanosomes." **93**: 59-80.
- Kagabadouno, M. (2018). "Ebola outbreak brings to light an unforeseen impact of tsetse control on sleeping sickness transmission in Guinea." bioRxiv.
- Kee, H. L., J. F. Dishinger, T. L. Blasius, C. J. Liu, B. Margolis and K. J. Verhey (2012). "A size-exclusion permeability barrier and nucleoporins characterize a ciliary pore complex that regulates transport into cilia." Nat Cell Biol **14**(4): 431-437.
- Kelly, S., J. Reed, S. Kramer, L. Ellis, H. Webb, J. Sunter, J. Salje, N. Marinsek, K. Gull, B. Wickstead and M. Carrington (2007). "Functional genomics in *Trypanosoma brucei*: a collection of vectors for the expression of tagged proteins from endogenous and ectopic gene loci." Mol Biochem Parasitol **154**(1): 103-109.
- Kennedy, P. G. (2008). "The continuing problem of human African trypanosomiasis (sleeping sickness)." Ann Neurol **64**(2): 116-126.
- Kleine, F. (1909). "Weitere wissenschaftliche Beobachtungen über die Entwicklung von Trypanosomen in Glossinen." **35**: 924-925.
- Kohl, L. and K. Gull (1998). "Molecular architecture of the trypanosome cytoskeleton." Mol Biochem Parasitol **93**(1): 1-9.
- Kohl, L., D. Robinson and P. Bastin (2003). "Novel roles for the flagellum in cell morphogenesis and cytokinesis of trypanosomes." EMBO J **22**(20): 5336-5346.
- Kooy, R. F., H. Hirumi, S. K. Moloo, V. M. Nantulya, P. Dukes, P. M. Van der Linden, W. A. Duijndam, C. J. Janse and J. P. Overdulve (1989). "Evidence for diploidy in metacyclic forms of African trypanosomes." Proc Natl Acad Sci U S A **86**(14): 5469-5472.

## References

Koyfman, A. Y., M. F. Schmid, L. Gheiratmand, C. J. Fu, H. A. Khant, D. Huang, C. Y. He and W. Chiu (2011). "Structure of *Trypanosoma brucei* flagellum accounts for its bihelical motion." Proc Natl Acad Sci U S A **108**(27): 11105-11108.

Kozminski, K. G., P. L. Beech and J. L. Rosenbaum (1995). "The Chlamydomonas kinesin-like protein FLA10 is involved in motility associated with the flagellar membrane." J Cell Biol **131**(6 Pt 1): 1517-1527.

Kozminski, K. G., K. A. Johnson, P. Forscher and J. L. Rosenbaum (1993). "A motility in the eukaryotic flagellum unrelated to flagellar beating." Proc Natl Acad Sci U S A **90**(12): 5519-5523.

L'Hernault, S. W. and J. L. Rosenbaum (1985). "Reversal of the posttranslational modification on Chlamydomonas flagellar alpha-tubulin occurs during flagellar resorption." J Cell Biol **100**(2): 457-462.

Lacomble, S., S. Vaughan, C. Gadelha, M. K. Morphew, M. K. Shaw, J. R. McIntosh and K. Gull (2009). "Three-dimensional cellular architecture of the flagellar pocket and associated cytoskeleton in trypanosomes revealed by electron microscope tomography." J Cell Sci **122**(Pt 8): 1081-1090.

Lacomble, S., S. Vaughan, C. Gadelha, M. K. Morphew, M. K. Shaw, J. R. McIntosh and K. Gull (2010). "Basal body movements orchestrate membrane organelle division and cell morphogenesis in *Trypanosoma brucei*." J Cell Sci **123**(Pt 17): 2884-2891.

LaCount, D. J., B. Barrett and J. E. Donelson (2002). "Trypanosoma brucei FLA1 is required for flagellum attachment and cytokinesis." J Biol Chem **277**(20): 17580-17588.

Lakkis, M. and J. Zhou (2003). "Molecular complexes formed with polycystins." Nephron Exp Nephrol **93**(1): e3-8.

Lambacher, N. J., A. L. Bruel, T. J. van Dam, K. Szymanska, G. G. Slaats, S. Kuhns, G. J. McManus, J. E. Kennedy, K. Gaff, K. M. Wu, R. van der Lee, L. Burglen, D. Doummar, J. B. Riviere, L. Faivre, T. Attie-Bitach, S. Saunier, A. Curd, M. Peckham, R. H. Giles, C. A. Johnson, M. A. Huynen, C. Thauvin-Robinet and O. E. Blacque (2016). "TMEM107 recruits ciliopathy proteins to subdomains of the ciliary transition zone and causes Joubert syndrome." Nat Cell Biol **18**(1): 122-131.

Langerhans, P. (1876). "Zur Anatomie des *Amphioxus*." Archiv fur Mikroskopische Anatomie **12**: 290-348.

## References

Laurencon, A., R. Dubruille, E. Efimenko, G. Grenier, R. Bissett, E. Cortier, V. Rolland, P. Swoboda and B. Durand (2007). "Identification of novel regulatory factor X (RFX) target genes by comparative genomics in *Drosophila* species." Genome Biol **8**(9): R195.

Le Ray, D., J. D. Barry, C. Easton and K. Vickerman (1977). "First tsetse fly transmission of the "AnTat" serodeme of *Trypanosoma brucei*." Ann Soc Belg Med Trop **57**(4-5): 369-381.

Lechtreck, K. F. and S. Geimer (2000). "Distribution of polyglutamylated tubulin in the flagellar apparatus of green flagellates." Cell Motil Cytoskeleton **47**(3): 219-235.

Lechtreck, K. F., S. Luro, J. Awata and G. B. Witman (2009). "HA-tagging of putative flagellar proteins in *Chlamydomonas reinhardtii* identifies a novel protein of intraflagellar transport complex B." Cell Motil Cytoskeleton **66**(8): 469-482.

Lee, E., E. Sivan-Loukianova, D. F. Eberl and M. J. Kernan (2008). "An IFT-A protein is required to delimit functionally distinct zones in mechanosensory cilia." Curr Biol **18**(24): 1899-1906.

Lee, L. (2013). "Riding the wave of ependymal cilia: genetic susceptibility to hydrocephalus in primary ciliary dyskinesia." J Neurosci Res **91**(9): 1117-1132.

Li, J. B., J. M. Gerdes, C. J. Haycraft, Y. Fan, T. M. Teslovich, H. May-Simera, H. Li, O. E. Blacque, L. Li, C. C. Leitch, R. A. Lewis, J. S. Green, P. S. Parfrey, M. R. Leroux, W. S. Davidson, P. L. Beales, L. M. Guay-Woodford, B. K. Yoder, G. D. Stormo, N. Katsanis and S. K. Dutcher (2004). "Comparative genomics identifies a flagellar and basal body proteome that includes the BBS5 human disease gene." Cell **117**(4): 541-552.

Liang, Y., Y. Pang, Q. Wu, Z. Hu, X. Han, Y. Xu, H. Deng and J. Pan (2014). "FLA8/KIF3B phosphorylation regulates kinesin-II interaction with IFT-B to control IFT entry and turnaround." Dev Cell **30**(5): 585-597.

Livingstone, D. (1857). Missionary travels and researches in South Africa, including a sketch of sixteen year's residence in the interior of Africa, J.Murray.

Lucker, B. F., R. H. Behal, H. Qin, L. C. Siron, W. D. Taggart, J. L. Rosenbaum and D. G. Cole (2005). "Characterization of the intraflagellar transport complex B core: direct interaction of the IFT81 and IFT74/72 subunits." J Biol Chem **280**(30): 27688-27696.

## References

- Lucker, B. F., M. S. Miller, S. A. Dziedzic, P. T. Blackmarr and D. G. Cole (2010). "Direct interactions of intraflagellar transport complex B proteins IFT88, IFT52, and IFT46." J Biol Chem **285**(28): 21508-21518.
- Ludington, W. B., K. A. Wemmer, K. F. Lehtreck, G. B. Witman and W. F. Marshall (2013). "Avalanche-like behavior in ciliary import." Proc Natl Acad Sci U S A **110**(10): 3925-3930.
- Luo, M., M. Cao, Y. Kan, G. Li, W. Snell and J. Pan (2011). "The phosphorylation state of an aurora-like kinase marks the length of growing flagella in *Chlamydomonas*." Curr Biol **21**(7): 586-591.
- M. Farina, M. A., T. souto-Padron, W. De Souza (1986). Further Studies on the Organization of the Paraxial Rod of Trypanosomatids.
- MacLeod, E. T., I. Maudlin, A. C. Darby and S. C. Welburn (2007). "Antioxidants promote establishment of trypanosome infections in tsetse." Parasitology **134**(Pt 6): 827-831.
- Maga, J. A., T. Sherwin, S. Francis, K. Gull and J. H. LeBowitz (1999). "Genetic dissection of the *Leishmania* paraflagellar rod, a unique flagellar cytoskeleton structure." J Cell Sci **112 ( Pt 16)**: 2753-2763.
- Magnus, E., T. Vervoort and N. Van Meirvenne (1978). "A card-agglutination test with stained trypanosomes (C.A.T.T.) for the serological diagnosis of *T. B. gambiense* trypanosomiasis." Ann Soc Belg Med Trop **58**(3): 169-176.
- Maia-Brigagao, C., A. P. Gadelha and W. de Souza (2013). "New associated structures of the anterior flagella of *Giardia duodenalis*." Microsc Microanal **19**(5): 1374-1376.
- Marshall, W. F., H. Qin, M. Rodrigo Brenni and J. L. Rosenbaum (2005). "Flagellar length control system: testing a simple model based on intraflagellar transport and turnover." Mol Biol Cell **16**(1): 270-278.
- Marshall, W. F. and J. L. Rosenbaum (2001). "Intraflagellar transport balances continuous turnover of outer doublet microtubules: implications for flagellar length control." J Cell Biol **155**(3): 405-414.

## References

- Marszalek, J. R., X. Liu, E. A. Roberts, D. Chui, J. D. Marth, D. S. Williams and L. S. Goldstein (2000). "Genetic evidence for selective transport of opsin and arrestin by kinesin-II in mammalian photoreceptors." *Cell* **102**(2): 175-187.
- McGrath, J., S. Somlo, S. Makova, X. Tian and M. Brueckner (2003). "Two Populations of Node Monocilia Initiate Left-Right Asymmetry in the Mouse." *Cell* **114**(1): 61-73.
- Mesu, V., W. M. Kalonji, C. Bardonneau, O. V. Mordt, S. Blesson, F. Simon, S. Delhomme, S. Bernhard, W. Kuziena, J. F. Lubaki, S. L. Vuvu, P. N. Ngima, H. M. Mbembo, M. Ilunga, A. K. Bonama, J. A. Heradi, J. L. L. Solomo, G. Mandula, L. K. Badibabi, F. R. Dama, P. K. Lukula, D. N. Tete, C. Lumbala, B. Scherrer, N. Strub-Wourgaft and A. Tarral (2018). "Oral fexinidazole for late-stage African *Trypanosoma brucei gambiense* trypanosomiasis: a pivotal multicentre, randomised, non-inferiority trial." *Lancet* **391**(10116): 144-154.
- Migchelsen, S. J., P. Buscher, A. I. Hoepelman, H. D. Schallig and E. R. Adams (2011). "Human African trypanosomiasis: a review of non-endemic cases in the past 20 years." *Int J Infect Dis* **15**(8): e517-524.
- Miki, K., W. Qu, E. H. Goulding, W. D. Willis, D. O. Bunch, L. F. Strader, S. D. Perreault, E. M. Eddy and D. A. O'Brien (2004). "Glyceraldehyde 3-phosphate dehydrogenase-S, a sperm-specific glycolytic enzyme, is required for sperm motility and male fertility." *Proc Natl Acad Sci U S A* **101**(47): 16501-16506.
- Milenkovic, L., M. P. Scott and R. Rohatgi (2009). "Lateral transport of Smoothed from the plasma membrane to the membrane of the cilium." *J Cell Biol* **187**(3): 365-374.
- Mitashi, P., E. Hasker, V. Lejon, V. Kande, J. J. Muyembe, P. Lutumba and M. Boelaert (2012). "Human african trypanosomiasis diagnosis in first-line health services of endemic countries, a systematic review." *PLoS Negl Trop Dis* **6**(11): e1919.
- Montesano, R. (1979). "Inhomogeneous distribution of filipin-sterol complexes in the ciliary membrane of rat tracheal epithelium." *Am J Anat* **156**(1): 139-145.
- Moore, L. L., C. Santrich and J. H. LeBowitz (1996). "Stage-specific expression of the *Leishmania mexicana* paraflagellar rod protein PFR-2." *Mol Biochem Parasitol* **80**(2): 125-135.

## References

- Moreira-Leite, F. F., T. Sherwin, L. Kohl and K. Gull (2001). "A trypanosome structure involved in transmitting cytoplasmic information during cell division." Science **294**(5542): 610-612.
- Mugnier, M. R., G. A. Cross and F. N. Papavasiliou (2015). "The in vivo dynamics of antigenic variation in *Trypanosoma brucei*." Science **347**(6229): 1470-1473.
- Mukhopadhyay, S., X. Wen, B. Chih, C. D. Nelson, W. S. Lane, S. J. Scales and P. K. Jackson (2010). "TULP3 bridges the IFT-A complex and membrane phosphoinositides to promote trafficking of G protein-coupled receptors into primary cilia." Genes Dev **24**(19): 2180-2193.
- Muller, O. (1786). "Animalcula infusoria; fluvia tilia et marina, que detexit, systematice descripsit et ad vivum delineari curavit." Molleri, Havniae.
- Mullor, J. L., P. Sanchez and A. Ruiz i Altaba (2002). "Pathways and consequences: Hedgehog signaling in human disease." Trends Cell Biol **12**(12): 562-569.
- N Chenouard, J. B., I Bloch, P Bastin, JC Olivo-Marin (2010). Curvelet analysis of kymograph for tracking bi-directional particles in fluorescence microscopy images. 17th IEEE International Conference on. I. P. (ICIP). **3657-3660**.
- Nachury, M. V., E. S. Seeley and H. Jin (2010). "Trafficking to the ciliary membrane: how to get across the periciliary diffusion barrier?" Annu Rev Cell Dev Biol **26**: 59-87.
- Ngo, H. M. and G. B. Bouck (1998). "Heterogeneity and a coiled coil prediction of trypanosomatid-like flagellar rod proteins in *Euglena*." J Eukaryot Microbiol **45**(3): 323-333.
- Nicastro, D., J. R. McIntosh and W. Baumeister (2005). "3D structure of eukaryotic flagella in a quiescent state revealed by cryo-electron tomography." Proc Natl Acad Sci U S A **102**(44): 15889-15894.
- Njiokou, F., H. Nimpaye, G. Simo, G. R. Njitchouang, T. Asonganyi, G. Cuny and S. Herder (2010). "Domestic animals as potential reservoir hosts of *Trypanosoma brucei gambiense* in sleeping sickness foci in Cameroon." Parasite **17**(1): 61-66.

## References

- Nonaka, S., Y. Tanaka, Y. Okada, S. Takeda, A. Harada, Y. Kanai, M. Kido and N. Hirokawa (1998). "Randomization of left-right asymmetry due to loss of nodal cilia generating leftward flow of extraembryonic fluid in mice lacking KIF3B motor protein." Cell **95**(6): 829-837.
- O'Hagan, R., B. P. Piasecki, M. Silva, P. Phirke, K. C. Nguyen, D. H. Hall, P. Swoboda and M. M. Barr (2011). "The tubulin deglutamylase CCPP-1 regulates the function and stability of sensory cilia in *C. elegans*." Curr Biol **21**(20): 1685-1694.
- Oberholzer, M., G. Langousis, H. T. Nguyen, E. A. Saada, M. M. Shimogawa, Z. O. Jonsson, S. M. Nguyen, J. A. Wohlschlegel and K. L. Hill (2011). "Independent analysis of the flagellum surface and matrix proteomes provides insight into flagellum signaling in mammalian-infectious *Trypanosoma brucei*." Mol Cell Proteomics **10**(10): M111 010538.
- Ogbadoyi, E. O., D. R. Robinson and K. Gull (2003). "A high-order trans-membrane structural linkage is responsible for mitochondrial genome positioning and segregation by flagellar basal bodies in trypanosomes." Mol Biol Cell **14**(5): 1769-1779.
- Ooi, C. P. and P. Bastin (2013). "More than meets the eye: understanding *Trypanosoma brucei* morphology in the tsetse." Front Cell Infect Microbiol **3**: 71.
- Orozco, J. T., K. P. Wedaman, D. Signor, H. Brown, L. Rose and J. M. Scholey (1999). "Movement of motor and cargo along cilia." Nature **398**(6729): 674.
- Otieno, L. H. and N. Darji (1979). "The abundance of pathogenic African trypanosomes in the salivary secretions of wild *Glossina pallidipes*." Ann Trop Med Parasitol **73**(6): 583-588.
- Ou, G., O. E. Blacque, J. J. Snow, M. R. Leroux and J. M. Scholey (2005). "Functional coordination of intraflagellar transport motors." Nature **436**(7050): 583-587.
- Pan, J. a. S., W (2002). "Kinesin-II Is Required for Flagellar Sensory Transduction during Fertilization in *Chlamydomonas*."
- Pan, X., G. Ou, G. Civelekoglu-Scholey, O. E. Blacque, N. F. Endres, L. Tao, A. Mogilner, M. R. Leroux, R. D. Vale and J. M. Scholey (2006). "Mechanism of transport of IFT particles in *C. elegans* cilia by the concerted action of kinesin-II and OSM-3 motors." J Cell Biol **174**(7): 1035-1045.

## References

Pays, E., B. Vanhollebeke, L. Vanhamme, F. Paturiaux-Hanocq, D. P. Nolan and D. Perez-Morga (2006). "The trypanolytic factor of human serum." Nat Rev Microbiol **4**(6): 477-486.

Pazour, G. J., N. Agrin, J. Leszyk and G. B. Witman (2005). "Proteomic analysis of a eukaryotic cilium." J Cell Biol **170**(1): 103-113.

Pazour, G. J., S. A. Baker, J. A. Deane, D. G. Cole, B. L. Dickert, J. L. Rosenbaum, G. B. Witman and J. C. Besharse (2002). "The intraflagellar transport protein, IFT88, is essential for vertebrate photoreceptor assembly and maintenance." J Cell Biol **157**(1): 103-113.

Pazour, G. J., B. L. Dickert, Y. Vucica, E. S. Seeley, J. L. Rosenbaum, G. B. Witman and D. G. Cole (2000). "Chlamydomonas IFT88 and Its Mouse Homologue, Polycystic Kidney Disease GeneTg737, Are Required for Assembly of Cilia and Flagella." The Journal of Cell Biology **151**(3): 709-718.

Pazour, G. J., B. L. Dickert and G. B. Witman (1999). "The DHC1b (DHC2) isoform of cytoplasmic dynein is required for flagellar assembly." J Cell Biol **144**(3): 473-481.

Pazour, G. J., J. T. San Agustin, J. A. Follit, J. L. Rosenbaum and G. B. Witman (2002). "Polycystin-2 localizes to kidney cilia and the ciliary level is elevated in orpk mice with polycystic kidney disease." Curr Biol **12**(11): R378-380.

Pedersen, L. B., S. Geimer and J. L. Rosenbaum (2006). "Dissecting the molecular mechanisms of intraflagellar transport in chlamydomonas." Curr Biol **16**(5): 450-459.

Pedersen, L. B., M. S. Miller, S. Geimer, J. M. Leitch, J. L. Rosenbaum and D. G. Cole (2005). "Chlamydomonas IFT172 is encoded by FLA11, interacts with CrEB1, and regulates IFT at the flagellar tip." Curr Biol **15**(3): 262-266.

Pedersen, L. B. and J. L. Rosenbaum (2008). "Intraflagellar transport (IFT) role in ciliary assembly, resorption and signalling." Curr Top Dev Biol **85**: 23-61.

Perkins, L. A., E. M. Hedgecock, J. N. Thomson and J. G. Culotti (1986). "Mutant sensory cilia in the nematode *Caenorhabditis elegans*." Dev Biol **117**(2): 456-487.

Perrone, C. A., D. Tritschler, P. Taulman, R. Bower, B. K. Yoder and M. E. Porter (2003). "A novel dynein light intermediate chain colocalizes with the retrograde motor

## References

for intraflagellar transport at sites of axoneme assembly in chlamydomonas and Mammalian cells." Mol Biol Cell **14**(5): 2041-2056.

Phillips, D. M. (1966). "Fine structure of *Sciara coprophila* sperm." J Cell Biol **30**(3): 499-517.

Pigino, G., S. Geimer, S. Lanzavecchia, E. Paccagnini, F. Cantele, D. R. Diener, J. L. Rosenbaum and P. Lupetti (2009). "Electron-tomographic analysis of intraflagellar transport particle trains in situ." J Cell Biol **187**(1): 135-148.

Piperno, G. and K. Mead (1997). "Transport of a novel complex in the cytoplasmic matrix of *Chlamydomonas* flagella." Proc Natl Acad Sci U S A **94**(9): 4457-4462.

Porter, M. E., R. Bower, J. A. Knott, P. Byrd and W. Dentler (1999). "Cytoplasmic dynein heavy chain 1b is required for flagellar assembly in *Chlamydomonas*." Mol Biol Cell **10**(3): 693-712.

Porter, M. E. and W. S. Sale (2000). "The 9 + 2 axoneme anchors multiple inner arm dyneins and a network of kinases and phosphatases that control motility." J Cell Biol **151**(5): F37-42.

Portman, N., S. Lacomble, B. Thomas, P. G. McKean and K. Gull (2009). "Combining RNA interference mutants and comparative proteomics to identify protein components and dependences in a eukaryotic flagellum." J Biol Chem **284**(9): 5610-5619.

Pradel, L. C., M. Bonhivers, N. Landrein and D. R. Robinson (2006). "NIMA-related kinase TbNRKC is involved in basal body separation in *Trypanosoma brucei*." J Cell Sci **119**(Pt 9): 1852-1863.

Praetorius, H. A. and K. R. Spring (2003). "Removal of the MDCK cell primary cilium abolishes flow sensing." J Membr Biol **191**(1): 69-76.

Prensier, G., E. Vivier, S. Goldstein and J. Schrevel (1980). "Motile flagellum with a "3 + 0" ultrastructure." Science **207**(4438): 1493-1494.

Prevo, B., P. Mangeol, F. Oswald, J. M. Scholey and E. J. Peterman (2015). "Functional differentiation of cooperating kinesin-2 motors orchestrates cargo import and transport in *C. elegans* cilia." Nat Cell Biol **17**(12): 1536-1545.

## References

- Prevo, B., J. M. Scholey and E. J. G. Peterman (2017). "Intraflagellar transport: mechanisms of motor action, cooperation, and cargo delivery." FEBS J **284**(18): 2905-2931.
- Priotto, G., S. Kasparian, W. Mutombo, D. Ngouama, S. Ghorashian, U. Arnold, S. Ghabri, E. Baudin, V. Buard, S. Kazadi-Kyanza, M. Ilunga, W. Mutangala, G. Pohlig, C. Schmid, U. Karunakara, E. Torreele and V. Kande (2009). "Nifurtimox-eflornithine combination therapy for second-stage African *Trypanosoma brucei gambiense* trypanosomiasis: a multicentre, randomised, phase III, non-inferiority trial." Lancet **374**(9683): 56-64.
- Pugacheva, E. N., S. A. Jablonski, T. R. Hartman, E. P. Henske and E. A. Golemis (2007). "HEF1-dependent Aurora A activation induces disassembly of the primary cilium." Cell **129**(7): 1351-1363.
- Pullen, T. J., M. L. Ginger, S. J. Gaskell and K. Gull (2004). "Protein targeting of an unusual, evolutionarily conserved adenylate kinase to a eukaryotic flagellum." Mol Biol Cell **15**(7): 3257-3265.
- Qin, H., D. T. Burnette, Y. K. Bae, P. Forscher, M. M. Barr and J. L. Rosenbaum (2005). "Intraflagellar transport is required for the vectorial movement of TRPV channels in the ciliary membrane." Curr Biol **15**(18): 1695-1699.
- Qin, H., D. R. Diener, S. Geimer, D. G. Cole and J. L. Rosenbaum (2004). "Intraflagellar transport (IFT) cargo: IFT transports flagellar precursors to the tip and turnover products to the cell body." J Cell Biol **164**(2): 255-266.
- Qin, H., Z. Wang, D. Diener and J. Rosenbaum (2007). "Intraflagellar transport protein 27 is a small G protein involved in cell-cycle control." Curr Biol **17**(3): 193-202.
- Ralston, K. S., Z. P. Kabututu, J. H. Melehani, M. Oberholzer and K. L. Hill (2009). "The *Trypanosoma brucei* flagellum: moving parasites in new directions." Annu Rev Microbiol **63**: 335-362.
- Ralston, K. S., A. G. Lerner, D. R. Diener and K. L. Hill (2006). "Flagellar motility contributes to cytokinesis in *Trypanosoma brucei* and is modulated by an evolutionarily conserved dynein regulatory system." Eukaryot Cell **5**(4): 696-711.

## References

- Rasooly, R. and N. Balaban (2004). "Trypanosome microtubule-associated protein p15 as a vaccine for the prevention of African sleeping sickness." *Vaccine* **22**(8): 1007-1015.
- Reiter, J. F., O. E. Blacque and M. R. Leroux (2012). "The base of the cilium: roles for transition fibres and the transition zone in ciliary formation, maintenance and compartmentalization." *EMBO Rep* **13**(7): 608-618.
- Reiter, J. F. and M. R. Leroux (2017). "Genes and molecular pathways underpinning ciliopathies." *Nat Rev Mol Cell Biol* **18**(9): 533-547.
- Reuner, B., E. Vassella, B. Yutzy and M. Boshart (1997). "Cell density triggers slender to stumpy differentiation of *Trypanosoma brucei* bloodstream forms in culture." *Mol Biochem Parasitol* **90**(1): 269-280.
- Rico, E., L. Jeacock, J. Kovarova and D. Horn (2018). "Inducible high-efficiency CRISPR-Cas9-targeted gene editing and precision base editing in African trypanosomes." *Sci Rep* **8**(1): 7960.
- Ringo, D. L. (1967). "Flagellar Motion and Fine Structure of the Flagellar Apparatus in *Chlamydomonas*." *The Journal of Cell Biology* **33**(3): 543-571.
- Robinson, D. R. (1995). "Microtubule polarity and dynamics in the control of organelle positioning, segregation, and cytokinesis in the trypanosome cell cycle." *The Journal of Cell Biology* **128**(6): 1163-1172.
- Robinson, D. R. and K. Gull (1991). "Basal body movements as a mechanism for mitochondrial genome segregation in the trypanosome cell cycle." *Nature* **352**(6337): 731-733.
- Roditi, I. and C. Clayton (1999). "An unambiguous nomenclature for the major surface glycoproteins of the procyclic form of *Trypanosoma brucei*." *Mol Biochem Parasitol* **103**(1): 99-100.
- Rogowski, K., F. Juge, J. van Dijk, D. Wloga, J. M. Strub, N. Levilliers, D. Thomas, M. H. Bre, A. Van Dorsselaer, J. Gaertig and C. Janke (2009). "Evolutionary divergence of enzymatic mechanisms for posttranslational polyglycylation." *Cell* **137**(6): 1076-1087.

## References

- Rohatgi, R. and W. J. Snell (2010). "The ciliary membrane." Curr Opin Cell Biol **22**(4): 541-546.
- Rosenbaum, J. L. and F. M. Child (1967). "Flagellar regeneration in protozoan flagellates." J Cell Biol **34**(1): 345-364.
- Rosenbaum, J. L. and G. B. Witman (2002). "Intraflagellar transport." Nat Rev Mol Cell Biol **3**(11): 813-825.
- Rotureau, B., T. Blisnick, I. Subota, D. Julkowska, N. Cayet, S. Perrot and P. Bastin (2014). "Flagellar adhesion in *Trypanosoma brucei* relies on interactions between different skeletal structures in the flagellum and cell body." J Cell Sci **127**(Pt 1): 204-215.
- Rotureau, B., C. P. Ooi, D. Huet, S. Perrot and P. Bastin (2014). "Forward motility is essential for trypanosome infection in the tsetse fly." Cell Microbiol **16**(3): 425-433.
- Rotureau, B., I. Subota and P. Bastin (2011). "Molecular bases of cytoskeleton plasticity during the *Trypanosoma brucei* parasite cycle." Cell Microbiol **13**(5): 705-716.
- Rotureau, B., I. Subota, J. Buisson and P. Bastin (2012). "A new asymmetric division contributes to the continuous production of infective trypanosomes in the tsetse fly." Development **139**(10): 1842-1850.
- Rudiger, M., U. Plessmann, A. H. Rudiger and K. Weber (1995). "Beta tubulin of bull sperm is polyglycylated." FEBS Lett **364**(2): 147-151.
- San Agustin, J. T., G. J. Pazour and G. B. Witman (2015). "Intraflagellar transport is essential for mammalian spermiogenesis but is absent in mature sperm." Mol Biol Cell **26**(24): 4358-4372.
- Santrich, C., L. Moore, T. Sherwin, P. Bastin, C. Brokaw, K. Gull and J. H. LeBowitz (1997). "A motility function for the paraflagellar rod of *Leishmania* parasites revealed by PFR-2 gene knockouts." Mol Biochem Parasitol **90**(1): 95-109.
- Sasse, R. and K. Gull (1988). "Tubulin post-translational modifications and the construction of microtubular organelles in *Trypanosoma brucei*." J Cell Sci **90** ( Pt 4): 577-589.

## References

- Satir, P. (1968). "Studies on cilia. 3. Further studies on the cilium tip and a "sliding filament" model of ciliary motility." J Cell Biol **39**(1): 77-94.
- Satir, P. and S. T. Christensen (2007). "Overview of structure and function of mammalian cilia." Annu Rev Physiol **69**: 377-400.
- Schafer, J. C., C. J. Haycraft, J. H. Thomas, B. K. Yoder and P. Swoboda (2003). "XBX-1 encodes a dynein light intermediate chain required for retrograde intraflagellar transport and cilia assembly in *Caenorhabditis elegans*." Mol Biol Cell **14**(5): 2057-2070.
- Schneider, A., U. Plessmann and K. Weber (1997). "Subpellicular and flagellar microtubules of *Trypanosoma brucei* are extensively glutamylated." J Cell Sci **110** ( Pt 4): 431-437.
- Schneider, A., T. Sherwin, R. Sasse, D. G. Russell, K. Gull and T. Seebeck (1987). "Subpellicular and flagellar microtubules of *Trypanosoma brucei brucei* contain the same alpha-tubulin isoforms." J Cell Biol **104**(3): 431-438.
- Schrevel, J. and C. Besse (1975). "[A functional flagella with a 6 + 0 pattern]." J Cell Biol **66**(3): 492-507.
- Scott, V., T. Sherwin and K. Gull (1997). "gamma-tubulin in trypanosomes: molecular characterisation and localisation to multiple and diverse microtubule organising centres." J Cell Sci **110** ( Pt 2): 157-168.
- Sedmak, T. and U. Wolfrum (2010). "Intraflagellar transport molecules in ciliary and nonciliary cells of the retina." J Cell Biol **189**(1): 171-186.
- Serricchio, M., A. W. Schmid, M. E. Steinmann, E. Sigel, M. Rauch, D. Julkowska, S. Bonnefoy, C. Fort, P. Bastin and P. Butikofer (2015). "Flagellar membranes are rich in raft-forming phospholipids." Biol Open **4**(9): 1143-1153.
- Sharma, A. I., C. L. Olson and D. M. Engman (2017). "The Lipid Raft Proteome of African Trypanosomes Contains Many Flagellar Proteins." Pathogens **6**(3).
- Sharma, N., Z. A. Kosan, J. E. Stallworth, N. F. Berbari and B. K. Yoder (2011). "Soluble levels of cytosolic tubulin regulate ciliary length control." Mol Biol Cell **22**(6): 806-816.

## References

- Sharma, R., L. Peacock, E. Gluenz, K. Gull, W. Gibson and M. Carrington (2008). "Asymmetric cell division as a route to reduction in cell length and change in cell morphology in trypanosomes." Protist **159**(1): 137-151.
- Sheriff, O., L. F. Lim and C. Y. He (2014). "Tracking the biogenesis and inheritance of subpellicular microtubule in *Trypanosoma brucei* with inducible YFP-alpha-tubulin." Biomed Res Int **2014**: 893272.
- Sherwin, T. (1987). "Distinct localization and cell cycle dependence of COOH terminally tyrosinolated alpha-tubulin in the microtubules of *Trypanosoma brucei* brucei." The Journal of Cell Biology **104**(3): 439-446.
- Sherwin, T. and K. Gull (1989). "The cell division cycle of *Trypanosoma brucei* brucei: timing of event markers and cytoskeletal modulations." Philos Trans R Soc Lond B Biol Sci **323**(1218): 573-588.
- Sherwin, T., A. Schneider, R. Sasse, T. Seebeck and K. Gull (1987). "Distinct localization and cell cycle dependence of COOH terminally tyrosinolated alpha-tubulin in the microtubules of *Trypanosoma brucei* brucei." J Cell Biol **104**(3): 439-446.
- Signor, D., K. P. Wedaman, J. T. Orozco, N. D. Dwyer, C. I. Bargmann, L. S. Rose and J. M. Scholey (1999). "Role of a class DHC1b dynein in retrograde transport of IFT motors and IFT raft particles along cilia, but not dendrites, in chemosensory neurons of living *Caenorhabditis elegans*." J Cell Biol **147**(3): 519-530.
- Silva, D. A., X. Huang, R. H. Behal, D. G. Cole and H. Qin (2012). "The RABL5 homolog IFT22 regulates the cellular pool size and the amount of IFT particles partitioned to the flagellar compartment in *Chlamydomonas reinhardtii*." Cytoskeleton (Hoboken) **69**(1): 33-48.
- Simarro, P. P., J. Jannin and P. Cattand (2008). "Eliminating human African trypanosomiasis: where do we stand and what comes next?" PLoS Med **5**(2): e55.
- Singla, V. and J. F. Reiter (2006). "The primary cilium as the cell's antenna: signaling at a sensory organelle." Science **313**(5787): 629-633.
- Sirajuddin, M., L. M. Rice and R. D. Vale (2014). "Regulation of microtubule motors by tubulin isoforms and post-translational modifications." Nat Cell Biol **16**(4): 335-344.

## References

- Sluder, G. and C. L. Rieder (1985). "Experimental separation of pronuclei in fertilized sea urchin eggs: chromosomes do not organize a spindle in the absence of centrosomes." *J Cell Biol* **100**(3): 897-903.
- Smith, T. K., F. Bringaud, D. P. Nolan and L. M. Figueiredo (2017). "Metabolic reprogramming during the *Trypanosoma brucei* life cycle." *F1000Res* **6**.
- Snow, J. J., G. Ou, A. L. Gunnarson, M. R. Walker, H. M. Zhou, I. Brust-Mascher and J. M. Scholey (2004). "Two anterograde intraflagellar transport motors cooperate to build sensory cilia on *C. elegans* neurons." *Nat Cell Biol* **6**(11): 1109-1113.
- Sorokin, S. (1962). "Centrioles and the formation of rudimentary cilia by fibroblasts and smooth muscle cells." *J Cell Biol* **15**: 363-377.
- Sorokin, S. P. (1968). "Reconstructions of centriole formation and ciliogenesis in mammalian lungs." *J Cell Sci* **3**(2): 207-230.
- Stepanek, L. and G. Pigino (2016). "Microtubule doublets are double-track railways for intraflagellar transport trains." *Science* **352**(6286): 721-724.
- Stephan, A., S. Vaughan, M. K. Shaw, K. Gull and P. G. McKean (2007). "An essential quality control mechanism at the eukaryotic basal body prior to intraflagellar transport." *Traffic* **8**(10): 1323-1330.
- Subota, I., D. Julkowska, L. Vincensini, N. Reeg, J. Buisson, T. Blisnick, D. Huet, S. Perrot, J. Santi-Rocca, M. Duchateau, V. Hourdel, J. C. Rousselle, N. Cayet, A. Namane, J. Chamot-Rooke and P. Bastin (2014). "Proteomic analysis of intact flagella of procyclic *Trypanosoma brucei* cells identifies novel flagellar proteins with unique sub-localization and dynamics." *Mol Cell Proteomics* **13**(7): 1769-1786.
- Sun, S. Y., C. Wang, Y. A. Yuan and C. Y. He (2013). "An intracellular membrane junction consisting of flagellum adhesion glycoproteins links flagellum biogenesis to cell morphogenesis in *Trypanosoma brucei*." *J Cell Sci* **126**(Pt 2): 520-531.
- Sunter, J. D., C. Benz, J. Andre, S. Whipple, P. G. McKean, K. Gull, M. L. Ginger and J. Lukes (2015). "Modulation of flagellum attachment zone protein FLAM3 and regulation of the cell shape in *Trypanosoma brucei* life cycle transitions." *J Cell Sci* **128**(16): 3117-3130.

## References

- Swoboda, P., H. T. Adler and J. H. Thomas (2000). "The RFX-type transcription factor DAF-19 regulates sensory neuron cilium formation in *C. elegans*." Mol Cell **5**(3): 411-421.
- Tabish, M., Z. K. Siddiqui, K. Nishikawa and S. S. Siddiqui (1995). "Exclusive expression of *C. elegans* *osm-3* kinesin gene in chemosensory neurons open to the external environment." J Mol Biol **247**(3): 377-389.
- Tam, L. W., N. F. Wilson and P. A. Lefebvre (2007). "A CDK-related kinase regulates the length and assembly of flagella in *Chlamydomonas*." J Cell Biol **176**(6): 819-829.
- Tanos, B. E., H. J. Yang, R. Soni, W. J. Wang, F. P. Macaluso, J. M. Asara and M. F. Tsou (2013). "Centriole distal appendages promote membrane docking, leading to cilia initiation." Genes Dev **27**(2): 163-168.
- Taschner, M., S. Bhogaraju and E. Lorentzen (2012). "Architecture and function of IFT complex proteins in ciliogenesis." Differentiation **83**(2): S12-22.
- Taschner, M., S. Bhogaraju, M. Vetter, M. Morawetz and E. Lorentzen (2011). "Biochemical mapping of interactions within the intraflagellar transport (IFT) B core complex: IFT52 binds directly to four other IFT-B subunits." J Biol Chem **286**(30): 26344-26352.
- Taschner, M., K. Weber, A. Mourao, M. Vetter, M. Awasthi, M. Stiegler, S. Bhogaraju and E. Lorentzen (2016). "Intraflagellar transport proteins 172, 80, 57, 54, 38, and 20 form a stable tubulin-binding IFT-B2 complex." EMBO J **35**(7): 773-790.
- Trepout, S., A. M. Tassin, S. Marco and P. Bastin (2018). "STEM tomography analysis of the trypanosome transition zone." J Struct Biol **202**(1): 51-60.
- Tsao, C. C. and M. A. Gorovsky (2008). "Tetrahymena IFT122A is not essential for cilia assembly but plays a role in returning IFT proteins from the ciliary tip to the cell body." J Cell Sci **121**(Pt 4): 428-436.
- Tyler, K. M., A. Fridberg, K. M. Toriello, C. L. Olson, J. A. Cieslak, T. L. Hazlett and D. M. Engman (2009). "Flagellar membrane localization via association with lipid rafts." J Cell Sci **122**(Pt 6): 859-866.

## References

- Tyler, K. M., K. R. Matthews and K. Gull (1997). "The bloodstream differentiation-division of *Trypanosoma brucei* studied using mitochondrial markers." Proc Biol Sci **264**(1387): 1481-1490.
- Urwyler, S., E. Studer, C. K. Renggli and I. Roditi (2007). "A family of stage-specific alanine-rich proteins on the surface of epimastigote forms of *Trypanosoma brucei*." Mol Microbiol **63**(1): 218-228.
- Uzureau, P., S. Uzureau, L. Lecordier, F. Fontaine, P. Tebabi, F. Homble, A. Grelard, V. Zhendre, D. P. Nolan, L. Lins, J. M. Crowet, A. Pays, C. Felu, P. Poelvoorde, B. Vanhollebeke, S. K. Moestrup, J. Lyngso, J. S. Pedersen, J. C. Mottram, E. J. Dufourc, D. Perez-Morga and E. Pays (2013). "Mechanism of *Trypanosoma brucei* gambiense resistance to human serum." Nature **501**(7467): 430-434.
- van Dam, T. J., M. J. Townsend, M. Turk, A. Schlessinger, A. Sali, M. C. Field and M. A. Huynen (2013). "Evolution of modular intraflagellar transport from a coatomer-like progenitor." Proc Natl Acad Sci U S A **110**(17): 6943-6948.
- Van Den Abbeele, J., Y. Claes, D. van Bockstaele, D. Le Ray and M. Coosemans (1999). "*Trypanosoma brucei* spp. development in the tsetse fly: characterization of the post-mesocyclic stages in the foregut and proboscis." Parasitology **118** ( Pt 5): 469-478.
- Vanhamme, L., F. Paturiaux-Hanocq, P. Poelvoorde, D. P. Nolan, L. Lins, J. Van Den Abbeele, A. Pays, P. Tebabi, H. Van Xong, A. Jacquet, N. Moguelevsky, M. Dieu, J. P. Kane, P. De Baetselier, R. Brasseur and E. Pays (2003). "Apolipoprotein L-I is the trypanosome lytic factor of human serum." Nature **422**(6927): 83-87.
- Vannuccini, E., E. Paccagnini, F. Cantele, M. Gentile, D. Dini, F. Fino, D. Diener, C. Mencarelli and P. Lupetti (2016). "Two classes of short intraflagellar transport train with different 3D structures are present in *Chlamydomonas* flagella." J Cell Sci **129**(10): 2064-2074.
- Varga, V., F. Moreira-Leite, N. Portman and K. Gull (2017). "Protein diversity in discrete structures at the distal tip of the trypanosome flagellum." Proc Natl Acad Sci U S A **114**(32): E6546-E6555.
- Vaughan, S., T. Attwood, M. Navarro, V. Scott, P. McKean and K. Gull (2000). "New tubulins in protozoal parasites." Curr Biol **10**(7): R258-259.

## References

- Vaughan, S. and K. Gull (2008). "The structural mechanics of cell division in *Trypanosoma brucei*." Biochem Soc Trans **36**(Pt 3): 421-424.
- Vaughan, S. and K. Gull (2015). "Basal body structure and cell cycle-dependent biogenesis in *Trypanosoma brucei*." Cilia **5**: 5.
- Vickerman, K. (1962). "The mechanism of cyclical development in trypanosomes of the *Trypanosoma brucei* sub-group: an hypothesis based on ultrastructural observations." Trans R Soc Trop Med Hyg **56**: 487-495.
- Vickerman, K. (1969). "On the surface coat and flagellar adhesion in trypanosomes." J Cell Sci **5**(1): 163-193.
- Vickerman, K. (1985). "Developmental cycles and biology of pathogenic trypanosomes." Br Med Bull **41**(2): 105-114.
- Vickerman, L. T. a. K. (1985). "Differentiation in *trypanosoma brucei*: Host-parasite cell junctions and their Persistence during acquisition of the Variable antigen coat."
- Vincensini, L., T. Blisnick and P. Bastin (2011). "1001 model organisms to study cilia and flagella." Biol Cell **103**(3): 109-130.
- Vreysen, M. J., K. M. Saleh, M. Y. Ali, A. M. Abdulla, Z. R. Zhu, K. G. Juma, V. A. Dyck, A. R. Msangi, P. A. Mkonyi and H. U. Feldmann (2000). "Glossina austeni (Diptera: Glossinidae) eradicated on the island of Unguja, Zanzibar, using the sterile insect technique." J Econ Entomol **93**(1): 123-135.
- Wang, Z., Z. C. Fan, S. M. Williamson and H. Qin (2009). "Intraflagellar transport (IFT) protein IFT25 is a phosphoprotein component of IFT complex B and physically interacts with IFT27 in *Chlamydomonas*." PLoS One **4**(5): e5384.
- Warner, F. D. and P. Satir (1974). "The structural basis of ciliary bend formation. Radial spoke positional changes accompanying microtubule sliding." J Cell Biol **63**(1): 35-63.
- WHO (1998). "Control and surveillance of African trypanosomiasis. Report of a WHO Expert Committee." World Health Organ Tech Rep Ser **881**: I-VI, 1-114.
- WHO (2018). Trypanosomiasis, human African.

## References

- Wickstead, B. and K. Gull (2006). "A "holistic" kinesin phylogeny reveals new kinesin families and predicts protein functions." *Mol Biol Cell* **17**(4): 1734-1743.
- Williams, C. L., C. Li, K. Kida, P. N. Inglis, S. Mohan, L. Semenc, N. J. Bialas, R. M. Stupay, N. Chen, O. E. Blacque, B. K. Yoder and M. R. Leroux (2011). "MKS and NPHP modules cooperate to establish basal body/transition zone membrane associations and ciliary gate function during ciliogenesis." *J Cell Biol* **192**(6): 1023-1041.
- Wilson, N. F., J. K. Iyer, J. A. Buchheim and W. Meek (2008). "Regulation of flagellar length in *Chlamydomonas*." *Semin Cell Dev Biol* **19**(6): 494-501.
- Wingfield, J. L., I. Mengoni, H. Bomberger, Y. Y. Jiang, J. D. Walsh, J. M. Brown, T. Picariello, D. A. Cochran, B. Zhu, J. Pan, J. Eggenschwiler, J. Gaertig, G. B. Witman, P. Kner and K. Lechtreck (2017). "IFT trains in different stages of assembly queue at the ciliary base for consecutive release into the cilium." *Elife* **6**.
- Wolff, A., B. de Nechaud, D. Chillet, H. Mazarguil, E. Desbruyeres, S. Audebert, B. Edde, F. Gros and P. Denoulet (1992). "Distribution of glutamylated alpha and beta-tubulin in mouse tissues using a specific monoclonal antibody, GT335." *Eur J Cell Biol* **59**(2): 425-432.
- Wren, K. N., J. M. Craft, D. Tritschler, A. Schauer, D. K. Patel, E. F. Smith, M. E. Porter, P. Kner and K. F. Lechtreck (2013). "A differential cargo-loading model of ciliary length regulation by IFT." *Curr Biol* **23**(24): 2463-2471.
- Yang, P., D. R. Diener, C. Yang, T. Kohno, G. J. Pazour, J. M. Dienes, N. S. Agrin, S. M. King, W. S. Sale, R. Kamiya, J. L. Rosenbaum and G. B. Witman (2006). "Radial spoke proteins of *Chlamydomonas* flagella." *J Cell Sci* **119**(Pt 6): 1165-1174.
- Yang, T. T., J. Su, W. J. Wang, B. Craige, G. B. Witman, M. F. Tsou and J. C. Liao (2015). "Superresolution Pattern Recognition Reveals the Architectural Map of the Ciliary Transition Zone." *Sci Rep* **5**: 14096.
- Zariwala, M. A., M. R. Knowles and H. Omran (2007). "Genetic defects in ciliary structure and function." *Annu Rev Physiol* **69**: 423-450.
- Zhou, Q., H. Hu, C. Y. He and Z. Li (2015). "Assembly and maintenance of the flagellum attachment zone filament in *Trypanosoma brucei*." *J Cell Sci* **128**(13): 2361-2372.

## **References**

Zhou, Q., B. Liu, Y. Sun and C. Y. He (2011). "A coiled-coil- and C2-domain-containing protein is required for FAZ assembly and cell morphology in *Trypanosoma brucei*." J Cell Sci **124**(Pt 22): 3848-3858.

Zimmermann, K. W. (1898). "Beitrage zur Kenntniss einiger Drusen und Epithelien." Archiv fur Mikroskopische Anatomie **52**: 552-706.

## 2) Figure references

Absalon, S., L. Kohl, C. Branche, T. Blisnick, G. Toutirais, F. Rusconi, J. Cosson, M. Bonhivers, D. Robinson and P. Bastin (2007). "Basal body positioning is controlled by flagellum formation in *Trypanosoma brucei*." PLoS One **2**(5): e437.

Absalon, S., T. Blisnick, L. Kohl, G. Toutirais, G. Dore, D. Julkowska, A. Tavenet and P. Bastin (2008). "Intraflagellar transport and functional analysis of genes required for flagellum formation in trypanosomes." Mol Biol Cell **19**(3): 929-944.

Afzelius, B. A. (2004). "Cilia-related diseases." J Pathol **204**(4): 470-477.

Bettencourt-Dias, M. (2013). "Q&A: Who needs a centrosome?" BMC Biol **11**: 28.

Bloodgood, R. A. (2009). "From central to rudimentary to primary: the history of an underappreciated organelle whose time has come. The primary cilium." Methods Cell Biol **94**: 3-52.

Brazelton, W. J., C. D. Amundsen, C. D. Silflow and P. A. Lefebvre (2001). "The bld1 mutation identifies the *Chlamydomonas* osm-6 homolog as a gene required for flagellar assembly." Curr Biol **11**(20): 1591-1594.

Briggs, L. J., P. G. McKean, A. Baines, F. Moreira-Leite, J. Davidge, S. Vaughan and K. Gull (2004). "The flagella connector of *Trypanosoma brucei*: an unusual mobile transmembrane junction." J Cell Sci **117**(Pt 9): 1641-1651.

Brown, J. M. and G. B. Witman (2014). "Cilia and Diseases." Bioscience **64**(12): 1126-1137.

Buisson, J. and P. Bastin (2010). "Flagellum Structure and Function in Trypanosomes." **17**: 63-86.

Bustamante-Marin, X. M. and L. E. Ostrowski (2017). "Cilia and Mucociliary Clearance." Cold Spring Harb Perspect Biol **9**(4).

Cote, R. H. (2006). Photoreceptor Phosphodiesterase (PDE6): A G-Protein-Activated PDE Regulating Visual Excitation in Rod and Cone Photoreceptor Cells, CRC Press.

## References

Dallai, R., P. Lupetti and C. Mencarelli (2006). "Unusual Axonemes of Hexapod Spermatozoa." *254*: 45-99.

Dean, S., J. D. Sunter and R. J. Wheeler (2017). "TrypTag.org: A Trypanosome Genome-wide Protein Localisation Resource." *Trends Parasitol* **33**(2): 80-82.

Demonchy, R., T. Blisnick, C. Deprez, G. Toutirais, C. Loussert, W. Marande, P. Grellier, P. Bastin and L. Kohl (2009). "Kinesin 9 family members perform separate functions in the trypanosome flagellum." *J Cell Biol* **187**(5): 615-622.

Elmendorf, H. G., S. C. Dawson and J. M. McCaffery (2003). "The cytoskeleton of *Giardia lamblia*." *International Journal for Parasitology* **33**(1): 3-28.

Engel, B. D., H. Ishikawa, K. A. Wemmer, S. Geimer, K. Wakabayashi, M. Hirono, B. Craige, G. J. Pazour, G. B. Witman, R. Kamiya and W. F. Marshall (2012). "The role of retrograde intraflagellar transport in flagellar assembly, maintenance, and function." *J Cell Biol* **199**(1): 151-167.

Engstler, M., T. Pfohl, S. Herminghaus, M. Boshart, G. Wiegertjes, N. Heddergott and P. Overath (2007). "Hydrodynamic flow-mediated protein sorting on the cell surface of trypanosomes." *Cell* **131**(3): 505-515.

Fawcett, D. W. (1975). "The mammalian spermatozoon." *Dev Biol* **44**(2): 394-436.

Franco, J. R., G. Cecchi, G. Priotto, M. Paone, A. Diarra, L. Grout, R. C. Mattioli and D. Argaw (2017). "Monitoring the elimination of human African trypanosomiasis: Update to 2014." *PLoS Negl Trop Dis* **11**(5): e0005585.

Hallmann, A. (2011). "Evolution of reproductive development in the volvocine algae." *Sex Plant Reprod* **24**(2): 97-112.

Hoog, J. L., S. Lacomble, C. Bouchet-Marquis, L. Briggs, K. Park, A. Hoenger and K. Gull (2016). "3D Architecture of the *Trypanosoma brucei* Flagella Connector, a Mobile Transmembrane Junction." *PLoS Negl Trop Dis* **10**(1): e0004312.

Johnson, K. A. and J. L. Rosenbaum (1992). "Polarity of flagellar assembly in *Chlamydomonas*." *J Cell Biol* **119**(6): 1605-1611. Knowles, M. R., L. A. Daniels, S. D. Davis, M. A. Zariwala and M. W. Leigh (2013). "Primary ciliary dyskinesia. Recent advances in diagnostics, genetics, and characterization of clinical disease." *Am J Respir Crit Care Med* **188**(8): 913-922.

## **References**

Kozminski, K. G., K. A. Johnson, P. Forscher and J. L. Rosenbaum (1993). "A motility in the eukaryotic flagellum unrelated to flagellar beating." Proc Natl Acad Sci U S A **90**(12): 5519-5523.

Linck, R. W., H. Chemes and D. F. Albertini (2016). "The axoneme: the propulsive engine of spermatozoa and cilia and associated ciliopathies leading to infertility." J Assist Reprod Genet **33**(2): 141-156.

Linck, R. W. and R. E. Stephens (2007). "Functional protofilament numbering of ciliary, flagellar, and centriolar microtubules." Cell Motil Cytoskeleton **64**(7): 489-495.

## **Abstract:**

Cilia and flagella are essential organelles in most eukaryotes including humans. They share a canonical cylindrical structure composed of nine doublets of microtubules called the axoneme that is conserved during evolution. They are built by an active mechanism termed Intraflagellar Transport or IFT. Despite some variations in composition and length between different types of cilia, the length for a given cell type is tightly controlled. Any defect in flagellum length or IFT machinery can lead to serious cellular dysfunctions, including in humans where it is associated to genetic diseases called ciliopathies. During my thesis, we have first investigated the role and functioning of IFT in *Trypanosoma brucei* a flagellated protozoan parasite that is a powerful model to investigate cilia. Using Focus Ion Beam-Scanning Electron Microscopy (FIB-SEM), we have demonstrated that IFT trains are present almost exclusively on only two out of nine microtubules doublets of the axoneme. Then, the use of high-resolution microscopy allowed us to observe in live cells that two tracks are actually used for bidirectional IFT trafficking. We have investigated mechanisms controlling flagellum length and propose a new model named “grow and lock” where the flagellum elongates at a constant growth-rate until a signal blocks further elongation or shortening. Finally this and other models have been investigated during the parasite cycle, when trypanosomes construct flagella with very different lengths.

**Keywords:** IFT, flagellum, length control, trypanosome.

## **Résumé:**

Les cils et les flagelles sont des organites essentiels chez la plupart des eucaryotes, y compris chez l'Homme. Ils possèdent une structure cylindrique composée de neuf doublets de microtubules appelée axonème qui est conservée au cours de l'évolution. Ils sont construits par un mécanisme appelé Transport IntraFlagellaire ou IFT. Malgré des variations de composition et de longueur entre différents types de cils, la longueur des cils d'un type cellulaire donné est étroitement contrôlée. Toute anomalie de la longueur du flagelle ou de la machinerie IFT peut entraîner de graves dysfonctionnements cellulaires, y compris chez l'homme, où elles sont associées à des maladies génétiques appelées ciliopathies. Au cours de ma thèse, nous avons dans un premier temps étudié le rôle et le fonctionnement de l'IFT chez *Trypanosoma brucei*, un parasite protozoaire flagellé qui est un excellent modèle pour étudier les cils. En utilisant le Focus Ion Beam-Scanning Electron Microscopy (FIB-SEM), nous avons démontré que les trains IFT n'étaient présents presque exclusivement que sur deux des neuf doublets microtubules de l'axonème. Puis, l'utilisation de la microscopie à haute résolution nous a permis de démontrer dans des cellules vivantes que ces deux voies sont utilisées pour l'IFT dans les deux sens sur chacun de ces doublets. Nous avons ensuite étudié les mécanismes contrôlant la longueur du flagelle et proposé un nouveau modèle appelé «grow and lock» où le flagelle s'allonge avec un taux de croissance constant jusqu'à ce qu'un signal bloque son élongation ou son raccourcissement. Pour finir nous avons étudié l'implication ce modèle ainsi que d'autres modèles durant le cycle parasitaire, lorsque les trypanosomes construisent des flagelles de longueurs très différentes.

**Mots clés:** IFT, flagelle, contrôle de longueur, trypanosome.

Unité de Biologie Cellulaire des Trypanosomes  
Institut Pasteur  
25 rue du Docteur Roux, 75015 Paris